#### Aus dem

#### Poliklinik für Zahnärztliche Prothetik

## Klinikum der Ludwig-Maximilians-Universität München



## TRP Channels in Toxicant-Induced Alveolar Barrier Dysfunction

Dissertation
zum Erwerb des Doctor of Philosophy (Ph.D.)
an der Medizinischen Fakultät
der Ludwig-Maximilians-Universität München

vorgelegt von Lena Baloo Schaller

> aus Illinois / USA

> > Jahr 2025

# Mit Genehmigung der Medizinischen Fakultät der Ludwig-Maximilians-Universität München

Erstes Gutachten: Prof. Dr. Alexander Dietrich

Zweites Gutachten: Priv. Doz. Dr. Claudia Staab-Weijnitz

Drittes Gutachten: Prof. Dr. Christian Wahl-Schott

Viertes Gutachten: Prof. Dr. Matthias Griese

Dekan: Prof. Dr. med. Thomas Gudermann

Tag der mündlichen Prüfung: 23.09.2025



LUDWIG-MAXIMILIANS-UNIVERSITÄT MÜNCHEN

Dean's Office Medical Faculty Faculty of Medicine



Affidavit			
Schaller, Lena			
Surname, first name			
I hereby declare, that the submitted t	hesis entitled		
TRP Channels in Tox	xicant-Induced Alveolar Barrier Dysfunction		
·	sources indicated and have not made unauthorised use of services hers has been quoted or reproduced, the source is always given.		
	n presented here has not been submitted in the same or simie purpose of obtaining an academic degree.		
Munich, 27.10.2025	Lena Schaller		
Place, Date	Signature doctoral candidate		



LUDWIG-MAXIMILIANS-UNIVERSITÄT MÜNCHEN

Dean's Office Medical Faculty Doctoral Office



# Confirmation of congruency between printed and electronic version of the doctoral thesis

Schaller, Lena	
Surname, first name	
I hereby declare that the electronic version of the sul	bmitted thesis, entitled
TRP Channels in Toxicant-Indu	ced Alveolar Barrier Dysfunction
is congruent with the printed version both in content	and format.
Munich, 27.10.2025	Lena Schaller
Place, Date	Signature doctoral candidate

## **Table of contents**

Affida	avit	1
Confi	rmation of congruency	2
Table	of contents	3
List o	of abbreviations	4
List o	of publications	6
Contr	ribution to the publications	7
1.1	Contribution to paper I	7
1.2	Contribution to paper II	7
1.3	Contribution to paper III (Appendix)	8
2.	Introduction	9
2.1	The composition and function of the alveolar barrier	9
2.1.1	The alveolar epithelium	9
2.1.2	The microvascular endothelium	10
2.2	Cell-cell junctions and their regulators	10
2.2.1	Adherens junctions, the blueprint of the junctional complex	10
2.2.2	Cadherins as substrates of MMP and ADAM proteins	11
2.2.3	N-Cadherin and its role in "cadherin-switching"	11
2.3	Effectors of altered barrier permeability	12
2.3.1	Acid exposure	12
2.3.2	Oxidative signaling	12
2.3.3	Immune cell trafficking and invasion	12
2.4	TRP channels in alveolar barrier function	13
2.4.1	TRPV4	14
2.4.2	TRPV2	15
2.4.3	TRPM2	15
2.5	Impedance-based assays of monolayer barrier integrity	15
2.5.1	Electrical cell-substrate impedance sensing (ECIS)	16
2.6	Aims	17
3.	Paper I	18
4.	Paper II	38
Refer	ences	55
Appe	ndix A: Paper III	61
Δckn	owledgements	88

## List of abbreviations

AC         Alternating Current           ADAN10         A Disintegrin and Metalloprotease Domain-Containing Protein 10           ADPR         Adenosine Diphosphate Ribose           ALI         Acute Lung Injury           ARD         Ankyrin Repeat Domain           ARDS         Acute Respiratory Distress Syndrome           AT1         Alveolar Epithelial Type 1           AT2         Alveolar Epithelial Type 2           E-Cadherin         Epithelial Cadherin           N-Cadherin         Neural Cadherin           VE-Cadherin         Vascular Endothelial Cadherin           Co2         Carbon Dioxide           CO2         Carbon Dioxide           COPD         Chronic Obstructive Pulmonary Disease           ECIS         Electrical Cell-substrate Impedance Sensing           ECM         Extracellular Matrix           GERD         Gastroesophageal Reflux Disease				
ADPR         Adenosine Diphosphate Ribose           ALI         Acute Lung Injury           ARD         Ankyrin Repeat Domain           ARDS         Acute Respiratory Distress Syndrome           AT1         Alveolar Epithelial Type 1           AT2         Alveolar Epithelial Type 2           E-Cadherin         Epithelial Cadherin           N-Cadherin         Neural Cadherin           Va-Cadherin         Vascular Endothelial Cadherin           Cadherin         Vascular Endothelial Cadherin           Ve-Cadherin         Vascular Endothelial Cadherin           Cadherin         Vascular Endothelial Cadherin           CaM         Calmodulin Binding Domain           CO2         Carbon Dioxide           COPD         Chronic Obstructive Pulmonary Disease           ECIS         Electrical Cell-substrate Impedance Sensing           ECIS         Electrical Matrix           GERD         Gastroesophageal Reflux Disease           H₂O2         Hydrogen Peroxide           H₂O2	AC	Alternating Current		
ALI Acute Lung Injury ARD Ankyrin Repeat Domain ARDS Acute Respiratory Distress Syndrome AT1 Alveolar Epithelial Type 1 AT2 Alveolar Epithelial Type 2 E-Cadherin Epithelial Cadherin N-Cadherin Neural Cadherin Ve-Cadherin Vascular Endothelial Cadherin [Ca²-]i Intracellular Calcium Concentration CaM Calmodulin Binding Domain CO2 Carbon Dioxide COPD Chronic Obstructive Pulmonary Disease ECIS Electrical Cell-substrate Impedance Sensing ECM Extracellular Matrix GERD Gastroesophageal Reflux Disease H2O2 Hydrogen Peroxide HCI Hydrochloric Acid HPMEC Human Pulmonary Microvascular Endothelial Cells AJ Adherens Junction TJ Tight Junction MMP Matrix Metalloprotease NADPH Nicotinamide Adenine Dinucleotide Phosphate O2 Oxygen P2X Purinergic receptor 2 type X PARP Poly-ADPR Polymerase PRD Proline-Rich Domain Rac1 Ras-related C3 Botulinum Toxin Substrate 1 RhoA Ras Homolog Family Member A ROS Reactive Oxygen Species siRNA Small Interfering RNA TEER Transepithelial/Transendothelial Electrical Resistance C-Terminal Carboxy-Terminal CTF Carboxy-Terminal Fragment N-Terminal Amino-terminal	ADAM10	A Disintegrin and Metalloprotease Domain-Containing Protein 10		
ARD Ankyrin Repeat Domain ARDS Acute Respiratory Distress Syndrome AT1 Alveolar Epithelial Type 1 AT2 Alveolar Epithelial Type 2 E-Cadherin Epithelial Cadherin N-Cadherin Neural Cadherin VE-Cadherin Vascular Endothelial Cadherin [Ca²¹]; Intracellular Calcium Concentration Calmodulin Binding Domain CO2 Carbon Dioxide COPD Chronic Obstructive Pulmonary Disease ECIS Electrical Cell-substrate Impedance Sensing ECM Extracellular Matrix GERD Gastroesophageal Reflux Disease H2O2 Hydrogen Peroxide HCI Hydrochloric Acid HPMEC Human Pulmonary Microvascular Endothelial Cells AJ Adherens Junction TJ Tight Junction MMP Matrix Metalloprotease NADPH Nicotinamide Adenine Dinucleotide Phosphate O2 Oxygen P2X Purinergic receptor 2 type X PARP Poly-ADPR Polymerase PRD Proline-Rich Domain Rac1 Ras-related C3 Botulinum Toxin Substrate 1 RhoA Ras Homolog Family Member A ROS Reactive Oxygen Species siRNA Small Interfering RNA TEER Transepithelial/Transendothelial Electrical Resistance C-Terminal Carboxy-Terminal CTF Carboxy-Terminal Amino-terminal	ADPR	Adenosine Diphosphate Ribose		
ARDS Acute Respiratory Distress Syndrome AT1 Alveolar Epithelial Type 1 AT2 Alveolar Epithelial Type 2 E-Cadherin Epithelial Cadherin N-Cadherin Neural Cadherin VE-Cadherin Vascular Endothelial Cadherin VE-Cadherin Vascular Endothelial Cadherin  VE-Cadherin Vascular Endothelial Cadherin  [Ca²¹] Intracellular Calcium Concentration  CaM Calmodulin Binding Domain  CO₂ Carbon Dioxide  COPD Chronic Obstructive Pulmonary Disease ECIS Electrical Cell-substrate Impedance Sensing  ECM Extracellular Matrix  GERD Gastroesophageal Reflux Disease  H₂O₂ Hydrogen Peroxide  HCI Hydrochloric Acid  HPMEC Human Pulmonary Microvascular Endothelial Cells  AJ Adherens Junction  TJ Tight Junction  MMP Matrix Metalloprotease  NADPH Nicotinamide Adenine Dinucleotide Phosphate  O₂ Oxygen  P2X Purinergic receptor 2 type X  PARP Poly-ADPR Polymerase  PRD Proline-Rich Domain  Rac1 Ras-related C3 Botulinum Toxin Substrate 1  RhoA Ras Homolog Family Member A  ROS Reactive Oxygen Species  siRNA Small Interfering RNA  TEER Transepithelial/Transendothelial Electrical Resistance  C-Terminal Carboxy-Terminal  CTF Carboxy-Terminal Fragment  N-Terminal Amino-terminal	ALI	Acute Lung Injury		
AT1 Alveolar Epithelial Type 1 AT2 Alveolar Epithelial Type 2 E-Cadherin Epithelial Cadherin N-Cadherin Neural Cadherin VE-Cadherin Vascular Endothelial Cadherin VE-Cadherin Vascular Endothelial Cadherin  VE-Cadherin Vascular Endothelial Cadherin  [Ca²¹] Intracellular Calcium Concentration  CaM Calmodulin Binding Domain  CO₂ Carbon Dioxide  COPD Chronic Obstructive Pulmonary Disease  ECIS Electrical Cell-substrate Impedance Sensing  ECM Extracellular Matrix  GERD Gastroesophageal Reflux Disease  H₂O₂ Hydrogen Peroxide  HCI Hydrochloric Acid  HPMEC Human Pulmonary Microvascular Endothelial Cells  AJ Adherens Junction  TJ Tight Junction  MMP Matrix Metalloprotease  NADPH Nicotinamide Adenine Dinucleotide Phosphate  O₂ Oxygen  P2X Purinergic receptor 2 type X  PARP Poly-ADPR Polymerase  PRD Proline-Rich Domain  Rac1 Ras-related C3 Botulinum Toxin Substrate 1  RhoA Ras Homolog Family Member A  ROS Reactive Oxygen Species  siRNA Small Interfering RNA  TEER Transepithelial/Transendothelial Electrical Resistance  C-Terminal Carboxy-Terminal Fragment  N-Terminal Amino-terminal	ARD	Ankyrin Repeat Domain		
AT2 Alveolar Epithelial Type 2 E-Cadherin Epithelial Cadherin N-Cadherin Neural Cadherin VE-Cadherin Vascular Endothelial Cadherin VE-Cadherin Vascular Endothelial Cadherin (Ca²¹) Intracellular Calcium Concentration CaM Calmodulin Binding Domain CO₂ Carbon Dioxide COPD Chronic Obstructive Pulmonary Disease ECIS Electrical Cell-substrate Impedance Sensing ECM Extracellular Matrix GERD Gastroesophageal Reflux Disease H²₂O₂ Hydrogen Peroxide HCI Hydrochloric Acid HPMEC Human Pulmonary Microvascular Endothelial Cells AJ Adherens Junction TJ Tight Junction MMP Matrix Metalloprotease NADPH Nicotinamide Adenine Dinucleotide Phosphate O₂ Oxygen P2X Purinergic receptor 2 type X PARP Poly-ADPR Polymerase PRD Proline-Rich Domain Rac1 Ras-related C3 Botulinum Toxin Substrate 1 RhoA Ras Homolog Family Member A ROS Reactive Oxygen Species siRNA Small Interfering RNA TEER Transepithelial/Transendothelial Electrical Resistance C-Terminal Carboxy-Terminal Fragment N-Terminal Amino-terminal	ARDS	Acute Respiratory Distress Syndrome		
E-Cadherin Epithelial Cadherin N-Cadherin Neural Cadherin VE-Cadherin Vascular Endothelial Cadherin VE-Cadherin Vascular Endothelial Cadherin [Ca <sup>2+</sup> ]: Intracellular Calcium Concentration CaM Calmodulin Binding Domain CO <sub>2</sub> Carbon Dioxide COPD Chronic Obstructive Pulmonary Disease ECIS Electrical Cell-substrate Impedance Sensing ECM Extracellular Matrix GERD Gastroesophageal Reflux Disease H <sub>2</sub> O <sub>2</sub> Hydrogen Peroxide HCI Hydrochloric Acid HPMEC Human Pulmonary Microvascular Endothelial Cells AJ Adherens Junction TJ Tight Junction MMP Matrix Metalloprotease NADPH Nicotinamide Adenine Dinucleotide Phosphate O <sub>2</sub> Oxygen P2X Purinergic receptor 2 type X PARP Poly-ADPR Polymerase PRD Proline-Rich Domain Rac1 Ras-related C3 Botulinum Toxin Substrate 1 RhoA Ras Homolog Family Member A ROS Reactive Oxygen Species siRNA Small Interfering RNA TEER Transepithelial/Transendothelial Electrical Resistance C-Terminal Carboxy-Terminal CTF Carboxy-Terminal Fragment N-Terminal Amino-terminal	AT1	Alveolar Epithelial Type 1		
N-Cadherin  VE-Cadherin  VE-Cadherin  Ve-Cadherin  Vascular Endothelial Cadherin  [Ca²¹],  Intracellular Calcium Concentration  CaM  Calmodulin Binding Domain  CO₂  Carbon Dioxide  COPD  Chronic Obstructive Pulmonary Disease  ECIS  Electrical Cell-substrate Impedance Sensing  ECM  Extracellular Matrix  GERD  Gastroesophageal Reflux Disease  H₂O₂  Hydrogen Peroxide  HCI  Hydrochloric Acid  HPMEC  Human Pulmonary Microvascular Endothelial Cells  AJ  Adherens Junction  TJ  Tight Junction  MMP  Matrix Metalloprotease  NADPH  Nicotinamide Adenine Dinucleotide Phosphate  O₂  Oxygen  P2X  Purinergic receptor 2 type X  PARP  Poly-ADPR Polymerase  PRD  Proline-Rich Domain  Rac1  Ras-related C3 Botulinum Toxin Substrate 1  RhoA  Ras Homolog Family Member A  ROS  Reactive Oxygen Species  siRNA  Small Interfering RNA  TEER  Transepithelial/Transendothelial Electrical Resistance  C-Terminal  Carboxy-Terminal  Amino-terminal	AT2	Alveolar Epithelial Type 2		
VE-Cadherin Vascular Endothelial Cadherin  [Ca²¹]. Intracellular Calcium Concentration  CaM Calmodulin Binding Domain  CO₂ Carbon Dioxide  COPD Chronic Obstructive Pulmonary Disease  ECIS Electrical Cell-substrate Impedance Sensing  ECM Extracellular Matrix  GERD Gastroesophageal Reflux Disease  H₂O₂ Hydrogen Peroxide  HCI Hydrochloric Acid  HPMEC Human Pulmonary Microvascular Endothelial Cells  AJ Adherens Junction  TJ Tight Junction  MMP Matrix Metalloprotease  NADPH Nicotinamide Adenine Dinucleotide Phosphate  O₂ Oxygen  P2X Purinergic receptor 2 type X  PARP Poly-ADPR Polymerase  PRD Proline-Rich Domain  Rac1 Ras-related C3 Botulinum Toxin Substrate 1  RhoA Ras Homolog Family Member A  ROS Reactive Oxygen Species  siRNA Small Interfering RNA  TEER Transepithelial/Transendothelial Electrical Resistance  C-Terminal Carboxy-Terminal  Amino-terminal	E-Cadherin	Epithelial Cadherin		
[Ca²¹].       Intracellular Calcium Concentration         CaM       Calmodulin Binding Domain         CO₂       Carbon Dioxide         COPD       Chronic Obstructive Pulmonary Disease         ECIS       Electrical Cell-substrate Impedance Sensing         ECM       Extracellular Matrix         GERD       Gastroesophageal Reflux Disease         H₂O₂       Hydrogen Peroxide         HCI       Hydrochloric Acid         HPMEC       Human Pulmonary Microvascular Endothelial Cells         AJ       Adherens Junction         TJ       Tight Junction         MMP       Matrix Metalloprotease         NADPH       Nicotinamide Adenine Dinucleotide Phosphate         O₂       Oxygen         P2X       Purinergic receptor 2 type X         PARP       Poly-ADPR Polymerase         PRD       Proline-Rich Domain         Rac1       Ras-related C3 Botulinum Toxin Substrate 1         RhoA       Ras Homolog Family Member A         ROS       Reactive Oxygen Species         siRNA       Small Interfering RNA         TEER       Transepithelial/Transendothelial Electrical Resistance         C-Terminal       Carboxy-Terminal         C-Terminal       Amino-terminal	N-Cadherin	Neural Cadherin		
Calmodulin Binding Domain  CO2 Carbon Dioxide  COPD Chronic Obstructive Pulmonary Disease  ECIS Electrical Cell-substrate Impedance Sensing  ECM Extracellular Matrix  GERD Gastroesophageal Reflux Disease  H2O2 Hydrogen Peroxide HCI Hydrochloric Acid HPMEC Human Pulmonary Microvascular Endothelial Cells  AJ Adherens Junction  TJ Tight Junction  MMP Matrix Metalloprotease  NADPH Nicotinamide Adenine Dinucleotide Phosphate  O2 Oxygen  P2X Purinergic receptor 2 type X  PARP Poly-ADPR Polymerase  PRD Proline-Rich Domain  Rac1 Ras-related C3 Botulinum Toxin Substrate 1  RhoA Ras Homolog Family Member A  ROS Reactive Oxygen Species  siRNA Small Interfering RNA  TEER Transepithelial/Transendothelial Electrical Resistance  C-Terminal Carboxy-Terminal Amino-terminal	VE-Cadherin	Vascular Endothelial Cadherin		
CO2 Carbon Dioxide  COPD Chronic Obstructive Pulmonary Disease  EGIS Electrical Cell-substrate Impedance Sensing  ECM Extracellular Matrix  GERD Gastroesophageal Reflux Disease  H <sub>2</sub> O <sub>2</sub> Hydrogen Peroxide  HCI Hydrochloric Acid  HPMEC Human Pulmonary Microvascular Endothelial Cells  AJ Adherens Junction  TJ Tight Junction  MMP Matrix Metalloprotease  NADPH Nicotinamide Adenine Dinucleotide Phosphate  O <sub>2</sub> Oxygen  P2X Purinergic receptor 2 type X  PARP Poly-ADPR Polymerase  PRD Proline-Rich Domain  Rac1 Ras-related C3 Botulinum Toxin Substrate 1  RhoA Ras Homolog Family Member A  ROS Reactive Oxygen Species  siRNA Small Interfering RNA  TEER Transepithelial/Transendothelial Electrical Resistance  C-Terminal Carboxy-Terminal  Fragment  N-Terminal Amino-terminal	[Ca <sup>2+</sup> ]i	Intracellular Calcium Concentration		
COPD Chronic Obstructive Pulmonary Disease  ECIS Electrical Cell-substrate Impedance Sensing  ECM Extracellular Matrix  GERD Gastroesophageal Reflux Disease  H <sub>2</sub> O <sub>2</sub> Hydrogen Peroxide  HCI Hydrochloric Acid  HPMEC Human Pulmonary Microvascular Endothelial Cells  AJ Adherens Junction  TJ Tight Junction  MMP Matrix Metalloprotease  NADPH Nicotinamide Adenine Dinucleotide Phosphate  O <sub>2</sub> Oxygen  P2X Purinergic receptor 2 type X  PARP Poly-ADPR Polymerase  PRD Proline-Rich Domain  Rac1 Ras-related C3 Botulinum Toxin Substrate 1  RhoA Ras Homolog Family Member A  ROS Reactive Oxygen Species  siRNA Small Interfering RNA  TEER Transepithelial/Transendothelial Electrical Resistance  C-Terminal Carboxy-Terminal  Fragment  Amino-terminal	CaM	Calmodulin Binding Domain		
ECIS Electrical Cell-substrate Impedance Sensing  ECM Extracellular Matrix  GERD Gastroesophageal Reflux Disease  H <sub>2</sub> O <sub>2</sub> Hydrogen Peroxide  HCI Hydrochloric Acid  HPMEC Human Pulmonary Microvascular Endothelial Cells  AJ Adherens Junction  TJ Tight Junction  MMP Matrix Metalloprotease  NADPH Nicotinamide Adenine Dinucleotide Phosphate  O <sub>2</sub> Oxygen  P2X Purinergic receptor 2 type X  PARP Poly-ADPR Polymerase  PRD Proline-Rich Domain  Rac1 Ras-related C3 Botulinum Toxin Substrate 1  RhoA Ras Homolog Family Member A  ROS Reactive Oxygen Species  siRNA Small Interfering RNA  TEER Transepithelial/Transendothelial Electrical Resistance  C-Terminal Carboxy-Terminal  CTF Carboxy-Terminal Fragment  N-Terminal	CO <sub>2</sub>	Carbon Dioxide		
ECM Extracellular Matrix  GERD Gastroesophageal Reflux Disease  H <sub>2</sub> O <sub>2</sub> Hydrogen Peroxide  HCl Hydrochloric Acid  HPMEC Human Pulmonary Microvascular Endothelial Cells  AJ Adherens Junction  TJ Tight Junction  MMP Matrix Metalloprotease  NADPH Nicotinamide Adenine Dinucleotide Phosphate  O <sub>2</sub> Oxygen  P2X Purinergic receptor 2 type X  PARP Poly-ADPR Polymerase  PRD Proline-Rich Domain  Rac1 Ras-related C3 Botulinum Toxin Substrate 1  RhoA Ras Homolog Family Member A  ROS Reactive Oxygen Species  siRNA Small Interfering RNA  TEER Transepithelial/Transendothelial Electrical Resistance  C-Terminal Carboxy-Terminal  CTF Carboxy-Terminal  Amino-terminal	COPD	Chronic Obstructive Pulmonary Disease		
GERD Gastroesophageal Reflux Disease  H <sub>2</sub> O <sub>2</sub> Hydrogen Peroxide  HCl Hydrochloric Acid  HPMEC Human Pulmonary Microvascular Endothelial Cells  AJ Adherens Junction  TJ Tight Junction  MMP Matrix Metalloprotease  NADPH Nicotinamide Adenine Dinucleotide Phosphate  O <sub>2</sub> Oxygen  P2X Purinergic receptor 2 type X  PARP Poly-ADPR Polymerase  PRD Proline-Rich Domain  Rac1 Ras-related C3 Botulinum Toxin Substrate 1  RhoA Ras Homolog Family Member A  ROS Reactive Oxygen Species  siRNA Small Interfering RNA  TEER Transepithelial/Transendothelial Electrical Resistance  C-Terminal Carboxy-Terminal  CTF Carboxy-Terminal Fragment  N-Terminal Amino-terminal	ECIS	Electrical Cell-substrate Impedance Sensing		
H2O2 Hydrogen Peroxide HCI Hydrochloric Acid HPMEC Human Pulmonary Microvascular Endothelial Cells AJ Adherens Junction TJ Tight Junction MMP Matrix Metalloprotease NADPH Nicotinamide Adenine Dinucleotide Phosphate O2 Oxygen P2X Purinergic receptor 2 type X PARP Poly-ADPR Polymerase PRD Proline-Rich Domain Rac1 Ras-related C3 Botulinum Toxin Substrate 1 RhoA Ras Homolog Family Member A ROS Reactive Oxygen Species siRNA Small Interfering RNA TEER Transepithelial/Transendothelial Electrical Resistance C-Terminal Carboxy-Terminal CTF Carboxy-Terminal Fragment N-Terminal Amino-terminal	ECM	Extracellular Matrix		
HCI Hydrochloric Acid HPMEC Human Pulmonary Microvascular Endothelial Cells  AJ Adherens Junction  TJ Tight Junction  MMP Matrix Metalloprotease  NADPH Nicotinamide Adenine Dinucleotide Phosphate  O2 Oxygen  P2X Purinergic receptor 2 type X  PARP Poly-ADPR Polymerase  PRD Proline-Rich Domain  Rac1 Ras-related C3 Botulinum Toxin Substrate 1  RhoA Ras Homolog Family Member A  ROS Reactive Oxygen Species  siRNA Small Interfering RNA  TEER Transepithelial/Transendothelial Electrical Resistance  C-Terminal Carboxy-Terminal  CTF Carboxy-Terminal Fragment  N-Terminal Amino-terminal	GERD	Gastroesophageal Reflux Disease		
HPMEC Human Pulmonary Microvascular Endothelial Cells  AJ Adherens Junction  TJ Tight Junction  MMP Matrix Metalloprotease  NADPH Nicotinamide Adenine Dinucleotide Phosphate  O2 Oxygen  P2X Purinergic receptor 2 type X  PARP Poly-ADPR Polymerase  PRD Proline-Rich Domain  Rac1 Ras-related C3 Botulinum Toxin Substrate 1  RhoA Ras Homolog Family Member A  ROS Reactive Oxygen Species  siRNA Small Interfering RNA  TEER Transepithelial/Transendothelial Electrical Resistance  C-Terminal Carboxy-Terminal  CTF Carboxy-Terminal Fragment  N-Terminal Amino-terminal	H <sub>2</sub> O <sub>2</sub>	Hydrogen Peroxide		
AJ Adherens Junction  TJ Tight Junction  MMP Matrix Metalloprotease  NADPH Nicotinamide Adenine Dinucleotide Phosphate  O2 Oxygen  P2X Purinergic receptor 2 type X  PARP Poly-ADPR Polymerase  PRD Proline-Rich Domain  Rac1 Ras-related C3 Botulinum Toxin Substrate 1  RhoA Ras Homolog Family Member A  ROS Reactive Oxygen Species  siRNA Small Interfering RNA  TEER Transepithelial/Transendothelial Electrical Resistance  C-Terminal Carboxy-Terminal  CTF Carboxy-Terminal Fragment  N-Terminal Amino-terminal	HCI	Hydrochloric Acid		
TJ Tight Junction  MMP Matrix Metalloprotease  NADPH Nicotinamide Adenine Dinucleotide Phosphate  O2 Oxygen  P2X Purinergic receptor 2 type X  PARP Poly-ADPR Polymerase  PRD Proline-Rich Domain  Rac1 Ras-related C3 Botulinum Toxin Substrate 1  RhoA Ras Homolog Family Member A  ROS Reactive Oxygen Species  siRNA Small Interfering RNA  TEER Transepithelial/Transendothelial Electrical Resistance  C-Terminal Carboxy-Terminal  CTF Carboxy-Terminal Fragment  N-Terminal Amino-terminal	HPMEC	Human Pulmonary Microvascular Endothelial Cells		
MMP Matrix Metalloprotease  NADPH Nicotinamide Adenine Dinucleotide Phosphate  O2 Oxygen  P2X Purinergic receptor 2 type X  PARP Poly-ADPR Polymerase  PRD Proline-Rich Domain  Rac1 Ras-related C3 Botulinum Toxin Substrate 1  RhoA Ras Homolog Family Member A  ROS Reactive Oxygen Species  siRNA Small Interfering RNA  TEER Transepithelial/Transendothelial Electrical Resistance  C-Terminal Carboxy-Terminal  CTF Carboxy-Terminal Fragment  N-Terminal  Amino-terminal	AJ	Adherens Junction		
NADPH Nicotinamide Adenine Dinucleotide Phosphate  O2 Oxygen  P2X Purinergic receptor 2 type X  PARP Poly-ADPR Polymerase  PRD Proline-Rich Domain  Rac1 Ras-related C3 Botulinum Toxin Substrate 1  RhoA Ras Homolog Family Member A  ROS Reactive Oxygen Species  siRNA Small Interfering RNA  TEER Transepithelial/Transendothelial Electrical Resistance  C-Terminal Carboxy-Terminal  CTF Carboxy-Terminal Fragment  N-Terminal Amino-terminal	TJ	Tight Junction		
O2       Oxygen         P2X       Purinergic receptor 2 type X         PARP       Poly-ADPR Polymerase         PRD       Proline-Rich Domain         Rac1       Ras-related C3 Botulinum Toxin Substrate 1         RhoA       Ras Homolog Family Member A         ROS       Reactive Oxygen Species         siRNA       Small Interfering RNA         TEER       Transepithelial/Transendothelial Electrical Resistance         C-Terminal       Carboxy-Terminal         CTF       Carboxy-Terminal Fragment         N-Terminal       Amino-terminal	MMP	Matrix Metalloprotease		
P2X Purinergic receptor 2 type X  PARP Poly-ADPR Polymerase  PRD Proline-Rich Domain  Rac1 Ras-related C3 Botulinum Toxin Substrate 1  RhoA Ras Homolog Family Member A  ROS Reactive Oxygen Species  siRNA Small Interfering RNA  TEER Transepithelial/Transendothelial Electrical Resistance  C-Terminal Carboxy-Terminal  CTF Carboxy-Terminal Fragment  N-Terminal Amino-terminal	NADPH	Nicotinamide Adenine Dinucleotide Phosphate		
PARP Poly-ADPR Polymerase  PRD Proline-Rich Domain  Rac1 Ras-related C3 Botulinum Toxin Substrate 1  RhoA Ras Homolog Family Member A  ROS Reactive Oxygen Species  siRNA Small Interfering RNA  TEER Transepithelial/Transendothelial Electrical Resistance  C-Terminal Carboxy-Terminal  CTF Carboxy-Terminal Fragment  N-Terminal Amino-terminal	O <sub>2</sub>	Oxygen		
PRD Proline-Rich Domain  Rac1 Ras-related C3 Botulinum Toxin Substrate 1  RhoA Ras Homolog Family Member A  ROS Reactive Oxygen Species  siRNA Small Interfering RNA  TEER Transepithelial/Transendothelial Electrical Resistance  C-Terminal Carboxy-Terminal  CTF Carboxy-Terminal Fragment  N-Terminal Amino-terminal	P2X	Purinergic receptor 2 type X		
Rac1 Ras-related C3 Botulinum Toxin Substrate 1 RhoA Ras Homolog Family Member A ROS Reactive Oxygen Species siRNA Small Interfering RNA TEER Transepithelial/Transendothelial Electrical Resistance C-Terminal Carboxy-Terminal CTF Carboxy-Terminal Fragment N-Terminal Amino-terminal	PARP	Poly-ADPR Polymerase		
RhoA Ras Homolog Family Member A  ROS Reactive Oxygen Species  siRNA Small Interfering RNA  TEER Transepithelial/Transendothelial Electrical Resistance  C-Terminal Carboxy-Terminal  CTF Carboxy-Terminal Fragment  N-Terminal Amino-terminal	PRD	Proline-Rich Domain		
ROS Reactive Oxygen Species  siRNA Small Interfering RNA  TEER Transepithelial/Transendothelial Electrical Resistance  C-Terminal Carboxy-Terminal  CTF Carboxy-Terminal Fragment  N-Terminal Amino-terminal	Rac1	Ras-related C3 Botulinum Toxin Substrate 1		
siRNA Small Interfering RNA  TEER Transepithelial/Transendothelial Electrical Resistance  C-Terminal Carboxy-Terminal  CTF Carboxy-Terminal Fragment  N-Terminal Amino-terminal	RhoA	Ras Homolog Family Member A		
TEER Transepithelial/Transendothelial Electrical Resistance  C-Terminal Carboxy-Terminal  CTF Carboxy-Terminal Fragment  N-Terminal Amino-terminal	ROS	Reactive Oxygen Species		
C-Terminal Carboxy-Terminal  CTF Carboxy-Terminal Fragment  N-Terminal Amino-terminal	siRNA	Small Interfering RNA		
CTF Carboxy-Terminal Fragment  N-Terminal Amino-terminal	TEER	Transepithelial/Transendothelial Electrical Resistance		
N-Terminal Amino-terminal	C-Terminal	Carboxy-Terminal		
	CTF	Carboxy-Terminal Fragment		
TRP Transient Receptor Potential	N-Terminal	Amino-terminal		
	TRP	Transient Receptor Potential		

TRPA	Transient Receptor Potential, Ankyrin subfamily
TRPC	Transient Receptor Potential, Canonical subfamily
TRPM	Transient Receptor Potential, Melastatin subfamily
TRPV	Transient Receptor Potential, Vanilloid subfamily
VEGFα	Vascular Endothelial Growth Factor Alpha
WT	Wild-type

## List of publications

### Research paper I:

**Schaller, L.**, Gudermann, T., Dietrich, A. TRPV4 mediates alveolar epithelial barrier integrity and induces ADAM10-driven E-cadherin shedding. *Cells* **13**, 1717 (2024). https://doi.org/10.3390/cells13201717

#### Research paper II:

**Schaller, L.**, Kiefmann, M., Gudermann, T., Dietrich, A. TRPV2 channels facilitate pulmonary endothelial barrier recovery after ROS-induced permeability. *Redox biol* **85**, 103720 (2025). https://doi.org/10.1016/j.redox.2025.103720

#### Research paper III:

Sierra-Marquez, J., **Schaller, L.**, Sassenbach, L., Ramirez-Fernández, A., Alt, P., Rissiek, B., Zimmer, B., Schredelseker, J., Hector, J., Stähler, T., Koch-Nolte, F., Staab-Weijnitz, C., Dietrich, A., Kopp, R., Nicke, A. Different localization of P2X4 and P2X7 receptors in native mouse lung – lack of evidence for a direct P2X4-P2X7 receptor interaction. *Front Immunol* **15**, (2024). https://doi.org/10.3389/fimmu.2024.1425938

#### Review paper I:

Müller, I., Alt, P., Rajan, S., **Schaller, L.**, Geiger, F., Dietrich, A. Transient Receptor Potential (TRP) channels in airway toxicity and disease: an update. *Cells* **11**, 2907 (2022). https://doi.org/10.3390/cells1182907

#### **Review paper II:**

**Schaller, L.**, Hofmann, K., Geiger, F., Dietrich, A. Electrical cell-substrate impedance sensing (ECIS) in lung biology and disease. *Appl. Res.*, e202400059 (2024). https://doi.org/10.1002/appl.202400059

## Contribution to the publications

## 1.1 Contribution to paper I

As the first author of this publication, my contributions included the planning and conducting of all experiments, data acquisition and analysis, data visualization in GraphPad Prism version 10, and the preparation of the first draft of the manuscript.

My aim in this project was to determine if the TRPV4 ion channel was involved in toxicant-induced changes in alveolar epithelial barrier integrity. To this end, I was responsible for isolating primary alveolar epithelial type 2 (AT2) cells from the lungs of wild-type (WT) and TRPV4-deficient (TRPV4-/-) mice, differentiating them to alveolar epithelial type 1 (AT1) cells, and running all subsequent experiments with these primary cells. I assessed the role of TRPV4 in the context of pharmacological activation through the use of a specific TRPV4 agonist and antagonist (GSK1016790A and GSK2193874, respectively). I was able to confirm the specificity of these pharmacological agents through calcium imaging experiments conducted in WT and TRPV4-/-AT1 cells. Moreover, I established a model of acid-induced acute lung injury (ALI) through HCI-induced media acidification in order to investigate TRPV4's role in pH-sensing. I assessed the effects of these two TRPV4 activation conditions on the alveolar epithelial barrier integrity of WT and TRPV4-/- AT1 cells using electrical cell-substrate impedance sensing (ECIS) in the Z-theta system from Applied Biophysics (Troy, NY, USA). In parallel, I performed Western blotting to determine the effects of TRPV4 activation on the alveolar epithelial adherens junction protein, epithelial cadherin (E-cadherin).

My experiments revealed that both GSK1016790A and acidic pH exposure triggered an acute loss of alveolar epithelial barrier resistance and the formation of an E-cadherin C-terminal fragment (CTF). These effects were significantly reduced in the absence of TRPV4 functionality, confirming a role for TRPV4 in mediating toxicant-induced alveolar epithelial barrier dysfunction. In addition, through the use of the specific inhibitor Gl254023X, I determined that the TRPV4-driven E-cadherin CTF formation was, in part, due to the activity of a disintegrin and metalloprotease-containing protein 10 (ADAM10).

## 1.2 Contribution to paper II

Where my first paper addressed TRPV4 in the alveolar epithelial barrier, this second paper focused on the roles of TRP channels in oxidative stress-induced pulmonary microvascular endothelial barrier dysfunction. I was the first author of this manuscript, and was responsible for the complete experimental setup, as well as the data generation, analysis, and visualization in GraphPad Prism 10. Additionally, I was responsible for preparing the first draft of the manuscript, and for conducting the additional experiments requested by the reviewers.

Due to the restricted cell yield and low proliferation rates resulting from my preliminary tests of murine pulmonary endothelial cell isolation protocols, I conducted my experiments on primary human pulmonary microvascular endothelial cells (HPMEC, Promocell, Heidelberg, Germany) from four healthy donors. I characterized the effects of oxidative stress on HPMEC barrier integrity using ECIS-based cellular resistance measurements and Western blotting (see paper I) for vascular endothelial cadherin (VE-cadherin) protein levels following the application of different concentrations of hydrogen peroxide ( $H_2O_2$ ). I found that 300  $\mu$ M  $H_2O_2$  exposure caused an acute, persistent loss of HPMEC barrier resistance, coinciding with the appearance of a VE-cadherin CTF, and that these effects were not reflective of cytolysis. HPMECs treated with 75  $\mu$ M  $H_2O_2$  also experienced an acute loss of barrier resistance, but were able to recover after 90 minutes. I was able to completely prevent the formation of the  $H_2O_2$ -induced VE-cadherin CTF through the pharmacological inhibition of ADAM10.

We chose to investigate the redox-sensitive TRP channels, TRPM2 and TRPV2, after my initial quantitative real-time PCR revealed that they were among the top four expressed TRP genes in HPMECs, after TRPM7 and TRPC1. I performed calcium imaging experiments in HPMECs with the pharmacological inhibitors econazole and tranilast for TRPM2 and TRPV2, respectively, and confirmed that the increase in intracellular calcium concentration ([Ca²+]i) following H<sub>2</sub>O<sub>2</sub> exposure could be partially reduced if either channel was independently inhibited. I determined that TRPV2 inhibition prevented H<sub>2</sub>O<sub>2</sub>-induced VE-cadherin cleavage, while TRPM2 inhibition increased the

degree of VE-cadherin CTF formation. TRPV4 inhibition had no effect on the degree of  $H_2O_2$ -induced VE-cadherin cleavage. These Western blot results were corroborated with experiments using the alternate TRPM2 and TRPV2 inhibitors, JNJ28583113 and valdecoxib, respectively, as well as with siRNA-mediated gene silencing. I further confirmed the TRPV2/ADAM10/VE-cadherin pathway with the application of the TRPV2 agonist, cannabidiol, which also induced ADAM10-dependent VE-cadherin cleavage. I could not determine a role for TRPM2 in mediating VE-cadherin internalization, but did find that TRPM2 inhibition induced increased baseline HPMEC reactive oxygen species (ROS) levels and VE-cadherin cleavage, suggesting that TRPM2 could maintain redox homeostasis in HPMECs.

I next addressed the roles of TRPM2 and TRPV2 in HPMEC barrier recovery following 75 μΜ H<sub>2</sub>O<sub>2</sub> exposure. The inhibition of either TRPM2, TRPV2, or ADAM10 significantly impaired the recovery of HPMEC barrier resistance, which I investigated further in a time course of immunofluorescence stainings following 75 μM H<sub>2</sub>O<sub>2</sub> exposure. In cells pretreated with the solvent DMSO as a control, I observed a distinct, transient disorganization of VE-cadherin at the HPMEC plasma membrane 15 minutes after initial H<sub>2</sub>O<sub>2</sub> exposure, with a recovery of membrane localization and organization after 90 minutes. The disruption of VE-cadherin was accompanied by a transient localization of N-cadherin at cell-cell junctions, which then returned to its baseline, intracellular localization at 90 minutes. Inhibition of the TRPM2 or TRPV2/ADAM10 pathways disrupted the H<sub>2</sub>O<sub>2</sub>-induced N- and VE-cadherin "switching" in different forms; TRPM2 inhibition in the presence of 75 μM H<sub>2</sub>O<sub>2</sub> led to a permanent loss of VE-cadherin at the plasma membrane, while TRPV2 or ADAM10 inhibition prevented the initial disorganization of VE-cadherin and impaired the subsequent membrane localization of N-cadherin. The results of these experiments indicated that TRPV2 promotes HPMEC barrier recovery following oxidative stress by facilitating the HPMEC wound healing response by mediating the temporary "switching" of VE- and N-cadherin at adherens junctions.

## 1.3 Contribution to paper III (Appendix)

This manuscript was the product of a fruitful and extensive collaboration between our lab and the working group of Prof. Dr. Annette Nicke. The aim of the project was to ascertain which pulmonary cell types expressed the purinergic receptors P2X4 and/or P2X7, and whether there was evidence for a physical association of these two ion channels in pulmonary tissue. As co-first author, I performed immunofluorescence stainings of isolated murine alveolar, intraperitoneal, and bone-marrow-derived macrophages. I also provided advice on and executed confocal imaging for colocalization analyses. Most relevant for this thesis, I was responsible for the harvest and preparation of murine lung tissue for immunofluorescence. I selected appropriate pulmonary epithelial and endothelial markers and performed the subsequent staining and imaging in order to determine the cellular localization of P2X7 and P2X4 in whole-lung tissue. The results of our experiments determined that the overlap between the two ion channels in terms of cell type and subcellular localization was limited, providing further evidence against a physiologically relevant, direct interaction between P2X4 and P2X7 in the lungs. In addition to the experimental portion of the project, I also contributed to the preparation and editing of the final manuscript.

## 2. Introduction

## 2.1 The composition and function of the alveolar barrier

The lungs are considered the primary organ of the mammalian respiratory system and are responsible for facilitating gas exchange, supplying oxygen  $(O_2)$  to the blood and removing carbon dioxide  $(CO_2)$ . In one breath, air is distributed from the upper respiratory tract, moving from the mouth and trachea through the branching system of conducting airways, the bronchi and bronchioles, and eventually reaching the alveoli, the main sites of gas exchange [1,2]. This distal, alveolar region comprises nearly 90 % of the total volume of the lung, with an approximate surface area of 140 m² [3]. At the alveoli,  $O_2$  and  $CO_2$  move between the blood-gas barrier through passive diffusion, a type of transport made possible by the microscopically ( $\sim$ 2  $\mu$ m) thin nature of the barrier [3]. The alveolar barrier consists of three layers: the alveolar epithelium; the interstitial space, filled with an extracellular matrix (ECM), scattered fibroblasts, and a central band of collagen providing tensile strength; and the microvascular endothelium [3-5] (Figure 1). The alveolar unit's role in gas exchange was acknowledged as early as 1910 [6], but the thin, delicate barrier also contributes to the physical, chemical, and immunological defense of the airways from inspired toxins and pathogens [7]. As such, the alveolar barrier is both essential for respiratory health and function, and is also a prime toxicological target.

#### 2.1.1 The alveolar epithelium

The alveolar epithelium mainly consists of the alveolar epithelial type 1 (AT1) and type 2 (AT2) cells. In healthy alveoli, AT2 cells produce and secrete pulmonary surfactant, which lowers the alveolar surface tension and aids in host defense, as surfactant proteins A and D bind to pathogens to promote their recognition by alveolar macrophages [8]. AT2 cells can also act as AT1 progenitor cells, with greater proliferative and migratory capabilities than their AT1 cell counterparts, and are known to differentiate into AT1 cells in cases of pulmonary injury [9,10]. In contrast to the pseudostratified, columnar epithelium of the upper respiratory tract, AT1 cells are large, squamous cells that are cytologically similar to endothelial cells [11]. AT1 cells span approximately 95 % of the total alveolar surface, are responsible for the tight alveolar epithelial barrier, and are the site of gas exchange in the alveoli [9]. In addition, AT1 cells secrete vascular endothelial growth factor alpha (VEGFα), an angiogenic protein, which could play a role in epithelial-to-endothelial paracrine signaling in the developing or healing alveolus [12].

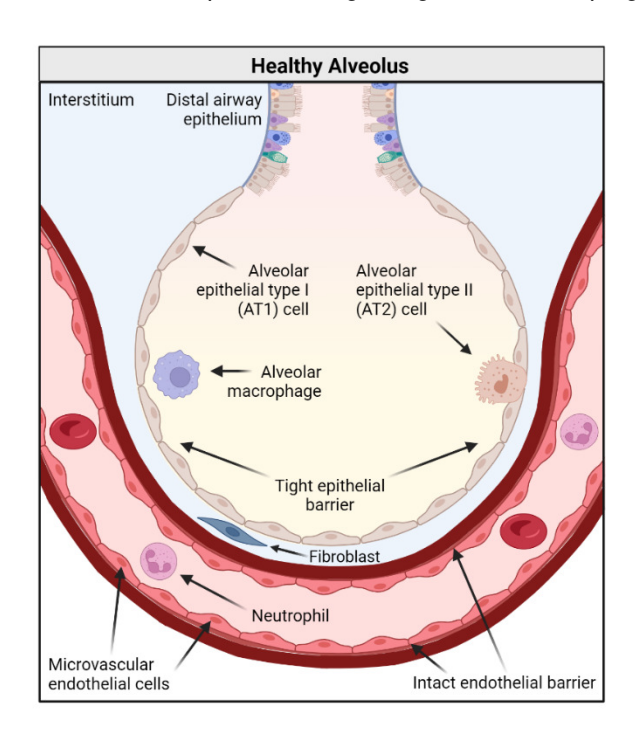


Figure 1: Structure of the alveolar barrier. The alveolar unit consists of a layer of alveolar epithelial cells, an interstitial space populated by fibroblasts, and a layer of microvascular endothelial cells. Alveolar macrophages act as a first line of defense against infiltrating pathogens (modified from [5,13]).

#### 2.1.2 The microvascular endothelium

AT1 cells facilitate gas exchange by interfacing with microvascular endothelial cells across the thin interstitial border [10]. These pulmonary microvascular endothelial cells line a capillary network that surrounds the alveoli in a dense, mesh-like structure [3]. The endothelium serves many roles, including in angiogenesis, blood coagulation, and wound healing [14]. Additionally, the microvascular endothelium is responsible for the regulation of paracellular and transcellular transport of metabolites, gases, and signaling factors [14]. Vascular barrier integrity varies across organ systems, as well as between vascular regions within a single organ [15]. While endothelial cell-cell junctions are typically less restrictive than those between epithelial cells, the barrier formed by the microvascular endothelium is significantly more constrained than that of the arterial or venous endothelium [15-17].

## 2.2 Cell-cell junctions and their regulators

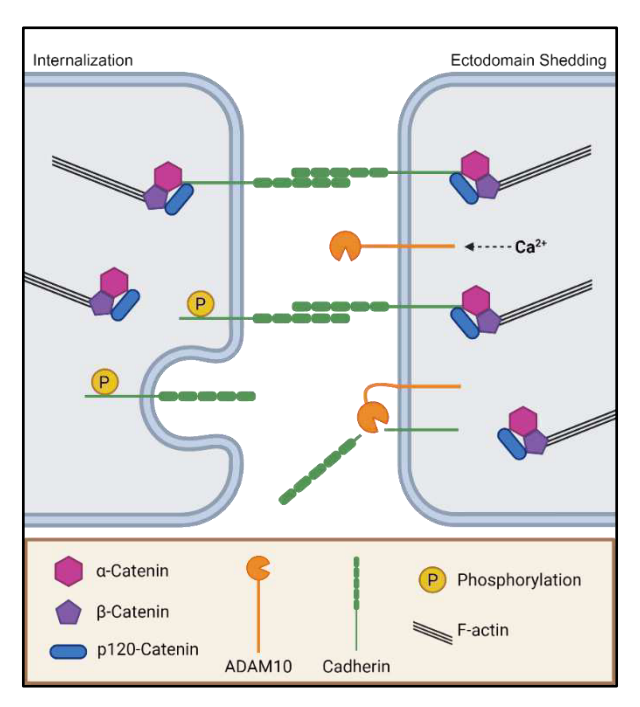
The integrity of the barriers formed by the alveolar epithelium and the microvascular endothelium depend on the junctional complexes between individual cells, which are composed of tight junctions (TJs), adherens junctions (AJs), and desmosomes [18,19]. Tight junctions are aptly named for their pivotal role in maintaining a restrictive paracellular permeability, and are made up of the transmembrane proteins of the claudin family, as well as occludin, tricellulin, and junctional adhesion molecules [18,19]. TJs interface with the actin cytoskeleton through interactions with zona occludens proteins [18,19]. AJs are mainly responsible for providing mechanical strength to the cell layer, regulating cell-cell adhesion and maintaining cell polarity [18,20]. Finally, desmosomes, consisting of the desmogleins and desmocollins proteins, confer mechanical stability through their connections to intermediate filaments [18].

#### 2.2.1 Adherens junctions, the blueprint of the junctional complex

Adherens junctions consist of Ca<sup>2+</sup>-dependent, homophilic interactions between the cadherin proteins of neighboring cells [21]. These proteins, including vascular endothelial cadherin (VE-cadherin) and epithelial cadherin (E-cadherin) are single-pass, transmembrane glycoproteins with a highly conserved, intracellular C-terminal domain [22]. This intracellular region interfaces with the actin cytoskeleton through several protein mediators, including vinculin, alpha-actinin, and several catenins [23,24]. In addition to being a functional tether between neighboring cells, adherens junctions are also essential for the formation and integrity of other junctional complexes. Epithelial tight junction assembly, for example, is restricted and disorganized in the absence of E-cadherin [25,26]. Not only that, but the formation of desmosomes, or the endothelial equivalent, syndesmos [27], is dependent on cadherins and their interaction with plakoglobin [28,29].

Cadherin proteins are in a state of constant turnover and, upon internalization into early endosomes, can either be degraded or reintroduced to the plasma membrane [30]. The rate of cadherin internalization is significantly increased upon its decoupling from p120-catenin [31-33] which, in the case of VE-cadherin, can result from the phosphorylation of serine or tyrosine residues at its C-terminus [32,34,35] (Figure 2). It has also been theorized that, aside from internalization, the disruption of extracellular binding domains can lead to a diffusion of cadherins from AJs to the greater plasma membrane [24]. Whether a result of diffusion or internalization, altered localization of cadherins at AJs often accompanies an increase in paracellular permeability [36].

Figure 2: Processes governing the removal of cadherin proteins from AJs. Cadherin proteins can undergo internalization following C-terminus phosphorylation and dissociation from the catenin complex. Cadherins can also be cleaved by several metalloproteases, including ADAM10 (modified from [24,37]) The disruption of cadherin complexes can lead to cytoskeletal reorganization following the dissociation of cadherins from filamentous actin (F-actin).



#### 2.2.2 Cadherins as substrates of MMP and ADAM proteins

Cadherin proteins at the plasma membrane can also the target of proteases, including matrix metalloproteases (MMPs) and members of the a disintegrin and metalloprotease (ADAM) family, in a process of proteolytic ectodomain cleavage, or "shedding" [38,39] (Figure 2). The regulation of VE-cadherin levels at the cell membrane through protease cleavage was first described in 1998 [40], and it is presently accepted that MMP activation leads to endothelial remodeling and the degradation of the ECM, leading to junctional disruption and cell detachment, which are necessary steps in wound healing and angiogenesis [21]. The majority of protease-driven shedding of E- and VE-cadherin is the result of ADAM10 activity [41-43], while other proteases, including MMPs 3 and 7, ADAMs 15 and 17, and cathepsins can also cleave cadherins [39,44]. Protease-driven cadherin cleavage is likely Ca<sup>2+</sup>-dependent, as ionomycin-induced Ca<sup>2+</sup>-influx significantly increases the extracellular shedding of E-cadherin [45]. Protease-mediated cadherin shedding reduces cell adhesion while increasing cell migration, and serves an essential role in cell-cell communication, angiogenesis, and wound healing [38,42].

#### 2.2.3 N-Cadherin and its role in "cadherin-switching"

In addition to VE- and E-cadherin, endothelial and epithelial cells also express neural cadherin (N-cadherin) [24,46]. Where VE- and E-cadherin are associated with contact inhibition of cell growth [47-49] and constrained cell motility [50-52], N-cadherin expression and localization at AJs is associated with a migratory phenotype [51,53]. While the former are the most prominent cadherins at the AJs of their respective cell types at steady-state, N-cadherin remains dispersed both along the cell membrane and intracellularly [46,54]. Several reports suggest that the presence of E- and VE-cadherin at AJs restricts N-cadherin translocation, and demonstrate that, in the absence of E- or VE-cadherin, N-cadherin rapidly translocates to and organizes at AJs [46,51]. This phenomenon of "cadherin-switching" has been noted across a variety of metastatic cancers [53,55-58]. N-cadherin is also known to activate the Rac1/RhoA signaling pathway, which subsequently induces the recruitment of VE-cadherin to AJs [59]. Therefore, "cadherin-switching" may serve an essential biological role to allow cells to transition into a temporary state of elevated motility to facilitate efficient wound healing, returning to a steady-state once cell-cell contacts have been reestablished.

### 2.3 Effectors of altered barrier permeability

The epithelial and endothelial cell layers that make up the alveolar barrier are constitutively restrictive, and paracellular transport across these barriers is strictly regulated. However, the thin, delicate nature of these cells predisposes the alveolar barrier to permeability-inducing agents from endogenous and exogenous sources. Airway epithelial barrier dysfunction, for example, can be caused by various environmental exposures, including cigarette smoke [60], allergens, air pollution, respiratory viruses and bacteria [61,62]. In comparison to the arterial or venous endothelium, the pulmonary microvascular endothelium is far more sensitive to injury [63]. The barrier integrity of the pulmonary microvasculature can be disrupted by mechanical stress (as in the case of ventilator induced lung injury), oxidative stress, and by signaling from neutrophils, platelets, or lymphocytes [64]. Extensive, prolonged microvascular leakage has been attributed to numerous inflammatory diseases, such as anaphylaxis, sepsis, and acute lung injury (ALI) [65]. Regardless of the initial trigger, prolonged elevated barrier permeability can lead to a buildup of fluid from the plasma in the interstitial and alveolar spaces. This condition, termed pulmonary edema, can lead to acute respiratory distress syndrome (ARDS) [66], with an estimated mortality rate of 40 % in moderate cases [67]. As such, a deeper understanding of the mechanisms underlying alveolar epithelial and microvascular endothelial barrier dysfunction would be beneficial for advancing clinical care.

#### 2.3.1 Acid exposure

A drop in extracellular pH is a dangerous trigger of altered alveolar epithelial barrier integrity, leading to pulmonary injury known as aspiration pneumonitis [68]. The average airway pH is approximately 7.3 [69], but it can drop significantly to acidic levels upon the aspiration of gastric fluid, the pH of which ranges from 1.5 to 3 [70]. Gastroesophageal reflux disease (GERD), experienced by 10-20 % of the Western adult population, is a major risk factor for gastric acid aspiration [68]. Although gastric acid aspiration is associated with increased alveolar neutrophil number and inflammation in humans, the underlying signaling pathways are still unclear [71]. Acid-induced ALI has been modeled *in vivo* by intra-tracheal instillation of HCI in rodents, resulting in increased alveolar permeability, impaired gas exchange, and an increase in inflammatory cell infiltration [72-77]. However, these *in vivo* experiments do not give insight into the acute signaling following acidic exposure in the alveoli, as lung function and tissue analyses were conducted only 3-6 hours after exposure. Therefore, supplementing the aforementioned findings with results from *in vitro* assessments would greatly improve our understanding of the mechanisms behind acid-induced ALI.

#### 2.3.2 Oxidative signaling

Reactive oxygen species (ROS), such as hydrogen peroxide (H<sub>2</sub>O<sub>2</sub>) and the superoxide anion, are important endogenous signaling molecules. ROS are produced during mitochondrial respiration as well as by nicotinamide adenine dinucleotide phosphate (NADPH) oxidase in the phagolysosomes of activated inflammatory cells [78,79]. Endothelial cells, in particular, require low levels of ROS for processes such as wound healing and angiogenesis [80,81]. Elevated ROS levels, however, can cause cellular oxidative distress, which can lead to altered signaling and apoptosis [80]. Therefore, the concept of a "redox window" has been introduced to describe the range of cellular redox rates wherein ROS signaling is optimal [80,82]. Interestingly, alveolar acidification experiments have shown a downstream increase in endothelial ROS levels. This finding has significant implications regarding the alveolar barrier, as ROS are known to alter endothelial barrier integrity. ROS exposure has been shown to trigger a permanent loss of endothelial resistance [83,84], and increase myosin light chain phosphorylation, which causes cell contraction [85]. ROS exposure has also been shown to induce endothelial VE-cadherin phosphorylation [86] and internalization [84,87].

#### 2.3.3 Immune cell trafficking and invasion

Of all the circulating immune cells, neutrophils are the first to migrate to sites of injury, inflammation, or infection [7,88]. Not only do neutrophils respond to oxidative stress and inflammation, but they are also major endogenous sources of ROS, capable of adhering to the endothelial cell surface and releasing ROS in a respiratory burst [23,89-91]. Migrating leukocytes preferentially

target AJs over TJs [92,93], and trigger a localized loss of VE-cadherin at the site of transmigration, which is reversed once the cell has transversed the endothelium [93]. Epithelial AJs are also affected during neutrophil transmigration, as transepithelial neutrophil migration induces protease-driven E-cadherin cleavage [94]. Experimental models of pulmonary acid exposure [75,76] or microvascular oxidative stress [95,96] have shown an increase in leukocyte recruitment and transmigration in response to the respective stimulus. As such, neutrophil extravasation, and the associated respiratory burst, could be an additional endogenous effector of altered alveolar barrier integrity in response to an exogenous trigger, such as acid-induced ALI (Figure 3).

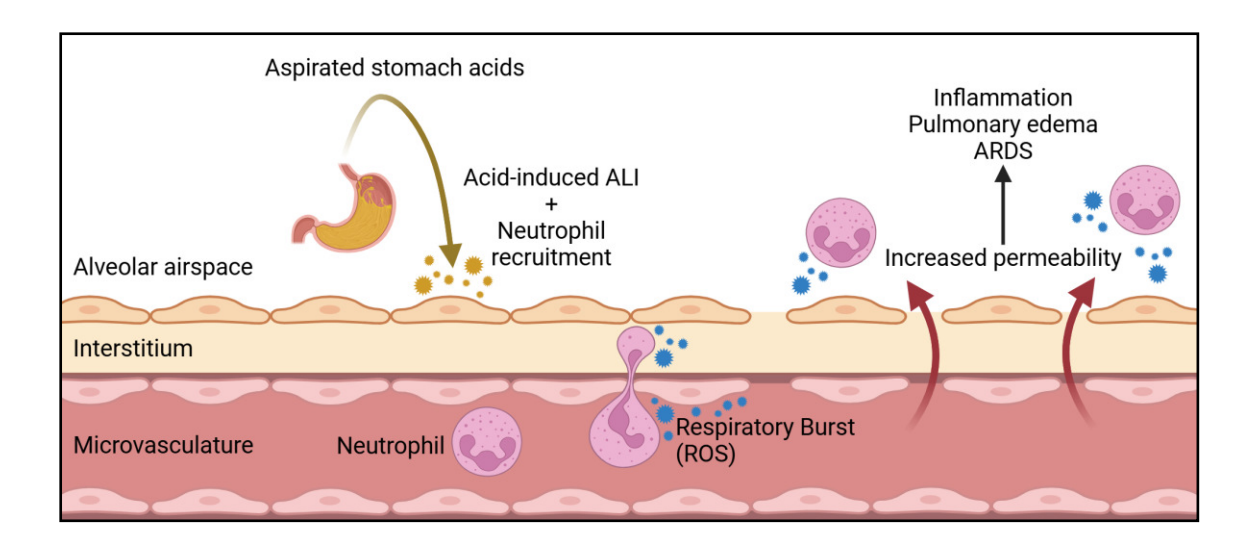
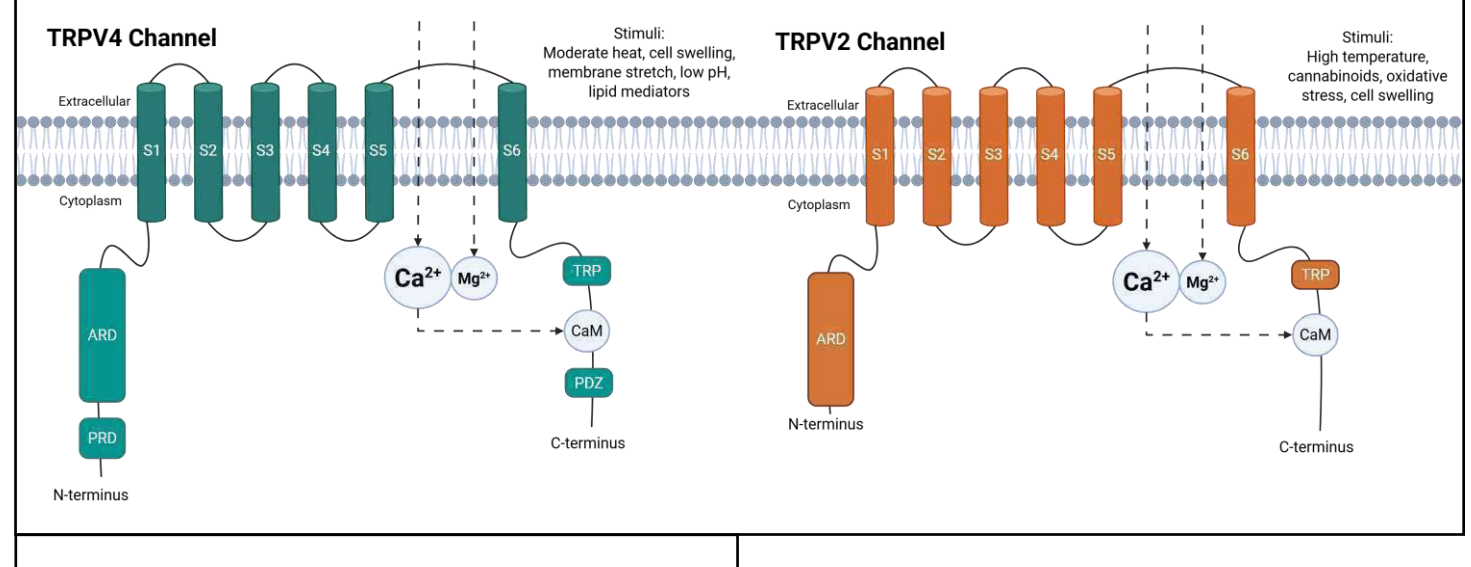


Figure 3: Acid aspiration and oxidative signaling induce alveolar barrier permeability. The integrity of the alveolar barrier can be compromised during acute lung injury (ALI), such as in the case of acid aspiration, or as a result of oxidative signaling by reactive oxygen species (ROS), including the respiratory burst released by invading neutrophils. Extensive permeability can lead to the development of acute respiratory distress syndrome (ARDS).

#### 2.4 TRP channels in alveolar barrier function

The integrity of AJs depends on extracellular Ca<sup>2+</sup>, and Ca<sup>2+</sup> influx is a well-recognized effector of barrier permeability [97], lending the family of non-selective transient receptor potential (TRP) cation channels particular toxicological interest for Ca<sup>2+</sup>-signaling in barrier dysfunction. The TRP locus, first identified in a 1989 study on *Drosophila* mutants [98], has since been characterized as a genetic superfamily of 28 mammalian homologues spanning 6 subfamilies [78,99]. TRP proteins share a common structure, with intracellular N- and C-termini and 6 transmembrane domains [99]. In addition, the majority of TRP members share a conserved sequence called the TRP box (comprised of the amino acid sequence: EWKFAR) [99]. TRP monomers form functional ion channels as either homotetrameric or heterotetrameric structures [100] (Figure 4).

The proteins within the TRPV subfamily have been extensively tied to pulmonary health, with TRPV1 known to play a role in asthma and cough [101] and TRPV4 associated with numerous respiratory diseases including pulmonary hypertension, cystic fibrosis, chronic obstructive pulmonary disease (COPD) [102], and lung fibrosis [103]. Like TRPV1, TRPA1 in tracheal and bronchial epithelial cells plays a role in the cough response following exposure to ozone [104], while in fibroblasts the channel may serve a protective role against the development of pulmonary fibrosis [105]. TRPC1, 4, and 6 are demonstrated mediators of endothelial permeability, possibly via RhoA-driven reorganization of the actin cytoskeleton [21,106]. Interestingly, TRP-mediated Ca<sup>2+</sup> influx has recently been associated with proteolytic ectodomain shedding, raising the possibility that TRP activation can lead to downstream cleavage of cadherin proteins and AJ destabilization [37].



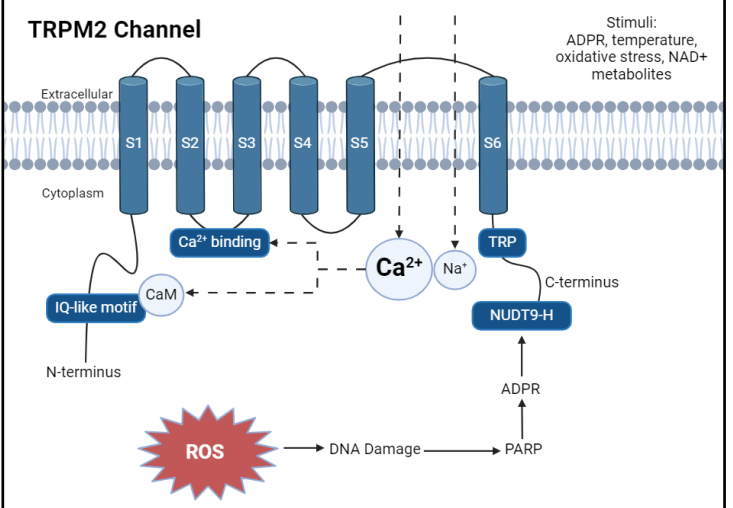


Figure 4: Basic structure and features of TRPV4, TRPV2, and TRPM2 proteins. While all three TRP proteins share a core structure of six transmembrane domains and form ion channels that conduct Ca<sup>2+</sup>, the proteins can be distinguished by their unique domains, including proline-rich domains (PRD), ankyrin repeat domains (ARD), TRP-box and NUDT9-H domains, and calmodulin (CaM) binding sites. Reactive oxygen species (ROS) trigger the production of ADP ribose (ADPR) by poly-ADP ribose polymerase (PARP), which can activate TRPM2 by binding to the NUDT9-H domain.

#### 2.4.1 TRPV4

The fourth member of the vanilloid TRP family, TRPV4, is ubiquitously expressed throughout the body [99,101,107] including in alveolar macrophages and the endo- and epithelial cells of the respiratory tract [99,108]. TRPV4 can be activated by numerous stimuli, such as cell swelling, shear stress, and low extracelluar pH [109], as well as by a variety of endogenous and exogenous ligands, including arachidonic acid and its metabolites [107]. TRPV4's roles in pulmonary injury and disease are both significant and multifaceted. For instance, in mice, TRPV4 has been proven to protect against ischemia-reperfusion-associated pulmonary edema [110], while its ablation reduced the extent of ventilator-induced pulmonary edema [111]. Although the interplay between TRPV4 signaling and altered pulmonary barrier permeability has been a topic of extensive study [112], the majority of research into TRPV4's role in mediating alveolar barrier function has been restricted to the endothelial cell layer [101]. The few studies conducted with a focus on the alveolar epithelium have reported an acute loss of barrier resistance [113] and increased membrane blebbing in alveolar epithelial cells [111] following TRPV4 activation. Therefore, it is likely that TRPV4 plays a similar role in mediating alveolar epithelial barrier integrity as in endothelial cells.

TRPV4's activation under conditions of low extracellular pH [109] makes the channel a prime target in the case of acid-induced ALI. Along this line, *in vivo* ALI models have demonstrated that TRPV4 directly contributes to the inflammation and edema following an intra-tracheal administration of HCI [75,76]. In addition to reduced inflammatory cytokine levels and edema, TRPV4-deficient mice in these studies showed significantly reduced neutrophil recruitment in the lung parenchyma, suggesting that both barrier permeability and neutrophil extravasation were restricted in the absence of TRPV4. The mechanistic pathways underlying these observations, however, have not been determined.

#### 2.4.2 TRPV2

The expression of TRPV2 is as broad as that of TRPV4, and the two share a highly conserved sequence of N-terminal ankyrin-repeats characteristic of the TRPV subfamily [114]. In contrast to TRPV4, however, far less is known about the role of TRPV2 in pulmonary function and disease. TRPV2 expression has been shown to be increased in an ovalbumin mouse model of asthma [115], and macrophages lacking TRPV2 functionality have limited phagocytic [116] and migration [117] capabilities. In fact, TRPV2 has been connected with signaling pathways mediating chemotaxis and migration in several cell types, including immune cells [118], metastatic cancer cells [119,120], and human brain microvascular endothelial cells [121]. TRPV2 shares several activation conditions with its TRPV family members, including high temperatures (TRPV1) [122], mechanical stress (TRPV4) [114] and cannabinoids (TRPV1) [123]. Recently, it was determined that TRPV2 can also act as a redox sensor, with ROS-induced oxidation of a methionine residue lowering the channel's threshold for temperature activation to physiological levels [124,125]. These findings, paired with TRPV2's expression in the microvascular endothelium, highlight a potential role for TRPV2 in mediating endothelial barrier permeability in response to ROS, such as those produced by invading neutrophils in cases of ALI [90].

#### 2.4.3 TRPM2

While the exact role of TRPV2 as a redox sensor in the pulmonary microvascular endothelium is not well established, the second member of the melastatin TRP subfamily, TRPM2, is known to mediate ROS-induced changes in endothelial barrier integrity [126]. TRPM2 is expressed throughout the body, including in the brain, heart, and lung, as well as in numerous cell types, such as cardiomyocytes, neurons, immune cells, and endothelial cells [78]. At the cellular level, TRPM2 is present at both the plasma membrane and the lysosomal membrane [127]. As with TRPV2, TRPM2 activation is temperature-dependent, and is reportedly gated by Ca<sup>2+</sup> and H<sub>2</sub>O<sub>2</sub> [78]. Although there are few specific, well-characterized pharmacological activators of TRPM2 at present, TRPM2 is known to be endogenously activated by adenosine diphosphate ribose (ADPR) [78]. In response to ROS-induced DNA damage, poly-ADPR polymerase (PARP) generates ADPR, which binds to TRPM2's C-terminal NUDT9-H domain and activates the channel, making TRPM2 an indirect redox-sensitive ion channel [78].

TRPM2's role in ROS-induced endothelial barrier permeability was first discussed in 2008, when Hecquet *et al.* determined that H<sub>2</sub>O<sub>2</sub> exposure caused an acute loss of barrier resistance in human pulmonary arterial endothelial cells, and that this effect was reduced in the absence of TRPM2 functionality [128]. These results were corroborated in 2015, when Mittal *et al.* found that TRPM2 mediated VE-cadherin phosphorylation in murine endothelial cells exposed to H<sub>2</sub>O<sub>2</sub> [129]. Additionally, the authors observed that TRPM2-deficient endothelial cells had reduced migratory capacities and that TRPM2-deficient mice showed altered angiogenesis in a model of hindlimb ischemia and neovascularization [129]. As such, the general consensus is that TRPM2 is, in part, responsible for endothelial barrier dysfunction following oxidative stress. However, the underlying mechanisms therein and the possible involvement of additional ion channels remain unclear.

## 2.5 Impedance-based assays of monolayer barrier integrity

The function and integrity of the cell barrier can be assessed by a variety of techniques. While permeability assays, such as macromolecular tracer assays, can provide basic information regarding the rate and extent of perfusion across a monolayer, the invasive nature of these assays severely limits their application [130]. Electrical impedance spectroscopy, the measurement of the electrical, ohmic resistance of a cellular monolayer, offers a noninvasive alternative for the assessment of barrier integrity [131]. While there are currently a variety of devices available for the monitoring of electrical cell resistance, all share the general principles of impedance spectroscopy. In brief, a frequency of an alternating current (AC) voltage is applied to a cell layer, and the resulting amplitude and phase of the AC current is measured, yielding a total impedance value [131]. Ohmic resistance measurements of cell monolayers were traditionally taken using handheld "chopstick" electrodes spanning a transwell insert, generating values of the transendothelial or transepithelial electrical resistance (TEER) [130]. However, recent developments in noninvasive real-time electrical impedance measurement devices have allowed for significant advancement in studies of monolayer barrier properties. Current instruments on the market include the cellZscope (nanoAnalytics, Münster, Germany), the xCELLigence (Agilent, Santa Clara, CA,

USA), and the electrical cell-substrate impedance sensing (ECIS, Applied Biophysics, Troy, NY, USA) systems [132].

### 2.5.1 Electrical cell-substrate impedance sensing (ECIS)

Electrical cell-substrate impedance sensing (ECIS) offers several advantages over other conventional impedance spectroscopy techniques. A typical ECIS array consists of an 8-well plate with 40 gold-coated electrodes [133], ECIS, in comparison to the chopstick method of TEER measurement, minimizes the potential for user error and unintended perturbations of the monolayer. Cells are seeded directly upon the ECIS electrodes (Figure 5), allowing for real-time, quantitative measurements of cell behavior with a high degree of sensitivity [131], as opposed to the timepointrestricted measurement of the chopstick method. Impedance measurements reflect different monolayer properties, depending on the AC frequency applied. Impedance values from relatively high AC frequencies, such as those above 32000 Hz, are affected by the degree of confluency and coverage on the plate, and therefore are a better indicator of cell growth rates. AC frequencies below 4000 Hz, in contrast, are more influenced by changes in the spaces below and between cells, and are more suitable for studies on barrier function [133]. An ECIS experiment can be performed using a multi-frequency scan, which rotates through a range of AC frequencies from 62.5 Hz to 64000 Hz [133], allowing for measurements of both electrode coverage and barrier integrity. When compared with the xCELLigence and cellZscope devices, the ECIS arrays were determined to be the most sensitive, with the capacity to distinguish micromotions (<1 nm) of individual cells [132,134]. One limitation of the original ECIS system is the lack of a basolateral fluid compartment, which excludes the potential for permeability or transport experiments [131]. However, recent developments in ECIS technology will amend this drawback through the incorporation of transwell inserts [135]. While the ECIS is compatible with most cell types, ECIS spectroscopy is most often applied in studies on endothelial cells [13].

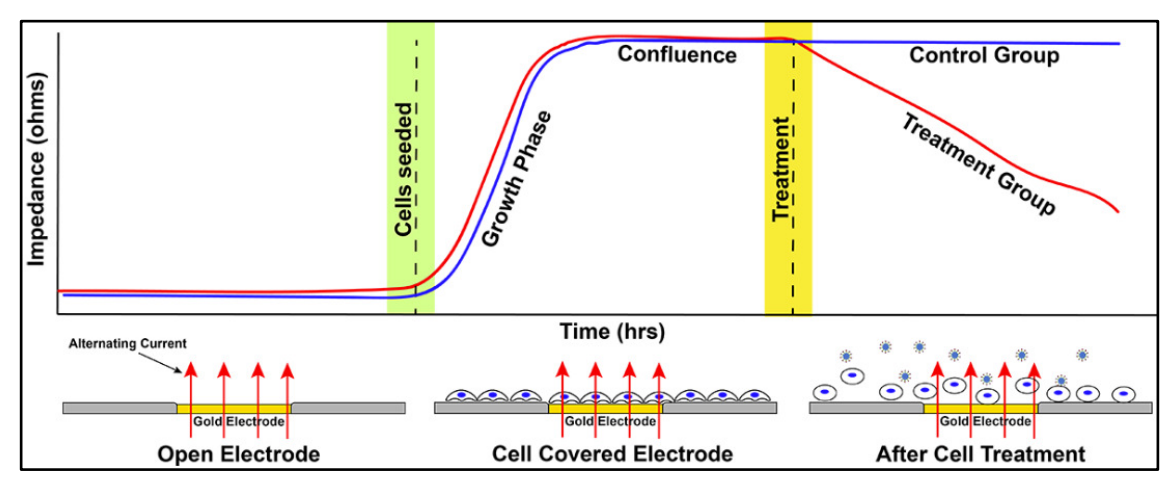


Figure 5. Principles of ECIS impedance spectroscopy. Cells are plated on gold electrodes, and an alternating current (AC) is passed through the cell layer. The monolayer impedance is calculated from the resulting electric potential across the electrodes. Impedance values increase as the cells grow to confluency, and remain at a plateau while the cell barrier rests at steady-state. Any treatment-related decreases in cell adhesion and barrier integrity will register as a loss of impedance. From [133].

## 2.6 Aims

As TRPV4 is known to affect endothelial barrier integrity and is expressed in AT1 cells, the first aim of this thesis is:

- To determine the effects of TRPV4 activation on the AT1 cell barrier and
- To investigate the role of TRPV4 in the alveolar epithelial response to acid-induced ALI.

The second aim of the thesis turns its focus to the microvascular endothelial barrier of the alveolar unit, with the goal to:

- Validate and investigate the contribution of TRPV2 to endothelial barrier dysfunction following ROS exposure, and
- Determine if additional redox-sensitive TRP channels, such as TRPM2 and TRPV4, are also involved.





Article

# TRPV4 Mediates Alveolar Epithelial Barrier Integrity and Induces ADAM10-Driven E-Cadherin Shedding

Lena Schaller, Thomas Gudermann and Alexander Dietrich \*

Walther Straub Institute for Pharmacology and Toxicology, Member of the German Center for Lung Research (DZL), Medical Faculty, LMU-Munich, Nussbaumstrasse 26, 80336 Munich, Germany; lena.schaller@lrz.uni-muenchen.de (L.S.); thomas.gudermann@lrz.uni-muenchen.de (T.G.)

\* Correspondence: alexander.dietrich@lrz.uni-muenchen.de

Abstract: Transient receptor potential vanilloid 4 (TRPV4) channels have been associated with numerous pulmonary pathologies, including hypertension, asthma, and acute lung injury. However, their role in the alveolar epithelium remains unclear. We performed impedance-based resistance measurements in primary differentiated alveolar epithelial type I (AT1) cells from wild-type (WT) and TRPV4-deficient (TRPV4-/-) C57/BL6J mice to detect changes in AT1 barrier integrity upon TRPV4 activation. Both pharmacological (GSK1016790A) and a low pH-driven activation of TRPV4 were quantified, and the downstream effects on adherens junctions were assessed through the Western blotting of epithelial cadherin (E-cadherin) protein levels. Importantly, a drop in pH caused a rapid decrease in AT1 barrier resistance and increased the formation of a ~35 kDa E-cadherin C-terminal fragment, with both effects significantly reduced in TRPV4-/- AT1 cells. Similarly, the pharmacological activation of TRPV4 in AT1 cells triggered an immediate transient loss of barrier resistance and the formation of the same E-cadherin fragment, which was again diminished by TRPV4 deficiency. Moreover, TRPV4-mediated E-cadherin cleavage was significantly reduced by GI254023X, an antagonist of a disintegrin and metalloprotease 10 (ADAM10). Our results confirm the role of TRPV4 in regulating alveolar epithelial barrier permeability and provide insight into a novel signaling pathway by which TRPV4-induced Ca<sup>2+</sup> influx stimulates metalloprotease-driven ectodomain shedding.

**Keywords:** a disintegrin and metalloprotease 10 (ADAM10); electrical cell–substrate impedance sensing (ECIS); epithelial cadherin (E-cadherin); transient receptor potential vanilloid 4 (TRPV4)



Citation: Schaller, L.; Gudermann, T.; Dietrich, A. TRPV4 Mediates Alveolar Epithelial Barrier Integrity and Induces ADAM10-Driven E-Cadherin Shedding. *Cells* **2024**, *13*, 1717. https://doi.org/10.3390/cells13201717

Academic Editor: Konstantin G. Birukov

Received: 23 September 2024 Revised: 11 October 2024 Accepted: 15 October 2024 Published: 17 October 2024



Copyright: © 2024 by the authors. Licensee MDPI, Basel, Switzerland. This article is an open access article distributed under the terms and conditions of the Creative Commons Attribution (CC BY) license (https://creativecommons.org/licenses/by/4.0/).

#### 1. Introduction

The alveolar epithelial barrier is crucial for maintaining effective gas exchange and protecting the lungs from environmental pathogens and toxicants. This barrier consists primarily of thin alveolar type 1 (AT1) cells, which are responsible for 95% of respiratory gas exchange, and cuboidal alveolar type 2 (AT2) cells, which produce surfactants and act as AT1 progenitor cells [1,2]. Due to its delicate yet restrictive nature, the permeability of the alveolar epithelial barrier is tightly regulated. Disruptions in alveolar barrier integrity can lead to pulmonary edema, characterized by the accumulation of protein-rich extravascular fluid in the interstitium and alveoli. Extensive pulmonary edema can develop into acute respiratory distress syndrome (ARDS), with an approximate mortality rate of 30–40% [3].

The integrity of the alveolar epithelium strongly depends on the intercellular junctions that regulate paracellular permeability. These junctions, including tight junctions (TJs), adherens junctions (AJs) and desmosomes, also facilitate cell-cell communication and maintain cell polarity [4]. While TJs are primarily responsible for maintaining a restrictive paracellular barrier, AJs play integral roles in the formation and regulation of TJs and their associated proteins [4–7]. Epithelial AJs consist of Ca<sup>2+</sup>-dependent homotypic adhesions between the extracellular regions of E-cadherin proteins on neighboring cells [4]. The

cytoplasmic tail of E-cadherin, like other classical cadherins, is highly conserved and interacts with the actin cytoskeleton through the anchor proteins p120 catenin,  $\beta$ -catenin, and  $\alpha$ -catenin [4,6,8]. The absence of E-cadherin has been associated with hallmarks of altered barrier integrity, including increased cell proliferation, motility, and invasiveness [5,9–12].

The E-cadherin proteins of AJs undergo constant turnover and are readily ubiquitinated, endocytosed, and returned to the plasma membrane, possibly through a protein kinase C- and/or Rho-dependent pathway [9,13,14]. However, these proteins are also susceptible to cleavage by various proteases, resulting in multiple cleavage products that may possibly trigger downstream signaling cascades. For instance, the intracellular C-terminal region of E-cadherin can be cleaved by gamma-secretase and caspase, while the extracellular region is targeted by numerous metalloproteases [8,15–17]. One such metalloprotease, a disintegrin and metalloprotease 10 (ADAM10), is widely expressed in epithelial tissue and plays a significant role in cadherin cleavage [15,18]. ADAM10 activation requires intracellular Ca<sup>2+</sup> influx, although the exact upstream pathway leading to ADAM10 activation remains unclear [19].

Recent research suggests that members of the transient receptor potential (TRP) superfamily may initiate the Ca<sup>2+</sup> influx necessary for ADAM10 activation [19]. Of the potential candidates, the fourth member of the vanilloid family (TRPV4) is of particular interest. TRPV4, like other TRP proteins, has intracellular N- and C-termini and consists of six transmembrane domains with a pore-forming loop spanning helices 5 and 6 [20–22]. TRPV proteins are identified through their long N-terminal ankyrin repeat domains and typically form homotetrameric nonselective ion channels [20,23]. TRPV4 channels are expressed in many organ systems, including the lungs, where they are found in immune cells, endothelial cells, and epithelial cells of the trachea, bronchi, and alveoli [21,22,24–27]. Functional TRPV4 channel homotetramers are mechano-, pH-, osmo- and thermosensitive, and are also activated by chemical mediators including phorbol esters and arachidonic acid metabolites [22,24,28].

The roles of TRPV4 channels in pulmonary injury are complex. On one hand, TRPV4 ablation increased pulmonary edema formation in a model of ischemia-reperfusion, highlighting an important function in the chronic expression and regulation of proteins for the protection of cell barrier integrity ([27] reviewed in [22]). On the other hand, isolated lungs from TRPV4-/- mice developed significantly reduced edema following ventilation-induced lung damage, most probably due to the absence of these channels in endothelial cells and their acute activation by mechanical stress [29]. While TRPV4's role in inducing pulmonary endothelial barrier permeability is well documented (reviewed in [20–22,24,25,30,31]), its acute effects on the alveolar epithelial barrier are less understood. Studies on epithelial cell lines have shown conflicting results. The activation of TRPV4 induced barrier permeability and altered tight junction morphology in a mouse mammary cell line HC11 [32] and Madin-Darby canine kidney II [33] monolayers. Conversely, in corneal epithelial RCE1(5T5) cells [34] and keratinocytes [35], TRPV4 activation increased barrier resistance and upregulated the expression of TJ-associated proteins. Isolated alveolar epithelial cells from rats exhibited decreased barrier resistance immediately after exposure to a specific TRPV4 activator [36]. Observations of TRPV4-mediated blebbing in endothelial and epithelial cells in the alveoli [29] demand further investigation of the molecular mechanisms of the AT1 cell-induced loss of cell barrier function by TRPV4-driven Ca<sup>2+</sup> entry.

In addition to its association with fibrosis and pulmonary hypertension (reviewed in [24,25]), TRPV4 has also been linked to acid-induced acute lung injury (ALI) [30,37]. Acid-induced ALI can occur in cases of occupational exposure, as well as in patients suffering from gastroesophageal reflux disease (GERD), the latter of which is a known risk factor for recurrent ALI [38]. Two independent studies in 2014 [30] and 2016 [37] working with similar murine models of acid-induced ALI found that TRPV4—/— mice were protected from inflammation and pulmonary edema following intratracheal HCl instillation, with reduced inflammatory cytokine levels and neutrophil recruitment in the

lungs. Acid-induced ALI may be in part due to the activity of TRPV4 in immune cells. In 2010, Hamanaka et al. showed that TRPV4-expressing macrophages could restore the susceptibility of TRPV4-/- lungs to mechanically induced lung injury [26]. However, transcriptomic analysis identified only a minimal TRPV4 expression in neutrophils [30], suggesting TRPV4 may influence neutrophil function and recruitment indirectly, possibly by controlling AT1 paracellular permeability.

Only a limited number of studies indicate that TRPV4 activation may induce instability in the alveolar epithelial barrier, similar to its effect on microvascular endothelial cells. To validate these findings and further explore the underlying mechanisms, we isolated AT1 cells from WT and TRPV4—/— mice and assessed the effects of pH- and agonist-driven TRPV4 activation on alveolar epithelial barrier integrity through electrical cell–substrate impedance sensing (ECIS) [39,40]. We determined that TRPV4 activation triggered an immediate but transient reduction in barrier resistance, accompanied by the ADAM10-mediated cleavage of E-cadherin.

#### 2. Materials and Methods

#### 2.1. Animals

TRPV4—/— (B6.199X1-Trpv4<sup>tm1MSZ</sup> from Riken BioResource Research Center RBRC01939, Ibaraki, Japan) mice were backcrossed 10 times with the C57/BL6J strain. The correct knockout of the TRPV4 protein was approved by Western blotting in our recent manuscript [27]. Sex- and age-matched mice between 2 and 4 months of age and wild-type controls from the same colony were used in all experiments.

## 2.2. Isolation and Culture of Primary Alveolar Epithelial Cells and In Vitro Differentiation of AT1 Cells

The isolation of primary alveolar epithelial cells from murine lungs was performed as previously described [27]. In brief, 3-6 mice were sacrificed via cervical dislocation. Lungs were transcardially perfused with 20 mL of Dulbecco's phosphate-buffered saline (PBS, Merck, Darmstadt, Germany, D8537), inflated intratracheally with 1.5 mL of dispase solution (Corning, New York, NY, USA, 354235), followed by 400 µL of 1% low gelling temperature agarose (Merck, A9414) in Dulbecco's Modified Eagle Medium (DMEM, Thermo Fisher Scientific, Waltham, MA, USA, 41965039). Once the agarose had solidified, lungs were resected and digested in a 1 mL dispase solution for 45 min at room temperature (RT). Lung lobes were then manually dissociated in 5 mL HEPES-buffered DMEM with 100 U/mL DNase I (AppliChem, Darmstadt, Germany, A3778). The tissue suspension from each mouse was pooled and passed through a series of 100 μm, 20 μm, and 10 μm filters (Sefar, Helden, Switzerland, 3A03-0010-102-00, 3A03-0020-102-10 and 3A03-0100-115-01) to ensure a dispersed cell suspension. The resulting suspension was then centrifuged (10 min,  $200 \times g$ ), the media removed, and the pellet resuspended in HEPES-buffered DMEM. The cell suspension was then plated out on CD16/32- and CD45-coated (BD Biosciences, Franklin Lakes, NJ, USA, 553142 and 553076) Petri dishes in a negative selection step for macrophages and lymphocytes. Following a 30 min incubation step at 37 °C, the dishes were washed thrice with HEPES-buffered DMEM, and the nonadherent cells were transferred to uncoated, tissue culture-treated 10 cm dishes (Sarstedt, Nümbrecht, Germany, 83.3900.300). After allowing 1 h for fibroblast deposition, the suspension was carefully removed from all plates and centrifuged (see above settings). The media was aspirated, and the resulting AT2 cell pellet was resuspended in culture media (HEPESbuffered DMEM supplemented with 10% FCS, 1% P/S) and seeded according to intended experimental requirements. Cells were either harvested after 48 h in culture for AT2 immunocytochemistry or allowed to differentiate to AT1 cells over 7 days.

#### 2.3. Indirect Immunocytochemistry

Isolated WT alveolar epithelial cells were seeded on poly-L-lysine-coated 12 mm glass coverslips. After 48 h or 7 days of culture at 37 °C and 5% CO<sub>2</sub>, cells were washed once with

cold PBS, fixed in 4% PFA/PBS (15 min, RT), and then washed thrice with cold PBS. Cells were permeabilized for 10 min at RT in a 0.2% Triton X-100/PBS solution and then washed  $4 \times 5$  min in PBS-T (0.1% Tween20 in PBS). Cells were blocked for 1 h in PBS containing 0.1% Tween20 and 5% BSA, after which they were incubated overnight at 4 °C in primary antibody solutions prepared in blocking buffer (see Supplementary Table S1 for antibodies and dilutions). The following day, cells were washed ( $4 \times 5$  min, PBS-T), incubated for 2 h at RT in secondary antibody solutions, and subsequently washed ( $4 \times 5$  min, PBS-T). All antibodies were diluted in the blocking buffer. Next, nuclei were stained with DAPI (0.1 mg/L in PBS) for 3 min at RT, after which cells were washed ( $4 \times 5$  min, PBS-T). Coverslips were mounted with PermaFluor mounting medium (Epredia, Kalamazoo, MI, USA, #TA-030-FM) and kept at 4 °C. Confocal images were taken with a Zeiss LSM 880 microscope using the ZEN Black software (2.3 SP1 FP3). Images were processed with FIJI software (Image J v.1.53c, Wayne Rasband, NIH, Bethesda, MD, USA) [41].

#### 2.4. Ca<sup>2+</sup> Imaging

Isolated TRPV4—/— and WT AT2 cells were grown on 24 mm glass coverslips for 7 days. On the day of measurement, differentiated AT1 cells were loaded with 2  $\mu$ M Fura-2-AM (Merck, #47989-1MG-F) in Ca<sup>2+</sup> buffer (0.1% BSA in HBSS (with Ca<sup>2+</sup>, Mg<sup>2+</sup> and 0.5 M HEPES)) for 25 min at RT. Coverslips were then washed with HEPES/HBSS buffer, inserted in a quick-change chamber (Warner instruments, Holliston, MA, USA, #64-0367) with 450  $\mu$ L HEPES/HBSS, and placed on the 40x oil objective of a Leica DM98 fluorescence microscope. Any changes in intracellular Ca<sup>2+</sup> concentration following TRPV4 activation (100 nM GSK1016790A, GlaxoSmithKline, Brentford, UK) were recorded at 340 and 380 nm wavelengths, as described [42].

#### 2.5. Quantification of Alveolar Epithelial Barrier Resistance

Freshly isolated WT and TRPV4-/- AT2 cells were seeded at a density of  $2 \times 10^4$  cells/well on electrical cell–substrate impedance sensing (ECIS) plates (Applied Biophysics, Troy, NY, USA, 8W10E+), which had been treated with 10 mM of L-Cysteine, as per the manufacturer's recommendation. Cells were kept in culture at 37 °C and 5% CO<sub>2</sub> for 7 days, at which point barrier integrity experiments were conducted, with resistance measured at 500 Hz using the ECIS  $Z\Phi$  device (Applied Biophysics).

#### 2.6. SDS-PAGE and Western Blot Analysis

The expression of full-length and degraded E-cadherin protein were evaluated by Western blot analysis, as previously described [42]. Following treatment, AT1 cells were lysed in 100 µL of RIPA buffer (20 mM Tris-HCl, pH 7.5, 150 mM NaCl, 1% Nonidet P40, 0.5% sodium deoxycholate, 1% SDS, 5 mM EDTA) with protease and phosphatase inhibitors (Roche, Mannheim, Germany, #04906837001, #05892791001) for 30 min on ice and sonicated for 30 s. Protein concentration was quantified with the Pierce BCA Protein Assay Kit (Thermo Fisher Scientific, #23225) according to the manufacturer's protocol. Prepared protein samples (5 μg lysate, 1× Laemmli buffer (prepared from 5× stock: 3 mL TRIS/HCl (2.6 M), pH 6.8; 10 mL glycerin; 2 g SDS; 2 mg bromophenol blue; 5 mL β-mercaptoethanol)) were heated for 10 min at 95 °C, then loaded onto an SDS-PAGE gel (4% stacking, 10% separating). Gel electrophoresis was run for 30 min at 80 V, then at 120 V for 90 min. Proteins were then transferred from the gel to a Roti®-PVDF membrane (Roth, Karlsruhe, Germany, #T830.1) in a wet transfer system (BioRad, Feldkirchen, Germany) at 50-60 V for 1.5 h. After the transfer, the membrane was blocked with 5% low-fat milk (Roth, #T145.2) in TBS-T (0.1% Tween20) for 1 h at RT. All antibodies were diluted in the milk blocking solution. Membranes were incubated in the primary antibody solutions overnight at 4 °C. The next day, membranes were washed (3  $\times$  10 min, TBS-T) and incubated for 2 h at RT in peroxidase-conjugated secondary antibody solutions. Chemiluminescence was imaged following incubation in SuperSignal West Femto or Pico maximum sensitivity substrates (Life Technologies, Carlsbad, CA, USA, #34095 and #34580), using an Odyssey Fc unit

(Licor, Lincoln, NE, USA). For antibody information and dilutions, see Supplementary Table S1.

#### 2.7. Statistical Analysis

Statistical tests were performed using GraphPad Prism 10 software (GraphPad Software, San Diego, CA, USA). Significant differences are indicated by asterisks, where p < 0.05 (\*), 0.01 (\*\*\*), 0.001 (\*\*\*), and 0.0001 (\*\*\*\*).

#### 3. Results

#### 3.1. Differentiation and Characterization of Primary Murine Alveolar Epithelial Type I Cells

In order to assess the effects of TRPV4 activation upon AT1 cells, we first validated our isolation and differentiation procedure. Freshly isolated murine AT2 cells were fixed 2 and 7 days after isolation and stained for the epithelial markers prosurfactant protein C (pSPC) and aquaporin-5 (AQP5), which are specifically expressed by AT2 and AT1 cells, respectively (Figure 1) [43]. The process of AT2-to-AT1 differentiation was clearly delineated, with the 2-day epithelial cells staining positive for pSPC and negative for AQP5, and the 7-day epithelial cells only showing positive staining for AQP5. These results confirm that our isolation protocol yields a small population of AT2 cells, which differentiate into a confluent monolayer of AT1 cells within 7 days, as previously described [27].

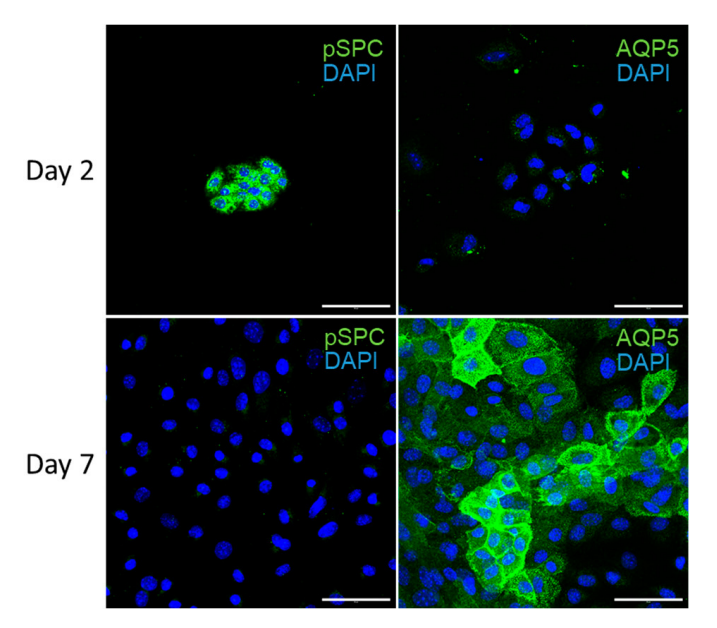


**Figure 1.** Differentiation and characterization of isolated primary murine alveolar epithelial type I (AT1) cells. Alveolar epithelial cells were fixed 2 (day 2) and 7 days (day 7) after isolation and stained for the AT2 and AT1 markers prosurfactant protein C (pSPC) and aquaporin 5 (AQP5), respectively. Nuclei staining was performed with DAPI dye (DAPI). Scale bar:  $50 \mu m$ .

#### 3.2. TRPV4 Mediates Acid-Induced Alveolar Epithelial Barrier Dysfunction

As TRPV4 is known to be activated under acidic conditions, we tested the effect of HCl application on isolated AT1 cells to represent acid-induced ALI. We obtained real-time quantitative measurements of AT1 barrier integrity through electrical cell-substrate impedance sensing (ECIS). A drop in media pH from 7.5 to 4.5 induced a rapid decrease in AT1 barrier resistance in WT cells (Figure 2A). Although TRPV4—/— AT1 cells also experienced a drop in resistance, it was less pronounced than in WT AT1 cells. The difference between genotypes became apparent as soon as 10 min after exposure, with a barrier resistance of only  $12\% \pm 3.5\%$  in WT AT1 cells, which was significantly decreased compared to TRPV4—/— cells (Figure 2B). Along this line, the drop in pH had a strong impact on the AT1 monolayer and affected cell–matrix adhesion, as well as cell–cell junctions, as indicated

by changes in the monolayer capacitance. AT1 monolayers of both genotypes showed a noticeable increase in capacitance upon media acidification, although the increase was only significant in WT cells (Figure S1A,B). At the protein level, HCl exposure resulted in an increased formation of a ~35 kDa C-terminal fragment (CTF) of E-cadherin (Figure 2C). The amount of this CTF was increased in all HCl-treated samples but was more pronounced in lysates from WT AT1 cells. Quantification revealed that the amount of E-cadherin CTF generated in WT HCl-treated cells was significantly larger than in the respective control samples and HCl-treated TRPV4—/— cells (Figure 2D). HCl exposure did not significantly alter the levels of full-length E-cadherin in any genotype (Figure S2A).

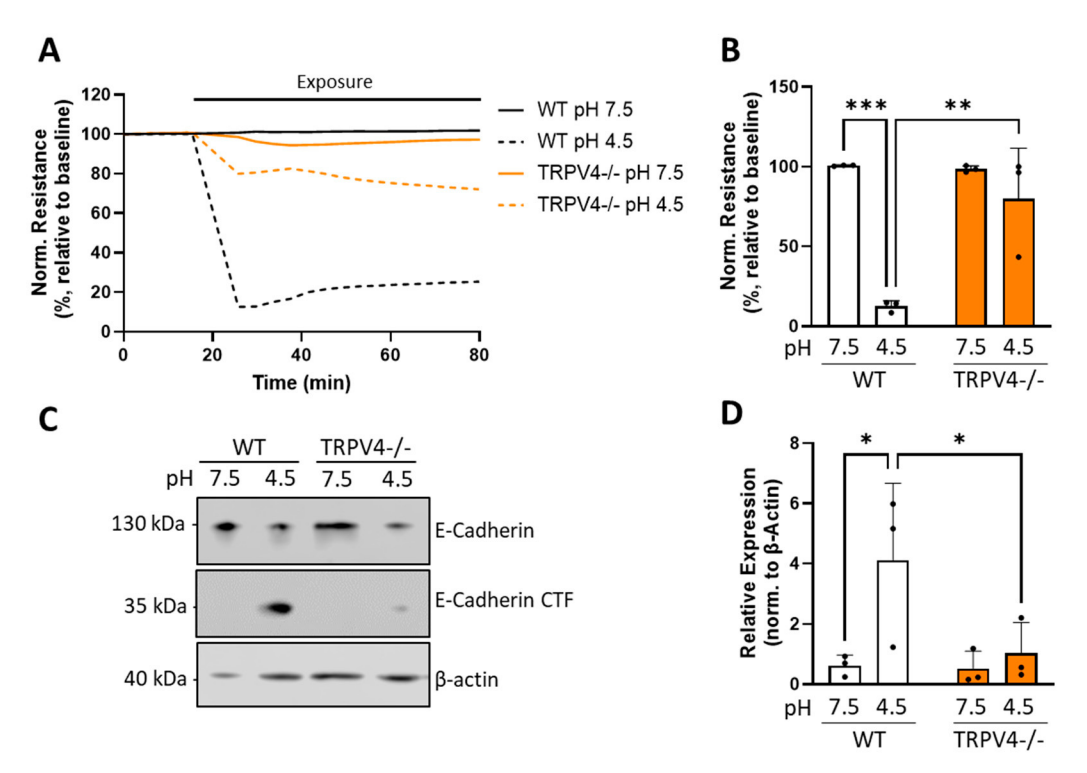


**Figure 2.** Changes in normalized electrical cell resistance (**A**,**B**) and expression/proteolyis of E-cadherin (**C**,**D**) of wild-type (WT) and TRPV4-/- AT1 cells. Cell resistance was recorded at 500 Hz for 1 h following an HCl-induced drop in media pH (**A**) and normalized monolayer resistance values 10 min after exposure were quantified (**B**). Cells from the same isolations and treatment conditions were lysed after 1 h of exposure, levels of E-cadherin and E-cadherin CTF were assessed by Western blotting (**C**) (see original blot in Figure S2B,C), and the results of the latter were summarized (**D**). Data are presented as mean  $\pm$  SD (**B**,**D**) from 3 independent cell isolations of 6 mice each (n = 3). Significance between means was analyzed using a two-way ANOVA; \* p < 0.05, \*\* p < 0.01, \*\*\* p < 0.001.

### 3.3. Pharmacological Activation of TRPV4 Induces a Rapid Transient Drop in Barrier Resistance

To better explore the mechanisms underlying TRPV4-mediated AT1 barrier dysfunction, we applied characterized pharmacological modulators of TRPV4. We tested a specific TRPV4 activator, GSK1016790A, with an EC $_{50}$  of 5 nM (GSK101, Tocris, #6433 [44]), on differentiated AT1 cells using Ca $^{2+}$  imaging, along with the TRPV4 inhibitor GSK2193874, with an IC $_{50}$  of 2–40 nM (GSK219, Tocris, #5106 [45]). The application of GSK101 in WT AT1 cells resulted in a transient increase in intracellular Ca $^{2+}$  ([Ca $^{2+}$ ] $_i$ ), which was absent in WT AT1 cells pre- and co-treated with GSK219 (Figure 3A). In TRPV4–/– AT1 cells, the application of GSK101 had no effect on [Ca $^{2+}$ ] $_i$  (Figure 3B).

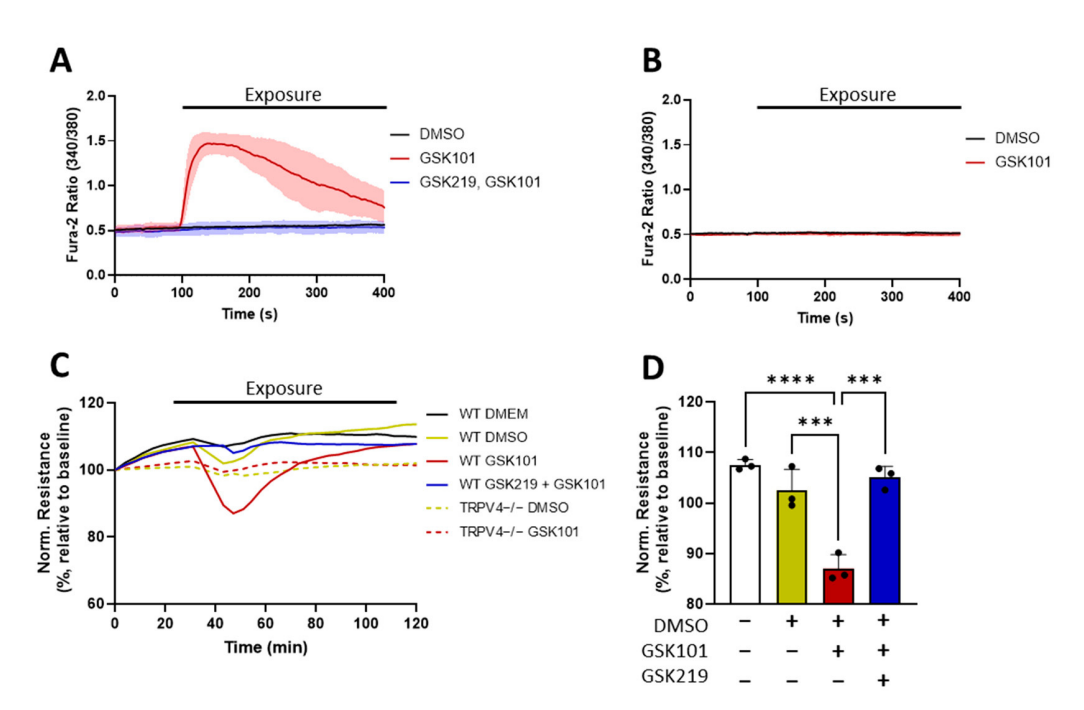


**Figure 3.** Intracellular  $Ca^{2+}$  concentration ( $[Ca^{2+}]_i$ ) (**A,B**) and cell barrier function (**C,D**) of AT1 cells after activation (GSK1016790A (GSK101)) and inhibition (GSK2193874 (GSK219)) of TRPV4 channels.  $[Ca^{2+}]_i$  was quantified in primary differentiated AT1 cells from WT (**A**) and TRPV4-/- mice (**B**) upon application of a specific TRPV4 activator (GSK101, 100 nM) in the presence and absence of a specific TRPV4 blocker (GSK219, 300 nM). One representative experiment (n = 10 cells, mean  $\pm$  SD) out of three independent isolations is shown. Changes in electrical cell resistance (normalized to baseline levels) were recorded with an ECIS device at 500 Hz for WT and TRPV4-/- AT1 cells upon application of GSK101 (100 nM) in the presence and absence of GSK219 (300 nM) for 90 min (**C**). Data represent mean values from 3 independent cell isolations of 6 mice each (n = 3). The normalized electrical cell resistance for WT treatment groups 15 min after exposure was quantified (**D**). Data represent mean  $\pm$  SD, and significance between means was analyzed with a one-way ANOVA; \*\*\*\* p < 0.001, \*\*\*\* p < 0.0001.

With the specificity of GSK101 in AT1 cells confirmed, we next examined the effect of TRPV4 activation upon AT1 barrier integrity. Dose–response ECIS experiments established that 100 nM GSK101 was the optimal concentration for TRPV4-driven AT1 barrier disruption, as the effect plateaued at higher concentrations (up to 3  $\mu$ M, Figure S3). The activation of TRPV4 resulted in a transient drop in barrier resistance in WT AT1 cells, peaking approximately 15 min after GSK101 application and recovering to baseline levels after 90 min (Figure 3C). In line with our previous results on TRPV4-induced [Ca²+]i, GSK101 had no effect on AT1 cell permeability after pre- and co-treatment with GSK219, nor in TRPV4-/- cells. The quantification of the barrier function 15 min after GSK101 exposure revealed that the 13%  $\pm$  2.7% loss of cell resistance in WT AT1 cells was significantly larger than in untreated controls and GSK219-treated WT cells (Figure 3D). Similarly, the loss in barrier integrity upon GSK101 exposure in WT AT1 cells was significantly larger than in TRPV4-/- AT1 cells (Figure S4A). In all ECIS experiments, the capacitance of the AT1 monolayer remained constant, indicating that the observed changes in resistance were due to altered cell–cell junction integrity and not cell-substrate detachment (Figure S4B).

#### 3.4. TRPV4 Activation Triggers an ADAM10-Mediated Cleavage of E-Cadherin

The drop in AT1 cell barrier resistance following TRPV4 activation suggested a loss in paracellular junction integrity. One possible explanation for this sudden drop in resistance might be a TRPV4-driven activation of one or more metalloproteinases, causing a rapid shedding of the AT1 protein ectodomain [19]. Through a Western blot protein analysis, we identified an increased presence of a  $\sim$ 35 kDa E-cadherin CTF 15 min after treatment with

GSK101 (Figure 4A). This CTF was detected in far lower quantities in samples pre- and co-treated with GSK219 and was absent in TRPV4-/- AT1 cells. As E-cadherin is a known substrate of ADAM10 [18], we also assessed whether treatment with an ADAM10 inhibitor, GI254023X, with an IC $_{50}$  of 5.3 nM (GI254, Tocris, #3995 [46]), would limit the TRPV4-driven formation of this CTF. Western blot quantification confirmed that the significant increase in the E-cadherin CTF formation upon GSK101 application in WT AT1 cells was entirely dependent on TRPV4, as pre- and co-incubation with GSK219 maintained E-cadherin CTF levels equal to those in untreated controls (Figure 4A,B). Additionally, ADAM10 inhibition through GI254 partially but significantly reduced the GSK101-driven formation of the E-cadherin CTF (Figure 4A,B). In TRPV4-/- AT1 cells, Western blot quantification revealed no significant change in E-cadherin CTF formation after GSK101 exposure (Figure S5A). Additionally, in all treatment groups and genotypes, the effect of TRPV4 activation on the expression of full-length E-cadherin protein levels was not significantly different (Figure S5B,C).

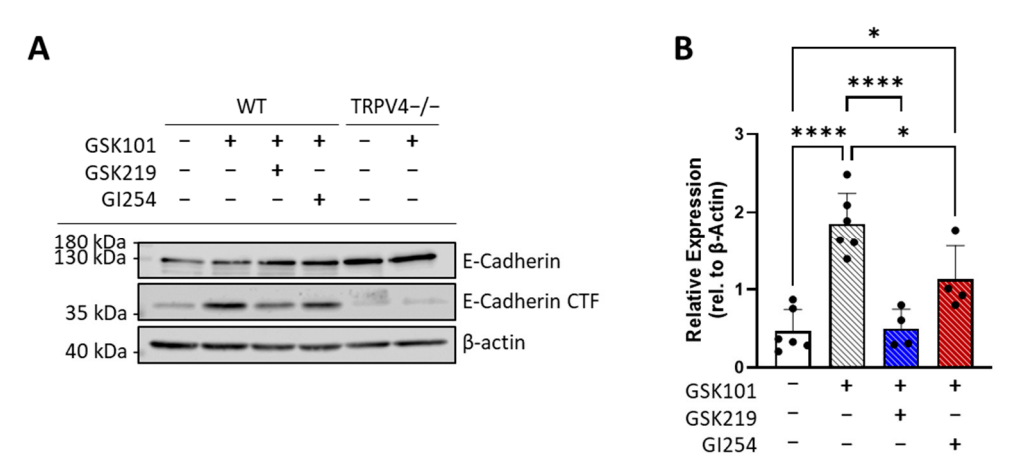


Figure 4. Quantification of E-cadherin and E-cadherin C-terminal fragment (CTF) by Western blotting of protein lysates from primary differentiated AT1 cells isolated from wild-type (WT) and TRPV4-deficient (TRPV4-/-) mice (A,B). Representative Western blot showing levels of E-cadherin and E-cadherin CTF in WT and TRPV4-/- AT1 cells 15 min after application of GSK101 (100 nM) in the presence and absence of either GSK219 (300 nM) or an ADAM10 inhibitor GI254023X (GI254 3  $\mu$ M) (A) (see original blot in Figure S5D-F). Changes in the levels of E-cadherin CTF in WT AT1 cells were quantified 15 min after exposure to the indicated compounds (B). Data represent mean  $\pm$  SD (B) from at least 4 independent cell isolations from 3 to 5 mice, each (n = 4–6). Significance between means was analyzed with one-way ANOVA; \* p < 0.05, \*\*\*\*\* p < 0.0001.

#### 4. Discussion

TRPV4 is a well-recognized mediator of lung function and has also been implicated in various pulmonary disease states, including fibrosis, inflammation, and pulmonary edema formation [22,24,25,27,47]. Numerous studies in endothelial cells and pulmonary arterial smooth muscle cells have demonstrated that TRPV4 activation increases monolayer permeability through mechanisms such as the downregulation of TJ-associated genes, the contraction of actin–myosin rings, the disorganization of F-actin, and the loss of cell–matrix adhesion [20,25,32,48,49]. However, the role of TRPV4 in alveolar epithelial barrier function and integrity is still elusive. Through real-time impedance measurements and protein analysis of isolated differentiated murine AT1 cells, we confirmed that TRPV4 activation induces a rapid transient drop in AT1 barrier resistance. Here, we showed for the first time that TRPV4 activation in primary AT1 cells destabilizes AJs through an ADAM10-mediated extracellular cleavage of E-cadherin. Additionally, we found that TRPV4 mediates AT1 barrier dysfunction in a model of acid-induced ALI, suggesting that TRPV4-driven disruption of paracellular barrier integrity might occur, irrespective of the initial stimulus.

We began by assessing the role of TRPV4 in a clinically relevant context. Patch clamp electrophysiology performed in Chinese hamster ovary (CHO) cells demonstrated that TRPV4 responds significantly to low pH [28]. As the pH necessary to open the channel is lower than physiological levels in most compartments, the pH activation of TRPV4 is mainly relevant in conditions of acid-induced ALI, as occurs through occupational exposure or in patients suffering from gastroesophageal reflux disease (GERD) [50]. Consistent with in vivo results from previous studies [30,37], we observed that TRPV4 deficiency reduces the effects of low pH on AT1 barrier integrity. Both the HCl-induced drop in barrier resistance and the accompanying degradation of E-cadherin were significantly increased in WT AT1 cells compared to those from TRPV4—/— mice. Thus, by facilitating barrier permeabilization, TRPV4 in alveolar epithelial cells may also support the neutrophil recruitment observed in whole lungs following HCl instillation [30,37].

Our ECIS experiments in WT AT1 cells revealed that unlike HCl exposure, the drop in barrier resistance following the application of the specific TRPV4 activator GSK101 was transient, with a return to baseline resistance within 90 min of exposure. This discrepancy may be due to the caustic effects of the acidic media. Studies in the human alveolar cell line A549 have demonstrated that incubation with low-pH media suppresses cell proliferation rates [51] and induces significant persistent reductions in barrier resistance [52]. Few studies have assessed GSK101-driven changes in epithelial barrier resistance, showing varying results. Martinez-Rendon et al., in 2016, found that GSK101 treatment led to a gradual increase in the transepithelial resistance (TER) of corneal epithelial cells from the RCE1(5T5) cell line [34]. However, these results reflect measurements taken hours after GSK101 application, while we and others have shown that dynamic changes in barrier resistance occur within the first 30 min of TRPV4 activation in primary differentiated AT1 cells [36,53].

While the inhibitory effects of GSK219 pretreatment on GSK101-induced TRPV4 activity (Figure 3A), the loss of AT1 barrier resistance (Figure 3C,D), and E-cadherin degradation (Figure 4) were very effective, we are also aware that two other TRPV4 inhibitors applied after HCl incorporation that were able to suppress acute lung injury in vivo [30]. Whether GSK219 is similarly effective in post-exposure treatments needs to be explored.

Our results also give some insight into the downstream mechanisms underlying TRPV4-induced AT1 barrier dysfunction. As with our model of acid-induced ALI, GSK101 application increased the formation of a ~35 kDa C-terminal fragment of E-cadherin, detected as early as 15 min after exposure, at the point of greatest loss of barrier resistance. The formation of this fragment was TRPV4 specific, as its levels did not increase in TRPV4—/— AT1 cells or cells treated with the specific TRPV4 antagonist GSK219. The size of this fragment indicates an extracellular metalloprotease cleavage event. A recent study by Tatsumi et al. proposed that TRP-induced Ca<sup>2+</sup> influx could activate certain ADAM proteins, including ADAM10 and ADAM17, by the Ca<sup>2+</sup> sensitive protein ANO6 [54], leading to the ectodomain shedding of their respective ligands [19]. Although mechanistic connections between TRPV4 and the matrix metalloproteases MMP2 and MMP9 have been reported [55], a physiological relationship between TRPV4 channels and ADAM10 had not yet been identified [19]. Using an ADAM10-specific antagonist, we showed that TRPV4driven E-cadherin cleavage in AT1 cells is partially mediated by ADAM10 (Figure 5). As it is likely that additional MMPs and ADAM proteins are activated by TRPV4-induced Ca<sup>2+</sup> influx, future experiments characterizing the resulting ectodomain cleavage would be beneficial to determine to what extent TRPV4-induced cell detachment is dependent on protease activity.

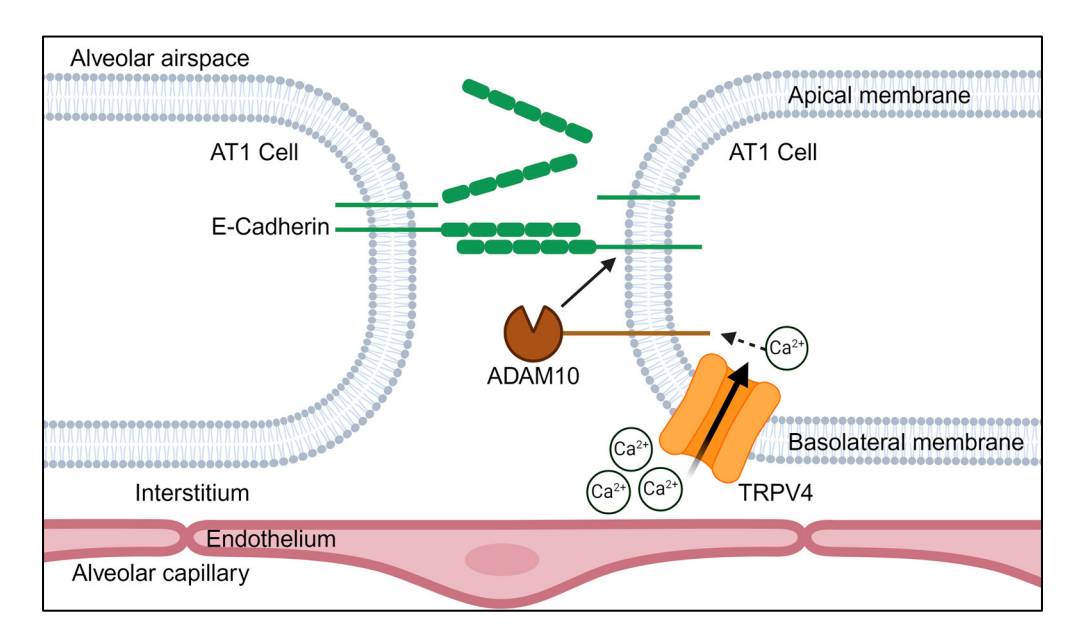


**Figure 5.** Schematic describing a possible interaction between TRPV4 and ADAM10, resulting in ectodomain shedding of E-cadherin in AT1 cells (modified from [19]). See text for more details.

Altered alveolar epithelial barrier integrity can often lead to the development of pulmonary edema, which can progress to acute respiratory distress syndrome (ARDS) Matthay, Zemans, Zimmerman, Arabi, Beitler, Mercat, Herridge, Randolph and Calfee [3]. It is possible, however, that increased barrier permeability could be physiologically beneficial. Edema fluid could dilute inflammatory mediators, neutralize an acidic environment, or carry pathogen-combating neutrophils. Along this line, there is strong biological support for a mechanism by which TRPV4 at the plasma membrane of AT1 cells facilitates neutrophil transmigration. E-cadherin and TRPV4 show similar staining patterns at the plasma membrane in various epithelial cell types [32], with immunoprecipitation pulldown experiments revealing a molecular connection between TRPV4 and  $\alpha$ -catenin,  $\beta$ -catenin, and E-cadherin [56]. Epithelial TRPV4 is localized to the basolateral membrane, which comprises the alveolar septal wall [29,32]. Neutrophil adhesion to the alveolar epithelium is restricted to the basolateral side, with eventual transmigration across the epithelial barrier limited to the paracellular route [57]. TRPV4's localization to the basolateral membrane, paired with its colocalization with E-cadherin, would allow targeted Ca<sup>2+</sup> influx at sites requiring AJ weakening. The transient drop in AT1 barrier resistance upon GSK101 application indicates that the barrier disruption induced by TRPV4 activity is quickly resolved. Therefore, the TRPV4-ADAM10-E-cadherin cleavage may facilitate efficient regulated neutrophil transmigration.

In addition to the alveolar epithelium, the alveolar barrier also includes the microvascular endothelium. Our ECIS measurements in WT AT1 cells are consistent with those previously performed in human lung microvascular endothelial cells, characterized by a  $\sim 10-20\%$  drop in barrier resistance within 15 min of GSK101 application and a return to baseline resistance within 3 h [53]. Although a pathway involving TRPV4 and vascular endothelial cadherin (VE-cadherin) cleavage has not yet been investigated, it is possible that metalloprotease activity occurs downstream of TRPV4. Activation occurs in endothelial cells as well, further supporting neutrophil transmigration from the microvasculature to the alveolar epithelium.

#### 5. Conclusions

In summary, our study highlights the significant role of TRPV4 in regulating alveolar epithelial barrier integrity. We confirmed that TRPV4 is involved in acid-induced lung injury, as channel activation under conditions of low pH triggered an immediate drop in AT1 barrier resistance with a destabilization of AJ proteins. These observations were corroborated using specific agonists and antagonists of TRPV4. In addition, we discovered a novel mechanism by which TRPV4 activation affects AT1 cell junctions, namely through the ADAM10-mediated cleavage of E-cadherin. These insights into the TRPV4-ADAM10-E-cadherin pathway may be confirmed in an ex vivo lung model in the future [58] and provide a basis for further research into targeted therapies for pulmonary diseases involving epithelial barrier dysfunction.

Supplementary Materials: The following supporting information can be downloaded at: https://www.mdpi.com/article/10.3390/cells13201717/s1, Figure S1: Low pH induces TRPV4-mediated changes in cell adhesion; Figure S2: Low pH does not significantly change E-cadherin protein expression in AT1 cells; Figure S3: Loss of AT1 cell resistance upon GSK101 application plateaus at 100 nM concentration; Figure S4: GSK101-induced loss of AT1 barrier resistance is TRPV4-dependent and does not cause cell detachment; Figure S5: GSK101 exposure triggers TRPV4-dependent formation of an E-cadherin CTF but does not significantly change the protein expression of E-cadherin; Table S1: Antibodies used for cell isolation, Western blotting and immunocytochemistry; File: WB (S2B C) (S5D-F).

**Author Contributions:** Conceptualization, L.S. and A.D.; methodology, L.S.; validation, L.S.; formal analysis, L.S.; investigation, L.S.; resources, A.D.; writing—original draft preparation, L.S.; writing—review and editing, L.S., A.D. and T.G.; visualization, L.S.; supervision, A.D.; project administration, L.S., A.D. and T.G.; funding acquisition, A.D. and T.G. All authors have read and agreed to the published version of the manuscript.

**Funding:** This research was funded by the Deutsche Forschungsgemeinschaft (DFG) (GRK 2338 Project 04 (LS, AD, TG) and TRR152 project 16 (AD, TG)) and the Deutsche Zentrum für Lungenforschung (DZL) (AD, TG).

**Institutional Review Board Statement:** The animal study protocol was approved by the Ethics Committee Regierung Oberbayern Munich, Germany, ROB-55.2-2532.Vet\_02-20-105.

**Informed Consent Statement:** Not applicable.

**Data Availability Statement:** All data supporting the findings of this study are available in the paper and its Supplementary Information section.

**Acknowledgments:** The authors would like to thank Bettina Braun and Benedikt Kirmayer for excellent technical assistance.

**Conflicts of Interest:** The authors declare no conflicts of interest.

#### References

- 1. Yang, J.; Hernandez, B.J.; Martinez Alanis, D.; Narvaez del Pilar, O.; Vila-Ellis, L.; Akiyama, H.; Evans, S.E.; Ostrin, E.J.; Chen, J. The development and plasticity of alveolar type 1 cells. *Development* **2016**, *143*, 54–65. [CrossRef]
- 2. Rackley, C.R.; Stripp, B.R. Building and maintaining the epithelium of the lung. J. Clin. Investig. 2012, 122, 2724–2730. [CrossRef]
- 3. Matthay, M.A.; Zemans, R.L.; Zimmerman, G.A.; Arabi, Y.M.; Beitler, J.R.; Mercat, A.; Herridge, M.; Randolph, A.G.; Calfee, C.S. Acute respiratory distress syndrome. *Nat. Rev. Dis. Primers* **2019**, *5*, 18. [CrossRef]
- 4. Nawijn, M.C.; Hackett, T.L.; Postma, D.S.; van Oosterhout, A.J.; Heijink, I.H. E-cadherin: Gatekeeper of airway mucosa and allergic sensitization. *Trends Immunol.* **2011**, *32*, 248–255. [CrossRef]
- 5. Hartsock, A.; Nelson, W.J. Adherens and tight junctions: Structure, function and connections to the actin cytoskeleton. *Biochim. Biophys. Acta* **2008**, *1778*, 660–669. [CrossRef]
- 6. Post, S.; Heijink, I.H.; Hesse, L.; Koo, H.K.; Shaheen, F.; Fouadi, M.; Kuchibhotla, V.N.S.; Lambrecht, B.N.; Van Oosterhout, A.J.M.; Hackett, T.L.; et al. Characterization of a lung epithelium specific E-cadherin knock-out model: Implications for obstructive lung pathology. Sci. Rep. 2018, 8, 13275. [CrossRef]
- 7. Tunggal, J.A.; Helfrich, I.; Schmitz, A.; Schwarz, H.; Gunzel, D.; Fromm, M.; Kemler, R.; Krieg, T.; Niessen, C.M. E-cadherin is essential for in vivo epidermal barrier function by regulating tight junctions. *EMBO J.* **2005**, 24, 1146–1156. [CrossRef]

8. Ferber, E.C.; Kajita, M.; Wadlow, A.; Tobiansky, L.; Niessen, C.; Ariga, H.; Daniel, J.; Fujita, Y. A role for the cleaved cytoplasmic domain of E-cadherin in the nucleus. *J. Biol. Chem.* **2008**, 283, 12691–12700. [CrossRef]

- 9. Fujita, Y.; Krause, G.; Scheffner, M.; Zechner, D.; Leddy, H.E.; Behrens, J.; Sommer, T.; Birchmeier, W. Hakai, a c-Cbl-like protein, ubiquitinates and induces endocytosis of the E-cadherin complex. *Nat. Cell Biol.* **2002**, *4*, 222–231. [CrossRef] [PubMed]
- 10. Nieman, M.T.; Prudoff, R.S.; Johnson, K.R.; Wheelock, M.J. N-cadherin promotes motility in human breast cancer cells regardless of their E-cadherin expression. *J. Cell Biol.* **1999**, 147, 631–644. [CrossRef] [PubMed]
- 11. Frixen, U.H.; Behrens, J.; Sachs, M.; Eberle, G.; Voss, B.; Warda, A.; Löchner, D.; Birchmeier, W. E-cadherin-mediated cell-cell adhesion prevents invasiveness of human carcinoma cells. *J. Cell Biol.* **1991**, *113*, 173–185. [CrossRef] [PubMed]
- 12. Bringuier, P.P.; Umbas, R.; Schaafsma, H.E.; Karthaus, H.F.; Debruyne, F.M.; Schalken, J.A. Decreased E-cadherin immunoreactivity correlates with poor survival in patients with bladder tumors. *Cancer Res.* **1993**, *53*, 3241–3245. [PubMed]
- 13. Kamei, T.; Matozaki, T.; Sakisaka, T.; Kodama, A.; Yokoyama, S.; Peng, Y.F.; Nakano, K.; Takaishi, K.; Takai, Y. Coendocytosis of cadherin and c-Met coupled to disruption of cell-cell adhesion in MDCK cells-regulation by Rho, Rac and Rab small G proteins. *Oncogene* 1999, 18, 6776–6784. [CrossRef] [PubMed]
- 14. Le, T.L.; Joseph, S.R.; Yap, A.S.; Stow, J.L. Protein kinase C regulates endocytosis and recycling of E-cadherin. *Am. J. Physiol. Cell Physiol.* **2002**, 283, C489–C499. [CrossRef] [PubMed]
- 15. Maretzky, T.; Reiss, K.; Ludwig, A.; Buchholz, J.; Scholz, F.; Proksch, E.; de Strooper, B.; Hartmann, D.; Saftig, P. ADAM10 mediates E-cadherin shedding and regulates epithelial cell-cell adhesion, migration, and beta-catenin translocation. *Proc. Natl. Acad. Sci. USA* 2005, 102, 9182–9187. [CrossRef]
- 16. Lynch, C.C.; Vargo-Gogola, T.; Matrisian, L.M.; Fingleton, B. Cleavage of E-Cadherin by Matrix Metalloproteinase-7 Promotes Cellular Proliferation in Nontransformed Cell Lines via Activation of RhoA. *J. Oncol.* **2010**, 2010, 530745. [CrossRef]
- 17. Noë, V.; Fingleton, B.; Jacobs, K.; Crawford, H.C.; Vermeulen, S.; Steelant, W.; Bruyneel, E.; Matrisian, L.M.; Mareel, M. Release of an invasion promoter E-cadherin fragment by matrilysin and stromelysin-1. *J. Cell Sci.* **2001**, *114*, 111–118. [CrossRef]
- 18. Reiss, K.; Ludwig, A.; Saftig, P. Breaking up the tie: Disintegrin-like metalloproteinases as regulators of cell migration in inflammation and invasion. *Pharmacol. Ther.* **2006**, *111*, 985–1006. [CrossRef]
- 19. Tatsumi, M.; Kishi, T.; Ishida, S.; Kawana, H.; Uwamizu, A.; Ono, Y.; Kawakami, K.; Aoki, J.; Inoue, A. Ectodomain shedding of EGFR ligands serves as an activation readout for TRP channels. *PLoS ONE* **2023**, *18*, e0280448. [CrossRef]
- Villalta, P.C.; Townsley, M.I. Transient receptor potential channels and regulation of lung endothelial permeability. *Pulm. Circ.* 2013, 3, 802–815. [CrossRef]
- 21. Rosenbaum, T.; Benitez-Angeles, M.; Sanchez-Hernandez, R.; Morales-Lazaro, S.L.; Hiriart, M.; Morales-Buenrostro, L.E.; Torres-Quiroz, F. TRPV4: A Physio and Pathophysiologically Significant Ion Channel. *Int. J. Mol. Sci.* 2020, 21, 3837. [CrossRef] [PubMed]
- 22. Rajan, S.; Schremmer, C.; Weber, J.; Alt, P.; Geiger, F.; Dietrich, A. Ca<sup>2+</sup> Signaling by TRPV4 Channels in Respiratory Function and Disease. *Cells* **2021**, *10*, 822. [CrossRef] [PubMed]
- 23. Miller, B.A.; Hoffman, N.E.; Merali, S.; Zhang, X.Q.; Wang, J.; Rajan, S.; Shanmughapriya, S.; Gao, E.; Barrero, C.A.; Mallilankaraman, K.; et al. TRPM2 channels protect against cardiac ischemia-reperfusion injury: Role of mitochondria. *J. Biol. Chem.* **2014**, 289, 7615–7629. [CrossRef] [PubMed]
- 24. Goldenberg, N.M.; Ravindran, K.; Kuebler, W.M. TRPV4: Physiological role and therapeutic potential in respiratory diseases. *Naunyn-Schmiedebergs Arch. Pharmacol.* **2015**, *388*, 421–436. [CrossRef] [PubMed]
- 25. Kumar, M.; Zaman, M.K.; Das, S.; Goyary, D.; Pathak, M.P.; Chattopadhyay, P. Transient Receptor Potential Vanilloid (TRPV4) channel inhibition: A novel promising approach for the treatment of lung diseases. *Biomed. Pharmacother.* **2023**, *163*, 114861. [CrossRef]
- 26. Hamanaka, K.; Jian, M.Y.; Townsley, M.I.; King, J.A.; Liedtke, W.; Weber, D.S.; Eyal, F.G.; Clapp, M.M.; Parker, J.C. TRPV4 channels augment macrophage activation and ventilator-induced lung injury. *Am. J. Physiol. Lung Cell. Mol. Physiol.* **2010**, 299, L353–L362. [CrossRef]
- 27. Weber, J.; Rajan, S.; Schremmer, C.; Chao, Y.K.; Krasteva-Christ, G.; Kannler, M.; Yildirim, A.O.; Brosien, M.; Schredelseker, J.; Weissmann, N.; et al. TRPV4 channels are essential for alveolar epithelial barrier function as protection from lung edema. *JCI Insight* 2020, 5, e134464. [CrossRef]
- 28. Suzuki, M.; Mizuno, A.; Kodaira, K.; Imai, M. Impaired pressure sensation in mice lacking TRPV4. *J. Biol. Chem.* **2003**, 278, 22664–22668. [CrossRef]
- 29. Alvarez, D.F.; King, J.A.; Weber, D.; Addison, E.; Liedtke, W.; Townsley, M.I. Transient receptor potential vanilloid 4-mediated disruption of the alveolar septal barrier: A novel mechanism of acute lung injury. *Circ. Res.* **2006**, *99*, 988–995. [CrossRef]
- 30. Balakrishna, S.; Song, W.; Achanta, S.; Doran, S.F.; Liu, B.; Kaelberer, M.M.; Yu, Z.; Sui, A.; Cheung, M.; Leishman, E.; et al. TRPV4 inhibition counteracts edema and inflammation and improves pulmonary function and oxygen saturation in chemically induced acute lung injury. *Am. J. Physiol. Lung Cell Mol. Physiol.* **2014**, *307*, L158–L172. [CrossRef]
- 31. Achanta, S.; Jordt, S.E. Transient receptor potential channels in pulmonary chemical injuries and as countermeasure targets. *Ann. N. Y. Acad. Sci.* **2020**, *1480*, 73–103. [CrossRef] [PubMed]
- 32. Reiter, B.; Kraft, R.; Gunzel, D.; Zeissig, S.; Schulzke, J.D.; Fromm, M.; Harteneck, C. TRPV4-mediated regulation of epithelial permeability. *FASEB J.* **2006**, 20, 1802–1812. [CrossRef] [PubMed]

33. Mukaiyama, M.; Yamasaki, Y.; Usui, T.; Nagumo, Y. Transient receptor potential V4 channel stimulation induces reversible epithelial cell permeability in MDCK cell monolayers. *FEBS Lett.* **2019**, *593*, 2250–2260. [CrossRef] [PubMed]

- 34. Martinez-Rendon, J.; Sanchez-Guzman, E.; Rueda, A.; Gonzalez, J.; Gulias-Canizo, R.; Aquino-Jarquin, G.; Castro-Munozledo, F.; Garcia-Villegas, R. TRPV4 Regulates Tight Junctions and Affects Differentiation in a Cell Culture Model of the Corneal Epithelium. *J. Cell Physiol.* 2017, 232, 1794–1807. [CrossRef] [PubMed]
- 35. Kida, N.; Sokabe, T.; Kashio, M.; Haruna, K.; Mizuno, Y.; Suga, Y.; Nishikawa, K.; Kanamaru, A.; Hongo, M.; Oba, A. Importance of transient receptor potential vanilloid 4 (TRPV4) in epidermal barrier function in human skin keratinocytes. *Pflügers Arch.-Eur. J. Physiol.* **2012**, 463, 715–725. [CrossRef]
- 36. Dagenais, A.; Desjardins, J.; Shabbir, W.; Roy, A.; Filion, D.; Sauve, R.; Berthiaume, Y. Loss of barrier integrity in alveolar epithelial cells downregulates ENaC expression and activity via Ca(<sup>2+</sup>) and TRPV4 activation. *Pflugers Arch.* **2018**, 470, 1615–1631. [CrossRef]
- 37. Yin, J.; Michalick, L.; Tang, C.; Tabuchi, A.; Goldenberg, N.; Dan, Q.; Awwad, K.; Wang, L.; Erfinanda, L.; Nouailles, G.; et al. Role of Transient Receptor Potential Vanilloid 4 in Neutrophil Activation and Acute Lung Injury. *Am. J. Respir. Cell Mol. Biol.* **2016**, *54*, 370–383. [CrossRef]
- 38. Bice, T.; Li, G.; Malinchoc, M.; Lee, A.S.; Gajic, O. Incidence and risk factors of recurrent acute lung injury. *Crit. Care Med.* **2011**, 39, 1069–1073. [CrossRef]
- 39. Stolwijk, J.A.; Matrougui, K.; Renken, C.W.; Trebak, M. Impedance analysis of GPCR-mediated changes in endothelial barrier function: Overview and fundamental considerations for stable and reproducible measurements. *Pflugers Arch.* **2015**, 467, 2193–2218. [CrossRef]
- 40. Schaller, L.; Hofmann, K.; Geiger, F.; Dietrich, A. Electrical cell-substrate impedance sensing (ECIS) in lung biology and disease. *Appl. Res.* **2024**, e202400059. [CrossRef]
- 41. Schindelin, J.; Arganda-Carreras, I.; Frise, E.; Kaynig, V.; Longair, M.; Pietzsch, T.; Preibisch, S.; Rueden, C.; Saalfeld, S.; Schmid, B.; et al. Fiji: An open-source platform for biological-image analysis. *Nat. Methods* **2012**, *9*, 676–682. [CrossRef] [PubMed]
- 42. Hofmann, K.; Fiedler, S.; Vierkotten, S.; Weber, J.; Klee, S.; Jia, J.; Zwickenpflug, W.; Flockerzi, V.; Storch, U.; Yildirim, A.; et al. Classical transient receptor potential 6 (TRPC6) channels support myofibroblast differentiation and development of experimental pulmonary fibrosis. *Biochim. Biophys. Acta Mol. Basis Dis.* 2017, 1863, 560–568. [CrossRef] [PubMed]
- 43. Marconett, C.N.; Zhou, B.; Sunohara, M.; Pouldar, T.M.; Wang, H.; Liu, Y.; Rieger, M.E.; Tran, E.; Flodby, P.; Siegmund, K.D.; et al. Cross-Species Transcriptome Profiling Identifies New Alveolar Epithelial Type I Cell-Specific Genes. *Am. J. Respir. Cell Mol. Biol.* **2017**, *56*, 310–321. [CrossRef] [PubMed]
- 44. Thorneloe, K.S.; Sulpizio, A.C.; Lin, Z.; Figueroa, D.J.; Clouse, A.K.; McCafferty, G.P.; Chendrimada, T.P.; Lashinger, E.S.; Gordon, E.; Evans, L.; et al. N-((1S)-1-{[4-((2S)-2-{[(2,4-dichlorophenyl)sulfonyl]amino}-3-hydroxypropanoyl)-1-piperazinyl]carbonyl}-3-methylbutyl)-1-benzothiophene-2-carboxamide (GSK1016790A), a novel and potent transient receptor potential vanilloid 4 channel agonist induces urinary bladder contraction and hyperactivity: Part I. *J. Pharmacol. Exp. Ther.* **2008**, 326, 432–442. [CrossRef] [PubMed]
- 45. Cheung, M.; Bao, W.; Behm, D.J.; Brooks, C.A.; Bury, M.J.; Dowdell, S.E.; Eidam, H.S.; Fox, R.M.; Goodman, K.B.; Holt, D.A.; et al. Discovery of GSK2193874: An Orally Active, Potent, and Selective Blocker of Transient Receptor Potential Vanilloid 4. *ACS Med. Chem. Lett.* 2017, *8*, 549–554. [CrossRef]
- 46. Ludwig, A.; Hundhausen, C.; Lambert, M.H.; Broadway, N.; Andrews, R.C.; Bickett, D.M.; Leesnitzer, M.A.; Becherer, J.D. Metalloproteinase inhibitors for the disintegrin-like metalloproteinases ADAM10 and ADAM17 that differentially block constitutive and phorbol ester-inducible shedding of cell surface molecules. *Comb. Chem. High. Throughput Screen.* 2005, 8, 161–171. [CrossRef]
- 47. Darby, W.G.; Grace, M.S.; Baratchi, S.; McIntyre, P. Modulation of TRPV4 by diverse mechanisms. *Int. J. Biochem. Cell Biol.* **2016**, 78, 217–228. [CrossRef]
- 48. Phuong, T.T.T.; Redmon, S.N.; Yarishkin, O.; Winter, J.M.; Li, D.Y.; Krizaj, D. Calcium influx through TRPV4 channels modulates the adherens contacts between retinal microvascular endothelial cells. *J. Physiol.* **2017**, *595*, 6869–6885. [CrossRef]
- 49. Willette, R.N.; Bao, W.; Nerurkar, S.; Yue, T.L.; Doe, C.P.; Stankus, G.; Turner, G.H.; Ju, H.; Thomas, H.; Fishman, C.E.; et al. Systemic activation of the transient receptor potential vanilloid subtype 4 channel causes endothelial failure and circulatory collapse: Part 2. *J. Pharmacol. Exp. Ther.* **2008**, *326*, 443–452. [CrossRef]
- 50. Gaude, G.S. Pulmonary manifestations of gastroesophageal reflux disease. Ann. Thorac. Med. 2009, 4, 115–123. [CrossRef]
- 51. Ohwada, A.; Yoshioka, Y.; Iwabuchi, K.; Nagaoka, I.; Dambara, T.; Fukuchi, Y. VEGF regulates the proliferation of acid-exposed alveolar lining epithelial cells. *Thorax* **2003**, *58*, 328–332. [CrossRef] [PubMed]
- 52. Bourgois, A.; Crouzier, D.; Legrand, F.X.; Raffin, F.; Boyard, A.; Girleanu, M.; Favier, A.L.; François, S.; Dekali, S. Alumina nanoparticles size and crystalline phase impact on cytotoxic effect on alveolar epithelial cells after simple or HCl combined exposures. *Toxicol. In Vitro* 2019, 59, 135–149. [CrossRef] [PubMed]
- 53. Suresh, K.; Servinsky, L.; Reyes, J.; Baksh, S.; Undem, C.; Caterina, M.; Pearse, D.B.; Shimoda, L.A. Hydrogen peroxide-induced calcium influx in lung microvascular endothelial cells involves TRPV4. *Am. J. Physiol. Lung Cell. Mol. Physiol.* **2015**, 309, L1467–L1477. [CrossRef] [PubMed]
- 54. Bleibaum, F.; Sommer, A.; Veit, M.; Rabe, B.; Andrä, J.; Kunzelmann, K.; Nehls, C.; Correa, W.; Gutsmann, T.; Grötzinger, J.; et al. ADAM10 sheddase activation is controlled by cell membrane asymmetry. *J. Mol. Cell Biol.* **2019**, *11*, 979–993. [CrossRef] [PubMed]

55. Villalta, P.C.; Rocic, P.; Townsley, M.I. Role of MMP2 and MMP9 in TRPV4-induced lung injury. *Am. J. Physiol. Lung Cell. Mol. Physiol.* **2014**, 307, L652–L659. [CrossRef]

- 56. Janssen, D.A.; Jansen, C.J.; Hafmans, T.G.; Verhaegh, G.W.; Hoenderop, J.G.; Heesakkers, J.P.; Schalken, J.A. TRPV4 channels in the human urogenital tract play a role in cell junction formation and epithelial barrier. *Acta Physiol.* **2016**, 218, 38–48. [CrossRef]
- 57. Zemans, R.L.; Colgan, S.P.; Downey, G.P. Transepithelial migration of neutrophils: Mechanisms and implications for acute lung injury. *Am. J. Respir. Cell Mol. Biol.* **2009**, *40*, 519–535. [CrossRef]
- 58. Schremmer, C.; Steinritz, D.; Gudermann, T.; Beech, D.; Dietrich, A. An ex vivo perfused ventilated murine lung model suggests lack of acute pulmonary toxicity of the potential novel anticancer agent (–)-englerin A. *Arch. Toxicol.* **2022**, *96*, 1055–1063. [CrossRef]

**Disclaimer/Publisher's Note:** The statements, opinions and data contained in all publications are solely those of the individual author(s) and contributor(s) and not of MDPI and/or the editor(s). MDPI and/or the editor(s) disclaim responsibility for any injury to people or property resulting from any ideas, methods, instructions or products referred to in the content.

# TRPV4 mediates alveolar epithelial barrier integrity and induces ADAM10-driven E-cadherin shedding

Lena Schaller, Thomas Gudermann and Alexander Dietrich

# **Supplementary Information**

Table S1: Antibodies used for cell isolation, Western blotting and immunocytochemistry

Primary antibodies	Supplier	Cat. # / RRID	Dilution
E-Cadherin (mo pAb)	BD Biosciences	610181 / AB_397580	WB: 1:1000
B-actin-HRP (mo pAb)	Merck	A3854 / AB_262011	WB: 1:10000
Aquaporin 5 (AQP5) (rb pAb)	Alomone Labs	AQP005 / AB_2039736	ICC: 1:200
Prosurfactant protein C (pSPC)	Merck	AB3786 / AB_91588	ICC: 1:200
(rb pAb)			
CD16/CD32	BD Pharmingen	553142 / AB_394656	Iso: 1:666
CD45	BD Pharmingen	553076 / AB_394606	Iso: 1:666

Secondary antibodies	Supplier	Cat. # / RRID	Dilution
Mouse-HRP	Cell Signaling	7076 / AB_330924	WB: 1:10000
Rabbit Alexa Fluor 488	ThermoFisher Scientific	A32731 / AB_2633280	ICC: 1:250

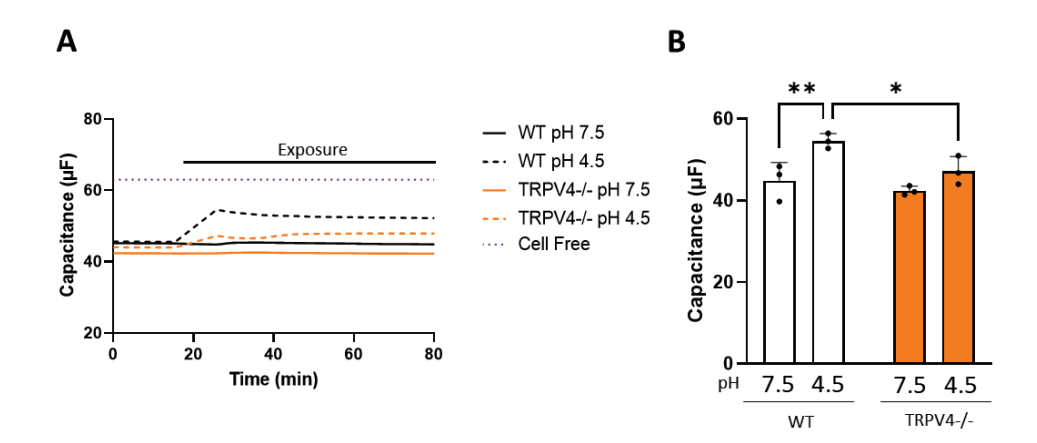


**Figure S1:** Low pH induces TRPV4-mediated changes in cell adhesion. (A) Capacitance values for WT and TRPV4-/- AT1 cells upon an HCl-induced change in media pH were recorded using an ECIS system at 500 Hz. Capacitance values 10 minutes after media change (pH 7.5 or pH 4.5) were quantified (B). Data represent the mean  $\pm$  SD (B) of 3 independent cell preparations from 6 mice each. Significance was assessed using a two-way ANOVA. \* p < 0.05, \*\* p < 0.01

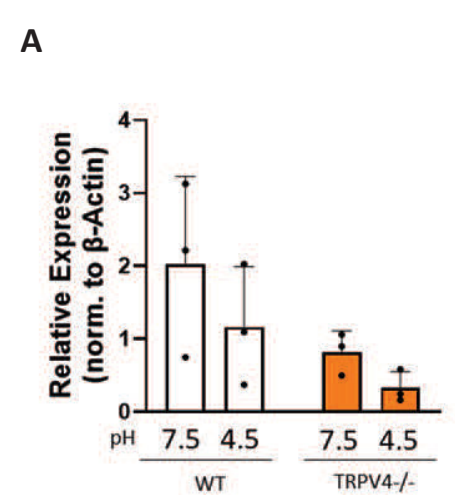


**Figure S2:** Low pH does not significantly change E-cadherin protein expression in AT1 cells. Quantification of Western blot results for E-cadherin protein expression in AT1 cells 1 h after a change in media pH. Data represent the mean ± SD of 3 independent cell preparations from 6 mice each. Significance was assessed using a two-way ANOVA.

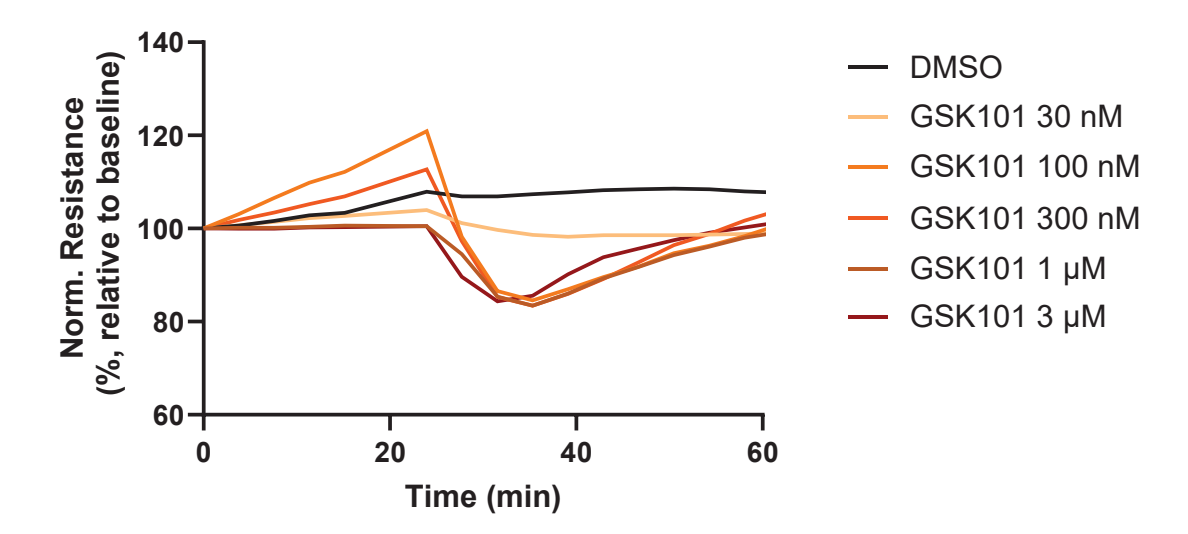


**Figure S3:** Loss of AT1 cell resistance upon GSK101 application plateaus at 100 nM concentration. Changes in normalized electrical cell resistance were recorded at 500 Hz in WT AT1 cells upon application of increasing concentrations of GSK101. Data represent the results from one cell preparation of 5 mice.

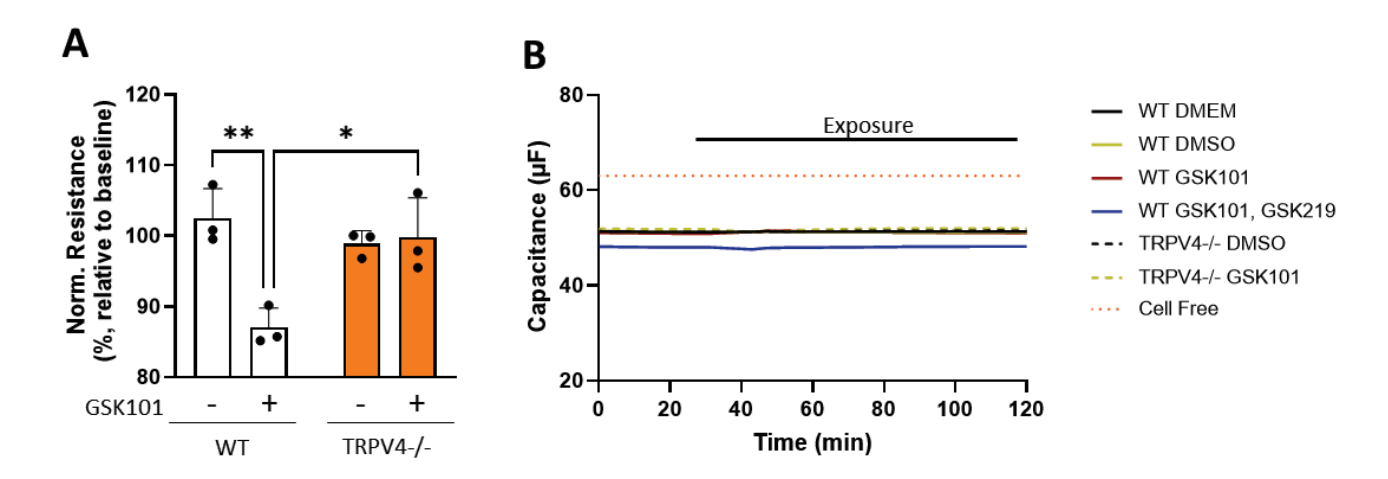


**Figure S4:** GSK101-induced loss of AT1 barrier resistance is TRPV4-dependant, and does not cause cell detachment. (A) The normalized electrical cell resistance for WT and Trpv4-/- AT1 cells 15 minutes after GSK101 (100 nM) exposure was quantified. (B) Mean capacitance values for WT and Trpv4-/- AT1 cells upon application of GSK101 (100 nM) in the presence and absence of GSK219 (300 nM) were recorded using an ECIS system at 500 Hz. Data represent mean  $\pm$  SD (A) from 3 independent cell isolations from 5 mice each. Significance between means was analyzed with a two-way ANOVA; \* p < 0.05, \*\* p < 0.01.

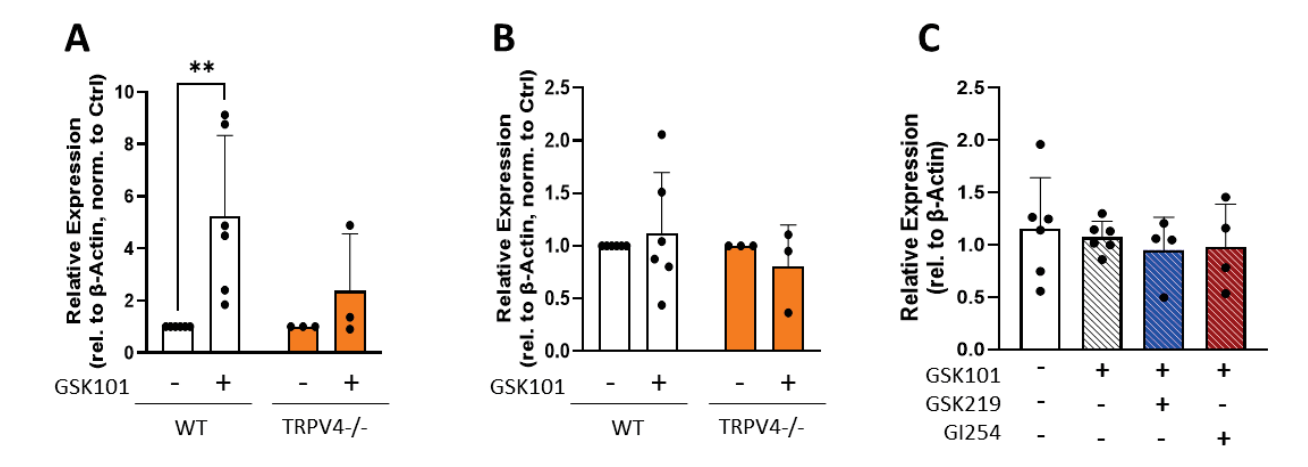


**Figure S5:** GSK101 exposure triggers TRPV4-dependent formation of an E-cadherin CTF, but does not significantly change the protein expression of E-cadherin. Quantification of Western blot results for the level of E-cadherin CTF (A) and E-cadherin (B) in WT and Trpv4-/- AT1 cells 15 minutes after the addition of GSK101 (100 nM). (C) Quantification of Western blot results for E-cadherin protein expression levels in WT AT1 cells 15 minutes following the addition of GSK101 (100 nM) in theh presence and absence of either the TRPV4 inhibitor GSK219 (300 nM) or the ADAM10 inhibitor GI254 (3  $\mu$ M). Data represent the mean  $\pm$  SD from at least 3 independent cell preparations from 3-5 mice, each. Significance was assessed using two-way (A, B) and one-way (C) ANOVA; \*\* p < 0.01.

# Paper II



Contents lists available at ScienceDirect

# Redox Biology

journal homepage: www.elsevier.com/locate/redox



# TRPV2 channels facilitate pulmonary endothelial barrier recovery after ROS-induced permeability

Lena Schaller, Martina Kiefmann, Thomas Gudermann, Alexander Dietrich \* ©

Walther Straub Institute of Pharmacology and Toxicology, Member of the German Center for Lung Research (DZL), Medical Faculty, LMU Munich, Nußbaumstrasse 26, 80336, Munich, Germany

### ARTICLE INFO

Keywords: TRPV2 ADAM10 ROS Impedance Cadherin Endothelial barrier function

### ABSTRACT

Reactive oxygen species (ROS), such as hydrogen peroxide (H2O2), are known signaling molecules that increase endothelial barrier permeability. In this study, we investigated the roles of redox-sensitive transient receptor potential (TRP) ion channels, TRPM2, TRPV2 and TRPV4, in H2O2-induced endothelial barrier dysfunction. Using primary human pulmonary microvascular endothelial cells (HPMEC), we employed impedance-based resistance measurements, Western blot, and immunofluorescence staining to assess the effects of H<sub>2</sub>O<sub>2</sub> on the endothelial barrier. Exposure to sublytic concentrations of H2O2 caused an acute loss of endothelial barrier integrity, accompanied by the cleavage of vascular endothelial cadherin (VE-cadherin), which was also apparent after application of the TRPV2 activator cannabidiol. The inhibition of either TRPV2 with tranilast or a disintegrin and metalloprotease domain-containing protein 10 (ADAM10) with GI254023X significantly reduced H<sub>2</sub>O<sub>2</sub>-induced VE-cadherin cleavage, while TRPM2 inhibition by econazole significantly increased H<sub>2</sub>O<sub>2</sub>-driven VE-cadherin cleavage and blockage of TRPV4 showed no effect. Although inhibition of either TRPV2 or ADAM10 did not prevent the initial loss of barrier resistance upon H<sub>2</sub>O<sub>2</sub> exposure, both were essential for the subsequent recovery of barrier integrity. Time-course immunofluorescence stainings revealed that HPMEC barrier recovery involved a transient localization of N-cadherin proteins at adherens junctions. This process of cadherin-switching did not occur upon inhibition of TRPV2 or ADAM10. Our results highlight a novel role for TRPV2 as a redox sensitive ion channels in the microvascular endothelium and provide insight into the mechanisms underlying pulmonary microvascular endothelial barrier recovery.

## 1. Introduction

The barrier formed by the pulmonary microvasculature is constitutively restrictive, preventing both pathogen infiltration and edema formation while facilitating the exchange of gases and nutrients between the bloodstream and surrounding tissue [1,2]. While a transient increase in permeability supports biological functions such as wound repair, angiogenesis and immune cell trafficking [3,4], prolonged or extensive permeability can result in pulmonary edema, acute respiratory distress syndrome (ARDS) [5] and atherosclerosis [6].

Reactive oxygen species (ROS), such as hydrogen peroxide (H<sub>2</sub>O<sub>2</sub>), are known effectors of altered endothelial barrier function [7–10]. ROS can arise from exogenous triggers, including infection, ionizing radiation or toxicants, but also occur naturally in the body, such as during mitochondrial respiration [11,12]. The concept of an "oxidative window" describes the optimal range of ROS levels that facilitate cellular

processes such as neovascularization, cell proliferation and wound healing [7,8,13]. Deviations from this balance, resulting in oxidative or reductive stress, lead to cellular dysfunction [8].

Adherens junctions (AJs), comprised of Ca<sup>2+</sup>-dependent, homotypic adhesions between the vascular endothelial cadherin (VE-cadherin) proteins of neighboring cells, are essential components of the endothelial barrier [3,14]. While the formation of AJs depends on extracellular Ca<sup>2+</sup>, an increase in intracellular Ca<sup>2+</sup> can induce endothelial barrier permeability [3,15]. Members of the Transient Receptor Potential (TRP) superfamily form nonselective cation channels that conduct Ca<sup>2+</sup>, and several TRP channels have been implicated in Ca<sup>2+</sup>-induced barrier dysfunction [3]. It has been reported that TRP-induced Ca<sup>2+</sup> influx could activate a disintegrin and metalloprotease domain-containing protein 10 (ADAM10) [16], a metalloprotease known to cleave VE-cadherin at its extracellular domain [17]. However, a ROS-driven, ADAM10-mediated cleavage of VE-cadherin has yet to be reported in pulmonary

E-mail address: alexander.dietrich@lrz.uni-muenchen.de (A. Dietrich).

https://doi.org/10.1016/j.redox.2025.103720

Received 21 May 2025; Received in revised form 5 June 2025; Accepted 6 June 2025 Available online 7 June 2025

2213-2317/© 2025 The Authors. Published by Elsevier B.V. This is an open access article under the CC BY license (http://creativecommons.org/licenses/by/4.0/).

<sup>\*</sup> Corresponding author.

microvascular endothelial cells.

TRPM2 is a recognized mediator of ROS-induced  $Ca^{2+}$  influx. Expressed in the brain, immune cells, and vasculature, TRPM2 forms a tetrameric, nonselective ion channel that conducts  $Ca^{2+}$  and is gated by adenosine diphosphate ribose (ADPR) [18–21], which is generated as a result of ROS-induced DNA damage [18,19]. While TRPM2 is a known modulator of pulmonary endothelial barrier permeability, its knockdown does not completely abolish endothelial  $Ca^{2+}$  influx following ROS exposure, suggesting the involvement of additional redox-sensitive  $Ca^{2+}$  channels [9,22].

The second member of the vanilloid TRP subfamily, TRPV2, is a potential candidate for the undefined source of ROS-induced pulmonary endothelial Ca<sup>2+</sup> influx. Originally associated with mechanoreception [23], TRPV2 also operates as a redox-sensitive ion channel [24,25], and is highly expressed in the microvascular endothelium in relation to other redox-sensitive TRP channels, including TRPM2 and TRPV4 [26]. While TRPV2 has been linked to changes in blood-brain barrier integrity [27], there is no evidence to date linking the channel to altered pulmonary microvascular endothelial barrier function [28].

Here, we applied pharmacological inhibitors to investigate the role of TRPM2 and TRPV2 in  $\rm H_2O_2$ -induced pulmonary endothelial barrier dysfunction. Neither channel was responsible for the initial loss of barrier resistance, but both channels facilitated the subsequent recovery of barrier integrity. In this model, TRPV2 mediated AJ integrity by inducing ADAM10-driven VE-cadherin cleavage, which was further increased upon TRPM2 inhibition. Endothelial barrier recovery was characterized by the translocation of neural cadherin (N-cadherin) to the plasma membrane, suggesting a role for TRP-mediated cadherin switching in the restoration of endothelial barrier function following ROS-induced permeability.

## 2. Methods

## 2.1. Cells

Primary human pulmonary microvascular endothelial cells (HPMECs) [29] from healthy donors were obtained from Promocell (Heidelberg, Germany, #C-12281) and cultured in endothelial cell growth medium MV (Promocell, #C-22020) at 37  $^{\circ}$ C and 5  $^{\circ}$ C Co<sub>2</sub>, and were kept until passage 12. Donor information is provided in Supp. Table S1. Relevant ethical statements were provided by Promocell. For experiments involving pharmacological inhibition, HPMECs were pre-incubated for 1 h in DMEM containing the respective inhibitor(s), which were also present during the subsequent exposure period.

# 2.2. Quantification of endothelial barrier resistance

HPMECs were seeded onto electrical cell-substrate impedance sensing (ECIS) plates at a density of 8  $\times$  10^4 cells/well (Applied Biophysics, Troy, NY, USA, 8W10E+), which had been treated with 10 mM of 1-Cysteine according to the manufacturer's recommendation. HPMEC barrier resistance was measured at 4000 Hz using the ECIS ZΦ device (Applied Biophysics), and experiments were conducted once the monolayer resistance had reached a constant state (after  $\sim\!48~h)$ .

## 3. Results

3.1.  $H_2O_2$  exposure at non-cytolytic concentrations increases HPMEC barrier permeability, triggers ADAM10-dependent VE-cadherin cleavage, and induces TRP-mediated  $Ca^{2+}$  flux

Using  $\rm H_2O_2$  to mimic ROS production in response to infection, radiation or other toxicants, we monitored changes in barrier resistance of human pulmonary microvascular endothelial cells (HPMEC). While  $\rm H_2O_2$  exposure did not exert detectable cytolytic effects after 2 h (Supp. Fig. S1), changes in HPMEC barrier resistance were observed within 5

min of exposure (Fig. 1A). 15 min post H<sub>2</sub>O<sub>2</sub> addition, mean HPMEC barrier resistance dropped to 45 %  $\pm$  11 % and 47 %  $\pm$  14 % of the control in cells treated with 75 µM and 300 µM H<sub>2</sub>O<sub>2</sub>, respectively, with recovery noted only in HPMECs treated with 75 µM H<sub>2</sub>O<sub>2</sub> (quantified in Fig. 1B). Additionally, Western blot analysis revealed that H<sub>2</sub>O<sub>2</sub> exposure caused the formation of a single ~35 kDa VE-cadherin C-terminal fragment (CTF) (Fig. 1C, Supp. Fig. S1B), the formation of which was prevented by the addition of the specific ADAM10 inhibitor GI254023X [30] (GI254, see Supp. Table S2 for IC50 values) (Fig. 1C, quantified in D). Cell fractionation through surface biotinylation revealed that this CTF was present as early as 15 min after exposure, and was detected at both the plasma membrane and the intracellular space (Supp. Fig. 1C). As ADAM10 is activated upon Ca<sup>2+</sup> influx, we first turned our attention to two redox-sensitive TRP channels, TRPM2 and TRPV2. Quantitative rt-PCR confirmed that both genes were transcribed in HPMECs (Supp. Fig. S1D), and both proteins were detected in cell lysates via Western blot (Supp. Fig. S1E and F).  $Ca^{2+}$  imaging experiments revealed that the increase of intracellular  $Ca^{2+}$  ( $[Ca^{2+}]_i$ ) upon  $H_2O_2$  exposure was dependent on both channels (Fig. 1E and F).

# 3.2. TRPV2 mediates ADAM10-driven VE-cadherin shedding upon $H_2O_2$ exposure

Having demonstrated that  $\rm H_2O_2$  exposure triggers TRP-dependent  $\rm Ca^{2+}$  influx, we next investigated the specific contributions of TRPV2 and TRPM2 to the associated VE-cadherin cleavage. HPMECs pretreated with the TRPV2 inhibitor tranilast [31] had significantly reduced  $\rm H_2O_2$ -driven, ADAM10-mediated cleavage of VE-cadherin (Fig. 2A) when quantified (Fig. 2B). These results were corroborated using the alternate TRPV2 inhibitor valdecoxib [32] (Supp. Fig. S2A and B), as well as through siRNA-mediated TRPV2 knockdown (Supp. Fig. S2C and D). The TRPV2/ADAM10/VE-cadherin cleavage pathway was further confirmed with the TRPV2 activator, cannabidiol (CBD) [27] (Fig. 2C, quantified in D). Notably, while gene transcripts of the redox-sensitive TRPV4 channel were also detected in HPMECs (Supp. Fig. S1D), pretreatment with the specific TRPV4 inhibitor GSK2193874 [33] had no effect on the degree of  $\rm H_2O_2$ -induced VE-cadherin CTF formation (Supp. Fig. S2E and F).

In contrast to TRPV2, we observed that the H2O2-induced VEcadherin cleavage was more potent in the absence of TRPM2 functionality, as VE-cadherin CTF levels increased tenfold in HPMECs pretreated with the TRPM2 inhibitor econazole [34] (Fig. 2E, quantified in F). This finding was corroborated using the alternate TRPM2 inhibitor JNJ-28583113 [35] (Supp. Fig. S3A and B), as well as through siRNA-mediated TRPM2 knockdown (Supp. Fig. S3C and D). We observed that ADAM10 inhibition completely abolished H<sub>2</sub>O<sub>2</sub>-induced VE-cadherin CTF formation in econazole-treated HPMECs (Fig. 2G, quantified in H), suggesting that the absence of TRPM2 functionality exacerbates the TRPV2/ADAM10/VE-cadherin cleavage pathway. Further experiments into an underlying mechanism did not indicate direct involvement of TRPM2 in AJ destabilization, as H2O2-induced dephosphorylation of VE-cadherin was not altered in the presence of econazole (Supp. Fig. S3E and F). However, assays with the fluorigenic ROS probe H<sub>2</sub>DCFDA revealed that TRPM2 inhibition increased baseline intracellular ROS levels by 16.2 %  $\pm$  4.3 % relative to DMSO controls (Supp. Fig. S3G) within 30 min.

# 3.3. Recovery of HPMEC barrier integrity requires TRPV2 and TRPM2 functionality

We next assessed whether inhibition of TRPV2 and TRPM2 channels would influence the HPMEC barrier response to  $H_2O_2$ . The protective effect of TRPM2 on VE-cadherin cleavage was also evident in our measurements of barrier resistance, as application of the TRPM2 inhibitor econazole prior to the addition of 75  $\mu$ M  $H_2O_2$  significantly impaired HPMEC barrier recovery (Fig. 3A), with resistance values dropping to

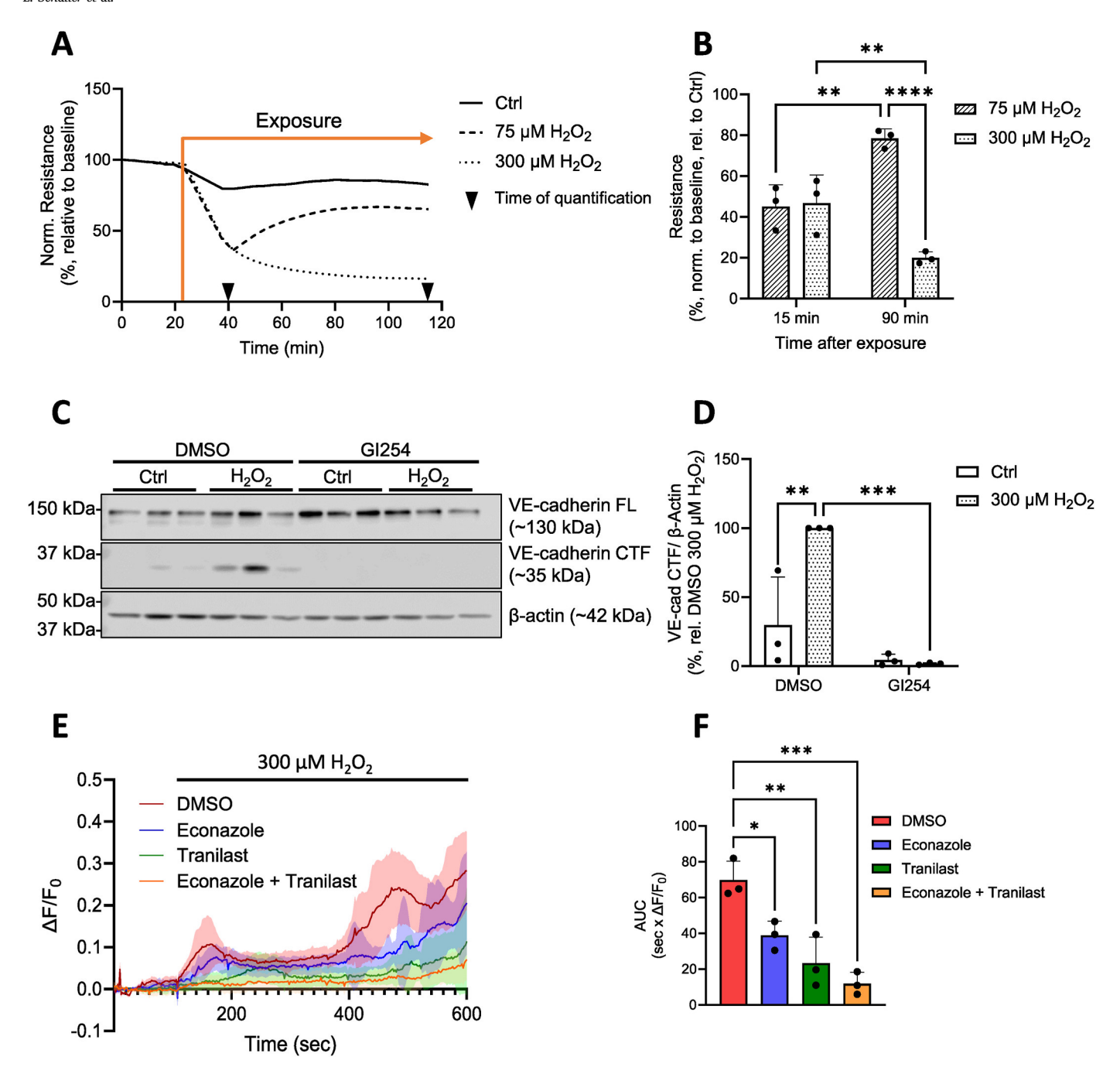


Fig. 1.  $H_2O_2$  induces HPMEC barrier instability and ADAM10-dependent VE-cadherin cleavage. Changes in HPMEC electrical resistance (normalized to baseline levels) were recorded with an ECIS device at 4000 Hz upon application of  $H_2O_2$  (75 μM, 300 μM) (**A**). The normalized resistance values 15 and 90 min after exposure were quantified (**B**). Representative Western blot (from one donor, 3 technical replicates) of the full length (FL) and C-terminal fragment (CTF) levels of VE-cadherin protein in HPMECs 2 h after  $H_2O_2$  exposure (300 μM) in the presence and absence of the ADAM10 inhibitor GI254023X (GI254, 3 μM) (**C**). β-actin was probed as a loading control. Normalized levels of VE-Cadherin CTF from these Western blots were quantified (**D**). Data reflect the mean (**A**, **B**, **D**) + SD (**B**, **D**) from 3 independent donors (n = 3). (**E**) Mean  $\Delta F/F_0$  traces of HPMEC monolayer  $Ca^{2+}$  influx following  $H_2O_2$  exposure (300 μM) in the presence and absence of the TRPM2 and TRPV2 inhibitors, econazole (10 μM) and tranilast (50 μM). Data represent the mean  $\pm$  SD from one experiment, 35–50 cells/treatment group. This experiment was performed three times in HPMECs from a single donor at different passage numbers (n = 3), and the area under the curve (AUC) of each mean  $\Delta F/F_0$   $Ca^{2+}$  trace was quantified (**E**), with bars reflecting the mean + SEM. Normality of data was confirmed using the Shapiro-Wilk test, and significance between means was analyzed using two- or one-way ANOVA and Tukey post hoc tests (**B**, **D**, **E**); \*p < 0.1, \*\*p < 0.01, \*\*\*p < 0.001, \*\*\*\*p < 0.0001.

33 %  $\pm$  23 % of control values after 90 min of treatment (Fig. 3B). In addition to TRPM2, the TRPV2/ADAM10 axis was also necessary for HPMEC barrier recovery. HPMECs exposed to 75  $\mu$ M H<sub>2</sub>O<sub>2</sub> experienced significantly reduced recovery when pretreated with tranilast (Fig. 3C, quantified in Fig. 3D) or GI254023X (Fig. 3E, quantified in 3F).

3.4. TRPV2 facilitates HPMEC barrier recovery through "cadherin switching"

TRPV2-driven VE-cadherin cleavage could facilitate HPMEC barrier recovery by destabilizing AJs and enabling the translocation of neural cadherin (N-cadherin) to the plasma membrane, promoting wound healing. A time-course series of immunofluorescence stainings (Fig. 4A)

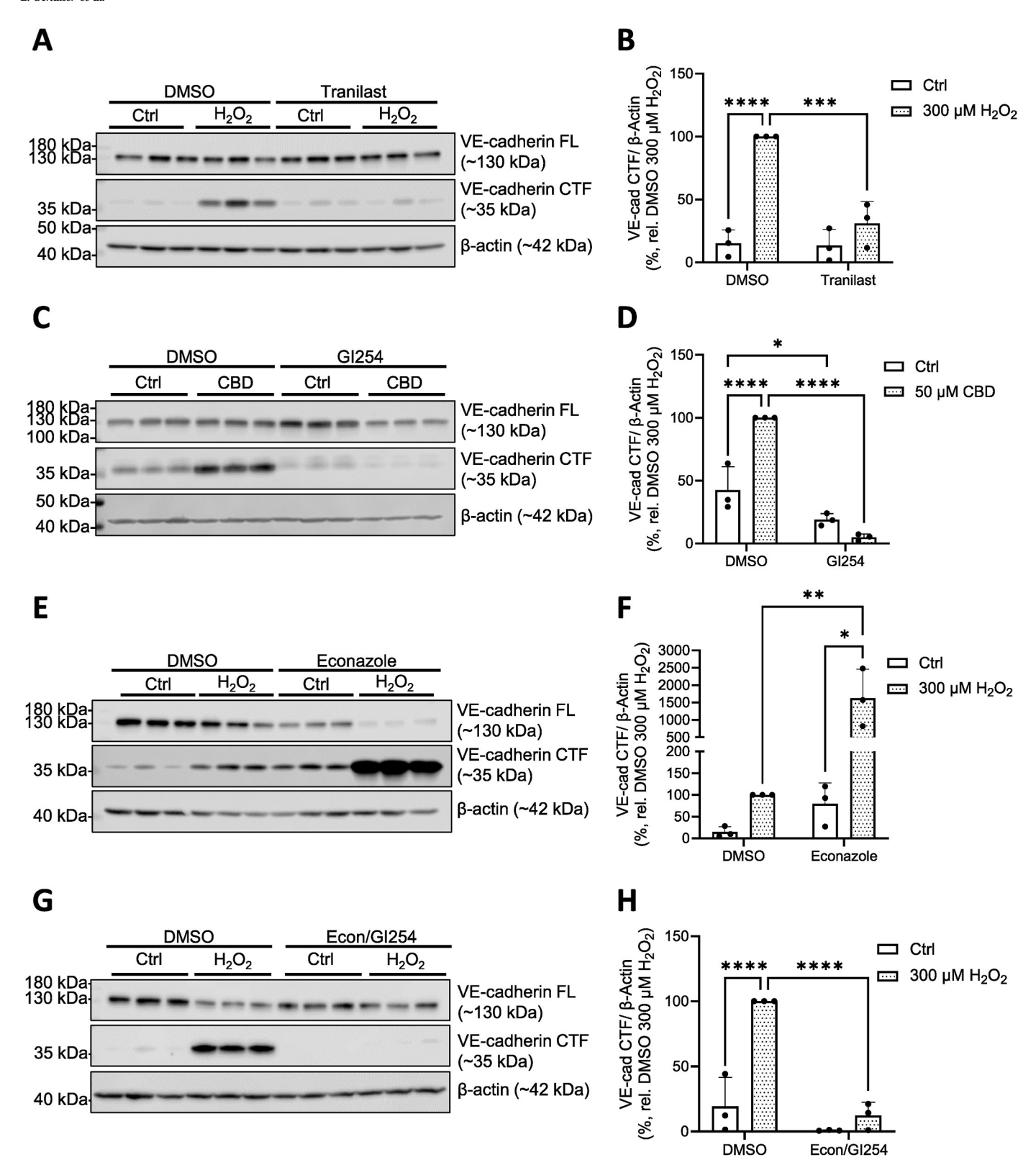


Fig. 2. TRPV2 and TRPM2 mediate VE-cadherin cleavage in HPMECs. Representative Western blot of FL and CTF VE-cadherin protein levels in HPMECs upon TRPV2 inhibition (50 μM tranilast) and 2 h exposure to  $H_2O_2$  (300 μM; **A**, quantified in **B**). (**C**) Representative Western blot of FL and CTF VE-cadherin protein levels in HPMECs upon ADAM10 inhibition (3 μM GI254023X, GI254) and 2 h exposure to cannabidiol (CBD, 50 μM), quantified in (**D**). Representative Western blot of FL and CTF VE-cadherin protein levels in HPMECs upon TRPM2 inhibition (10 μM econazole) and 2 h exposure to  $H_2O_2$  (300 μM; **E**, quantified in **F**). Representative Western blot of FL and CTF VE-cadherin protein levels after  $H_2O_2$  exposure (2 h, 300 μM) upon co-inhibition of TRPM2 and ADAM10 (10 μM econazole, 3 μM GI254023X, (**G**, quantified in **H**)). For all Western blots, β-actin was probed for as a loading control; samples shown are from a single donor, 3 technical replicates. Quantified data reflect the mean + SD from 3 independent donors (**B**, **D**, **F**) or 3 consecutive passages from one donor (**H**); (n = 3). Normality of data was confirmed using the Shapiro-Wilk test, and significance between means was analyzed using two-way ANOVA, with Tukey post hoc tests; \*p < 0.05, \*\*p < 0.01, \*\*\*\*p < 0.001, \*\*\*\*p < 0.0001.

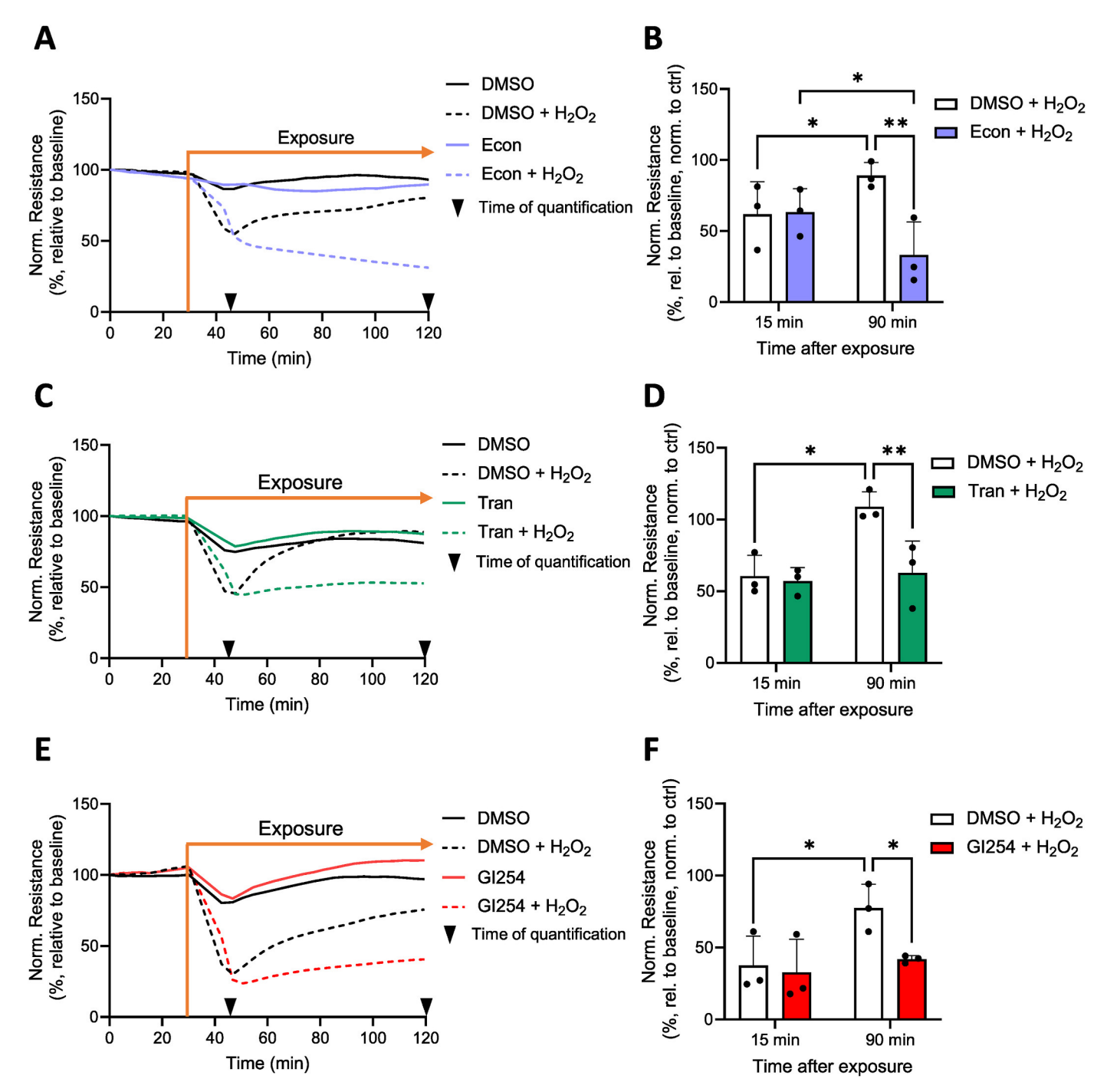


Fig. 3. TRPM2 and TRPV2 facilitate HPMEC barrier recovery following  $H_2O_2$  exposure. Changes in barrier resistance (normalized to baseline) were measured in HPMECs which were preincubated with DMSO or econazole (econ,  $10 \mu M$ , 1 h) and subsequently exposed to  $75 \mu M$   $H_2O_2$  (A). HPMEC resistance values (presented as % of control values) were quantified 15 and 90 min after  $H_2O_2$  application (B). Similar experiments were conducted with the TRPV2 inhibitor tranilast (tran,  $50 \mu M$ , 1 h preincubation, (C, D)) and the ADAM10 inhibitor GI254023X (GI254,  $3 \mu M$ , 1 h preincubation, (E, F)). Data represent the mean (A-F) + SD (B, D, F) of results from 3 independent donors (n = 3). Normality of data was confirmed using the Shapiro-Wilk test, and significance between means was analyzed with two-way ANOVA and Tukey post hoc tests; \*p < 0.05, \*\*p < 0.01.

revealed that, upon exposure to 75  $\mu$ M H<sub>2</sub>O<sub>2</sub>, VE-cadherin signal became disorganized at the plasma membrane after 15 min, recovering within 90 min. In contrast, N-cadherin, while initially dispersed in the intracellular space, organized at the plasma membrane 15 min after H<sub>2</sub>O<sub>2</sub> exposure, returning to the intracellular space within 90 min. N-cadherin may also be a target of ADAM10 ectodomain cleavage, as an H<sub>2</sub>O<sub>2</sub>-dependent ~37 kDa N-cadherin CTF was detected in HPMEC lysates (Supp. Fig. 4). Quantification of VE-cadherin signal intensities at the borders of adjacent cells revealed that econazole-treated HPMECs

showed a significant loss of VE-cadherin signal after 90 min of  $\rm H_2O_2$  exposure (Fig. 4B). 15 min after  $\rm H_2O_2$  exposure, N-cadherin signal intensities at the junctions of DMSO and econazole treated HPMECs were significantly elevated, while HPMECs pretreated with either TRPV2 or ADAM10 inhibitors showed no significant change in N-cadherin signal (Fig. 4C). Colocalization analyses of VE-cadherin and N-cadherin further confirmed that 75  $\mu$ M  $\rm H_2O_2$  induced a transient localization of N-cadherin at AJs with VE-cadherin, a process that was significantly impaired upon either TRPV2 or ADAM10 inhibition (Fig. 4D).

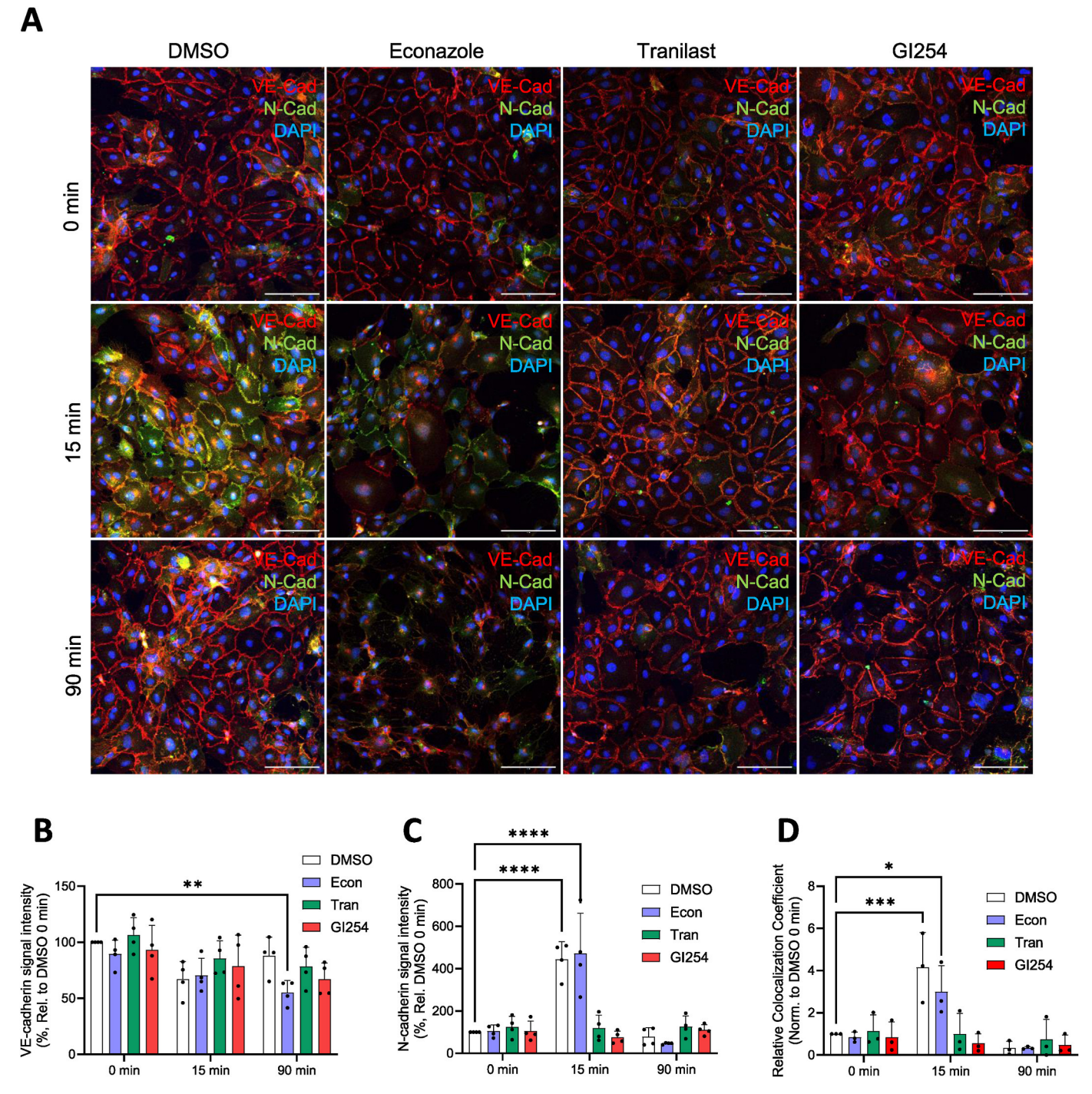


Fig. 4. TRPV2 and ADAM10 are necessary for altered localization of N- and VE-cadherin following  $H_2O_2$  exposure. (A) HPMEC immunofluorescence staining of VE-cadherin (red) and N-cadherin (green) over a timecourse of  $H_2O_2$  exposure (75  $\mu$ M; 0 min, 15 min, 90 min) in the presence and absence of TRPM2, TRPV2 or ADAM10 inhibitors (10  $\mu$ M econazole, 50  $\mu$ M tranilast, 3  $\mu$ M GI254023X, respectively). Nuclei were stained with DAPI (blue), scale bars: 100  $\mu$ m. Signal intensities of VE-cadherin (B) and N-cadherin (C) at cell-cell junctions were quantified from stainings performed in HPMECs from one donor at 4 consecutive passages (n=4, 30 regions per n). Colocalization analyses for N- and VE-cadherin were conducted for the same regions in three experiments (n=3, 30 regions per n), and mean weighted colocalization coefficients for VE-cadherin – N-cadherin were plotted (D). Normality of data was confirmed using the Shapiro-Wilk test, and significance between means (B–D) were analyzed with two-way ANOVA and Tukey post hoc tests; p < 0.05, p < 0.01, p < 0.01, p < 0.001, p < 0.001, p < 0.0001.

## 4. Discussion

ROS are not only mediators of vascular pathology, but are also critical signaling molecules for endothelial cell proliferation, growth and motility [7,8,13,36]. In this study, we describe a pathway by which TRPV2 channels, alongside TRPM2 channels, modulate AJ protein composition and facilitate the recovery of HPMEC barrier function after

## H<sub>2</sub>O<sub>2</sub> exposure.

We found that TRPV2, a redox-sensitive channel, played a significant role in mediating HPMEC response to ROS.  $\rm H_2O_2$  exposure triggered an  $\rm [Ca^{2+}]_i$  increase within 5 min, a reaction which was significantly reduced upon pharmacological inhibition of TRPV2. While the intracellular localization pattern of TRPV2 has not been determined in pulmonary endothelial cells, TRPV2 is rapidly translocated from internal

stores to the plasma membrane upon application of insulin-like growth factor 1 (IGF-1) to CHO cells [37] or the chemotactic peptide fMetLeu-Phe to macrophages [38]. Upon stimulation, TRPV2 localizes at the cell podosome [39], a membrane region of endothelial cells [40] that supports cell motility through localized proteolysis [41]. While we did not study the mechanisms of TRPV2 translocation, we observed that TRPV2 inhibition prevented the H<sub>2</sub>O<sub>2</sub>-driven proteolytic cleavage of VE-cadherin (Fig. 2A), a known substrate of the Ca<sup>2+</sup>-activated protease ADAM10 Therefore, we propose [17]. TRPV2/ADAM10/VE-cadherin pathway through which HPMECs respond to ROS via ectodomain cleavage of VE-cadherin. Upon exposure to ROS, TRPV2 is activated, and the resulting Ca<sup>2+</sup> influx activates the metalloprotease ADAM10, possibly through the Ca<sup>2+</sup>-activated scramblase, anoctamin 6 (ANO6) [42]. This cleavage event may not be restricted to ADAM10 and VE-cadherin, and the involvement of other Ca<sup>2+</sup>-activated proteases and their cell-adhesion substrates presents a promising avenue for further study. In addition, it remains to be determined whether the extracellular fragment of VE-cadherin released during this process plays a role in downstream signaling, as is the case with its epithelial counterpart E-cadherin [43].

Our study also offers insight into the complex function of TRPM2 in mediating vascular permeability. We observed that the initial H<sub>2</sub>O<sub>2</sub>driven [Ca<sup>2+</sup>]<sub>i</sub> increase in HPMECs was significantly reduced upon pharmacological inhibition of TRPM2, confirming the findings of previous studies [9,22]. In one such study, Mittal et al. described TRPM2-dependent changes in the VE-cadherin phosphorylation state at tyrosine residue 731, a site involved in VE-cadherin internalization [22, 44-46]. Our results demonstrated that VE-cadherin Y731 was dephosphorylated within 5 min of H<sub>2</sub>O<sub>2</sub> exposure, but that this process occurred independent of TRPM2 signaling. Our data suggest that, instead, TRPM2 facilitates HPMEC barrier recovery by maintaining cellular redox homeostasis, as has been described in interstitial macrophages [47], neutrophils [48], and myocytes [49]. As in these other cell types, we found that HPMECs pretreated with the TRPM2 inhibitor econazole had significantly elevated ROS levels compared to DMSO treated controls. This elevated oxidative stress in the absence of TRPM2 functionality could activate the TRPV2/ADAM10 pathway, which would account for the enhanced VE-cadherin cleavage observed under both baseline and H<sub>2</sub>O<sub>2</sub>-stimulated conditions upon TRPM2 inhibition. While both TRPM2 and TRPV2 mediate H<sub>2</sub>O<sub>2</sub> –induced Ca<sup>2+</sup> influx, our results demonstrate that the two channels serve different roles in HPMEC response to H<sub>2</sub>O<sub>2</sub>. This discrepancy could be attributed to channel localization and density, the study of which may be more feasible with the advent of novel specific antibodies and nanobodies. There is also the possibility that TRPV2 may facilitate localized Ca<sup>2+</sup> influx, or "Ca2+ sparklets," as has been described for TRPV4 in the vascular endothelium (reviewed in Ref. [50]).

The protective role of TRPM2 was also apparent in our measurements of HPMEC barrier resistance. Not only were HPMECs pretreated with econazole unable to recover their barrier integrity following 75 μM H<sub>2</sub>O<sub>2</sub> exposure, but their barrier resistance continued to drop significantly over the course of 90 min. Unexpectedly, inhibition of the TRPV2/ADAM10 pathway also significantly limited the recovery of HPMEC barrier integrity after H2O2 exposure. One possible biological explanation for why a destructive process such as ectodomain cleavage could be beneficial for barrier recovery is to facilitate the process of "cadherin switching". In the endothelium, VE-cadherin localizes primarily to AJs at the plasma membrane, where it is thought to contribute to contact inhibition of cell growth and proliferation [51,52]. N-cadherin, in contrast, is associated with cell migration and wound healing and is unable to translocate to the plasma membrane in the presence of VE-cadherin complexes at AJs [51,53]. Upon the disruption of VE-cadherin junctional organization, N-cadherin translocates to the cell surface, where it can form heterotypic adhesions with neighboring cells. The resulting N-cadherin adhesion complex promotes Rac1 activation, which in turn induces the reorganization of VE-cadherin at AJs [54]. We

were able to observe this transient localization of N-cadherin at AJs in our timecourse immunofluorescence stainings, a process that did not occur upon inhibition of TRPV2 or ADAM10. Our results support a pathway by which redox-sensitive TRPV2 channels trigger the disruption of VE-cadherin dimers at HPMEC AJs through ADAM10-driven ectodomain cleavage. The resulting paracellular gaps are then rapidly repaired, possibly through N-cadherin-mediated recruitment of VE-cadherin. This pathway could be particularly relevant during leukocyte transmigration, which is characterized by  $\rm H_2O_2$  release [55], a temporary increase in paracellular permeability and a focal, transient loss of VE-cadherin complexes at AJs [4].

Future studies on the role of TRPV2 in pulmonary endothelial barrier function would benefit from the application of in vivo or ex vivo models. The isolated perfused and ventilated lung, for example, has been instrumental in toxicant screening [56], in highlighting TRPV4's role in ventilator-induced alveolar permeability [57], as well as in the investigation of H<sub>2</sub>O<sub>2</sub>-induced pulmonary edema [58,59]. Murine models could also give insight into the long-term transcriptional and translational regulation of the TRPV2/ADAM10 pathway. For example, mice exposed to cigarette smoke, an inducer of ROS and oxidative stress, showed reduced TRPV2 protein expression in alveolar macrophages [60]. It remains to be determined if this effect occurs in endothelial cells, but it is possible that TRPV2 and ADAM10-mediated VE-cadherin cleavage under chronic ROS exposure is kept in check through transcriptional regulation of TRPV2. Furthermore, additional histological studies on human biopsy tissue could provide more specific insight into the in situ membrane localization of TRPV2, which has previously been shown to differ from that of other TRP channels in epithelial cells [61]. Differing localization patterns could explain why TRPV2 was responsible for VE-cadherin cleavage in our HPMECs, in contrast to TRPV4, which has been reported to induce E-cadherin shedding in alveolar epithelial cells [62].

In summary, we confirmed that TRPM2 is only partially responsible for endothelial  ${\rm Ca}^{2+}$  influx following oxidative signaling and identified TRPV2 as an additional redox-sensitive contributor. We described a novel signaling pathway by which TRPV2 activation alters AJ composition through ADAM10-mediated VE-cadherin cleavage and determined that this pathway is essential for endothelial barrier recovery following oxidative injury. These findings establish a foundation for future studies exploring redox-regulated pulmonary endothelial repair pathways in translationally relevant model.

## CRediT authorship contribution statement

Lena Schaller: Writing – review & editing, Writing – original draft, Methodology, Investigation, Formal analysis, Data curation, Conceptualization. Martina Kiefmann: Writing – review & editing, Supervision, Conceptualization. Thomas Gudermann: Writing – review & editing, Project administration. Alexander Dietrich: Writing – review & editing, Visualization, Supervision, Resources, Project administration, Methodology, Investigation, Funding acquisition, Formal analysis, Conceptualization.

# Data availability

All data are available in the main text or the supplementary materials.

## **Funding**

This study was supported by grants from the Deutsche Forschungsgemeinschaft (TRR152 (TG, AD), and GRK 2338 (LS, TG, AD), Deutsches Zentrum für Lungenforschung (DZL) (TG, AD), Germany.

### Declaration of competing interest

The authors declare that they have no known competing financial interests or personal relationships that could have appeared to influence the work reported in this paper.

#### Acknowledgments

The authors would like to thank Bettina Braun and Benedikt Kirmayer for their excellent technical assistance.

## Appendix A. Supplementary data

Supplementary data to this article can be found online at https://doi.org/10.1016/j.redox.2025.103720.

#### References

- [1] S. Simmons, L. Erfinanda, C. Bartz, W.M. Kuebler, Novel mechanisms regulating endothelial barrier function in the pulmonary microcirculation, J. Physiol. 597 (2019) 997–1021, https://doi.org/10.1113/jp276245.
- [2] H.C. Müller-Redetzky, N. Suttorp, M. Witzenrath, Dynamics of pulmonary endothelial barrier function in acute inflammation: mechanisms and therapeutic perspectives, Cell Tissue Res. 355 (2014) 657–673, https://doi.org/10.1007/ s00441-014-1821-0.
- [3] D. Mehta, A.B. Malik, Signaling mechanisms regulating endothelial permeability, Physiol. Rev. 86 (2006) 279–367, https://doi.org/10.1152/physrev.00012.2005.
- [4] J.R. Allport, W.A. Muller, F.W. Luscinskas, Monocytes induce reversible focal changes in vascular endothelial cadherin complex during transendothelial migration under flow, J. Cell Biol. 148 (2000) 203–216, https://doi.org/10.1083/ ich.148 1 203
- [5] C.Y. Wang, C.S. Calfee, D.W. Paul, D.R. Janz, A.K. May, H. Zhuo, G.R. Bernard, M. A. Matthay, L.B. Ware, K.N. Kangelaris, One-year mortality and predictors of death among hospital survivors of acute respiratory distress syndrome, Intensive Care Med. 40 (2014) 388–396, https://doi.org/10.1007/s00134-013-3186-3.
- [6] P. Theofilis, M. Sagris, E. Oikonomou, A.S. Antonopoulos, G. Siasos, C. Tsioufis, D. Tousoulis, Inflammatory mechanisms contributing to endothelial dysfunction, Biomedicines 9 (2021), https://doi.org/10.3390/biomedicines9070781.
- [7] T. Fukai, M. Ushio-Fukai, Cross-talk between NADPH oxidase and mitochondria: role in ROS signaling and angiogenesis, Cells 9 (2020), https://doi.org/10.3390/cells9081849.
- [8] N. Urao, V. Sudhahar, S.J. Kim, G.F. Chen, R.D. McKinney, G. Kojda, T. Fukai, M. Ushio-Fukai, Critical role of endothelial hydrogen peroxide in post-ischemic neovascularization, PLoS One 8 (2013) e57618, https://doi.org/10.1371/journal. pone.0057618.
- [9] C.M. Hecquet, G.U. Ahmmed, S.M. Vogel, A.B. Malik, Role of TRPM2 channel in mediating H2O2-induced Ca2+ entry and endothelial hyperpermeability, Circ. Res. 102 (2008) 347–355, https://doi.org/10.1161/circresaha.107.160176.
- [10] M.A. Incalza, R. D'Oria, A. Natalicchio, S. Perrini, L. Laviola, F. Giorgino, Oxidative stress and reactive oxygen species in endothelial dysfunction associated with cardiovascular and metabolic diseases, Vasc. Pharmacol. 100 (2018) 1–19, https:// doi.org/10.1016/j.vph.2017.05.005.
- [11] H. Lum, K.A. Roebuck, Oxidant stress and endothelial cell dysfunction, Am. J. Physiol. Cell Physiol. 280 (2001) C719–C741, https://doi.org/10.1152/ aipcell.2001.280.4.C719.
- [12] N. Takahashi, D. Kozai, R. Kobayashi, M. Ebert, Y. Mori, Roles of TRPM2 in oxidative stress, Cell Calcium 50 (2011) 279–287, https://doi.org/10.1016/j. ceca.2011.04.006.
- [13] J. Yun, P. Rocic, Y.F. Pung, S. Belmadani, A.C. Carrao, V. Ohanyan, W.M. Chilian, Redox-dependent mechanisms in coronary collateral growth: the "redox window" hypothesis, Antioxidants Redox Signal. 11 (2009) 1961–1974, https://doi.org/ 10.1089/ars.2009.2476.
- [14] S.M. Troyanovsky, Adherens junction: the ensemble of specialized cadherin clusters, Trends Cell Biol. 33 (2023) 374–387, https://doi.org/10.1016/j. tcb.2022.08.007.
- [15] H. Lum, A.B. Malik, Regulation of vascular endothelial barrier function, Am. J. Physiol. 267 (1994) L223–L241, https://doi.org/10.1152/ajplung.1994.267.3.
- [16] M. Tatsumi, T. Kishi, S. Ishida, H. Kawana, A. Uwamizu, Y. Ono, K. Kawakami, J. Aoki, A. Inoue, Ectodomain shedding of EGFR ligands serves as an activation readout for TRP channels, PLoS One 18 (2023) e0280448, https://doi.org/ 10.1371/journal.pone.0280448.
- [17] B. Schulz, J. Pruessmeyer, T. Maretzky, A. Ludwig, C.P. Blobel, P. Saftig, K. Reiss, ADAM10 regulates endothelial permeability and T-Cell transmigration by proteolysis of vascular endothelial cadherin, Circ. Res. 102 (2008) 1192–1201, https://doi.org/10.1161/circresaha.107.169805.
- [18] R. Ding, Y.L. Yin, L.H. Jiang, Reactive oxygen species-induced TRPM2-mediated Ca (2+) signalling in endothelial cells, Antioxidants (Basel) 10 (2021), https://doi. org/10.3390/antiox10050718.
- [19] P. Malko, L.H. Jiang, TRPM2 channel-mediated cell death: an important mechanism linking oxidative stress-inducing pathological factors to associated

- pathological conditions, Redox Biol. 37 (2020) 101755, https://doi.org/10.1016/j.redox.2020.101755.
- [20] L.H. Jiang, W. Yang, J. Zou, D.J. Beech, TRPM2 channel properties, functions and therapeutic potentials, Expert Opin. Ther. Targets 14 (2010) 973–988, https://doi. org/10.1517/14728222.2010.510135.
- [21] B. Tóth, I. Iordanov, L. Csanády, Selective profiling of N- and C-terminal nucleotide-binding sites in a TRPM2 channel, J. Gen. Physiol. 152 (2020), https://doi.org/10.1085/jgp.201912533.
- [22] M. Mittal, N. Urao, C.M. Hecquet, M. Zhang, V. Sudhahar, X.P. Gao, Y. Komarova, M. Ushio-Fukai, A.B. Malik, Novel role of reactive oxygen species-activated Trp melastatin channel-2 in mediating angiogenesis and postischemic neovascularization, Arterioscler. Thromb. Vasc. Biol. 35 (2015) 877–887, https://doi.org/10.1161/atvbaha.114.304802.
- [23] A. Peralvarez-Marin, P. Donate-Macian, R. Gaudet, What do we know about the transient receptor potential vanilloid 2 (TRPV2) ion channel? FEBS J. 280 (2013) 5471–5487, https://doi.org/10.1111/febs.12302.
- [24] T.C. Fricke, F. Echtermeyer, J. Zielke, J. de la Roche, M.R. Filipovic, S. Claverol, C. Herzog, M. Tominaga, R.A. Pumroy, V.Y. Moiseenkova-Bell, et al., Oxidation of methionine residues activates the high-threshold heat-sensitive ion channel TRPV2, Proc. Natl. Acad. Sci. U. S. A. 116 (2019) 24359–24365, https://doi.org/10.1073/pnas.1904332116.
- [25] M. Oda, Y. Fujiwara, Y. Ishizaki, K. Shibasaki, Oxidation sensitizes TRPV2 to chemical and heat stimuli, but not mechanical stimulation, Biochem Biophys Rep 28 (2021) 101173, https://doi.org/10.1016/j.bbrep.2021.101173.
- [26] J.C. Schupp, T.S. Adams, C. Cosme, M.S.B. Raredon, Y. Yuan, N. Omote, S. Poli, M. Chioccioli, K.-A. Rose, E.P. Manning, et al., Integrated single-cell atlas of endothelial cells of the human lung, Circulation (New York, N. Y.) 144 (2021) 286–302, https://doi.org/10.1161/CIRCULATIONAHA.120.052318.
- [27] H. Luo, E. Rossi, B. Saubamea, S. Chasseigneaux, V. Cochois, N. Choublier, M. Smirnova, F. Glacial, N. Perriere, S. Bourdoulous, et al., Cannabidiol increases proliferation, migration, tubulogenesis, and integrity of human brain endothelial cells through TRPV2 activation, Mol. Pharm. 16 (2019) 1312–1326, https://doi. org/10.1021/acs.molpharmaceut.8b01252.
- [28] P.C. Villalta, M.I. Townsley, Transient receptor potential channels and regulation of lung endothelial permeability, Pulm. Circ. 3 (2013) 802–815, https://doi.org/ 10.1086/674765.
- [29] X. Zheng, W. Zhang, X. Hu, Different concentrations of lipopolysaccharide regulate barrier function through the PI3K/Akt signalling pathway in human pulmonary microvascular endothelial cells, Sci. Rep. 8 (2018) 9963, https://doi.org/10.1038/ s41598-018-28089-3.
- [30] A. Ludwig, C. Hundhausen, M.H. Lambert, N. Broadway, R.C. Andrews, D. M. Bickett, M.A. Leesnitzer, J.D. Becherer, Metalloproteinase inhibitors for the disintegrin-like metalloproteinases ADAM10 and ADAM17 that differentially block constitutive and phorbol ester-inducible shedding of cell surface molecules, Comb. Chem. High Throughput Screen. 8 (2005) 161–171, https://doi.org/10.2174/1386207053258488.
- [31] J. Conde, R.A. Pumroy, C. Baker, T. Rodrigues, A. Guerreiro, B.B. Sousa, M. C. Marques, B.P. de Almeida, S. Lee, E.P. Leites, et al., Allosteric antagonist modulation of TRPV2 by piperlongumine impairs glioblastoma progression, ACS Cent. Sci. 7 (2021) 868–881, https://doi.org/10.1021/acscentsci.1c00070.
- [32] Y. Bluhm, R. Raudszus, A. Wagner, N. Urban, M. Schaefer, K. Hill, Valdecoxib blocks rat TRPV2 channels, Eur. J. Pharmacol. 915 (2022) 174702, https://doi. org/10.1016/j.eiphar.2021.174702.
- [33] M. Cheung, W. Bao, D.J. Behm, C.A. Brooks, M.J. Bury, S.E. Dowdell, H.S. Eidam, R.M. Fox, K.B. Goodman, D.A. Holt, et al., Discovery of GSK2193874: an orally active, potent, and selective blocker of transient receptor potential vanilloid 4, ACS Med. Chem. Lett. 8 (2017) 549–554, https://doi.org/10.1021/acsmedchemlett.7b00094.
- [34] K. Hill, S. McNulty, A.D. Randall, Inhibition of TRPM2 channels by the antifungal agents clotrimazole and econazole, Naunyn-Schmiedebergs Arch Pharmacol 370 (2004) 227–237, https://doi.org/10.1007/s00210-004-0981-y.
- [35] L. Fourgeaud, C. Dvorak, M. Faouzi, J. Starkus, S. Sahdeo, Q. Wang, B. Lord, H. Coate, N. Taylor, Y. He, et al., Pharmacology of JNJ-28583113: a novel TRPM2 antagonist, Eur. J. Pharmacol. 853 (2019) 299–307, https://doi.org/10.1016/j. ejphar.2019.03.043.
- [36] T. Finkel, Signal transduction by reactive oxygen species, J. Cell Biol. 194 (2011) 7–15, https://doi.org/10.1083/jcb.201102095.
- [37] M. Kanzaki, Y.Q. Zhang, H. Mashima, L. Li, H. Shibata, I. Kojima, Translocation of a calcium-permeable cation channel induced by insulin-like growth factor-I, Nat. Cell Biol. 1 (1999) 165–170.
- [38] M. Nagasawa, Y. Nakagawa, S. Tanaka, I. Kojima, Chemotactic peptide fMetLeuPhe induces translocation of the TRPV2 channel in macrophages, J. Cell. Physiol. 210 (2007) 692–702, https://doi.org/10.1002/jcp.20883.
- [39] M. Nagasawa, I. Kojima, Translocation of calcium-permeable TRPV2 channel to the podosome: its role in the regulation of podosome assembly, Cell Calcium 51 (2012) 186–193, https://doi.org/10.1016/j.ceca.2011.12.012.
- [40] Y.N. Rui, Y. Chen, Y. Guo, C.E. Bock, J.P. Hagan, D.H. Kim, Z. Xu, Podosome formation impairs endothelial barrier function by sequestering zonula occludens proteins, J. Cell. Physiol. 235 (2020) 4655–4666, https://doi.org/10.1002/ jcp.29343.
- [41] S. Linder, M. Aepfelbacher, Podosomes: adhesion hot-spots of invasive cells, Trends Cell Biol. 13 (2003) 376–385, https://doi.org/10.1016/s0962-8924(03)00128-4.
- [42] K. Reiss, S. Leitzke, J. Seidel, M. Sperrhacke, S. Bhakdi, Scramblases as regulators of proteolytic ADAM function, Membranes 12 (2022) 185.
- [43] K. Reiss, A. Ludwig, P. Saftig, Breaking up the tie: disintegrin-like metalloproteinases as regulators of cell migration in inflammation and invasion,

- Pharmacol. Ther. 111 (2006) 985–1006, https://doi.org/10.1016/j.pharmthera.2006.02.009.
- [44] M. Mittal, S. Nepal, Y. Tsukasaki, C.M. Hecquet, D. Soni, J. Rehman, C. Tiruppathi, A.B. Malik, Neutrophil activation of endothelial cell-expressed TRPM2 mediates transendothelial neutrophil migration and vascular injury, Circ. Res. 121 (2017) 1081–1091, https://doi.org/10.1161/CIRCRESAHA.117.311747.
- [45] F. Wessel, M. Winderlich, M. Holm, M. Frye, R. Rivera-Galdos, M. Vockel, R. Linnepe, U. Ipe, A. Stadtmann, A. Zarbock, et al., Leukocyte extravasation and vascular permeability are each controlled in vivo by different tyrosine residues of VE-cadherin, Nat. Immunol. 15 (2014) 223–230, https://doi.org/10.1038/ ni.2824.
- [46] N. Arif, M. Zinnhardt, A. Nyamay'Antu, D. Teber, R. Brückner, K. Schaefer, Y.T. Li, B. Trappmann, C. Grashoff, D. Vestweber, PECAM-1 supports leukocyte diapedesis by tension-dependent dephosphorylation of VE-cadherin, EMBO J. 40 (2021) e106113, https://doi.org/10.15252/embj.2020106113.
- [47] S. Rajan, C. Schremmer, J. Weber, P. Alt, F. Geiger, A. Dietrich, Ca(2+) signaling by TRPV4 channels in respiratory function and disease, Cells 10 (2021), https://doi.org/10.3390/cells10040822.
- [48] A. Di, X.-P. Gao, F. Qian, T. Kawamura, J. Han, C. Hecquet, R.D. Ye, S.M. Vogel, A. B. Malik, The redox-sensitive cation channel TRPM2 modulates phagocyte ROS production and inflammation, Nat. Immunol. 13 (2012) 29–34, https://doi.org/10.1038/ni.2171.
- [49] B.A. Miller, J. Wang, I. Hirschler-Laszkiewicz, E. Gao, J. Song, X.Q. Zhang, W. J. Koch, M. Madesh, K. Mallilankaraman, T. Gu, et al., The second member of transient receptor potential-melastatin channel family protects hearts from ischemia-reperfusion injury, Am. J. Physiol. Heart Circ. Physiol. 304 (2013) H1010–H1022, https://doi.org/10.1152/ajpheart.00906.2012.
- [50] M.N. Sullivan, S. Earley, TRP channel Ca(2+) sparklets: fundamental signals underlying endothelium-dependent hyperpolarization, Am. J. Physiol. Cell Physiol. 305 (2013) C999–C1008, https://doi.org/10.1152/ajpcell.00273.2013.
- [51] G. Bazzoni, E. Dejana, Endothelial cell-to-cell junctions: molecular organization and role in vascular homeostasis, Physiol. Rev. 84 (2004) 869–901, https://doi. org/10.1152/physrev.00035.2003.
- [52] M. Grazia Lampugnani, A. Zanetti, M. Corada, T. Takahashi, G. Balconi, F. Breviario, F. Orsenigo, A. Cattelino, R. Kemler, T.O. Daniel, et al., Contact inhibition of VEGF-induced proliferation requires vascular endothelial cadherin, beta-catenin, and the phosphatase DEP-1/CD148, J. Cell Biol. 161 (2003) 793–804, https://doi.org/10.1083/jcb.200209019.

- [53] P. Navarro, L. Ruco, E. Dejana, Differential localization of VE- and N-cadherins in human endothelial cells: VE-cadherin competes with N-cadherin for junctional localization, J. Cell Biol. 140 (1998) 1475–1484, https://doi.org/10.1083/ ich.1406.1475
- [54] K. Kruse, Q.S. Lee, Y. Sun, J. Klomp, X. Yang, F. Huang, M.Y. Sun, S. Zhao, Z. Hong, S.M. Vogel, et al., N-cadherin signaling via Trio assembles adherens junctions to restrict endothelial permeability, J. Cell Biol. 218 (2019) 299–316, https://doi. org/10.1083/jcb.201802076.
- [55] X. Liu, J.L. Zweier, A real-time electrochemical technique for measurement of cellular hydrogen peroxide generation and consumption: evaluation in human polymorphonuclear leukocytes, Free Radic. Biol. Med. 31 (2001) 894–901, https:// doi.org/10.1016/S0891-5849(01)00665-7.
- [56] C. Schremmer, D. Steinritz, T. Gudermann, D.J. Beech, A. Dietrich, An ex vivo perfused ventilated murine lung model suggests lack of acute pulmonary toxicity of the potential novel anticancer agent (-)-englerin A, Arch. Toxicol. 96 (2022) 1055–1063, https://doi.org/10.1007/s00204-022-03235-z.
- [57] J. Weber, S. Rajan, C. Schremmer, Y.K. Chao, G. Krasteva-Christ, M. Kannler, A. O. Yildirim, M. Brosien, J. Schredelseker, N. Weissmann, et al., TRPV4 channels are essential for alveolar epithelial barrier function as protection from lung edema, JCI Insight 5 (2020), https://doi.org/10.1172/jci.insight.134464.
- [58] Y. Chiba, Y. Ishii, S. Kitamura, Y. Sugiyama, Activation of rho is involved in the mechanism of hydrogen-peroxide-induced lung edema in isolated perfused rabbit lung, Microvasc. Res. 62 (2001) 164–171, https://doi.org/10.1006/ mvre.2001.2329.
- [59] M.P. Habib, N.C. Clements, Effects of low-dose hydrogen peroxide in the isolated perfused rat lung, Exp. Lung Res. 21 (1995) 95–112, https://doi.org/10.3109/ 01902149509031747.
- [60] H. Masubuchi, M. Ueno, T. Maeno, K. Yamaguchi, K. Hara, H. Sunaga, H. Matsui, M. Nagasawa, I. Kojima, Y. Iwata, et al., Reduced transient receptor potential vanilloid 2 expression in alveolar macrophages causes COPD in mice through impaired phagocytic activity, BMC Pulm. Med. 19 (2019) 70, https://doi.org/10.1186/s12890-019-0821-y.
- [61] W. Yu, W.G. Hill, G. Apodaca, M.L. Zeidel, Expression and distribution of transient receptor potential (TRP) channels in bladder epithelium, Am. J. Physiol. Ren. Physiol. 300 (2011) F49–F59, https://doi.org/10.1152/ajprenal.00349.2010.
- [62] L. Schaller, T. Gudermann, A. Dietrich, TRPV4 mediates alveolar epithelial barrier integrity and induces ADAM10-driven E-cadherin shedding, Cells 13 (2024), https://doi.org/10.3390/cells13201717.

# TRPV2 channels facilitate pulmonary endothelial barrier recovery after ROS-induced permeability

Lena Schaller, Martina Kiefmann, Thomas Gudermann, Alexander Dietrich\*

Walther Straub Institute for Pharmacology and Toxicology, Member of the German Center for Lung Research (DZL), School of Medicine, LM University of Munich, Nußbaumstrasse 26, 80336 Munich, Germany.

\*Corresponding author. Email: <u>alexander.dietrich@lrz.uni-muenchen.de</u>.

# **Supplementary Methods**

# **Reagents and Antibodies**

The following reagents and antibodies were used: High glucose Dulbecco's Modified Eagle Medium (DMEM, Thermo Fisher Scientific, Waltham, MA, USA, #41965039); hydrogen peroxide solution (Merck, Darmstadt, Germany, H1009); Gl254023X (Tocris, Bristol, UK, #3995); econazole (Merck, Y0001236); JNJ-28583113 (MedChemExpress, Monmouth Junction, NJ, USA, #HY-149143); tranilast (Tocris, #1098); valdecoxib (Merck, #PZ0179); cannabidiol (Cayman Chemical, #90080, Ann Arbor, MI, USA); GSK2193874 (Tocris, #5106); anti-VE-Cadherin antibody (Cell Signaling, Danvers, MA, US, #2500); anti-phospho-VE-Cadherin (Tyr731) antibody (Thermo Fisher Scientific, #441145G); anti-N-Cadherin antibody (BD Biosciences, Franklin Lakes, NJ, US, #610920); horseradish peroxidase (HRP)-conjugated anti-β-actin antibody (Merck, #A3854); anti-TRPM2 antibody (Bethyl, Montgomery, TX, USA, #A300-414A); anti-TRPV2 antibody (Abcam, Cambridge, UK, Ab272862); peroxidase (POX)-conjugated anti-rabbit antibody (Merck, #A1654); horseradish peroxidase (HRP)-conjugated anti-mouse antibody (Cell Signaling, #7076); goat anti-rabbit IgG Alexa Fluor 488 (Thermo Fisher Scientific, #A11008); goat anti-mouse IgG Alexa Fluor 594 (Thermo Fisher Scientific, #A11005). See complete antibody information in Supp. Table S3.

## SiRNA knockdown of TRPV2 and TRPM2

Pools of TRPV2 siRNAs (100 nM, ON-TARGETplus, Horizon Discovery, Cambridge, UK, #L-004194-00-0050), TRPM2 siRNAs (30 nM, ON-TARGETplus, Horizon Discovery, #L-004193-00-0005), or nonspecific control siRNAs (ON-TARGETplus, Horizon Discovery, #D-001810-10-50) were introduced to HPMECs through reverse transcription using the DharmaFECT 2 transfection reagent (Horizon Discovery, #T-2002-03), per manufacturer's instructions. Media was replaced after 24 h, and cells were allowed to grow to confluency over a period of 3 days, at which point cells were lysed for RNA isolation or treated and harvested for Western blotting. Knockdown efficacy was determined through qRT-PCR and Western blotting.

# **Cell Surface Biotinylation and Cell Fractionation**

HPMEC surface proteins following H<sub>2</sub>O<sub>2</sub> exposure were isolated through surface biotinylation. Briefly, following exposure, HPMECs were washed once with ice cold PBS and incubated with the cell membrane impermeable biotinylation reagent EZ Link<sup>TM</sup> Sulfo-NHS-SS-Biotin (1 mg/ml, Thermo Fisher Scientific, #21217) for 1 h on ice. HPMECs were then washed with cold PBS, incubated with 50 mM glycine in PBS for 15 min to quench excess biotin, and subsequently washed twice in cold PBS. Cells were then lysed in 150 μl RIPA buffer (with protease and phosphatase inhibitors) for 1 h on ice. Lysates were spun at 14,000 rpm, 4 °C for 30 min. 50 μl of supernatant was added to 17 μl of streptavidinconjugated Dynabeads<sup>TM</sup> (Thermo Fisher Scientific, #11206D), and rotated overnight at 4 °C. The following day, biotin/bead bound proteins were magnetically separated from the unbiotinylated fraction, washed thrice in RIPA, and resuspended in RIPA with 1x Laemmli buffer (prepared from 5x stock: 3 ml TRIS/HCI (2.6 M), pH 6.8; 10 ml glycerin; 2 g SDS; 2 mg bromophenol blue; 5 ml β-mercaptoethanol). Samples for both fractions were then assessed using Western blot.

# **SDS-PAGE** and Western blot

The expression of VE-cadherin protein was evaluated by Western blot analysis as previously described [S1]. Following treatment, HPMECs were lysed in 150  $\mu$ l RIPA buffer (with protease and phosphatase inhibitors) for 30 min on ice. Protein concentration was quantified with the Pierce BCA Protein Assay Kit (Thermo Fisher Scientific, #23225) according to the manufacturer's protocol. Protein samples (10-30  $\mu$ g lysate, 1x Laemmli buffer (prepared from 5x stock: 3 ml TRIS/HCI (2.6 M), pH 6.8; 10 ml glycerin; 2 g

SDS; 2 mg bromophenol blue; 5 ml  $\beta$ -mercaptoethanol)) were heated for 10 min at 95 °C and loaded onto an SDS-PAGE gel (4 % stacking, 10 % separating). SDS-PAGE gel electrophoresis was run for 30 min at 80 V, and then at 120 V for 90 min. Proteins were then transferred from the gel to a Roti®-PVDF membrane (Roth, Karlsruhe, Germany, #T830.1) in a wet transfer system (BioRad, Feldkirchen, Germany) at 50 V for 1.5 h. The membrane was then blocked with 5 % low-fat milk (Roth, #T145.2) in TBS-T (0.1 % Tween20) for 1 h at RT. All antibodies were diluted in the milk blocking solution. See Supp. Table S3 for relevant antibody information. Membranes were incubated in the primary antibody solutions overnight at 4 °C. Afterwards, membranes were washed (3 x 10 min, TBS-T) and incubated for 2 h at RT in peroxidase-conjugated secondary antibody solutions. Chemiluminescence was detected following incubation in SuperSignal West Femto or Pico maximum sensitivity substrates (Life Technologies, CA, USA, #34095 and #34580), using an Odyssey-Fc unit (Licor, Lincoln, NE, USA). Uncut Western blot images for all samples and replicates can be found on the online Open Science Foundation repository, OSF DOI: 10.17605/OSF.IO/T3FJP.

# Ca<sup>2+</sup> Imaging

HPMECs were grown on poly-L-lysine-coated 24 mm glass coverslips until 80 % confluency. On the day of measurement, HPMECs were loaded with 2  $\mu$ M Fura-2-AM (Merck, #47989-1MG-F) in Ca<sup>2+</sup> buffer (0.1 % BSA in HBSS (with Ca<sup>2+</sup>, Mg<sup>2+</sup> and 0.5 M HEPES)) for 25 min at 37 °C. Coverslips were then washed with HEPES/HBSS buffer, placed into a quick-change chamber (Warner instruments, Holliston, USA, #64-0367) with 450 uL HEPES/HBSS, and positioned on the 40x oil-objective of a Leica DM98 fluorescence microscope. Changes in intracellular Ca<sup>2+</sup> concentration following the application of H<sub>2</sub>O<sub>2</sub> (300  $\mu$ M, Merck, #H1009) were recorded at 340 and 380 nm wavelengths, as described [S1]. For measurements involving pharmacological inhibition, the respective inhibitors were included in both the Fura incubation solution and the treatment solutions.

# **Immunocytochemistry**

HPMECs were seeded on poly-L-lysine-coated 12 mm glass coverslips. After treatment, cells were washed once with cold PBS, fixed in 4 % PFA/PBS (15 min, RT), and then washed thrice with cold PBS. Cells were permeabilized for 10 min at RT in a 0.2 % Triton X-100/PBS solution, and then washed 4 x 5 min in PBS-T (0.1 % Tween20 in PBS). HPMECs were blocked for 1 h in PBS with 0.1 % Tween20 and 5 % BSA, and then incubated overnight at 4 °C in primary antibody solutions prepared in blocking buffer. See complete antibody information in Supp. Table S3. The following day, cells were washed (4 x 5 min, PBS-T), incubated for 2 h at RT in secondary antibody solutions, and washed again (4 x 5 min, PBS-T). All antibodies were diluted in blocking buffer. Nuclei were stained with DAPI (0.1 mg/L in PBS) for 3 min at RT, after which cells were washed (4 x 5 min, PBS-T). Coverslips were mounted with PermaFluor mounting medium (Epredia, Kalamazoo, MI, USA, #TA-030-FM) and kept at 4 °C. Confocal images were taken with a Zeiss LSM 880 microscope (Zeiss, Oberkochen, Germany) using the ZEN Black software (Zeiss, version 2.3). Images were processed with FIJI software (Image J v.1.53c, Wayne Rasband, NIH, USA) [S2]. Signal quantification was performed with ZEN Blue and Black software (Zeiss, version 3.4). Regions of interest (ROI) were drawn along the borders of adjacent HPMECs. Mean Ncadherin and VE-cadherin signal intensity values from ten ROI were calculated for 3 images from each condition and timepoint. Colocalization analyses were conducted following the guidelines recommended by the software provider. Briefly, single-label control samples were used to set the gating for the experimental, double-labeled samples. VE-cadherin/N-cadherin colocalization coefficients were determined for ten ROI per image, with 3 images taken for each condition and timepoint. These immunocytochemistry experiments were replicated thrice in subsequent passages from one donor.

# **LDH Cytotoxicity Assay**

 $H_2O_2$ -induced cytotoxicity was assessed through an LDH assay (Merck, #11644793001), according to the manufacturer's protocol. Briefly, cells were incubated in 300  $\mu$ M  $H_2O_2$  for 2h, at which point the supernatant was collected and tested for the reduction of tetrazolium salt by NADH as a measure of LDH activity. Triton X100 (2 %) was applied as a positive control.

# Quantitative Reverse-Transcription (qRT)-PCR

Total RNA from HPMECs was isolated with the RNeasy Plus Mini Kit (Qiagen, Hilden, Germany, #74136). 1  $\mu$ g mRNA was then transcribed to cDNA using the RevertAid H Minus First Strand cDNA Synthesis Kit (Life Technologies, Darmstadt, Germany, #K1631), with reverse transcription polymerase and random primers according to the manufacturer's protocol. The levels of mRNA transcripts of target genes were assessed using real-time quantitative PCR, as described previously [S1]. Briefly, 3  $\mu$ l (15 ng) of template cDNA was added to 7  $\mu$ l of a master mix containing 2x Absolute QPCR SYBR Green Mix (Life Technologies, #AB1158B), 10 pmol of the respective primer pair (Metabion, Planegg, Germany, see table S4 for primer sequences) and water. For qRT-PCR, the following program was run in a light-cycler 480 device (Roche, Mannheim, Germany): activation (15 min, 94 °C); 45 cycles of

denaturation (12 s, 94  $^{\circ}$ C), annealing (30 s, 50  $^{\circ}$ C) and extension (30 s, 72  $^{\circ}$ C); and melting curve analysis. The default lightcycler software (Roche, Basel, Switzerland) allowed for the calculation of crossing points (Cps), which were used to calculate gene expression values.

# **Quantification of Reactive Oxygen Species (ROS)**

The cell-permeable, fluorigenic probe 2', 7'-dicholodihydrofluorescein diacetate (H<sub>2</sub>DCFDA) was used to semi-quantitatively assess ROS levels in HPMECs, as previously described [44]. HPMECs were plated at a density of 15,000 cells/well in 96 well plates and grown to confluency over 24-48 hrs, at which point HPMECs were pretreated with H<sub>2</sub>DCFDA (50  $\mu$ M, Thermo Fisher Scientific, #3135794) for 1 h in DMEM without phenol red. Cells were then washed once in warm DMEM without phenol red (Thermo Fisher Scientific, #21063029), and incubated with DMSO or econazole (10  $\mu$ M) in DMEM without phenol red for indicated time points. Fluorescence emitted by the oxidized DCF was detected using a microplate reader (Fluostar Omega, BMG labtech, Ortenberg, Germany). L-Cysteine (2 mM, Merck, #168159) was applied as an antioxidant negative control, and phorbol-12-myristat-13-acetate (PMA, 20  $\mu$ M) served as a positive control of intracellular ROS production.

## Statistical analysis

Statistical analysis was performed with GraphPad Prism 10 software (GraphPad Software, San Diego, USA). Significant differences are indicated by asterisks, where p < 0.05 (\*), 0.01 (\*\*\*), 0.001 (\*\*\*\*), and 0.0001 (\*\*\*\*\*).

# **Supplementary References**

- S1. Hofmann, K.; Fiedler S.; Vierkotten S.; Weber J.; Klee S.; Jia J.; Zwickenpflug, W.; Flockerzi, V.; Storch, U.; Yildirim AÖ.; Gudermann T.; Königshoff M, Dietrich A. Classical transient receptor potential 6 (TRPC6) channels support myofibroblast differentiation and development of experimental pulmonary fibrosis. *Biochim Biophys Acta Mol Basis Dis.* **2017**, *1863*, 560-568, doi: 10.1016/j.bbadis.2016.12.002.
- S2. Schindelin, J.; Arganda-Carreras, I..; Frise, E.; Kaynig, V.; Longair, M.; Pietzsch, T.; Preibisch S.; Rueden, C.; Saalfeld, S.; Schmid, B.; Tinevez, JY.; White, DJ.; Hartenstein, V.; Eliceiri, K.; Tomancak, P.; Cardona, A. Fiji: an open-source platform for biological-image analysis. *Nat Methods* **2012**, *9*, 676–682, doi: 10.1038/nmeth.2019.

# **Supplementary Tables and Figures**

**Table S1: HPMEC donor information (Promocell)** 

Donor ID (Lot #)	Catalogue #	Age	Sex	Ethnicity	Disease Status
467Z025.1	C-12281	61	Female	Caucasian	Healthy
463Z013.1	C-12281	57	Female	Caucasian	Healthy
489Z006.1	C-12281	51	Male	Caucasian	Healthy
489Z005	C-12281	52	Female	Caucasian	Healthy

Table S2: IC<sub>50</sub> values for TRP and ADAM inhibitors

Compound	Target	Expression System	Assay Type	IC <sub>50</sub>
Econazole	TRPM2	HEK293, hTRPM2	Electrophysiology	< 3 µM [34]
JNJ-28583113	TRPM2	HEK293, hTRPM2	Electrophysiology	126 nM [35]
Tranilast	TRPV2	HEK293T, hTRPV2	Fluorometric Assay	2.3 µM [31]
Valdecoxib	TRPV2	HEK293, rtTRPV2	Fluorometric Assay	9 µM [32]
GI254023X	ADAM10	COS-7, hADAM10	Enzymatic Cleavage Assay	5.3 nM [30]
GSK2193874	TRPV4	HEK293T, hTRPV4	Fluorometric Assay	2 nM [33]

Table S3: Antibodies used for Western blotting and immunocytochemistry

Primary Antibodies	Supplier	Cat. # / RRID	Dilution
VE-Cadherin (rb pAb)	Cell Signaling	2158 / AB_2077970	WB: 1:1,000; ICC: 1:400
Phospho-VE-cadherin	ThermoFisher	44-1145G / AB_2533584	WB: 1:1,000
(Tyr731) (rb pAb)	Scientific		
N-Cadherin (Mo pAb)	BD biosciences	610920 / AB_2077527	WB: 1:1,000; ICC: 1:400
TRPM2 (rb pAb)	Bethyl	A300-414A / AB_2208495	WB: 1:300
TRPV2 (rb pAb)	Abcam	Ab272862 / AB_2892218	WB: 1:300
B-actin-HRP (mo pAb)	Merck	A3854 / AB_262011	WB: 1:10,000

Secondary Antibodies	Supplier	Cat. # / RRID	Dilution
Rabbit IgG-POX	Merck	A6154 / AB_258284	WB: 1:10,000
Mouse IgG-HRP	Cell Signaling	7076 / AB_330924	WB: 1:10,000
Rabbit Alexa Fluor 488	ThermoFisher Scientific	A32731 / AB_2633280	ICC: 1:250
Mouse Alexa Fluor 594	ThermoFisher Scientific	A-11005 / AB_2534073	ICC: 1:250

Table S4: DNA-sequences of qRT-PCR primer pairs

Gene	Forward Primer	Reverse Primer
TRPC1	GAG AGC ATT TGA ACT TAG TGC TGA	TTA CAT TGC CGG GCT AGT TC
TRPC4	GGT CAG ACT TGA ACA GGC AAG	GTT TAA TTT CTC CCC ATA TGA AGC
TRPV2	CTG ACC GTT GGC ACT AAG C	CTC CCA TGA AGC CCA GTT C
TRPV4	GGA CAC GTG TGG GGA AGA	CAC AGC CAG CAT CTC GTG
TRPM2	GCC TCA GCT GCT TCG G	CTT CAC CAC CAG CAC TTC CA
TRPM7	AGA CTC GGC TTC TGC TGC TA	TCC AGG ATT TCT GGG ACA TTC TC

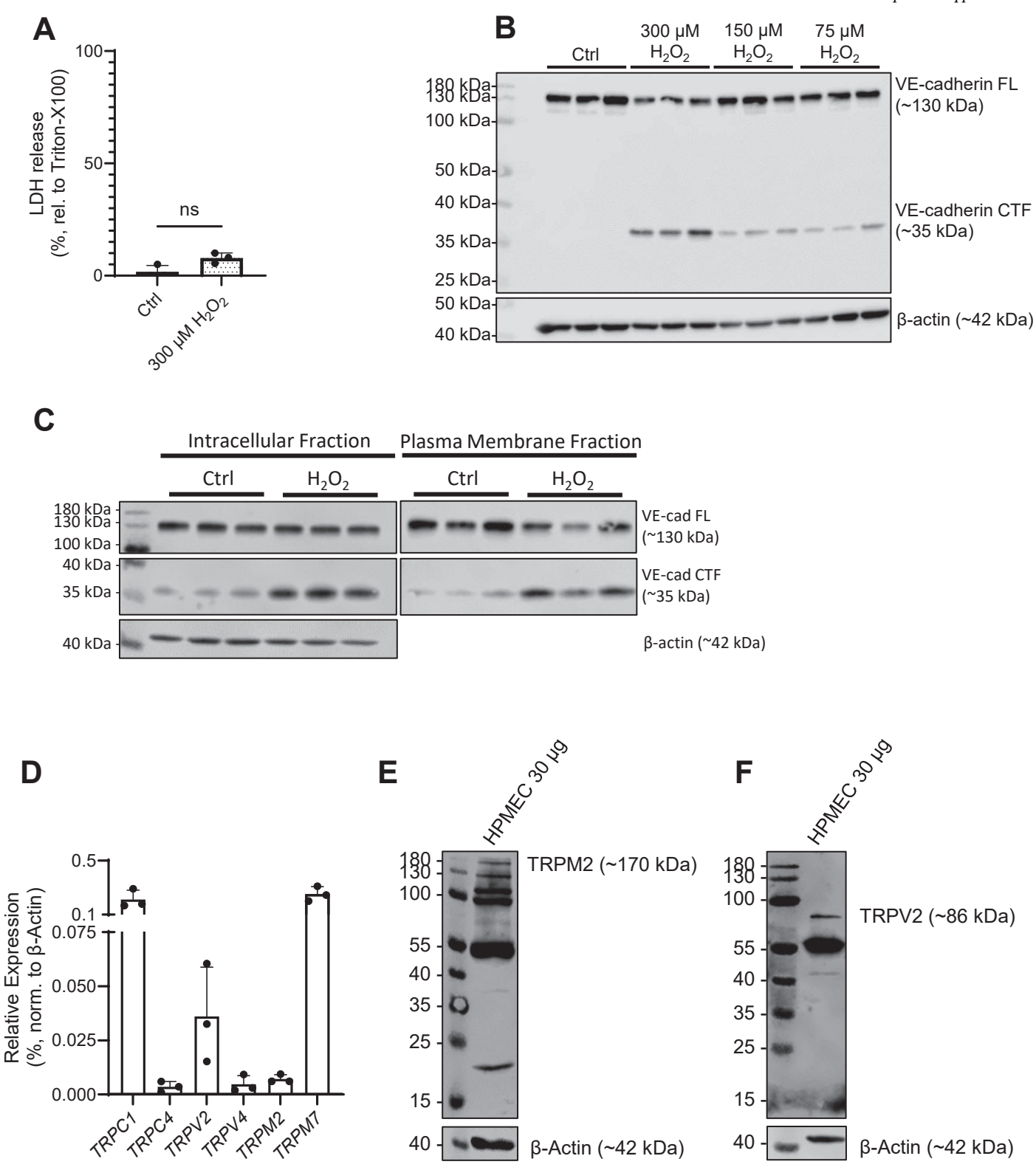


**Fig. S1.** Characterization of HPMECs and HPMEC response to  $H_2O_2$ . (A) Degree of cytolysis, measured in terms of lactate dehydrogenase (LDH) activity, in HPMECs after 2 h  $H_2O_2$  exposure (300 μM). Data represent the mean + SD of results from 3 independent donors (n = 3). Significance was assessed using a Wilcoxon test. ns = no significance. (B) Complete Western blot of the full length (FL) and C-terminal fragment (CTF) levels of VE-cadherin protein in HPMECs 2 h after  $H_2O_2$  exposure at varying concentrations (75 μM, 150 μM and 300 μM). β-actin was probed as a loading control. Data represent 3 technical replicates from one donor (n = 1). (C) Representative Western blot of VE-cadherin FL and CTF protein levels after 15 min  $H_2O_2$  exposure (300 μM). The intracellular and plasma membrane fractions of HPMEC protein lysates were separated through extracellular biotin labeling and streptavidin selection. β-actin was probed as a loading control. Data represent 3 technical replicates from one donor (n = 1). (D) TRP gene expression results, as detected by qRT-PCR, normalized to β-actin. Data reflect mean values + SD from 3 independent donors (n = 3). TRPM2 (E) and TRPV2 (F) proteins were detected in HPMEC lysates by Western blot, and β-actin was probed as a loading control.

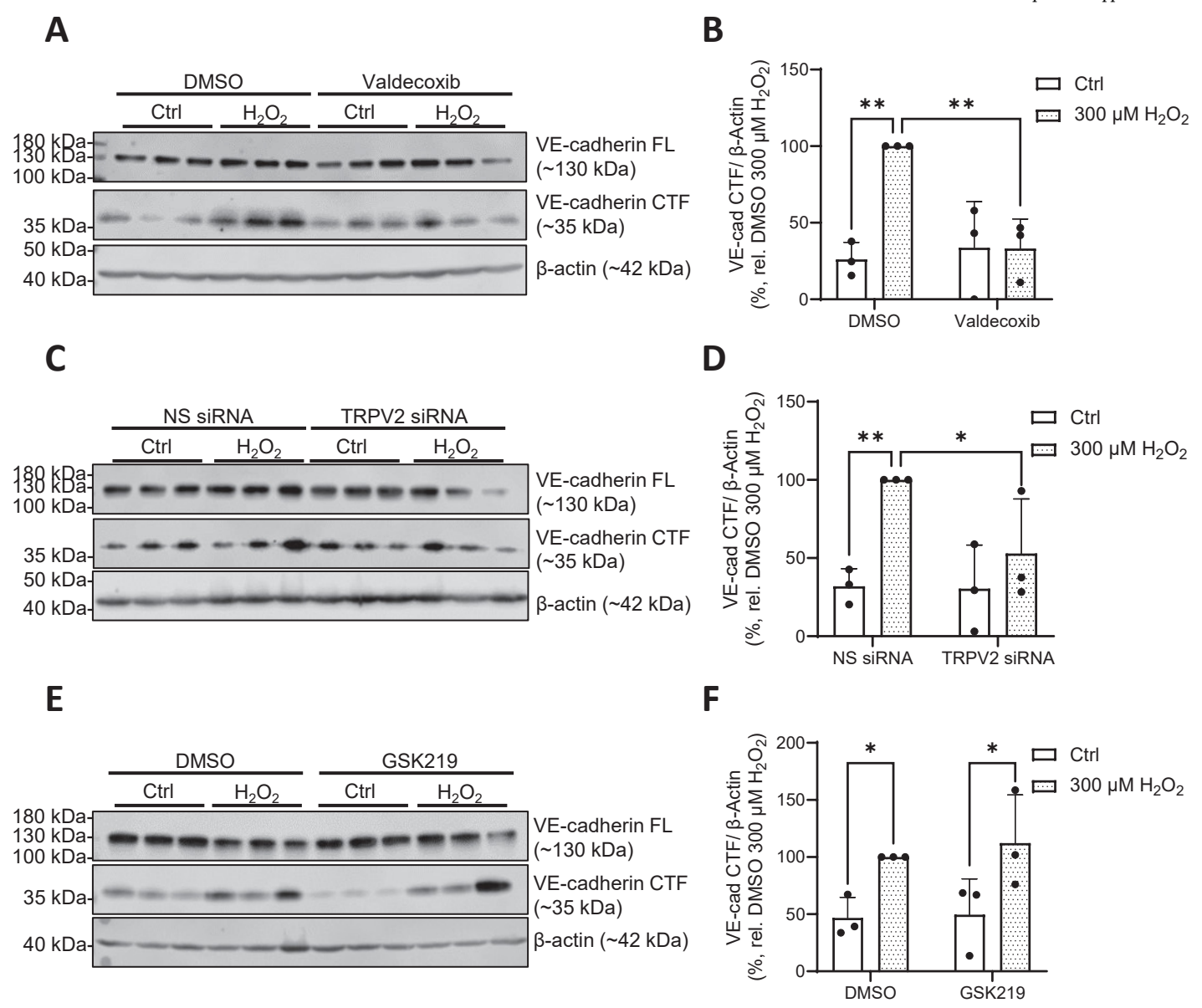


Fig. S2. Additional controls for TRPV2 modulation of HPMEC VE-cadherin upon  $H_2O_2$  exposure. Representative Western blots of FL and CTF VE-cadherin protein levels after  $H_2O_2$  exposure (2 h, 300 μM) upon TRPV2 inhibition (100 μM valdecoxib, (**A**, quantified in **B**)) or siRNA-mediated TRPV2 knockdown (100nM siRNA, NS = Nonspecific control, (**C**, quantified in **D**)). (**E**) Representative Western blot of FL and CTF VE-cadherin protein levels after  $H_2O_2$  exposure (2 h, 300 μM) upon TRPV4 inhibition (300 nM GSK2193874, quantified in **F**). For all Western blots, β-actin was probed for as a loading control, samples shown are from a single donor, 3 technical replicates. Western blot quantifications represent the mean + SD of results from 3 independent donors (**B**) or 3 consecutive passages from one donor (**D**, **F**); (n = 3). Normality of data was confirmed using the Shapiro-Wilk test, and significance between means was analyzed using two-way ANOVA, with Tukey post hoc test; \* p < 0.05, \*\* p < 0.01.

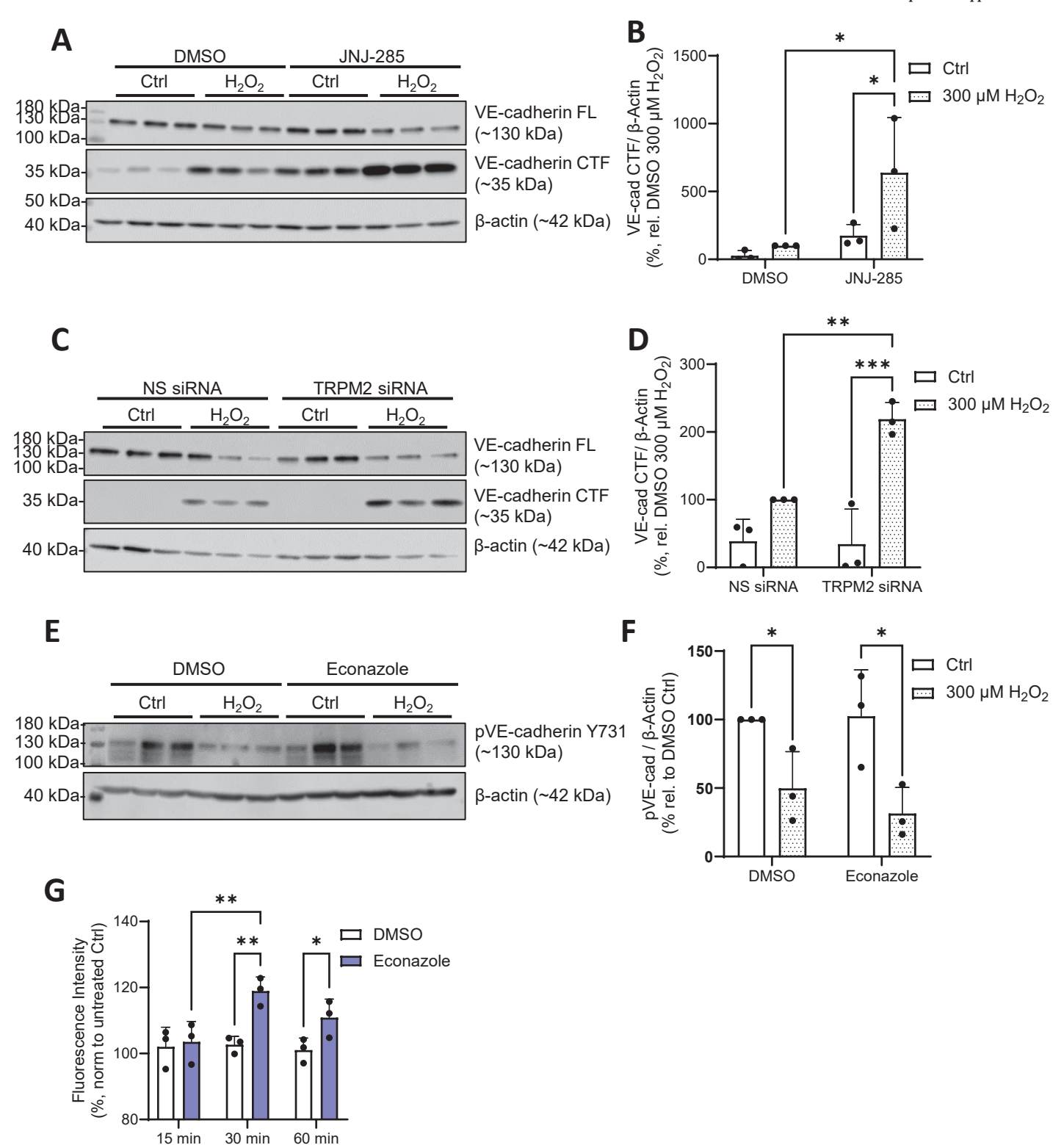


Fig. S3. Impaired TRPM2 functionality increases ADAM10-mediated HPMEC VE-cadherin cleavage. Representative Western blots of FL and CTF VE-cadherin protein levels after  $H_2O_2$  exposure (2 h, 300 μM) upon TRPM2 inhibition (10 μM JNJ-28583113, (**A**, quantified in **B**)) or siRNA-mediated TRPM2 knockdown (30 nM siRNA, NS = Nonspecific control, (**C**, quantified in **D**)). Representative Western blot of phosphorylated VE-cadherin (pY731) protein levels after  $H_2O_2$  exposure (5 min, 300 μM) upon TRPM2 inhibition (10 μM econazole, (**E**, quantified in **F**)). For all Western blots, β-actin was probed for as a loading control, samples shown are from a single donor, 3 technical replicates. Western blot quantifications represent the mean + SD of results from 3 independent donors (**B**, **D**) or 3 consecutive passages from one donor (**F**); (n = 3). (**G**) Detection of HPMEC ROS levels through the fluorigenic ROS probe  $H_2$ DCFDA after incubation with DMSO or econazole (10 μM) for the described timepoints. Data reflect the mean + SD of results from one donor at 3 consecutive passages (n = 3). Normality of data was confirmed using the Shapiro-Wilk test, and significance between means was analyzed using two-way ANOVA, with Tukey post hoc test; \* p < 0.05, \*\* p < 0.01, \*\*\* p < 0.001.

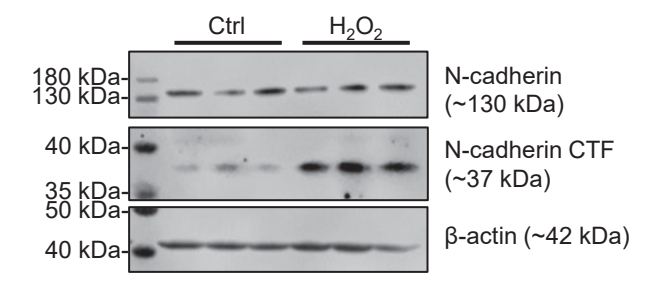


Figure S4.  $H_2O_2$  exposure induces N-cadherin cleavage in HPMECs. Representative Western blot of FL and CTF N-cadherin protein levels after  $H_2O_2$  exposure (2 h, 300 μM). β-actin was probed for as a loading control, samples shown are from a single donor, 3 technical replicates; (n = 1).

# References

- Hogan, B.; Tata, P.R. Cellular organization and biology of the respiratory system. Nature Cell Biology 2019, 10.1038/s41556-019-0357-7, doi:10.1038/s41556-019-0357-7.
- Hewitt, R.J.; Lloyd, C.M. Regulation of immune responses by the airway epithelial cell landscape. *Nature Reviews Immunology* 2021, 21, 347-362, doi:10.1038/s41577-020-00477-9.
- 3. Knudsen, L.; Ochs, M. The micromechanics of lung alveoli: structure and function of surfactant and tissue components. *Histochemistry and Cell Biology* **2018**, *150*, 661-676, doi:10.1007/s00418-018-1747-9.
- West, J.B. Comparative physiology of the pulmonary blood-gas barrier: the unique avian solution. Am J Physiol Regul Integr Comp Physiol 2009, 297, R1625-1634, doi:10.1152/ajpregu.00459.2009.
- Käsmann, L.; Dietrich, A.; Staab-Weijnitz, C.A.; Manapov, F.; Behr, J.; Rimner, A.; Jeremic, B.; Senan, S.; De Ruysscher, D.; Lauber, K., et al. Radiation-induced lung toxicity – cellular and molecular mechanisms of pathogenesis, management, and literature review. *Radiation Oncology* 2020, *15*, 214, doi:10.1186/s13014-020-01654-9.
- Krogh, A. On the Mechanism of the Gas-Exchange in the Lungs. Skandinavisches Archiv Für Physiologie 1910, 23, 248-278, doi:https://doi.org/10.1111/j.1748-1716.1910.tb00601.x.
- 7. Iwasaki, A.; Foxman, E.F.; Molony, R.D. Early local immune defences in the respiratory tract. *Nature Reviews Immunology* **2017**, *17*, 7-20, doi:10.1038/nri.2016.117.
- Fehrenbach, H. Alveolar epithelial type II cell: defender of the alveolus revisited. Respiratory Research 2001, 2, 33, doi:10.1186/rr36.
- Mason, R.J. Biology of alveolar type II cells. Respirology 2006, 11, S12-S15, doi:https://doi.org/10.1111/j.1440-1843.2006.00800.x.
- Rackley, C.R.; Stripp, B.R. Building and maintaining the epithelium of the lung. J Clin Invest 2012, 122, 2724-2730, doi:10.1172/JCl60519.
- Kapanci, Y.; Weibel, E.R.; Kaplan, H.P.; Robinson, F.R. Pathogenesis and reversibility of the pulmonary lesions of oxygen toxicity in monkeys. II. Ultrastructural and morphometric studies. *Lab Invest* 1969, 20, 101-118.
- 12. Yang, J.; Hernandez, B.J.; Martinez Alanis, D.; Narvaez del Pilar, O.; Vila-Ellis, L.; Akiyama, H.; Evans, S.E.; Ostrin, E.J.; Chen, J. The development and plasticity of alveolar type 1 cells. *Development* **2016**, *143*, 54-65, doi:10.1242/dev.130005.
- Schaller, L.; Hofmann, K.; Geiger, F.; Dietrich, A. Electrical cell-substrate impedance sensing (ECIS) in lung biology and disease. Applied Research 2024, 3, e202400059, doi:https://doi.org/10.1002/appl.202400059.
- Nilius, B.; Droogmans, G. Ion channels and their functional role in vascular endothelium. *Physiol Rev* 2001, 81, 1415-1459, doi:10.1152/physrev.2001.81.4.1415.
- Stevens, T.; Garcia, J.G.; Shasby, D.M.; Bhattacharya, J.; Malik, A.B. Mechanisms regulating endothelial cell barrier function. Am J Physiol Lung Cell Mol Physiol 2000, 279, L419-422, doi:10.1152/ajplung.2000.279.3.L419.
- Del Vecchio, P.J.; Siflinger-Birnboim, A.; Belloni, P.N.; Holleran, L.A.; Lum, H.; Malik, A.B. Culture and characterization of pulmonary microvascular endothelial cells. *In Vitro Cell Dev Biol* 1992, 28a, 711-715, doi:10.1007/bf02631058.
- 17. Blum, M.S.; Toninelli, E.; Anderson, J.M.; Balda, M.S.; Zhou, J.; O'Donnell, L.; Pardi, R.; Bender, J.R. Cytoskeletal rearrangement mediates human microvascular endothelial tight junction modulation by cytokines. *Am J Physiol* **1997**, *273*, H286-294, doi:10.1152/ajpheart.1997.273.1.H286.
- 18. Kageyama, T.; Ito, T.; Tanaka, S.; Nakajima, H. Physiological and immunological barriers in the lung. Seminars in Immunopathology 2024, 45, 533-547, doi:10.1007/s00281-024-01003-y.
- Nawijn, M.C.; Hackett, T.L.; Postma, D.S.; van Oosterhout, A.J.; Heijink, I.H. E-cadherin: gatekeeper of airway mucosa and allergic sensitization. *Trends Immunol* 2011, 32, 248-255, doi:10.1016/j.it.2011.03.004.
- Post, S.; Heijink, I.H.; Hesse, L.; Koo, H.K.; Shaheen, F.; Fouadi, M.; Kuchibhotla, V.N.S.; Lambrecht, B.N.; Van Oosterhout, A.J.M.; Hackett, T.L., et al. Characterization of a lung epithelium specific E-cadherin knock-out model: Implications for obstructive lung pathology. *Sci Rep* 2018, 8, 13275, doi:10.1038/s41598-018-31500-8.
- 21. Mehta, D.; Malik, A.B. Signaling mechanisms regulating endothelial permeability. *Physiol Rev* **2006**, *86*, 279-367, doi:10.1152/physrev.00012.2005.
- Hartsock, A.; Nelson, W.J. Adherens and tight junctions: structure, function and connections to the actin cytoskeleton. *Biochim Biophys Acta* 2008, 1778, 660-669, doi:10.1016/j.bbamem.2007.07.012.
- Lum, H.; Roebuck, K.A. Oxidant stress and endothelial cell dysfunction. Am J Physiol Cell Physiol 2001, 280, C719-741, doi:10.1152/ajpcell.2001.280.4.C719.
- 24. Giannotta, M.; Trani, M.; Dejana, E. VE-cadherin and endothelial adherens junctions: active guardians of vascular integrity. *Dev Cell* **2013**, *26*, 441-454, doi:10.1016/j.devcel.2013.08.020.

- Capaldo, C.T.; Macara, I.G. Depletion of E-Cadherin Disrupts Establishment but Not Maintenance of Cell Junctions in Madin-Darby Canine Kidney Epithelial Cells. *Molecular Biology of the Cell* 2007, 18, 189-200, doi:10.1091/mbc.e06-05-0471.
- Tunggal, J.A.; Helfrich, I.; Schmitz, A.; Schwarz, H.; Gunzel, D.; Fromm, M.; Kemler, R.; Krieg, T.; Niessen, C.M. E-cadherin is essential for in vivo epidermal barrier function by regulating tight junctions. *EMBO J* 2005, 24, 1146-1156, doi:10.1038/sj.emboj.7600605.
- 27. Dejana, E.; Corada, M.; Lampugnani, M.G. Endothelial cell-to-cell junctions. Faseb j 1995, 9, 910-918.
- 28. Kowalczyk, A.P.; Navarro, P.; Dejana, E.; Bornslaeger, E.A.; Green, K.J.; Kopp, D.S.; Borgwardt, J.E. VEcadherin and desmoplakin are assembled into dermal microvascular endothelial intercellular junctions: a pivotal role for plakoglobin in the recruitment of desmoplakin to intercellular junctions. *J Cell Sci* **1998**, *111* (*Pt 20*), 3045-3057, doi:10.1242/jcs.111.20.3045.
- Lewis, J.E.; Wahl, J.K., III; Sass, K.M.; Jensen, P.J.; Johnson, K.R.; Wheelock, M.J. Cross-Talk between Adherens Junctions and Desmosomes Depends on Plakoglobin. *Journal of Cell Biology* 1997, 136, 919-934, doi:10.1083/jcb.136.4.919.
- Le, T.L.; Joseph, S.R.; Yap, A.S.; Stow, J.L. Protein kinase C regulates endocytosis and recycling of Ecadherin. Am J Physiol Cell Physiol 2002, 283, C489-499, doi:10.1152/ajpcell.00566.2001.
- 31. Miyashita, Y.; Ozawa, M. Increased Internalization of p120-uncoupled E-cadherin and a Requirement for a Dileucine Motif in the Cytoplasmic Domain for Endocytosis of the Protein\*. *Journal of Biological Chemistry* **2007**, *282*, 11540-11548, doi:https://doi.org/10.1074/jbc.M608351200.
- Potter, M.D.; Barbero, S.; Cheresh, D.A. Tyrosine phosphorylation of VE-cadherin prevents binding of p120and beta-catenin and maintains the cellular mesenchymal state. *J Biol Chem* 2005, 280, 31906-31912, doi:10.1074/jbc.M505568200.
- 33. Ireton, R.C.; Davis, M.A.; van Hengel, J.; Mariner, D.J.; Barnes, K.; Thoreson, M.A.; Anastasiadis, P.Z.; Matrisian, L.; Bundy, L.M.; Sealy, L., et al. A novel role for p120 catenin in E-cadherin function. *J Cell Biol* **2002**, *159*, 465-476, doi:10.1083/jcb.200205115.
- 34. Gavard, J.; Gutkind, J.S. VEGF controls endothelial-cell permeability by promoting the β-arrestin-dependent endocytosis of VE-cadherin. *Nature Cell Biology* **2006**, *8*, 1223-1234, doi:10.1038/ncb1486.
- 35. Orsenigo, F.; Giampietro, C.; Ferrari, A.; Corada, M.; Galaup, A.; Sigismund, S.; Ristagno, G.; Maddaluno, L.; Koh, G.Y.; Franco, D., et al. Phosphorylation of VE-cadherin is modulated by haemodynamic forces and contributes to the regulation of vascular permeability in vivo. *Nat Commun* **2012**, *3*, 1208, doi:10.1038/ncomms2199.
- Corada, M.; Mariotti, M.; Thurston, G.; Smith, K.; Kunkel, R.; Brockhaus, M.; Lampugnani, M.G.; Martin-Padura, I.; Stoppacciaro, A.; Ruco, L., et al. Vascular endothelial-cadherin is an important determinant of microvascular integrity in vivo. *Proc Natl Acad Sci U S A* 1999, *96*, 9815-9820, doi:10.1073/pnas.96.17.9815.
- 37. Tatsumi, M.; Kishi, T.; Ishida, S.; Kawana, H.; Uwamizu, A.; Ono, Y.; Kawakami, K.; Aoki, J.; Inoue, A. Ectodomain shedding of EGFR ligands serves as an activation readout for TRP channels. *PLoS One* **2023**, *18*, e0280448, doi:10.1371/journal.pone.0280448.
- 38. Reiss, K.; Ludwig, A.; Saftig, P. Breaking up the tie: disintegrin-like metalloproteinases as regulators of cell migration in inflammation and invasion. *Pharmacol Ther* **2006**, *111*, 985-1006, doi:10.1016/j.pharmthera.2006.02.009.
- 39. Noë, V.; Fingleton, B.; Jacobs, K.; Crawford, H.C.; Vermeulen, S.; Steelant, W.; Bruyneel, E.; Matrisian, L.M.; Mareel, M. Release of an invasion promoter E-cadherin fragment by matrilysin and stromelysin-1. *J Cell Sci* **2001**, *114*, 111-118, doi:10.1242/jcs.114.1.111.
- Herren, B.; Levkau, B.; Raines, E.W.; Ross, R. Cleavage of beta-catenin and plakoglobin and shedding of VE-cadherin during endothelial apoptosis: evidence for a role for caspases and metalloproteinases. *Mol Biol Cell* 1998, 9, 1589-1601, doi:10.1091/mbc.9.6.1589.
- 41. Schulz, B.; Pruessmeyer, J.; Maretzky, T.; Ludwig, A.; Blobel, C.P.; Saftig, P.; Reiss, K. ADAM10 regulates endothelial permeability and T-Cell transmigration by proteolysis of vascular endothelial cadherin. *Circ Res* **2008**, *102*, 1192-1201, doi:10.1161/circresaha.107.169805.
- Maretzky, T.; Reiss, K.; Ludwig, A.; Buchholz, J.; Scholz, F.; Proksch, E.; de Strooper, B.; Hartmann, D.; Saftig, P. ADAM10 mediates E-cadherin shedding and regulates epithelial cell-cell adhesion, migration, and beta-catenin translocation. *Proc Natl Acad Sci U S A* 2005, 102, 9182-9187, doi:10.1073/pnas.0500918102.
- 43. Reiss, K.; Maretzky, T.; Ludwig, A.; Tousseyn, T.; de Strooper, B.; Hartmann, D.; Saftig, P. ADAM10 cleavage of N-cadherin and regulation of cell-cell adhesion and beta-catenin nuclear signalling. *Embo j* **2005**, *24*, 742-752, doi:10.1038/si.emboj.7600548.
- Lynch, C.C.; Vargo-Gogola, T.; Matrisian, L.M.; Fingleton, B. Cleavage of E-Cadherin by Matrix Metalloproteinase-7 Promotes Cellular Proliferation in Nontransformed Cell Lines via Activation of RhoA. *J Oncol* 2010, 2010, 530745, doi:10.1155/2010/530745.
- 45. Marambaud, P.; Shioi, J.; Serban, G.; Georgakopoulos, A.; Sarner, S.; Nagy, V.; Baki, L.; Wen, P.; Efthimiopoulos, S.; Shao, Z., et al. A presenilin-1/gamma-secretase cleavage releases the E-cadherin intracellular domain and regulates disassembly of adherens junctions. *Embo j* **2002**, *21*, 1948-1956, doi:10.1093/emboj/21.8.1948.

- 46. Navarro, P.; Ruco, L.; Dejana, E. Differential localization of VE- and N-cadherins in human endothelial cells: VE-cadherin competes with N-cadherin for junctional localization. *J Cell Biol* **1998**, *140*, 1475-1484, doi:10.1083/jcb.140.6.1475.
- 47. Lampugnani, M.G.; Zanetti, A.; Corada, M.; Takahashi, T.; Balconi, G.; Breviario, F.; Orsenigo, F.; Cattelino, A.; Kemler, R.; Daniel, T.O., et al. Contact inhibition of VEGF-induced proliferation requires vascular endothelial cadherin, beta-catenin, and the phosphatase DEP-1/CD148. *J Cell Biol* **2003**, *161*, 793-804, doi:10.1083/jcb.200209019.
- 48. Lampugnani, M.G.; Corada, M.; Caveda, L.; Breviario, F.; Ayalon, O.; Geiger, B.; Dejana, E. The molecular organization of endothelial cell to cell junctions: differential association of plakoglobin, beta-catenin, and alpha-catenin with vascular endothelial cadherin (VE-cadherin). *J Cell Biol* 1995, 129, 203-217, doi:10.1083/jcb.129.1.203.
- 49. Caveda, L.; Martin-Padura, I.; Navarro, P.; Breviario, F.; Corada, M.; Gulino, D.; Lampugnani, M.G.; Dejana, E. Inhibition of cultured cell growth by vascular endothelial cadherin (cadherin-5/VE-cadherin). *J Clin Invest* 1996, *98*, 886-893, doi:10.1172/jci118870.
- Frixen, U.H.; Behrens, J.; Sachs, M.; Eberle, G.; Voss, B.; Warda, A.; Löchner, D.; Birchmeier, W. E-cadherin-mediated cell-cell adhesion prevents invasiveness of human carcinoma cells. *J Cell Biol* 1991, 113, 173-185, doi:10.1083/jcb.113.1.173.
- 51. Giampietro, C.; Taddei, A.; Corada, M.; Sarra-Ferraris, G.M.; Alcalay, M.; Cavallaro, U.; Orsenigo, F.; Lampugnani, M.G.; Dejana, E. Overlapping and divergent signaling pathways of N-cadherin and VE-cadherin in endothelial cells. *Blood* **2012**, *119*, 2159-2170, doi:10.1182/blood-2011-09-381012.
- 52. Fujita, Y.; Krause, G.; Scheffner, M.; Zechner, D.; Leddy, H.E.; Behrens, J.; Sommer, T.; Birchmeier, W. Hakai, a c-Cbl-like protein, ubiquitinates and induces endocytosis of the E-cadherin complex. *Nat Cell Biol* **2002**, *4*, 222-231, doi:10.1038/ncb758.
- 53. Nieman, M.T.; Prudoff, R.S.; Johnson, K.R.; Wheelock, M.J. N-cadherin promotes motility in human breast cancer cells regardless of their E-cadherin expression. *J Cell Biol* **1999**, *147*, 631-644, doi:10.1083/icb.147.3.631.
- 54. Salomon, D.; Ayalon, O.; Patel-King, R.; Hynes, R.O.; Geiger, B. Extrajunctional distribution of N-cadherin in cultured human endothelial cells. *J Cell Sci* **1992**, *102* (*Pt* 1), 7-17, doi:10.1242/jcs.102.1.7.
- 55. Martìn-padura, I.; de Castellarnau, C.; Uccini, S.; Pilozzi, E.; Natali, P.G.; Nicotra, M.R.; Ughi, F.; Azzolini, C.; Dejana, E.; Ruco, L. Expression of VE (vascular endothelial)-cadherin and other endothelial-specific markers in haemangiomas. *The Journal of Pathology* **1995**, *175*, 51-57, doi:https://doi.org/10.1002/path.1711750109.
- 56. Umbas, R.; Isaacs, W.B.; Bringuier, P.P.; Schaafsma, H.E.; Karthaus, H.F.; Oosterhof, G.O.; Debruyne, F.M.; Schalken, J.A. Decreased E-cadherin expression is associated with poor prognosis in patients with prostate cancer. *Cancer Res* **1994**, *54*, 3929-3933.
- 57. Hazan, R.B.; Kang, L.; Whooley, B.P.; Borgen, P.I. N-cadherin promotes adhesion between invasive breast cancer cells and the stroma. *Cell Adhes Commun* **1997**, *4*, 399-411, doi:10.3109/15419069709004457.
- 58. Islam, S.; Carey, T.E.; Wolf, G.T.; Wheelock, M.J.; Johnson, K.R. Expression of N-cadherin by human squamous carcinoma cells induces a scattered fibroblastic phenotype with disrupted cell-cell adhesion. *J Cell Biol* **1996**, *135*, 1643-1654, doi:10.1083/jcb.135.6.1643.
- 59. Kruse, K.; Lee, Q.S.; Sun, Y.; Klomp, J.; Yang, X.; Huang, F.; Sun, M.Y.; Zhao, S.; Hong, Z.; Vogel, S.M., et al. N-cadherin signaling via Trio assembles adherens junctions to restrict endothelial permeability. *J Cell Biol* **2019**, *218*, 299-316, doi:10.1083/jcb.201802076.
- Aoshiba, K.; Nagai, A. Oxidative Stress, Cell Death, and Other Damage to Alveolar Epithelial Cells Induced by Cigarette Smoke. *Tobacco Induced Diseases* 2003, 1, 219, doi:10.1186/1617-9625-1-3-219.
- 61. Georas, S.N.; Rezaee, F. Epithelial barrier function: At the front line of asthma immunology and allergic airway inflammation. *Journal of Allergy and Clinical Immunology* **2014**, *134*, 509-520, doi:10.1016/j.jaci.2014.05.049.
- Brune, K.; Frank, J.; Schwingshackl, A.; Finigan, J.; Sidhaye, V.K. Pulmonary epithelial barrier function: some new players and mechanisms. *Am J Physiol Lung Cell Mol Physiol* 2015, 308, L731-745, doi:10.1152/ajplung.00309.2014.
- 63. Parker, J.C.; Yoshikawa, S. Vascular segmental permeabilities at high peak inflation pressure in isolated rat lungs. *Am J Physiol Lung Cell Mol Physiol* **2002**, *283*, L1203-1209, doi:10.1152/ajplung.00488.2001.
- Mehta, D.; Ravindran, K.; Kuebler, W.M. Novel regulators of endothelial barrier function. Am J Physiol Lung Cell Mol Physiol 2014, 307, L924-935, doi:10.1152/ajplung.00318.2014.
- 65. Armstrong, S.M.; Khajoee, V.; Wang, C.; Wang, T.; Tigdi, J.; Yin, J.; Kuebler, W.M.; Gillrie, M.; Davis, S.P.; Ho, M., et al. Co-Regulation of Transcellular and Paracellular Leak Across Microvascular Endothelium by Dynamin and Rac. *The American Journal of Pathology* **2012**, *180*, 1308-1323, doi:10.1016/j.ajpath.2011.12.002.
- Ware, L.B.; Matthay, M.A. The acute respiratory distress syndrome. N Engl J Med 2000, 342, 1334-1349, doi:10.1056/nejm200005043421806.
- 67. Bellani, G.; Laffey, J.G.; Pham, T.; Fan, E.; Brochard, L.; Esteban, A.; Gattinoni, L.; van Haren, F.; Larsson, A.; McAuley, D.F., et al. Epidemiology, Patterns of Care, and Mortality for Patients With Acute Respiratory

- Distress Syndrome in Intensive Care Units in 50 Countries. *JAMA* **2016**, *315*, 788-800, doi:10.1001/jama.2016.0291.
- Hu, X.; Lee, J.S.; Pianosi, P.T.; Ryu, J.H. Aspiration-related pulmonary syndromes. *Chest* 2015, 147, 815-823, doi:10.1378/chest.14-1049.
- Song , Y.; Thiagarajah , J.; Verkman , A.S. Sodium and Chloride Concentrations, pH, and Depth of Airway Surface Liquid in Distal Airways. *Journal of General Physiology* 2003, 122, 511-519, doi:10.1085/jgp.200308866.
- Balan, K.K.; Jones, A.T.; Roberts, N.B.; Pearson, J.P.; Critchley, M.; Jenkins, S.A. The effects of Helicobacter pylori colonization on gastric function and the incidence of portal hypertensive gastropathy in patients with cirrhosis of the liver. Am J Gastroenterol 1996, 91, 1400-1406.
- Hunt, E.B.; Sullivan, A.; Galvin, J.; MacSharry, J.; Murphy, D.M. Gastric Aspiration and Its Role in Airway Inflammation. Open Respir Med J 2018, 12, 1-10, doi:10.2174/1874306401812010001.
- 72. Imai, Y.; Kuba, K.; Neely, G.G.; Yaghubian-Malhami, R.; Perkmann, T.; van Loo, G.; Ermolaeva, M.; Veldhuizen, R.; Leung, Y.H.; Wang, H., et al. Identification of oxidative stress and Toll-like receptor 4 signaling as a key pathway of acute lung injury. *Cell* **2008**, *133*, 235-249, doi:10.1016/j.cell.2008.02.043.
- Weiser, M.R.; Pechet, T.T.V.; Williams, J.P.; Ma, M.; Frenette, P.S.; Moore, F.D.; Kobzik, L.; Hines, R.O.;
   Wagner, D.D.; Carroll, M.C., et al. Experimental murine acid aspiration injury is mediated by neutrophils and the alternative complement pathway. *Journal of Applied Physiology* 1997, 83, 1090-1095, doi:10.1152/jappl.1997.83.4.1090.
- Zarbock, A.; DiStasi, M.R.; Smith, E.; Sanders, J.M.; Kronke, G.; Harry, B.L.; von Vietinghoff, S.; Buscher, K.; Nadler, J.L.; Ley, K. Improved Survival and Reduced Vascular Permeability by Eliminating or Blocking 12/15-Lipoxygenase in Mouse Models of Acute Lung Injury (ALI)1. *The Journal of Immunology* 2009, 183, 4715-4722, doi:10.4049/jimmunol.0802592.
- 75. Balakrishna, S.; Song, W.; Achanta, S.; Doran, S.F.; Liu, B.; Kaelberer, M.M.; Yu, Z.; Sui, A.; Cheung, M.; Leishman, E., et al. TRPV4 inhibition counteracts edema and inflammation and improves pulmonary function and oxygen saturation in chemically induced acute lung injury. *Am J Physiol Lung Cell Mol Physiol* **2014**, *307*, L158-172, doi:10.1152/ajplung.00065.2014.
- Yin, J.; Michalick, L.; Tang, C.; Tabuchi, A.; Goldenberg, N.; Dan, Q.; Awwad, K.; Wang, L.; Erfinanda, L.;
   Nouailles, G., et al. Role of Transient Receptor Potential Vanilloid 4 in Neutrophil Activation and Acute Lung Injury. Am J Respir Cell Mol Biol 2016, 54, 370-383, doi:10.1165/rcmb.2014-0225OC.
- 77. Westphalen, K.; Monma, E.; Islam, M.N.; Bhattacharya, J. Acid contact in the rodent pulmonary alveolus causes proinflammatory signaling by membrane pore formation. *American Journal of Physiology-Lung Cellular and Molecular Physiology* **2012**, *303*, L107-L116, doi:10.1152/ajplung.00206.2011.
- 78. Takahashi, N.; Kozai, D.; Kobayashi, R.; Ebert, M.; Mori, Y. Roles of TRPM2 in oxidative stress. *Cell Calcium* **2011**, *50*, 279-287, doi:10.1016/j.ceca.2011.04.006.
- Finkel, T. Signal transduction by reactive oxygen species. J Cell Biol 2011, 194, 7-15, doi:10.1083/jcb.201102095.
- 80. Urao, N.; Sudhahar, V.; Kim, S.J.; Chen, G.F.; McKinney, R.D.; Kojda, G.; Fukai, T.; Ushio-Fukai, M. Critical role of endothelial hydrogen peroxide in post-ischemic neovascularization. *PLoS One* **2013**, *8*, e57618, doi:10.1371/journal.pone.0057618.
- Fukai, T.; Ushio-Fukai, M. Cross-Talk between NADPH Oxidase and Mitochondria: Role in ROS Signaling and Angiogenesis. Cells 2020, 9, doi:10.3390/cells9081849.
- 82. Yun, J.; Rocic, P.; Pung, Y.F.; Belmadani, S.; Carrao, A.C.; Ohanyan, V.; Chilian, W.M. Redox-dependent mechanisms in coronary collateral growth: the "redox window" hypothesis. *Antioxid Redox Signal* **2009**, *11*, 1961-1974, doi:10.1089/ars.2009.2476.
- 83. Nagababu, E.; Usatyuk, P.V.; Enika, D.; Natarajan, V.; Rifkind, J.M. Vascular endothelial barrier dysfunction mediated by amyloid-beta proteins. *J Alzheimers Dis* **2009**, *17*, 845-854, doi:10.3233/jad-2009-1104.
- 84. Kevil, C.G.; Okayama, N.; Alexander, J.S. H2O2-mediated permeability II: importance of tyrosine phosphatase and kinase activity. *American Journal of Physiology-Cell Physiology* **2001**, *281*, C1940-C1947, doi:10.1152/ajpcell.2001.281.6.C1940.
- 85. López-Ongil, S.; Torrecillas, G.; Pérez-Sala, D.; González-Santiago, L.; Rodríguez-Puyol, M.; Rodríguez-Puyol, D. Mechanisms involved in the contraction of endothelial cells by hydrogen peroxide. *Free Radical Biology and Medicine* **1999**, *26*, 501-510, doi:https://doi.org/10.1016/S0891-5849(98)00223-8.
- 86. Monaghan-Benson, E.; Burridge, K. The regulation of vascular endothelial growth factor-induced microvascular permeability requires Rac and reactive oxygen species. *J Biol Chem* **2009**, *284*, 25602-25611, doi:10.1074/jbc.M109.009894.
- 87. Kevil, C.G.; Ohno, N.; Gute, D.C.; Okayama, N.; Robinson, S.A.; Chaney, E.; Alexander, J.S. Role of cadherin internalization in hydrogen peroxide-mediated endothelial permeability. *Free Radic Biol Med* **1998**, *24*, 1015-1022, doi:10.1016/s0891-5849(97)00433-4.
- Rosales, C.; Demaurex, N.; Lowell, C.A.; Uribe-Querol, E. Neutrophils: Their Role in Innate and Adaptive Immunity. J Immunol Res 2016, 2016, 1469780, doi:10.1155/2016/1469780.
- 89. Tauber, A.I.; Brettler, D.B.; Kennington, E.A.; Blumberg, P.M. Relation of human neutrophil phorbol ester receptor occupancy and NADPH-oxidase activity. *Blood* **1982**, *60*, 333-339.

- 90. Nathan, C.F. Neutrophil activation on biological surfaces. Massive secretion of hydrogen peroxide in response to products of macrophages and lymphocytes. *J Clin Invest* **1987**, *80*, 1550-1560, doi:10.1172/jci113241.
- 91. Lum, H.; Gibbs, L.; Lai, L.; Malik, A.B. CD18 integrin-dependent endothelial injury: effects of opsonized zymosan and phorbol ester activation. *J Leukoc Biol* **1994**, *55*, 58-63, doi:10.1002/jlb.55.1.58.
- 92. Wolburg, H.; Wolburg-Buchholz, K.; Engelhardt, B. Diapedesis of mononuclear cells across cerebral venules during experimental autoimmune encephalomyelitis leaves tight junctions intact. *Acta Neuropathologica* **2005**, *109*, 181-190, doi:10.1007/s00401-004-0928-x.
- 93. Allport, J.R.; Muller, W.A.; Luscinskas, F.W. Monocytes induce reversible focal changes in vascular endothelial cadherin complex during transendothelial migration under flow. *J Cell Biol* **2000**, *148*, 203-216, doi:10.1083/jcb.148.1.203.
- 94. Chun, J.; Prince, A. TLR2-induced calpain cleavage of epithelial junctional proteins facilitates leukocyte transmigration. *Cell Host Microbe* **2009**, *5*, 47-58, doi:10.1016/j.chom.2008.11.009.
- 95. Rattan, V.; Sultana, C.; Shen, Y.; Kalra, V.K. Oxidant stress-induced transendothelial migration of monocytes is linked to phosphorylation of PECAM-1. *American Journal of Physiology-Endocrinology and Metabolism* **1997**, *273*, E453, doi:10.1152/ajpendo.1997.273.3.E453.
- 96. Scalia, R.; Lefer, A.M. In vivo regulation of PECAM-1 activity during acute endothelial dysfunction in the rat mesenteric microvasculature. *Journal of Leukocyte Biology* **1998**, *64*, 163-169, doi:https://doi.org/10.1002/jlb.64.2.163.
- 97. Cioffi, D.L.; Lowe, K.; Alvarez, D.F.; Barry, C.; Stevens, T. TRPing on the lung endothelium: calcium channels that regulate barrier function. *Antioxid Redox Signal* **2009**, *11*, 765-776, doi:10.1089/ars.2008.2221.
- 98. Montell, C.; Rubin, G.M. Molecular characterization of the Drosophila trp locus: a putative integral membrane protein required for phototransduction. *Neuron* **1989**, *2*, 1313-1323, doi:10.1016/0896-6273(89)90069-x.
- 99. Muller, I.; Alt, P.; Rajan, S.; Schaller, L.; Geiger, F.; Dietrich, A. Transient Receptor Potential (TRP) Channels in Airway Toxicity and Disease: An Update. *Cells* **2022**, *11*, doi:10.3390/cells11182907.
- Zergane, M.; Kuebler, W.M.; Michalick, L. Heteromeric TRP Channels in Lung Inflammation. Cells 2021, 10, 1654.
- Simmons, S.; Erfinanda, L.; Bartz, C.; Kuebler, W.M. Novel mechanisms regulating endothelial barrier function in the pulmonary microcirculation. *J Physiol* 2019, *597*, 997-1021, doi:10.1113/jp276245.
- 102. Kumar, M.; Zaman, M.K.; Das, S.; Goyary, D.; Pathak, M.P.; Chattopadhyay, P. Transient Receptor Potential Vanilloid (TRPV4) channel inhibition: A novel promising approach for the treatment of lung diseases. *Biomed Pharmacother* **2023**, *163*, 114861, doi:10.1016/j.biopha.2023.114861.
- 103. Rahaman, S.O.; Grove, L.M.; Paruchuri, S.; Southern, B.D.; Abraham, S.; Niese, K.A.; Scheraga, R.G.; Ghosh, S.; Thodeti, C.K.; Zhang, D.X., et al. TRPV4 mediates myofibroblast differentiation and pulmonary fibrosis in mice. *J Clin Invest* **2014**, *124*, 5225-5238, doi:10.1172/jci75331.
- 104. Li, C.; Zhang, H.; Wei, L.; Liu, Q.; Xie, M.; Weng, J.; Wang, X.; Chung, K.F.; Adcock, I.M.; Chen, Y., et al. Role of TRPA1/TRPV1 in acute ozone exposure induced murine model of airway inflammation and bronchial hyperresponsiveness. *J Thorac Dis* **2022**, *14*, 2698-2711, doi:10.21037/jtd-22-315.
- 105. Geiger, F.; Zeitlmayr, S.; Staab-Weijnitz, C.A.; Rajan, S.; Breit, A.; Gudermann, T.; Dietrich, A. An Inhibitory Function of TRPA1 Channels in TGF-β1-driven Fibroblast-to-Myofibroblast Differentiation. Am J Respir Cell Mol Biol 2023, 68, 314-325, doi:10.1165/rcmb.2022-0159OC.
- Tiruppathi, C.; Minshall, R.D.; Paria, B.C.; Vogel, S.M.; Malik, A.B. Role of Ca2+ signaling in the regulation of endothelial permeability. *Vascul Pharmacol* **2002**, *39*, 173-185, doi:10.1016/s1537-1891(03)00007-7.
- O'Neil, R.G.; Heller, S. The mechanosensitive nature of TRPV channels. *Pflugers Arch* 2005, 451, 193-203, doi:10.1007/s00424-005-1424-4.
- 108. Rosenbaum, T.; Benitez-Angeles, M.; Sanchez-Hernandez, R.; Morales-Lazaro, S.L.; Hiriart, M.; Morales-Buenrostro, L.E.; Torres-Quiroz, F. TRPV4: A Physio and Pathophysiologically Significant Ion Channel. Int J Mol Sci 2020, 21, doi:10.3390/ijms21113837.
- Suzuki, M.; Mizuno, A.; Kodaira, K.; Imai, M. Impaired pressure sensation in mice lacking TRPV4. *J Biol Chem* 2003, 278, 22664-22668, doi:10.1074/jbc.M302561200.
- 110. Weber, J.; Rajan, S.; Schremmer, C.; Chao, Y.K.; Krasteva-Christ, G.; Kannler, M.; Yildirim, A.; Brosien, M.; Schredelseker, J.; Weissmann, N., et al. TRPV4 channels are essential for alveolar epithelial barrier function as protection from lung edema. *JCI Insight* **2020**, *5*, doi:10.1172/jci.insight.134464.
- 111. Alvarez, D.F.; King, J.A.; Weber, D.; Addison, E.; Liedtke, W.; Townsley, M.I. Transient receptor potential vanilloid 4-mediated disruption of the alveolar septal barrier: a novel mechanism of acute lung injury. *Circ Res* **2006**, *99*, 988-995, doi:10.1161/01.RES.0000247065.11756.19.
- 112. Rajan, S.; Schremmer, C.; Weber, J.; Alt, P.; Geiger, F.; Dietrich, A. Ca(2+) Signaling by TRPV4 Channels in Respiratory Function and Disease. *Cells* **2021**, *10*, doi:10.3390/cells10040822.
- Dagenais, A.; Desjardins, J.; Shabbir, W.; Roy, A.; Filion, D.; Sauve, R.; Berthiaume, Y. Loss of barrier integrity in alveolar epithelial cells downregulates ENaC expression and activity via Ca(2+) and TRPV4 activation. *Pflugers Arch* 2018, 470, 1615-1631, doi:10.1007/s00424-018-2182-4.

- 114. Doñate-Macián, P.; Enrich-Bengoa, J.; Dégano, I.R.; Quintana, D.G.; Perálvarez-Marín, A. Trafficking of Stretch-Regulated TRPV2 and TRPV4 Channels Inferred Through Interactomics. *Biomolecules* 2019, 9, doi:10.3390/biom9120791.
- 115. Li, M.; Fan, X.; Ji, L.; Fan, Y.; Xu, L. Exacerbating effects of trimellitic anhydride in ovalbumin-induced asthmatic mice and the gene and protein expressions of TRPA1, TRPV1, TRPV2 in lung tissue. *Int Immunopharmacol* **2019**, *69*, 159-168, doi:10.1016/j.intimp.2019.01.038.
- Link, T.M.; Park, U.; Vonakis, B.M.; Raben, D.M.; Soloski, M.J.; Caterina, M.J. TRPV2 has a pivotal role in macrophage particle binding and phagocytosis. *Nat Immunol* **2010**, *11*, 232-239, doi:10.1038/ni.1842.
- 117. Nagasawa, M.; Nakagawa, Y.; Tanaka, S.; Kojima, I. Chemotactic peptide fMetLeuPhe induces translocation of the TRPV2 channel in macrophages. *J Cell Physiol* **2007**, *210*, 692-702, doi:10.1002/jcp.20883.
- Siveen, K.S.; Nizamuddin, P.B.; Uddin, S.; Al-Thani, M.; Frenneaux, M.P.; Janahi, I.A.; Steinhoff, M.; Azizi, F. TRPV2: A Cancer Biomarker and Potential Therapeutic Target. *Dis Markers* 2020, 2020, 8892312, doi:10.1155/2020/8892312.
- 119. Siveen, K.S.; Prabhu, K.S.; Parray, A.S.; Merhi, M.; Arredouani, A.; Chikri, M.; Uddin, S.; Dermime, S.; Mohammad, R.M.; Steinhoff, M., et al. Evaluation of cationic channel TRPV2 as a novel biomarker and therapeutic target in Leukemia-Implications concerning the resolution of pulmonary inflammation. *Sci Rep* **2019**, *9*, 1554, doi:10.1038/s41598-018-37469-8.
- 120. Peralvarez-Marin, A.; Donate-Macian, P.; Gaudet, R. What do we know about the transient receptor potential vanilloid 2 (TRPV2) ion channel? *FEBS J* **2013**, *280*, 5471-5487, doi:10.1111/febs.12302.
- 121. Luo, H.; Rossi, E.; Saubamea, B.; Chasseigneaux, S.; Cochois, V.; Choublier, N.; Smirnova, M.; Glacial, F.; Perriere, N.; Bourdoulous, S., et al. Cannabidiol Increases Proliferation, Migration, Tubulogenesis, and Integrity of Human Brain Endothelial Cells through TRPV2 Activation. *Mol Pharm* 2019, 16, 1312-1326, doi:10.1021/acs.molpharmaceut.8b01252.
- 122. Chugunov, A.O.; Volynsky, P.E.; Krylov, N.A.; Nolde, D.E.; Efremov, R.G. Temperature-sensitive gating of TRPV1 channel as probed by atomistic simulations of its trans- and juxtamembrane domains. *Scientific Reports* **2016**, *6*, 33112, doi:10.1038/srep33112.
- 123. Baylie, R.L.; Brayden, J.E. TRPV channels and vascular function. *Acta Physiol (Oxf)* **2011**, *203*, 99-116, doi:10.1111/j.1748-1716.2010.02217.x.
- 124. Fricke, T.C.; Echtermeyer, F.; Zielke, J.; de la Roche, J.; Filipovic, M.R.; Claverol, S.; Herzog, C.; Tominaga, M.; Pumroy, R.A.; Moiseenkova-Bell, V.Y., et al. Oxidation of methionine residues activates the high-threshold heat-sensitive ion channel TRPV2. *Proc Natl Acad Sci U S A* **2019**, *116*, 24359-24365, doi:10.1073/pnas.1904332116.
- Oda, M.; Fujiwara, Y.; Ishizaki, Y.; Shibasaki, K. Oxidation sensitizes TRPV2 to chemical and heat stimuli, but not mechanical stimulation. *Biochem Biophys Rep* **2021**, *28*, 101173, doi:10.1016/j.bbrep.2021.101173.
- 126. Wehage, E.; Eisfeld, J.; Heiner, I.; Jüngling, E.; Zitt, C.; Lückhoff, A. Activation of the cation channel long transient receptor potential channel 2 (LTRPC2) by hydrogen peroxide. A splice variant reveals a mode of activation independent of ADP-ribose. *J Biol Chem* 2002, 277, 23150-23156, doi:10.1074/jbc.M112096200.
- 127. Ding, R.; Yin, Y.L.; Jiang, L.H. Reactive Oxygen Species-Induced TRPM2-Mediated Ca(2+) Signalling in Endothelial Cells. Antioxidants (Basel) 2021, 10, doi:10.3390/antiox10050718.
- Hecquet, C.M.; Ahmmed, G.U.; Vogel, S.M.; Malik, A.B. Role of TRPM2 channel in mediating H2O2-induced Ca2+ entry and endothelial hyperpermeability. *Circ Res* 2008, 102, 347-355, doi:10.1161/circresaha.107.160176.
- Mittal, M.; Urao, N.; Hecquet, C.M.; Zhang, M.; Sudhahar, V.; Gao, X.P.; Komarova, Y.; Ushio-Fukai, M.; Malik, A.B. Novel role of reactive oxygen species-activated Trp melastatin channel-2 in mediating angiogenesis and postischemic neovascularization. *Arterioscler Thromb Vasc Biol* 2015, 35, 877-887, doi:10.1161/atvbaha.114.304802.
- 130. Bednarek, R. In Vitro Methods for Measuring the Permeability of Cell Monolayers. *Methods and Protocols* **2022**, *5*, 17.
- 131. Benson, K.; Cramer, S.; Galla, H.-J. Impedance-based cell monitoring: barrier properties and beyond. *Fluids and Barriers of the CNS* **2013**, *10*, 5, doi:10.1186/2045-8118-10-5.
- Hucklesby, J.J.W.; Anchan, A.; #039; Carroll, S.J.; Unsworth, C.P.; Graham, E.S.; Angel, C.E. Comparison of Leading Biosensor Technologies to Detect Changes in Human Endothelial Barrier Properties in Response to Pro-Inflammatory TNFα and IL1β in Real-Time. *Biosensors* **2021**, *11*, 159.
- 133. Applied Biophysics. What is ECIS. **2024**. Available online: https://www.biophysics.com/whatIsECIS.php (accessed on December 17, 2024).
- 134. Giaever, I.; Keese, C.R. Micromotion of mammalian cells measured electrically. *Proceedings of the National Academy of Sciences* **1991**, *88*, 7896-7900, doi:doi:10.1073/pnas.88.17.7896.
- Applied Biophysics. TEER. 2024. Available online: https://www.biophysics.com/teer.php (accessed on December 17, 2024).



TYPE Original Research
PUBLISHED 17 June 2024
DOI 10.3389/fimmu.2024.1425938



### **OPEN ACCESS**

EDITED BY Christa Elisabeth Müller, University of Bonn, Germany

REVIEWED BY
Günther Schmalzing,
RWTH Aachen University, Germany
Francois A. Rassendren,
INSERM U1191 Institut de Génomique
Fonctionnelle (IGF), France

\*CORRESPONDENCE Annette Nicke

□ annette.nicke@lrz.uni-muenchen.de

<sup>†</sup>These authors have contributed equally to this work and share first/last authorship

RECEIVED 30 April 2024 ACCEPTED 28 May 2024 PUBLISHED 17 June 2024

#### CITATION

Sierra-Marquez J, Schaller L, Sassenbach L, Ramírez-Fernández A, Alt P, Rissiek B, Zimmer B, Schredelseker J, Hector J, Stähler T, Koch-Nolte F, Staab-Weijnitz CA, Dietrich A, Kopp R and Nicke A (2024) Different localization of P2X4 and P2X7 receptors in native mouse lung - lack of evidence for a direct P2X4-P2X7 receptor interaction. Front. Immunol. 15:1425938. doi: 10.3389/fimmu.2024.1425938

## COPYRIGHT

© 2024 Sierra-Marquez, Schaller, Sassenbach, Ramírez-Fernández, Alt, Rissiek, Zimmer, Schredelseker, Hector, Stähler, Koch-Nolte, Staab-Weijnitz, Dietrich, Kopp and Nicke. This is an open-access article distributed under the terms of the Creative Commons Attribution License (CC BY). The use, distribution or reproduction in other forums is permitted, provided the original author(s) and the copyright owner(s) are credited and that the original publication in this journal is cited, in accordance with accepted academic practice. No use, distribution or reproduction is permitted which does not comply with these terms.

# Different localization of P2X4 and P2X7 receptors in native mouse lung - lack of evidence for a direct P2X4-P2X7 receptor interaction

Juan Sierra-Marquez<sup>1†</sup>, Lena Schaller<sup>1†</sup>, Lukas Sassenbach<sup>1</sup>, Antonio Ramírez-Fernández<sup>1</sup>, Philipp Alt<sup>1</sup>, Björn Rissiek<sup>2</sup>, Béla Zimmer<sup>1</sup>, Johann Schredelseker<sup>1,3</sup>, Julia Hector<sup>1</sup>, Tobias Stähler<sup>4</sup>, Friedrich Koch-Nolte<sup>4</sup>, Claudia A. Staab-Weijnitz<sup>5,6</sup>, Alexander Dietrich<sup>1</sup>, Robin Kopp<sup>1†</sup> and Annette Nicke<sup>1\*†</sup>

<sup>1</sup>Walther Straub Institute of Pharmacology and Toxicology, Member of the German Center for Lung Research (DZL), Faculty of Medicine, LMU Munich, Munich, Germany, <sup>2</sup>Department of Neurology, University Medical Centre Hamburg-Eppendorf, Hamburg, Germany, <sup>3</sup>Deutsches Zentrum für Herz-Kreislauf-Forschung, Partner Site Munich Heart Alliance, Munich, Germany, <sup>4</sup>Institute of Immunology, University Medical Centre Hamburg-Eppendorf, Hamburg, Germany, <sup>5</sup>Institute of Lung Health and Immunity (LHI), Helmholtz Munich, Comprehensive Pneumology Center (CPC-M), Member of the German Center for Lung Research (DZL), Germany, <sup>6</sup>Department of Pediatrics, University of Colorado Anschutz Medical Campus, Aurora, CO, United States

**Introduction:** P2X receptors are a family of homo- and heterotrimeric cation channels gated by extracellular ATP. The P2X4 and P2X7 subunits show overlapping expression patterns and have been involved in similar physiological processes, such as pain and inflammation as well as various immune cell functions. While formation of P2X2/P2X3 heterotrimers produces a distinct pharmacological phenotype and has been well established, functional identification of a P2X4/P2X7 heteromer has been difficult and evidence for and against a physical association has been found. Most of this evidence stems, however, from *in vitro* model systems.

**Methods:** Here, we used a P2X7-EGFP BAC transgenic mouse model as well as P2X4 and P2X7 knock-out mice to re-investigate a P2X4-P2X7 interaction in mouse lung by biochemical and immunohistochemical experiments as well as quantitative expression analysis.

**Results:** No detectable amounts of P2X4 could be co-purified from mouse lung via P2X7-EGFP. In agreement with these findings, immuno-histochemical analysis using a P2X7-specific nanobody revealed only limited overlap in the cellular and subcellular localizations of P2X4 and P2X7 in both the native lung tissue and primary cells. Comparison of P2X4 and P2X7 transcript and protein levels in the respective gene-deficient and wild type mice showed no mutual interrelation between their expression levels in whole lungs. However, a significantly reduced P2rx7 expression was found in alveolar macrophages of  $P2rx4^{-/-}$  mice.

**Discussion:** In summary, our detailed analysis of the cellular and subcellular P2X4 and P2X7 localization and expression does not support a physiologically relevant direct association of P2X4 and P2X7 subunits or receptors *in vivo*.

KEYWORDS

P2X7 receptor, P2X4 receptor, heteromerization, functional interaction, lung epithelial cells, macrophage, nanobody, BAC transgenic P2X7-EGFP mouse

# 1 Introduction

The P2X family of trimeric ion channel receptors comprises seven subtypes, P2X1-P2X7, of which all but the P2X6 subunit can form functional homomeric ion channels on their own (1). While a variety of possible P2X heteromers have been characterized *in vitro*, only few of them (such as P2X2/3 (2), P2X1/5 (3), and P2X2/5 (4)) have been confirmed *in vivo* also see (5–7). The P2X7 subtype differs structurally and functionally from other P2X receptors. The most significant differences are the presence of a palmitoylated cytoplasmic membrane anchor and a large intracellular so-called "ballast" domain (8), a low sensitivity to ATP (1), and its ability to initiate various downstream effects upon activation, such as the formation of large membrane pores (9).

Within the P2X receptor family, P2X4 and P2X7 are the most closely related subunits (47% and 48% amino acid sequence identity for the human and mouse proteins, respectively) and in humans and rodents both genes are direct neighbors on the same chromosome (10, 11). P2X4 and P2X7 are also co-expressed in many cell types including microglia (12), macrophages (13, 14), T cells (15), different cell types in the lung (16, 17) and secretory cells (18). While native P2X4 appears to be predominantly localized in lysosomes in many cell types (19), both subunits have been linked to similar processes, such as release of IL-1 $\beta$  and IL-18 and production of reactive oxygen species (ROS) (20–24), phagosome function (19, 25), autophagy, macrophage death (26), autocrine and paracrine activation of T cells (15, 27–31), and secretion of lung surfactant (32, 33).

Based on electrophysiological recordings, a functional P2X4/P2X7 interaction was originally suggested in airway ciliated cells (16) and subsequently described for the heterologously expressed subunits in HEK293 cells (14, 34). These studies are supported by measurements of dye uptake, where a positive effect of P2X4 on pore formation was identified in mouse macrophages (24, 26) while a negative P2X4 effect was observed in co-transfected HEK293 cells (34). However, neither a more recent study in *Xenopus laevis* oocytes, where both subunits were heterologously co-expressed (35), nor a detailed pharmacological analysis of endogenous subunits in BV-2 microglia did find evidence for a functional interaction (36).

A physical interaction of P2X4 and P2X7 subunits has been shown by co-purification experiments using transfected HEK293 and tsA201

cells as well as in mouse bone marrow-derived macrophages, the E10 mouse alveolar epithelial cell line, and primary gingival epithelial cells (14, 22, 24, 37–39). Further analysis by cross-linking, native polyacrylamide gel electrophoresis (PAGE) and atomic force microscopy indicated that the receptors formed complexes of interacting homotrimers rather than heterotrimers (37–39). In support of these studies, a close association of co-expressed P2X4 and P2X7 subunits was detected by Förster resonance energy transfer (FRET) analysis in *Xenopus laevis* oocytes and co-transfected HEK293 cells (24, 35) as well as in an *in situ* proximity ligation assay in HEK cells (39). Blue native PAGE analysis of P2X4 and P2X7-containing complexes across a variety of mouse tissues and a systematic co-precipitation study in HEK cells failed, however, to identify P2X4/P2X7 complexes that survived solubilization (5, 40).

A mutual interaction of both subunits was also reported at the transcriptional/translational level: in mouse kidney, a significant reduction of P2rx4 or P2rx7 mRNA levels was observed if the gene of the respective other P2X subtype was deleted (41). Likewise, P2X4 deficiency in bone marrow-derived dendritic cells led to reduced P2rx7 mRNA levels and decreased IL-1β release upon ATP treatment (42) and co-transfection of P2X7 and P2X4 increased surface expression of P2X4 in normal rat kidney (NRK) cells while total P2X4 levels remained unchanged (14). In mouse E10 alveolar epithelial cells, in contrast, downregulation of one subtype via shRNA resulted in an increased protein level of the respective other subtype (38). In RAW264.7 macrophage-like cells and bone marrow-derived dendritic cells, however, shRNAmediated downregulation of P2X4 did not affect P2X7 protein levels (23, 26) and most recently, evidence against an interdependent regulation or activation of both receptors and a heteromeric assembly was shown in the murine BV-2 microglia cell line (36).

Both subtypes are involved in immune cell function and are expressed in the lung where they have been shown to play a role in inflammatory processes (43, 44) and surfactant secretion (32, 33). Both have also been involved in a variety of pulmonary diseases, like asthma, acute lung injury (ALI), and chronic obstructive pulmonary disease (COPD) (42, 45–47). Due to its low ATP sensitivity, the proinflammatory P2X7 receptor is assumed to be mainly activated under pathophysiological conditions and it is therefore considered an interesting drug target (48, 49). In contrast, the P2X4 receptor has been shown to serve also important physiological functions

such as blood pressure regulation and cardiac myocyte contractility (50, 51). Its blockade, while shown to be beneficial in pain states (52), is therefore expected to cause unwanted side effects.

Thus, considering their physiological and potential pathophysiological roles and their potential to serve as drug targets, it is important to better understand the physiological relevance of their interaction and in particular, the possibility of heteromer formation as this would enable the development of subtype-specific antagonists. Here, we set out to reinvestigate this interaction in native mouse lung using a P2X7-EGFP overexpressing reporter mouse as well as P2X4 and P2X7-deficient mice ( $P2rx4^{-/-}$ ,  $P2rx7^{-/-}$ ).

# 2 Materials and methods

# 2.1 Animals

Tg(RP24–114E20P2X7451P-StrepHis-EGFP)Ani (P2X7-EGFP), P2rx7<sup>tm1d(EUCOMM)Wtsi</sup> (P2rx7<sup>-/-</sup>), and P2rx4<sup>tm1Rass</sup> (P2rx4<sup>-/-</sup>) mice have been described (53, 54). All mice were bred in a C57Bl/6N background and housed in standard conditions (22°C, 12 h light–dark cycle, water/food *ad libitum*). All animal experiments were performed in accordance with the principles of the European Communities Council Directive (2010/63/EU). Procedures were reviewed and approved by the Government of Upper Bavaria (ROB, 55.2–1-54–2532-59–2016, 55.2–2532.Vet\_02–20-147). All efforts were made to minimize suffering and number of animals.

# 2.2 Protein extraction from mouse tissue

Mice were euthanized by isoflurane exposure followed by cervical dislocation. The lung was dissected and milled in 600 µl of homogenization buffer (0.1 M sodium phosphate buffer, pH 8.0, 0.4 mM Pefabloc SC (Sigma) and Complete protease inhibitor (Roche Applied Science) using a Precellys 24 homogenizer (Peqlab) and 2.8 mm ceramic beads. Cell fragments, nuclei, and organelles were pelleted by centrifugation at 1000 x g and 4°C for 15 min. The supernatant, comprising membrane fragments and soluble proteins, was subsequently centrifuged at 21000 x g and 4°C for 60 min to pellet the crude membrane fraction. Membrane proteins were solubilized by resuspension in extraction buffer containing 1% NP-40 (Sigma), 0.5% n-dodecyl-β-D-maltoside (Calbiochem) or 1% digitonin (Sigma) and incubated for 15 min at 4°C. The protein extract was afterwards cleared from insoluble fragments by centrifugation (21000 x g, 4°C, 10 min) to obtain the supernatant with solubilized membrane proteins.

# 2.3 Protein expression in and extraction from *Xenopus laevis* oocytes

P2X4 and P2X7-EGFP were subcloned into the pNKS2 oocyte expression vector (55). Linearized (*XbaI*) plasmid DNA was purified with the Qiagen clean up kit and cRNA was synthesized using the mMESSAGE mMACHINE SP6 transcription kit. *Xenopus* 

laevis oocytes were kindly provided by Prof. Luis Pardo (Max Planck Institute for Experimental Medicine, Göttingen), injected with 25 ng cRNA, and kept at 16°C in ND96, supplemented with 500 μl/ml gentamycin. 2–3 days after injection, 6–12 oocytes were homogenized in extraction buffer (0.1 M phosphate buffer (pH 8.0), 0.4 mM Pefabloc SC, and 1% NP40 or 0.5% n-dodecyl-β-D-maltoside, 20 μl buffer/oocyte). After 15 min incubation on ice, the protein extract was cleared by two centrifugation steps (10 min, 15000 x g, 4°C).

# 2.4 Protein expression in and extraction from HEK cells

P2X4 and P2X7 were subcloned into the pcDNA3.1 mammalian expression vector. Cells were seeded on 6-well plates at a density of 2 x  $10^5$  cells per well in serum-free medium. The next day, DNA was introduced in the cells using the Turbofect transfection reagent (Thermo, Germany) following the indications of the manufacturer. Cells were kept at 37°C. 2 days after transfection, cells were detached by flushing them directly with sodium phosphate buffer (pH 8.0). The cells were pelleted by centrifugation at 800 x g for 5 min at 4°C, and later homogenized in 150–500 μl extraction buffer containing 0.1 M phosphate buffer (pH 8.0) supplemented with Pefabloc SC and 0.5% n-dodecyl-β-D-maltoside. After 15 min incubation on ice, the membrane fraction was obtained by centrifugation for 10 min at 21000 x g and 4°C and collection of the supernatant.

# 2.5 Immunoprecipitation

10–30 μl GFP-Trap <sup>®</sup> agarose beads (Chromotek) were washed three times (1000 x g, 1 minute, 4°C) with washing buffer (1:5 dilution of extraction buffer in sodium phosphate buffer (pH 8.0) supplemented with 150 mM NaCl). 300 μl of protein extracts were added to the beads and incubated under slow rotation for 1 h at 4°C. Beads were then washed three times with 500 μl of washing buffer and purified protein eluted by 2 min incubation with 45 μl 0.2 M glycine (pH 2.5) and subsequent neutralization with 5 μl 1 M Tris (pH 10.5), as recommended by the manufacturer.

# 2.6 SDS-PAGE and western blot analysis

Proteins (40  $\mu$ l extract, 20–40  $\mu$ l eluate) were separated on 8% SDS-PAGE gels and blotted onto Immobilon-FL PVDF membranes (Merck Millipore) for 16 h at 4°C using a Mini Trans-Blot cell (Bio-Rad). After transfer, membranes were blocked with Intercept (TBS) Blocking Buffer (LI-COR Biosciences) diluted 1:2 in TBS. For the immunological detection of proteins, the membrane was incubated with the specific primary antibodies diluted in blocking buffer for 60 min at RT or overnight at 4°C. After washing three times for 5 min with TBS-T (0.1% Tween-20), the membrane was incubated with the fluorescent dye-conjugated secondary antibodies diluted in TBS-T for 60 min at RT. The membrane was again washed three

times for 5 min with TBS-T and finally rinsed with TBS before detecting signals by using the Odyssey infrared imaging system (LICOR Biosciences). For antibodies see Supplementary Table S1.

# 2.7 Nanobody production

7E2-rbIgG and 7E2-hIgG1 heavy chain antibodies (hcAbs) were generated by cloning the mouse P2X7-specific nanobody 7E2 upstream of the hinge and Fc of rabbit IgG or the hinge and Fc of human IgG1 into the pCSE2.5 vector respectively (vector was kindly provided by Thomas Schirrmann, Braunschweig, Germany (56). HcAbs were produced by transiently transfected HEK-6E cells cultivated in serum-free medium. Six days post transfection supernatants were harvested and hcAbs were purified by protein A Sepharose affinity chromatography as described earlier (57).

# 2.8 Immunofluorescence staining of lung frozen sections

Mice were euthanized by careful cervical dislocation and subsequently transcardially perfused with 20 ml PBS (pH 7.4) followed by 20 ml 4% PFA/PBS. The lungs were then intratracheally inflated with 1ml of 4% PFA/Tissue-Tek O.C.T. and the trachea subsequentially sealed with a suture. Lungs were removed, post-fixed overnight in 4% PFA/PBS (at RT), and cryoprotected for 24 h at 4°C in a 10-25% sucrose gradient in PBS (pH 7.4) before they were embedded in Tissue-Tek O.C.T and frozen at -20°C. 10 or 20 µm sections were prepared and dried for 30 min at RT on glass slides, followed by an antigen retrieval step (25 min incubation at 37-50°C in citrate buffer (10 mM sodium citrate, 0.05% Tween20, pH 6.0). Slices were then blocked for 1 h at RT (0.4% Triton X-100, 1% BSA, 5% normal goat serum (NGS) in PBS). Lung sections were afterwards incubated for 16-24 h at 4°C with primary antibodies in a humidified chamber, washed 5 x 10 min with PBS-T (0.05% Tween20 in PBS), and stained for 2 h at RT with fluorescent dye-conjugated secondary antibodies. All antibodies were diluted (for antibody details and ratios see Supplementary Table S1) in blocking solution. After washing (5 x 10 min, PBS-T), slices were incubated for 1-3 min with 4', 6-diamidino-2-phenylindole (DAPI, 0.1 mg/l in PBS) and washed again (2 x 10 min, PBS). In some cases, Thiazole Red (TO-PRO-3, 1:1000, ThermoFisher Scientific) was used instead of DAPI and incubated together with the secondary antibodies. Coverslips were mounted using PermaFluor mounting medium, and slides were kept overnight at RT and then saved at 4°C until confocal scanning. For long-term storage, slices were kept at -20°C.

# 2.9 Preparation of alveolar macrophages

Mice were euthanized by cervical dislocation and lungs were then intra-tracheally lavaged (6x) with 1 ml PBS/0.5% BSA/2 mM EDTA (pH 7.4). Cells were collected by centrifugation (300 g at RT for 5 min), resuspended in RPMI1640 media containing 10% FCS, Pen/Strep (10 U/mL; 10  $\mu$ g/ml) and 50  $\mu$ M  $\beta$ -mercaptoethanol, and seeded in cell culture dishes (24-well for staining, and 5 cm for RNA

preparation). After 12-24 h (37°C, 5%  $CO_2$ ) cells were washed in PBS and either fixed for immunofluorescence staining or lysed in Trizol for subsequent RNA extraction.

# 2.10 Isolation and culture of alveolar epithelial type 2 cells

Isolation of alveolar epithelial cells was performed based on former protocols (58, 59) with some minor modifications (60). In brief, 4–5 mice were euthanized by cervical dislocation and lungs were perfused with 0.9% NaCl (B. Braun Melsungen AG) and instilled with 1.5 ml dispase solution (Corning) followed by 400 µl 1% low-melting agarose (Sigma) via the trachea. Lungs were removed and digested in dispase for 45 min. Tissues were treated with DNAse I (AppliChem) in DMEM (ThermoFisherScientific) with HEPES (AppliChem) and were processed through 100 µm, 20 µm and 10 µm meshes (Sefar) to obtain a single cell suspension. After centrifugation, the cell pellet was resuspended in medium without DNAse I, transferred to cell culture dishes coated with antibodies directed against CD16, CD32 and CD45 (see Supplementary Table S1) and incubated for 30 min at 37°C to remove immune cells. The supernatant and medium from an additional wash step were collected, transferred to cell culture dishes and incubated for 60 min at 37°C to remove fibroblasts. The suspension was centrifuged at 200 g for 5 min, cells were resuspended in DMEM medium buffered with HEPES containing 10% FCS, and seeded in a six-well plate. AT2 cells were collected 36-48 h after seeding for IF-staining. Cell identity was confirmed with an antibody against the cell type-specific marker protein pro-SP-C (Supplementary Table S1).

# 2.11 Immunofluorescence staining of adherent cells

Cells plated on 1.3 cm glass coverslips were fixed with 4% PFA/PBS (10 min at RT), washed twice with PBS, permeabilized for 10 min or 1 h at RT with 0.5% Triton X-100/PBS, and blocked (4% BSA, 4% normal goat serum diluted in PBS) for 60 min at RT. Cells were then incubated with primary antibodies (16–24 h at 4°C, see Supplementary Table S1), fluorescence conjugated secondary antibodies (60 min at RT) and DAPI staining solution (0.2 mg/ml DAPI/PBS, 1–3 min at RT). After each labeling step, cells were washed in 0.1% BSA/PBS (5 x 5 min at RT) and finally rinsed in milli-Q H<sub>2</sub>O before they were mounted on object slides with PermaFluor mounting medium. All antibodies were diluted in 2% BSA/PBS (see Supplementary Table S1). Images were obtained by confocal laser scanning microscopy using a Zeiss LSM 880.

# 2.12 Confocal imaging

Confocal images were taken using a Zeiss LSM 880 microscope with airyscan using the ZEN Black software (2.3 SP1 FP3). Each channel was imaged separately to avoid bleed-through between the channels. Tissue/cell samples and respective negative controls from

knock-out mice were prepared in parallel and used to determine background staining. The same settings (laser intensity and digital gain) were then applied for samples from wt and transgenic mice. Airyscan deconvolution was performed with automatic settings for all channels. Intensity profiles were created with the image processing suite from Zeiss ZEN 2.3 SP1 FP3 (black) at a representative position close to the nucleus. Images were processed with FIJI [Image J v.1.53c, Wayne Rasband, National Institutes of Health, USA, (61)].

# 2.13 RNA extraction and real-time PCR

Total mRNA was isolated from 20-30 mg of mouse tissue using the RNeasy plus mini kit (Qiagen). In the case of alveolar macrophages Trizol (ThermoFisher Scientific) was used for RNA extraction (1x10<sup>6</sup> cells/ml). Complementary DNA (cDNA) was synthesized with the QuantiNova reverse transcription kit (Qiagen) following the manufacturer's instructions from 1 µg of RNA. The quantitative PCR was carried out in a LightCycler 480 System using LightCycler 480 SYBR green I Master (Roche) and LightCycler 480 multiwell plates using 1 µl of cDNA. Primers were designed to span an exon-exon junction (see Supplementary Table S2). Relative mRNA levels were calculated by the ΔCtmethod using ribosomal protein lateral stalk subunit P0 and peptidylprolyl isomerase A (PPIA) (whole lung) or only PPIA (alveolar macrophages) as a reference (62): Relative mRNA level =  $2^{-\Delta Ct}$ , where  $\Delta Ct$  = Ct(target)- Ct(reference) and Ct = cycle threshold.

# 2.14 Statistical analysis

Statistical analysis was performed with Graph Pad Prism software and data are presented as means  $\pm$  standard deviation (SD). Shapiro-Wilk normality test was applied before mean comparison. After meeting the assumptions of normality and variance homogeneity, student's t-test was used to determine statistical differences between groups. Significance was accepted at \* p < 0.05, \*\* p < 0.01, \*\*\* p < 0.001 and \*\*\*\* p < 0.0001.

# **3 Results**

# 3.1 P2X4 is not co-purified with transgenic P2X7-EGFP from mouse lung

P2rx4 and P2rx7 have been shown to be widely expressed in lung tissue (17) and the physical interaction of the respective proteins as well as a mutual interrelation has been reported in a murine alveolar epithelial cell line (38) and in mouse primary macrophages (24). To verify and quantify this interaction in native lung tissue, we used a BAC transgenic P2X7-EGFP reporter mouse model and performed pull-down experiments using the transgenic EGFP-tagged P2X7 receptor as a bait and bead-coupled nanobodies against GFP for purification (Figure 1A).

As seen in Figure 1B, both P2X4 and P2X7 were clearly detected in extracts of the mouse lung, confirming their expression in this tissue. In contrast to the studies described above, however, no P2X4 subunits could be co-purified from lung extracts prepared with the non-denaturing detergents NP40, n-dodecyl-β-D-maltoside, and digitonin (Figure 1B). Since P2X4 was previously shown to associate closely with P2X7 in Xenopus laevis oocytes and to be purified with P2X7 from the tsA201 subclone of HEK cells (35, 39), we decided to use these same expression systems as a positive control and next co-expressed mouse P2X4 together with an EGFPtagged mouse P2X7 construct in these heterologous expression systems. Using the same conditions as applied for the mouse tissue and an identical P2X7-EGFP construct, P2X4 could be clearly co-purified with P2X7 from Xenopus oocytes (Figure 1C) but not from HEK cells stably expressing the P2X7-EGFP construct and transiently co-transfected with P2X4 (Figure 1D). Based on these results, we argue that there is no significant physical interaction (either heteromerization of subunits or dimerization of receptors) between P2X4 and P2X7 in native mouse lungs.

# 3.2 Cell type-specific localization of P2X7 in the mouse lung

Presence of both P2X4 and P2X7 protein has been shown in different cell types in the lung (38, 63). These studies mostly relied on pharmacological analysis and transcript identification in cultured primary cells or cell lines. More recent single-cell RNA-sequencing (scRNA-Seq) studies (64) indicate that, except for macrophages, single cell expression data of the corresponding genes *P2rx4* and *P2rx7* display limited overlap in intensity and cell type distribution, suggesting a subordinate role of co-expression in mouse lung tissue (Supplementary Figure 1A). Transcript data, however, often do not correlate with protein abundances (compare Supplementary Figure 1B) and some cell types, e.g. alveolar type 1 (AT1) cells, are frequently underrepresented in scRNA-Seq data (65).

Hence assessing the precise localization of the P2X7 receptor in non-transfected tissues at protein level is crucial, but has been difficult due to a lack of specificity of the available antibodies (66, 67). In particular, P2X4 and P2X7 co-staining in native tissues has been challenging because the commercially available antibodies are derived from the same host. Therefore, to determine sites of possible P2X4/P2X7 interaction in the mouse lung, we generated a P2X7-specific nanobody fused to the Fc domain of human IgG1 (7E2-hIgG hFcAb) and made use of the P2X7-EGFP reporter mouse, which was previously shown to reliably report the P2X7 expression pattern in mouse brain and gut nervous system (54, 68, 69). To confirm that this model also correctly mirrors endogenous P2rx7 expression in the lung, we first compared immunostainings of lung sections from wild-type (wt), P2X7-EGFP, and P2rx7<sup>/-</sup> mice using the previously described P2X7-specific nanobody fused to a rabbit Fc domain (7E2-rbFc, (54)). As seen in Figure 2A, both wt and P2X7-EGFP reporter mice present an evenly distributed staining along the lung alveoli, most likely representing epithelial cells, and a stronger signal in single cells, which likely represent

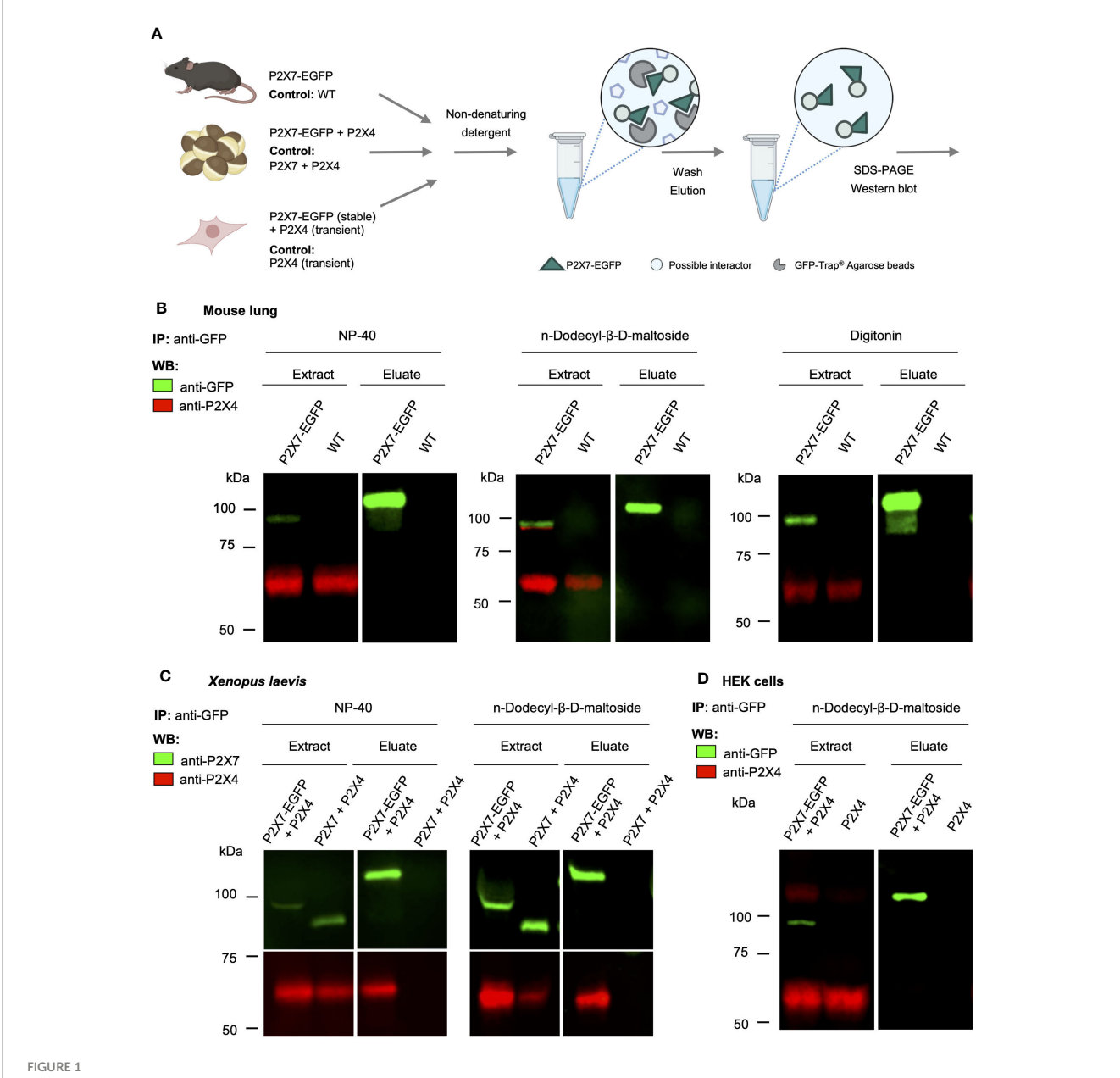


FIGURE 1
Lack of evidence for a physical interaction of P2X4 and P2X7 receptors in transgenic P2X7-EGFP mice. (A) Schematic representation of the purification of P2X7-containing complexes from mouse lung, cRNA-injected *Xenopus laevis* oocytes, and transfected HEK cells using anti-EGFP nanobodies (GFP-Trap®). (B) Immunoprecipitation of P2X7-EGFP complexes from lung tissue of BAC-transgenic P2X7-EGFP mice and wt controls using the indicated non-denaturing detergents for solubilization. Primary antibodies against GFP (from rat) and P2X4 (from rabbit) and secondary antibodies for infrared imaging were used for blot development and detection. Note that P2X4 has a tendency to form higher aggregates (dimers band in the middle image) but does not associate with P2X7 (absence of a band stained with both antibodies). (C) Co-purification of P2X4 with P2X7-EGFP from *Xenopus laevis* oocytes. cRNA encoding P2X4 subunits was injected together with cRNA encoding P2X7-EGFP or non-tagged P2X7 subunits (negative control). After 2 days, P2X7-EGFP complexes were immunoprecipitated as in B, using the indicated detergents. Blots were developed with antibodies against P2X4 and P2X7 (both derived from rabbit). (D) Immunoprecipitation of P2X7-EGFP complexes from HEK293 cells. P2X4-encoding DNA was transfected transiently into HEK293 cells stably expressing P2X7-EGFP and wt control cells. Proteins were extracted in n-dodecyl-β-D-maltoside and purified and detected as in (B). Representative results of at least two experiments are shown. Note that the harsh conditions required to elute the protein from the nanobody-coupled beads leads to a stronger protein denaturation than addition of SDS and results in a size shift of the P2X7-EGFP band as well as loss of EGFP fluorescence. Also note, that the eluate was about three times more concentrated than the extract. Panel (A) was created with BioRender.com.

macrophages (arrowheads in Figure 2A). As expected, sections from wt mice show a lower signal intensity than sections from P2X7-EGFP overexpressing mice.  $P2rx\mathcal{T}^{/-}$  mice showed only background fluorescence when imaged under identical conditions. Similar

results were obtained using a commercially available P2X7 antibody (Supplementary Figure 2A) and with the same nanobody linked to the human Fc-domain (Supplementary Figure 2B). To identify the *P2rx7*-expressing cell types, we next

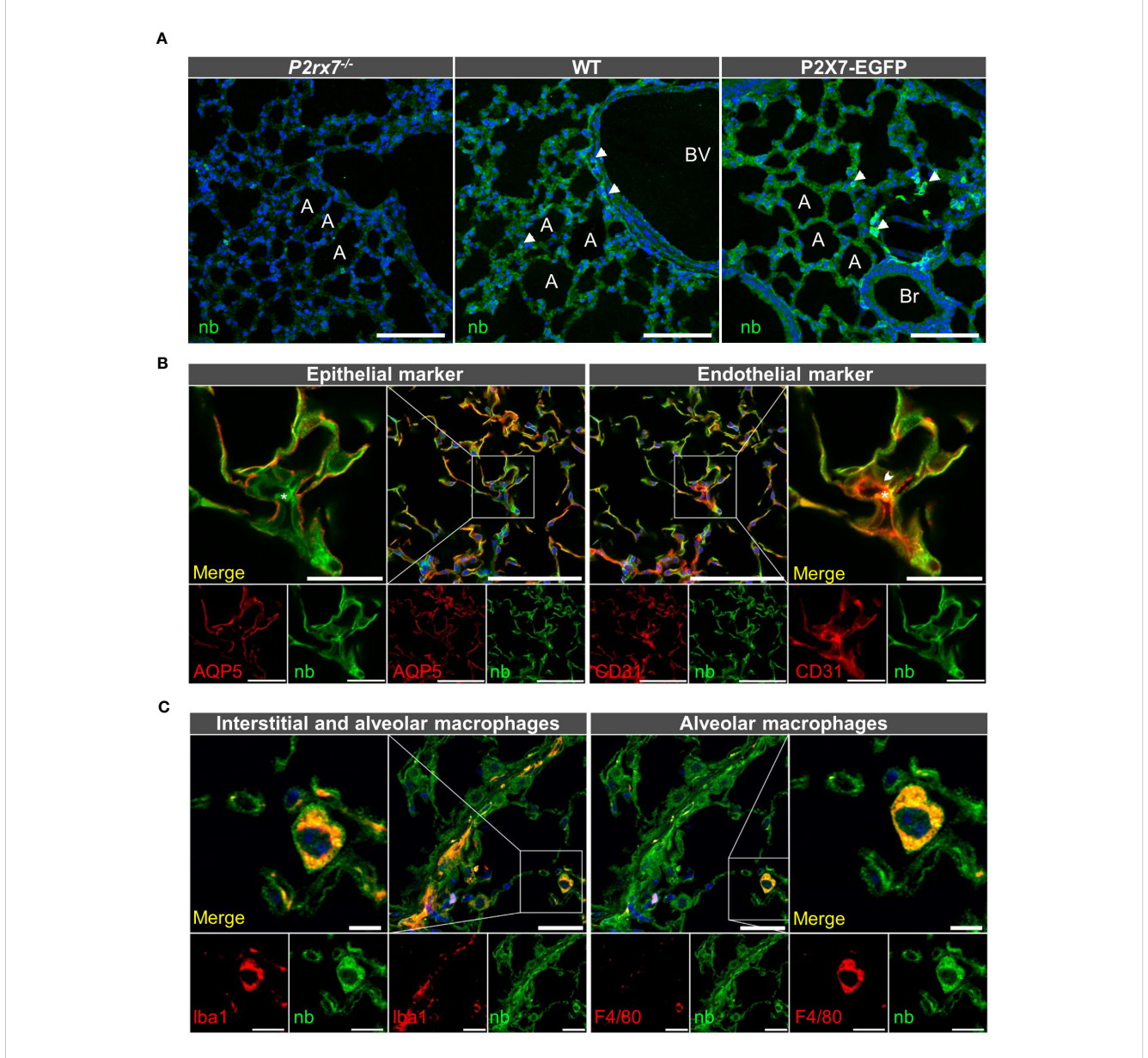


FIGURE 2
Cell type-specific P2X7 protein expression in the mouse lung. (A)  $10-20~\mu m$  lung cryosections from wt mice, P2X7-EGFP mice, and  $P2rx7^{-1}$  mice as negative control were prepared in parallel and immunostained with a P2X7-specifc nanobody (7E2-rbFc). Arrowheads show brighter cells, most likely macrophages. A = Alveolus, Br = Bronchiole, BV = Blood vessel. Scale bar  $100~\mu m$ . (B) Lung cryosections from wt mice were co-stained with the P2X7 nanobody (7E2 nb-hFc) and antibodies against the epithelial cell marker aquaporin 5 (AQP5) and the endothelial cell marker platelet endothelial cell adhesion molecule PECAM-1 (CD31). Insets show representative areas of differential staining for the two marker proteins. The arrowhead indicates a CD31 positive cell adjacent to a red blood cell (indicated by asterisk). Scale bar  $100~\mu m$ , inset scale bar  $100~\mu m$ . Nuclear staining with DAPI (in A, C) or TO-PRO-3 (in B) is shown in blue.

performed co-staining with cell type-specific markers. Figure 2B shows that the P2X7 staining lining the alveoli overlaps with the epithelial AT1 cell marker aquaporin 5 (70), in support of the previously reported presence of P2X7 in epithelial cells (38, 71). Due to their close association with epithelial cells, presence of P2X7 protein in aerocytes could not be reliably confirmed. However, in regions where a cross-section of a microvessel could be identified,

CD31-positive microvascular endothelial cells (arrowhead) show distinct P2X7-positive staining (see insets in Figure 2B). In addition, we confirmed that the single cells with more intense P2X7 staining are Iba1-positive macrophages [enlarged inset in Figure 2C, (72)]. Only a subset of these are F4/80-immunopositive, most likely representing alveolar macrophages (in Figure 2C). Presence of P2X7 in lung fibroblasts was excluded (Supplementary Figure 3).

# 3.3 P2X4 and P2X7 show distinct cellular localization

After identifying alveolar epithelial cells and macrophages as the dominant P2X7-positive cells in the lung parenchyma, we next performed co-staining of P2X4 and P2X7. To this aim, we first co-stained tissue from P2X7-EGFP transgenic mice with chicken anti-GFP and rabbit anti-P2X4 antibodies (Figure 3A). This revealed a clearly distinct cellular distribution of both receptors in the alveolar epithelium. While P2X7-EGFP is consistently localized along the respiratory epithelium, the P2X4 signal is mainly detected in single cells that are larger than AT1 cells and localized at the intersections

between alveoli. Only few P2X4-positive cells show clearly overlapping cellular expression with P2X7, and most likely represent macrophages (Figure 3B), as both subunits are co-expressed in this cell type [Supplementary Figure 1. (13, 73)]. However, a distinct subcellular localization of P2X4 and P2X7 is observed in these cells (Figure 3B). Based on the localization and morphology, the majority of P2X4-positive cells most likely represent AT2 cells, in agreement with the modulatory role of P2X4 in secretion of lung surfactant in these cells (33). To confirm the specific localization of P2X4 in AT2 cells, we next used a monoclonal rat anti-P2X4 antibody in combination with an antibody against the AT2 cell-specific marker pro-surfactant protein C (pro-SPC, Figure 3C).

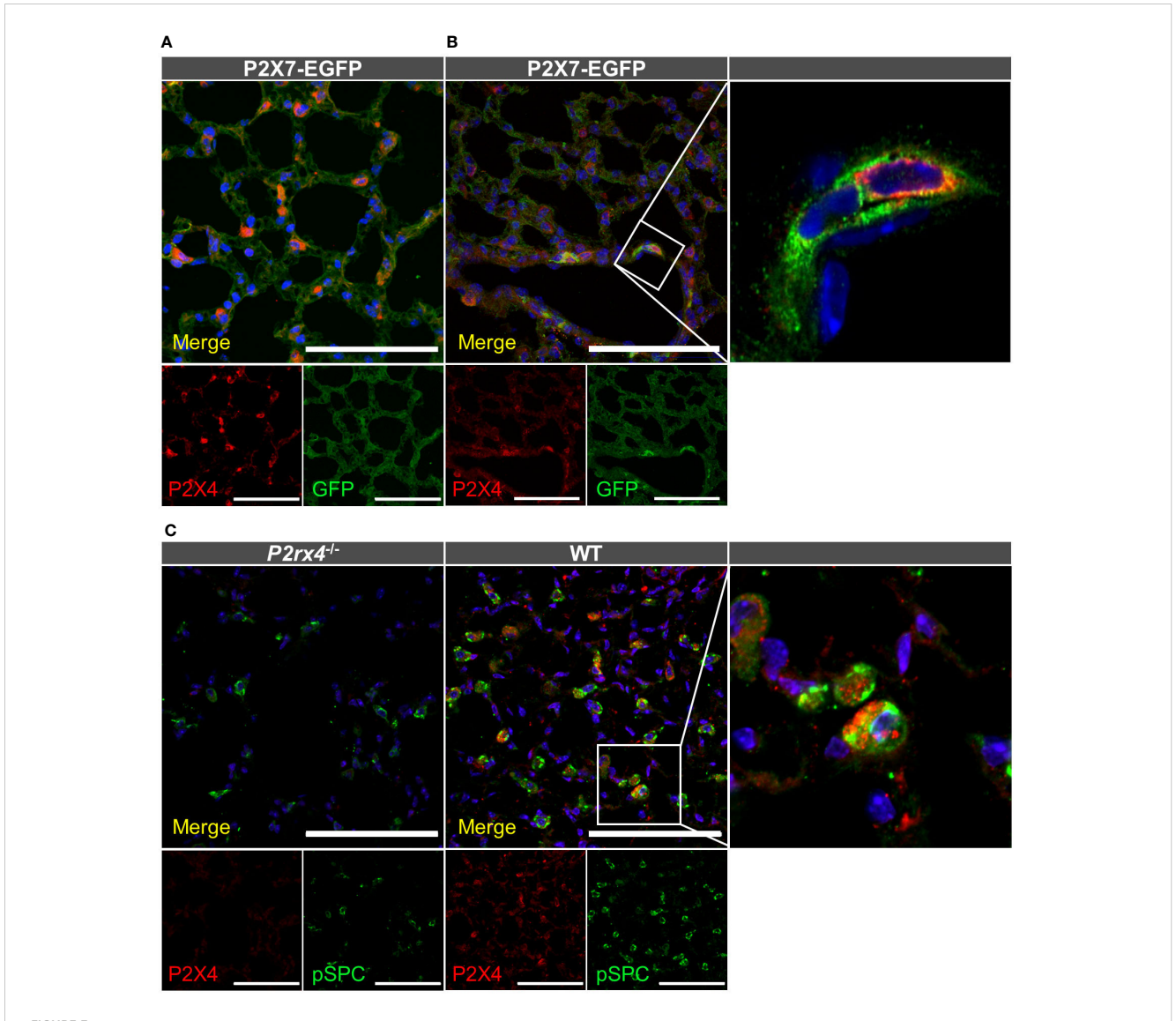


FIGURE 3
Cellular distribution of P2X4 and P2X7 protein in lung tissue. Cryosections (10–20 µm) of lung tissue from the indicated genotypes were immunostained with anti-GFP (green) and anti-P2X4 (red) antibodies and imaged by confocal microscopy (A) and Airyscan (B). Note that the enlarged inset in B was imaged separately (C) Specificity of the monoclonal rat anti-mP2X4 antibody in primary cells and co-staining with prosurfactant protein C as a marker for AT2 epithelial cells. Nuclear staining with DAPI (in A, B) or TO-PRO-3 (in C) is shown in blue. Scale bar 100 µm. Insets show the representative subcellular distribution of the respective proteins.

Despite the evident presence of P2X4 and pro-SPC in AT2 cells, both proteins also show a clearly distinct subcellular localization (Figure 3C inset). Whereas the anti-pro-SPC antibody appears to stain larger structures and most of the cell content (in agreement with staining of cytoplasmic pro-SPC), P2X4 shows a more restricted distribution in smaller compartments that most likely represent lamellar bodies. Mature lung surfactant is stored in lamellar bodies of AT2 cells and its exocytotic release has been shown to be facilitated by P2X4-mediated fusion-activated  $Ca^{2+}$  entry (FACE) into lamellar bodies (33). The specificity of the anti-P2X4 antibody was confirmed using lung tissue and macrophages from  $P2rx4^{-1-}$  mice as control (Figure 3C, Supplementary Figure S4).

In conclusion, we detect both P2X4 and P2X7 protein in interstitial macrophages and AT2 cells, in agreement with previous reports (17). However, both appear to have distinct subcellular localization.

# 3.4 P2X4 and P2X7 have distinct subcellular localization

To provide additional support for the cell type-specific localization and the distinct subcellular localizations of P2X7 and P2X4 in AT2 epithelial cells and macrophages and to better estimate possible regions of interaction, we next isolated primary AT2 epithelial cells as well as alveolar and bone marrow-derived macrophages from wt mice and the respective knock-out animals (Figure 4). These two types of macrophages were used since interstitial lung macrophages are difficult to obtain and require careful characterization. As expected, P2X4 shows a punctate and clearly intracellular localization in the case of AT2 cells (Figure 4A), often lining vesicle-like structures (arrows in Figure 4A, Supplementary Figure S5). P2X7 staining appears punctate without clear membrane localization (except for cells from transgenic mice (Supplementary Figure 5) but does not overlap with P2X4. While the reason for this unexpected intracellular localization is unclear, its presence in AT2 cells was further confirmed by Western blotting (Supplementary Figure 1B). In macrophages, a clear membrane localization is seen for both wt and P2X7-EGFP transgenic mice (Figures 4B, C, Supplementary Figure 5) and, importantly, no co-localization is observed for P2X4 and P2X7 (Figure 5). A very similar subcellular distribution of mainly membrane-localized P2X7 and intracellular P2X4 was confirmed in isolated peritoneal and primary microglia, the phagocytic cells of the brain (Supplementary Figure 6). Costaining of alveolar, peritoneal, and bone-marrow derived macrophages with CD68 (Figure 5) confirmed the presence of P2X4 in endosomal/lysosomal compartments, in agreement with previous findings, where P2X4 signal overlaps with the signal of LAMP-1 in macrophages, microglia, endothelial cells, and HEK293 cells (14, 19). Taken together, our findings argue against the possibility of substantial physical interactions between both subunits in the plasma membrane of phagocytic cells and might explain the absence of a clear electrophysiological phenotype resulting from their co-assembly (36).

# 3.5 Mutual interrelation between *P2rx4* and *P2rx7* expression?

In previous studies, the mutual interaction between P2rx4 and P2rx7 expression levels has been analyzed at mRNA and protein levels to identify a possible interrelation. Quantitative reverse transcription (qRT)-PCR data from mouse kidneys showed a significant reduction of P2rx4 and P2rx7 mRNA levels in genedeficient mouse models of the respective other subunit (41). In contrast, a reverse relationship was observed in a study that investigated expression at protein level of both subunits in an alveolar epithelial cell line and found that shRNA-mediated downregulation of one subtype resulted in an increased protein levels of the respective other subtype (38). Therefore, we asked whether overexpression of P2X7 in the BAC transgenic mouse model or the genetic ablation of one of both subtypes influenced protein levels of the respective other subunit in mouse lung tissue. No mutual interrelation on the protein level was observed in the whole mouse lung (Figure 6A). Likewise, the mRNA levels of the respective other subunit were not significantly altered by P2X7-EGFP overexpression or genetic ablation of either subunit (Figure 6B). Unexpectedly, but in line with the P2X7 staining in primary cells from P2rx4-/- mice (Figure 4) and Western blot analysis from AT2 cells Supplementary Figure 1B), a significantly decreased level of P2rx7 expression was found in alveolar macrophages of P2rx4<sup>-/-</sup> mice. (Figure 6C). These data were further supported by flow cytometric analyses of alveolar macrophages (characterized as CD11b+CD11c+CD64+CD206+), where cell surface-localized P2X7 expression levels were slightly reduced in P2rx4-/- mice when compared to WT mice (Supplementary Figure 8).

# 4 Discussion

Both P2X4 and P2X7 channels have been involved in several lung diseases including pulmonary fibrosis, COPD, and asthma (42, 45-47). Common cellular functions and evidence for and against their interaction have been reported and the formation of P2X4/7 complexes would be of important pharmacological relevance. Since much of this evidence stems from cell culture or overexpression systems, it is still an open question if these interactions take place at physiological expression levels in situ. Due to a lack of suitable antibodies, such studies have so far been difficult in native tissues or primary cells. Here, we used P2X7-specific nanobodies in combination with a P2X7-EGFP reporter mouse and P2X4 and P2X7 knock-out controls to investigate for the first time the physical interaction, co-localization, and mutual interrelation of the P2X7 and P2X4 subtypes in the native mouse lung as well as in primary macrophages and epithelial cell cultures. We find no physical association and show that both channels, while coexpressed in macrophages and AT2 epithelial cells, display clearly different subcellular localizations. Finally, we find that deletion of P2X4 reduces P2rx7 expression in macrophages and AT2 cells while

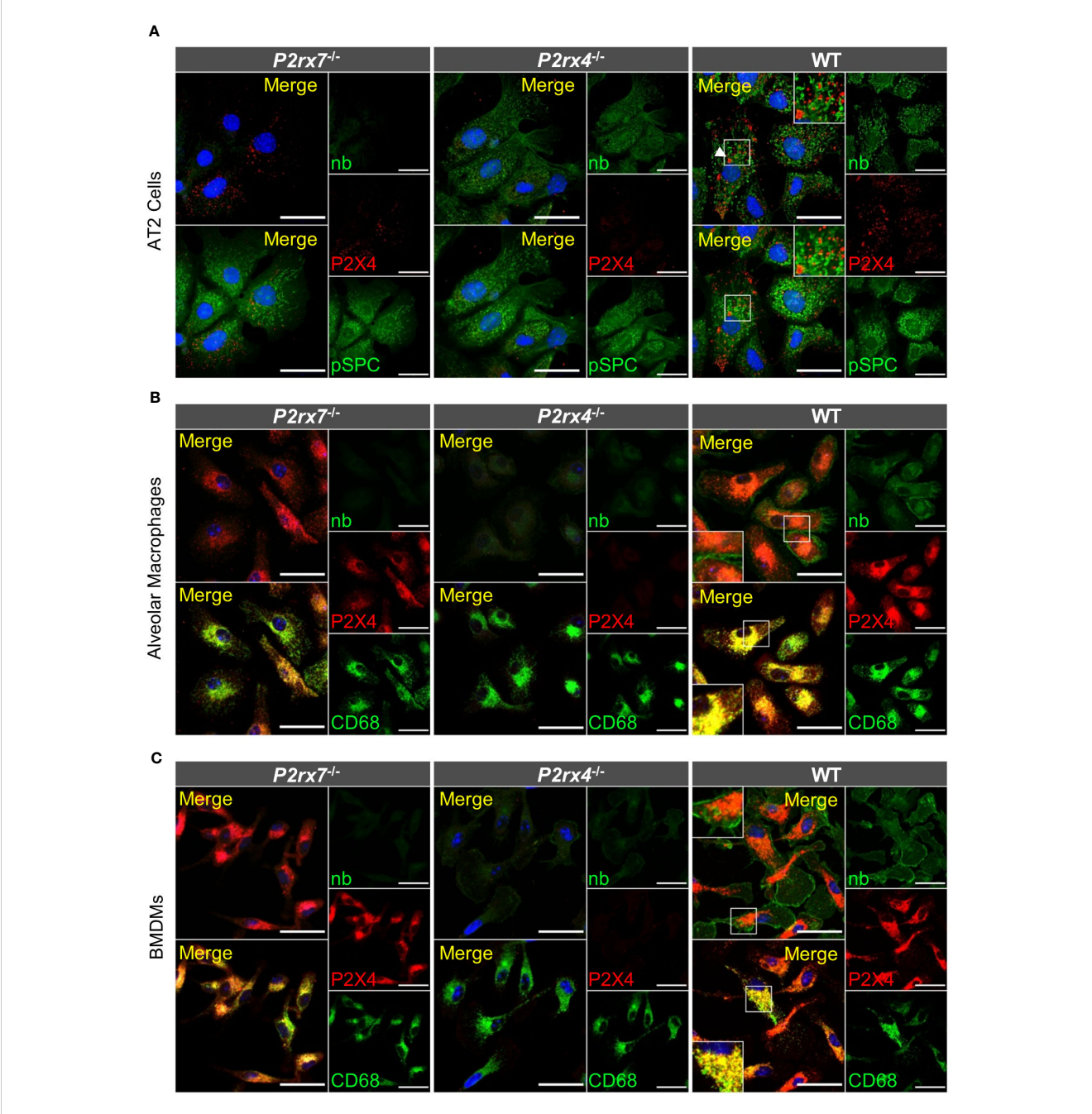
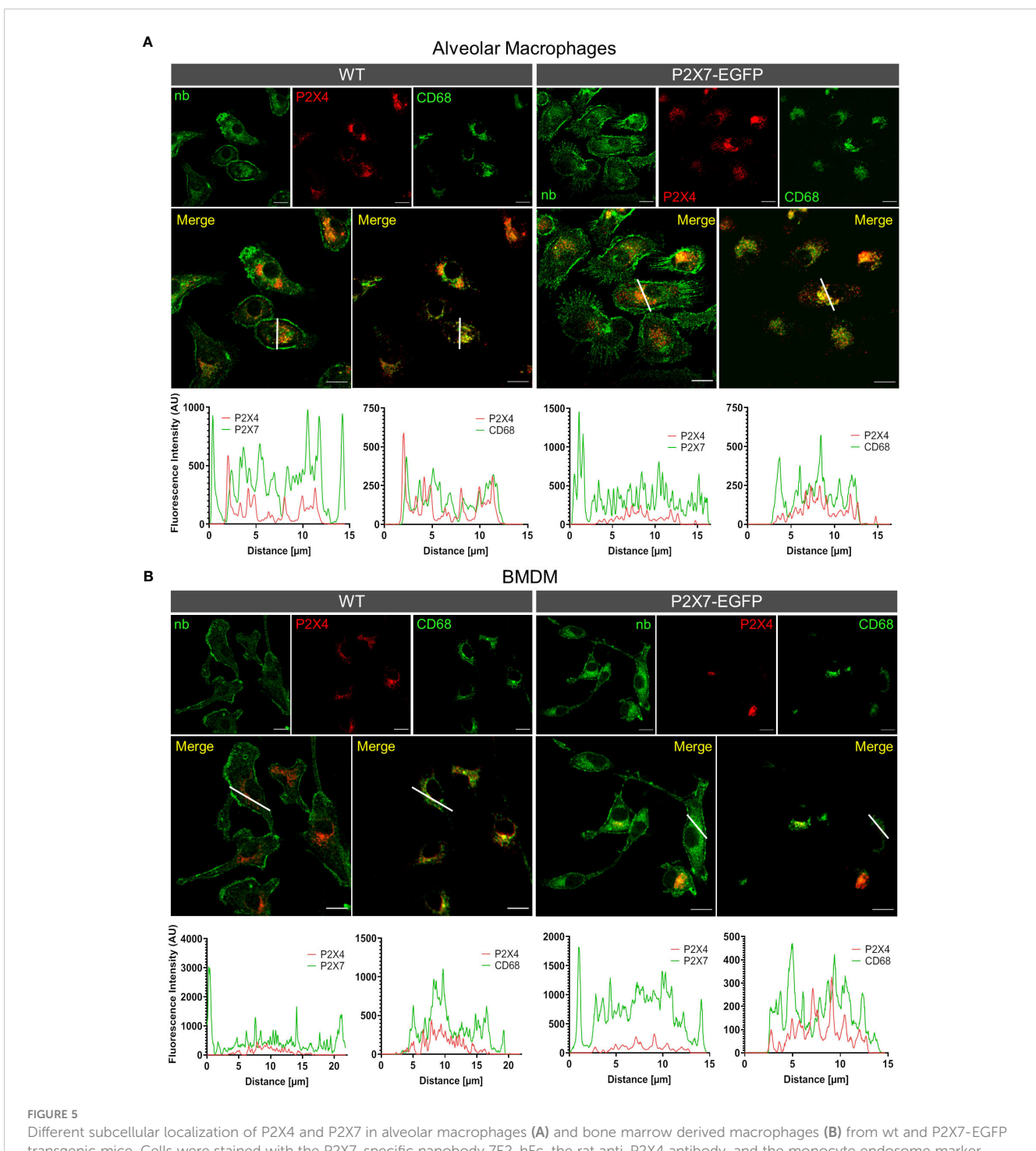


FIGURE 4
Subcellular localization of P2X4 and P2X7 in primary AT2 cells and macrophages. (A) Primary AT2 epithelial cells from wt mice and P2rx7<sup>-/-</sup>, P2rx4<sup>-/-</sup> controls, were stained 24 hours after plating with the P2X7-specific nanobody (7E2-hFc), rat anti-P2X4 antibody, and anti-prosurfactant protein C (SPC) as an AT2-type cell marker. (B) Alveolar macrophages and (C) bone marrow-derived macrophages (BMDM) isolated from wt and the respective P2X knock-out control mice were stained with the P2X7-specific nanobody (7E2-hFc), anti-P2X4 antibody, and an antibody against the lysosomal/ endosomal marker protein macrosialin (CD68). Nuclear staining with TO-PRO-3 is shown in blue. Scale bar 25 µm. Insets show intracellular puncta and/or membrane structures. Insets in upper panels show areas of intracellular P2X4 staining and comparable areas from control cells. Insets in lower panels show plasma membrane localization. Arrowheads indicate vesicle-like structures, where P2X4 is localized.

no mutual dependence was observed in whole lung tissue. Our data provide a detailed description of P2X4 and P2X7 protein localization in the mouse distal lung parenchyma and argue against a meaningful physical interaction between both receptors in this tissue.

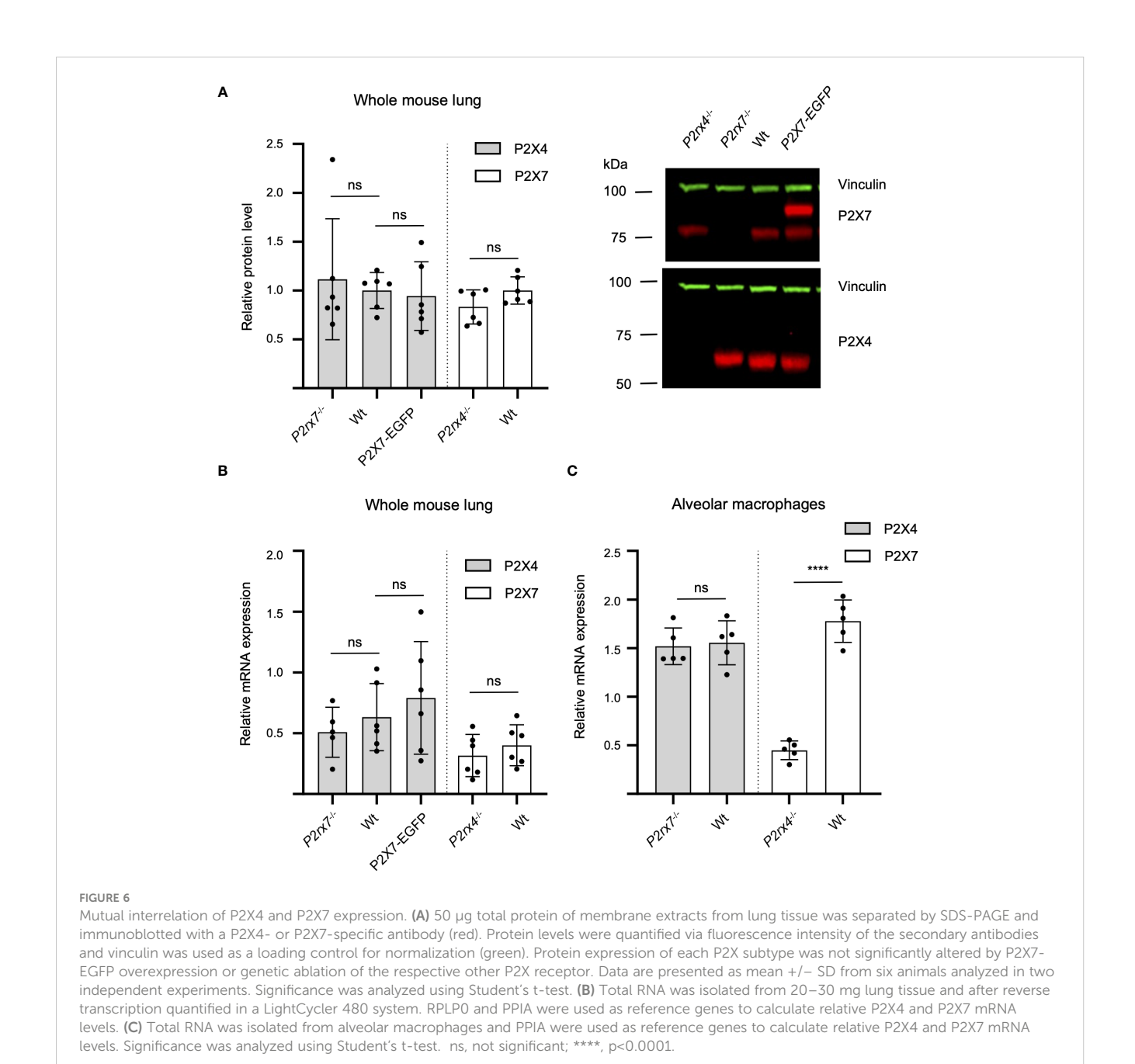
# 4.1 Do P2X4 and P2X7 receptors physically interact under native conditions?

A possible direct physical interaction and heteromerization of P2X4 and P2X7 receptors is an ongoing debate. The lack of evidence



Different subcellular localization of P2X4 and P2X7 in alveolar macrophages (A) and bone marrow derived macrophages (B) from wt and P2X7-EGFF transgenic mice. Cells were stained with the P2X7-specific nanobody 7E2-hFc, the rat anti-P2X4 antibody, and the monocyte endosome marker CD68. Images were obtained using a Zeiss LSM 880 with Airyscan, and intensity profiles obtained with the built-in image processing software (ZEN black) along the indicated lines. Scale bar 10 µm.

for a physical interaction found in this study is in contrast to many previously described findings where both subunits could be coimmunoprecipitated not only upon overexpression in HEK293 and tsA201 cells but also from a non-transfected cell line derived from alveolar epithelial cells (38) and primary epithelial cells and macrophages (14, 22, 24, 37, 39). Like in non-transfected cells, an almost similar physiological expression and only moderate overexpression levels can be expected in BAC transgenic mice. Along the same line, stably transfected P2X7-EGFP HEK cells presumably express less P2X7 than transiently transfected HEK cells. While we cannot exclude any P2X4/7 complexes below the detection level, the lack of detergent-resistant P2X4/P2X7



complexes is in agreement with a study where native rat tissues were investigated by BN-PAGE (40) and with a very limited overlap of co-localized subunits in native tissues. Thus, the described interaction of P2X4 and P2X7 in *Xenopus laevis* oocytes and HEK cells (24) might be a consequence of P2X4 and/or P2X7 over-expression in recombinant systems and possibly incorrect trafficking or accumulation in intracellular compartments such as the ER and is therefore of minor relevance in native tissue. This is supported by the fact that over-expressed P2X4 subunits show a high tendency to aggregate into oligomers (also seen in Figure 1) that likely include P2X7 subunits in case of strong overexpression. Similar findings have been described by Torres et al., who showed that P2X4 constructs were expressed at more than 10 times higher levels than other P2X subtypes in HEK293 cells and this resulted in unspecific interactions (5).

# 4.2 Are P2X4 and P2X7 receptors localized in the same subcellular compartments?

So far, due to limited availability of specific antibodies suitable for co-immunostainings, subcellular localization studies for P2X4 and P2X7 could only be performed by overexpression of tagged proteins and information about possible sites of interaction under native conditions has been lacking.

Compelling evidence for a close physical association of P2X4 and P2X7 receptors comes from co-precipitation studies with primary cells, like bone marrow-derived macrophages. However, despite the fact that both subunits are expressed in the same cell types and seem to be involved in the same signaling pathways, we and others have found a distinctly different subcellular localization. In both recombinant systems and primary cells, the P2X4 subtype

was mostly found intracellularly, co-localizing with lysosomal markers (14, 19, 74). In neurons but not primary macrophages, microglia, or vascular endothelial cells heterologously expressed GFP-tagged P2X4 receptors were also detected in the early endosomes (19, 74). P2X7, in contrast, is mainly found at the plasma membrane and only to some extent in intracellular compartments. Intracellular P2X7 signal was found to overlap with an ER marker in transfected NRK cells while the overlap of P2X4 and P2X7 signals in the plasma membrane was only limited (14). Using FRET-analysis and proximity ligation assays, colocalization was detected in transfected HEK cells and *Xenopus laevis* oocytes (24, 35, 39). This co-localization, however, might be limited to overexpressed proteins accumulated in the ER. Moreover, the tendency of some fluorescent protein tags to multimerize needs to be considered.

Nonetheless, trafficking of P2X4 to the plasma membrane is known to occur upon stimulation (e.g., via lipopolysacharide (LPS), (C-C motif chemokine 2 or 12 ionomycin) in microglia and macrophages (37, 75–77) and also in P2X4-transfected NRK (19). Thus, it is possible that in stimulated cells P2X4 receptors localize to the same compartments as P2X7 receptors (e.g. lipid rafts) and this could account for the observed co-precipitation from primary cells. Future studies on primary cells and tissues from our reporter mouse (eg. PLA with stimulated cells) and the presented antibody and nanobody tools might help to clarify this possibility. However, our immunofluorescence data support a pharmacological study in the BV-2 microglia cell line (36) and indicate that under physiological conditions, no, or only very limited amounts of P2X4 receptors are present in the plasma membrane.

# 4.3 Possible functional interactions/interrelations

Our experiments in macrophages show a significant effect of P2X4 deletion on P2X7 expression in alveolar macrophages and AT2 cells (but not vice versa), in contrast with previous studies on macrophage-like RAW264.7 cells and bone marrow-derived dendritic cells, which showed that shRNA-mediated downregulation of P2X4 did not affect P2X7 protein levels (21, 23). Together, these studies indicate that depletion of one subunit is neither limiting the expression of the respective other subunit, which would be the case if they are forming obligatory complexes, nor causing a compensatory overexpression of the other subunit, indicative of their interchangeable function in an essential physiological process. However, as mentioned above, data on mutual interrelation of the two P2X subtypes are inconclusive (38, 41) and tissue/cell type-specific differences or effects of cell manipulation might account for these findings and need to be explored. Thus, it has recently been demonstrated that the C57BL/ 6J P2rx4-/- mice carry a P2X7 SNP (78) that is not present in C57BL/6J wt controls. This passenger mutation has been shown to affect P2rx7 expression and P2X7 function in T cells (79). Likewise, we cannot exclude that the observed effect on P2rx7 expression is caused by alterations in the P2rx7 gene structure as a consequence of P2rx4 deletion rather than a functional interdependence. In support of this, a recent RNA sequencing study on microglia from P2X4-deficient mice showed that several genes that are located within 7.8 Mbase from the *P2rx4* gene, including *P2rx7*, are down regulated, likely due to chromatine alterations because of the presence of a β-galactosidase-neomycine cassette (80). Alternatively, P2X4 function in intracellular compartments might be required to regulate P2X7 plasma membrane transport and/ or turnover.

Since both P2X4 and P2X7 receptors are ATP-activated Ca2+permeable ion channels and are highly expressed in macrophages, it appears plausible that they can contribute to common signaling pathways and serve similar physiological function, at least if both were present in the plasma membrane. This could well explain the observed mutual influence on current kinetics, pore formation, ROS production and the secretion of mature IL-1beta and IL-18 through the activation of the NLRP3 inflammasome (20, 22, 24, 26). For example, rapid initial P2X4-mediated Ca2+ influx was suggested to initiate the P2X7-mediated IL-1b maturation and release (23). Likewise, P2X4 appears to be influence P2X7-mediated autophagy and cell death and both receptors were shown to play a role within the phagosome (19, 25, 26). However, in non-stimulated tissue, we do not see P2X4 in the membrane and the conditions and mechanisms for membrane transport in native tissue need to be further explored. In agreement with our data, (36) found independent activation of both subunits in the BV-2 microglia cell line via whole cell patch clamp. This argues against heteromeric assembly of both receptors, or against a physiological relevance of such.

#### 5 Conclusion

The P2X7-EGFP reporter mouse model and novel nanobody tools enabled for the first time the analysis of P2X4 and P2X7 localization and their interaction *in situ* and at physiological expression levels. The presented biochemical and immunofluorescence data argue against a physiological relevance of P2X4/P2X7 complexes in native mouse tissue. We suggest that previously described direct interactions of both subtypes result from over-expression in heterologous systems. Finally, passenger effects due to the close proximity of both genes need to be considered when investigating mutual interdependence.

## Data availability statement

The original contributions presented in the study are included in the article/Supplementary Material. Further inquiries can be directed to the corresponding author.

### **Ethics statement**

The animal experiments were approved by the Regierung von Oberbayern. The study was conducted in accordance with the local legislation and institutional requirements.

#### **Author contributions**

JS-M: Formal analysis, Investigation, Writing – review & editing. LSc: Formal analysis, Investigation, Writing – review & editing. LSa: Formal analysis, Investigation, Writing – review & editing. AR-F: Investigation, Formal analysis, Writing – review & editing. PA: Investigation, Writing – review & editing, Methodology. BR: Investigation, Writing – review & editing, Resources. BZ: Formal analysis, Investigation, Writing – review & editing. JS: Writing – review & editing, Methodology. JH: Writing – review & editing, Investigation. TS: Writing – review & editing, Resources. FK-N: Resources, Writing – review & editing, Funding acquisition. CS-W: Writing – review & editing, Funding acquisition, Methodology. RK: Conceptualization, Writing – original draft, Investigation. AN: Conceptualization, Funding acquisition, Supervision, Writing – original draft.

## **Funding**

The author(s) declare financial support was received for the research, authorship, and/or publication of this article. This work was supported by funding from the European Union's Horizon 2020 research and innovation programme under the Marie Skłodowska-Curie grant agreement (No 766124, AN), and the Deutsche Forschungsgemeinschaft (DFG, German Research Foundation): GRK2338 (AN, AD, CS-W), Project-ID 335447717 -SFB 1328 (AN, FK-N, BR), and RI 3540/2-1, Project-ID 533586492 (BR).

#### References

- 1. Illes P, Muller CE, Jacobson KA, Grutter T, Nicke A, Fountain SJ, et al. Update of P2X receptor properties and their pharmacology: IUPHAR Review 30. *Br J Pharmacol.* (2021) 178:489–514. doi: 10.1111/bph.15299
- 2. Lewis C, Neidhart S, Holy C, North RA, Buell G, Surprenant A. Coexpression of P2X2 and P2X3 receptor subunits can account for ATP-gated currents in sensory neurons. *Nature*. (1995) 377:432–5. doi: 10.1038/377432a0
- 3. Lalo U, Pankratov Y, Wichert SP, Rossner MJ, North RA, Kirchhoff F, et al. P2X1 and P2X5 subunits form the functional P2X receptor in mouse cortical astrocytes. *J Neurosci.* (2008) 28:5473–80. doi: 10.1523/JNEUROSCI.1149–08.2008
- 4. Compan V, Ulmann L, Stelmashenko O, Chemin J, Chaumont S, Rassendren F. P2X2 and P2X5 subunits define a new heteromeric receptor with P2X7-like properties. *J Neurosci.* (2012) 32:4284–96. doi: 10.1523/JNEUROSCI.6332–11.2012
- 5. Torres GE, Egan TM, Voigt MM. Hetero-oligomeric assembly of P2X receptor subunits. Specificities exist with regard to possible partners. *J Biol Chem.* (1999) 274:6653–9. doi: 10.1074/jbc.274.10.6653
- 6. Resende RR, Britto LR, Ulrich H. Pharmacological properties of purinergic receptors and their effects on proliferation and induction of neuronal differentiation of P19 embryonal carcinoma cells. *Int J Dev Neurosci.* (2008) 26:763–77. doi: 10.1016/j.ijdevneu.2008.07.008
- 7. Saul A, Hausmann R, Kless A, Nicke A. Heteromeric assembly of P2X subunits. Front Cell Neurosci. (2013) 7:250. doi: 10.3389/fncel.2013.00250
- 8. McCarthy AE, Yoshioka C, Mansoor SE. Full-length P2X7 structures reveal how palmitoylation prevents channel desensitization. *Cell.* (2019) 179:659–670 e613. doi: 10.1016/j.cell.2019.09.017
- 9. Di Virgilio F, Schmalzing G, Markwardt F. The elusive P2X7 macropore. Trends Cell Biol. (2018) 28:392–404. doi: 10.1016/j.tcb.2018.01.005
- 10. Dubyak GR. Go it alone no more–P2X7 joins the society of heteromeric ATP-gated receptor channels. *Mol Pharmacol.* (2007) 72:1402–5. doi: 10.1124/mol.107.042077

## Acknowledgments

We thank Stella Schieferstein and Heinz Janser for assistance. Images in Fig. 1B-D and Fig. 6A in this article were previously used in the thesis of Antonio Ramírez Fernández (Faculty of Medicine, LMU Munich, 2023).

#### Conflict of interest

The authors declare that the research was conducted in the absence of any commercial or financial relationships that could be construed as a potential conflict of interest.

The author(s) declared that they were an editorial board member of Frontiers, at the time of submission. This had no impact on the peer review process and the final decision.

#### Publisher's note

All claims expressed in this article are solely those of the authors and do not necessarily represent those of their affiliated organizations, or those of the publisher, the editors and the reviewers. Any product that may be evaluated in this article, or claim that may be made by its manufacturer, is not guaranteed or endorsed by the publisher.

## Supplementary material

The Supplementary Material for this article can be found online at: https://www.frontiersin.org/articles/10.3389/fimmu.2024. 1425938/full#supplementary-material

- 11. Hou Z, Cao J. Comparative study of the P2X gene family in animals and plants.  $Purinergic\ Signal.\ (2016)\ 12:269-81.\ doi: 10.1007/s11302-016-9501-z$
- 12. Xiang Z, Burnstock G. Expression of P2X receptors on rat microglial cells during early development. Glia.~(2005)~52:119-26.~doi:~10.1002/glia.20227
- 13. Bowler JW, Bailey RJ, North RA, Surprenant A. P2X4, P2Y1 and P2Y2 receptors on rat alveolar macrophages. *Br J Pharmacol.* (2003) 140:567–75. doi: 10.1038/sj.bjp.0705459
- 14. Guo C, Masin M, Qureshi OS, Murrell-Lagnado RD. Evidence for functional P2X4/P2X7 heteromeric receptors. *Mol Pharmacol.* (2007) 72:1447–56. doi: 10.1124/mol.107.035980
- 15. Brock VJ, Wolf IMA, Er-Lukowiak M, Lory N, Stahler T, Woelk LM, et al. P2X4 and P2X7 are essential players in basal T cell activity and Ca(2+) signaling milliseconds after T cell activation. *Sci Adv.* (2022) 8:eabl9770. doi: 10.1126/sciadv.abl9770
- 16. Ma W, Korngreen A, Weil S, Cohen EB, Priel A, Kuzin L, et al. Pore properties and pharmacological features of the P2X receptor channel in airway ciliated cells. *J Physiol.* (2006) 571:503–17. doi: 10.1113/jphysiol.2005.103408
- 17. Wirsching E, Fauler M, Fois G, Frick M. P2 purinergic signaling in the distal lung in health and disease. *Int J Mol Sci.* (2020) 21:4973. doi: 10.3390/ijms21144973
- 18. Novak I. Purinergic signalling in epithelial ion transport: regulation of secretion and absorption. *Acta Physiol (Oxf)*. (2011) 202:501–22. doi: 10.1111/j.1748-1716.2010.02225.x
- 19. Qureshi OS, Paramasivam A, Yu JC, Murrell-Lagnado RD. Regulation of P2X4 receptors by lysosomal targeting, glycan protection and exocytosis. *J Cell Sci.* (2007) 120:3838–49. doi: 10.1242/jcs.010348
- 20. Babelova A, Moreth K, Tsalastra-Greul W, Zeng-Brouwers J, Eickelberg O, Young MF, et al. Biglycan, a danger signal that activates the NLRP3 inflammasome via toll-like and P2X receptors. *J Biol Chem.* (2009) 284:24035–48. doi: 10.1074/jbc.M109.014266

- 21. Kawano A, Tsukimoto M, Mori D, Noguchi T, Harada H, Takenouchi T, et al. Regulation of P2X7-dependent inflammatory functions by P2X4 receptor in mouse macrophages. *Biochem Biophys Res Commun.* (2012) 420:102–7. doi: 10.1016/j.bbrc.2012.02.122
- 22. Hung SC, Choi CH, Said-Sadier N, Johnson L, Atanasova KR, Sellami H, et al. P2X4 assembles with P2X7 and pannexin-1 in gingival epithelial cells and modulates ATP-induced reactive oxygen species production and inflammasome activation. *PloS One.* (2013) 8:e70210. doi: 10.1371/journal.pone.0070210
- 23. Sakaki H, Fujiwaki T, Tsukimoto M, Kawano A, Harada H, Kojima S. P2X4 receptor regulates P2X7 receptor-dependent IL-1beta and IL-18 release in mouse bone marrow-derived dendritic cells. *Biochem Biophys Res Commun.* (2013) 432:406–11. doi: 10.1016/j.bbrc.2013.01.135
- 24. Perez-Flores G, Levesque SA, Pacheco J, Vaca L, Lacroix S, Perez-Cornejo P, et al. The P2X7/P2X4 interaction shapes the purinergic response in murine macrophages. *Biochem Biophys Res Commun.* (2015) 467:484–90. doi: 10.1016/j.bbrc.2015.10.025
- 25. Kuehnel MP, Rybin V, Anand PK, Anes E, Griffiths G. Lipids regulate P2X7-receptor-dependent actin assembly by phagosomes via ADP translocation and ATP synthesis in the phagosome lumen. *J Cell Sci.* (2009) 122:499–504. doi: 10.1242/jcs.034199
- 26. Kawano A, Tsukimoto M, Noguchi T, Hotta N, Harada H, Takenouchi T, et al. Involvement of P2X4 receptor in P2X7 receptor-dependent cell death of mouse macrophages. *Biochem Biophys Res Commun.* (2012) 419:374–80. doi: 10.1016/j.bbrc.2012.01.156
- 27. Schenk U, Westendorf AM, Radaelli E, Casati A, Ferro M, Fumagalli M, et al. Purinergic control of T cell activation by ATP released through pannexin-1 hemichannels. *Sci Signal.* (2008) 1:ra6. doi: 10.1126/scisignal.1160583
- 28. Yip L, Woehrle T, Corriden R, Hirsh M, Chen Y, Inoue Y, et al. Autocrine regulation of T-cell activation by ATP release and P2X7 receptors. *FASEB J.* (2009) 23:1685–93. doi: 10.1096/fj.08–126458
- 29. Woehrle T, Yip L, Elkhal A, Sumi Y, Chen Y, Yao Y, et al. Pannexin-1 hemichannel-mediated ATP release together with P2X1 and P2X4 receptors regulate T-cell activation at the immune synapse. *Blood.* (2010) 116:3475–84. doi: 10.1182/blood-2010-04-277707
- 30. Manohar M, Hirsh MI, Chen Y, Woehrle T, Karande AA, Junger WG. ATP release and autocrine signaling through P2X4 receptors regulate gammadelta T cell activation. *J Leukoc Biol.* (2012) 92:787–94. doi: 10.1189/jlb.0312121
- 31. Wang CM, Ploia C, Anselmi F, Sarukhan A, Viola A. Adenosine triphosphate acts as a paracrine signaling molecule to reduce the motility of T cells. *EMBO J.* (2014) 33:1354–64. doi: 10.15252/embj.201386666
- 32. Mishra A, Chintagari NR, Guo Y, Weng T, Su L, Liu L. Purinergic P2X7 receptor regulates lung surfactant secretion in a paracrine manner. *J Cell Sci.* (2011) 124:657–68. doi: 10.1242/jcs.066977
- 33. Miklavc P, Thompson KE, Frick M. A new role for P2X4 receptors as modulators of lung surfactant secretion. *Front Cell Neurosci.* (2013) 7:171. doi: 10.3389/fncel.2013.00171
- 34. Casas-Pruneda G, Reyes JP, Perez-Flores G, Perez-Cornejo P, Arreola J. Functional interactions between P2X4 and P2X7 receptors from mouse salivary epithelia. *J Physiol.* (2009) 587:2887–901. doi: 10.1113/jphysiol.2008.167395
- 35. Schneider M, Prudic K, Pippel A, Klapperstuck M, Braam U, Muller CE, et al. Interaction of purinergic P2X4 and P2X7 receptor subunits. *Front Pharmacol.* (2017) 8:860. doi: 10.3389/fphar.2017.00860
- 36. Trang M, Schmalzing G, Muller CE, Markwardt F. Dissection of P2X4 and P2X7 receptor current components in BV-2 microglia. Int J Mol Sci. (2020) 21:8489. doi: 10.3390/ijms21228489
- 37. Boumechache M, Masin M, Edwardson JM, Gorecki DC, Murrell-Lagnado R. Analysis of assembly and trafficking of native P2X4 and P2X7 receptor complexes in rodent immune cells. *J Biol Chem.* (2009) 284:13446–54. doi: 10.1074/jbc.M901255200
- 38. Weinhold K, Krause-Buchholz U, Rodel G, Kasper M, Barth K. Interaction and interrelation of P2X7 and P2X4 receptor complexes in mouse lung epithelial cells. *Cell Mol Life Sci.* (2010) 67:2631–42. doi: 10.1007/s00018–010-0355–1
- 39. Antonio LS, Stewart AP, Xu XJ, Varanda WA, Murrell-Lagnado RD, Edwardson JM. P2X4 receptors interact with both P2X2 and P2X7 receptors in the form of homotrimers. *Br J Pharmacol*. (2011) 163:1069–77. doi: 10.1111/j.1476-5381.2011.01303.x
- 40. Nicke A. Homotrimeric complexes are the dominant assembly state of native P2X7 subunits. *Biochem Biophys Res Commun.* (2008) 377:803–8. doi: 10.1016/j.bbrc.2008.10.042
- 41. Craigie E, Birch RE, Unwin RJ, Wildman SS. The relationship between P2X4 and P2X7: a physiologically important interaction? Front Physiol. (2013) 4:216. doi: 10.3389/fphys.2013.00216
- 42. Zech A, Wiesler B, Ayata CK, Schlaich T, Durk T, Hossfeld M, et al. P2rx4 deficiency in mice alleviates allergen-induced airway inflammation. *Oncotarget*. (2016) 7:80288–97. doi: 10.18632/oncotarget.13375
- 43. Riteau N, Gasse P, Fauconnier L, Gombault A, Couegnat M, Fick L, et al. Extracellular ATP is a danger signal activating P2X7 receptor in lung inflammation and

- fibrosis. Am J Respir Crit Care Med. (2010) 182:774-83. doi: 10.1164/rccm.201003-0359OC.
- 44. Winkelmann VE, Thompson KE, Neuland K, Jaramillo AM, Fois G, Schmidt H, et al. Inflammation-induced upregulation of P2X4 expression augments mucin secretion in airway epithelia. *Am J Physiol Lung Cell Mol Physiol.* (2019) 316:L58–70. doi: 10.1152/ajplung.00157.2018
- 45. Burnstock G, Brouns I, Adriaensen D, Timmermans JP. Purinergic signaling in the airways. *Pharmacol Rev.* (2012) 64:834–68. doi: 10.1124/pr.111.005389
- 46. Savio LEB, de Andrade Mello P, da Silva CG, Coutinho-Silva R. The P2X7 receptor in inflammatory diseases: angel or demon? *Front Pharmacol.* (2018) 9:52. doi: 10.3389/fphar.2018.00052
- 47. Schneider S, Merfort I, Idzko M, Zech A. Blocking P2X purinoceptor 4 signalling alleviates cigarette smoke induced pulmonary inflammation. *Respir Res.* (2022) 23:148. doi: 10.1186/s12931-022-02072-z
- 48. Sperlagh B, Illes P. P2X7 receptor: an emerging target in central nervous system diseases. *Trends Pharmacol Sci.* (2014) 35:537–47. doi: 10.1016/j.tips.2014.08.002
- 49. Di Virgilio F, Dal Ben D, Sarti AC, Giuliani AL, Falzoni S. The P2X7 receptor in infection and inflammation. *Immunity*. (2017) 47:15–31. doi: 10.1016/j.immuni 2017 06 020
- 50. Yamamoto K, Sokabe T, Matsumoto T, Yoshimura K, Shibata M, Ohura N, et al. Impaired flow-dependent control of vascular tone and remodeling in P2X4-deficient mice. *Nat Med.* (2006) 12:133–7. doi: 10.1038/nm1338
- 51. Yang T, Shen JB, Yang R, Redden J, Dodge-Kafka K, Grady J, et al. Novel protective role of endogenous cardiac myocyte P2X4 receptors in heart failure. *Circ Heart Fail.* (2014) 7:510–8. doi: 10.1161/CIRCHEARTFAILURE.113.001023
- 52. Inoue K, Tsuda M. Nociceptive signaling mediated by P2X3, P2X4 and P2X7 receptors. *Biochem Pharmacol.* (2020) 187:114309. doi: 10.1016/j.bcp.2020.114309
- 53. Sim JA, Chaumont S, Jo J, Ulmann L, Young MT, Cho K, et al. Altered hippocampal synaptic potentiation in P2X4 knock-out mice. *J Neurosci.* (2006) 26:9006–9. doi: 10.1523/JNEUROSCI.2370–06.2006
- 54. Kaczmarek-Hajek K, Zhang J, Kopp R, Grosche A, Rissiek B, Saul A, et al. Reevaluation of neuronal P2X7 expression using novel mouse models and a P2X7-specific nanobody. *Elife*. (2018) 7:e36217. doi: 10.7554/eLife.36217
- 55. Gloor S, Pongs O, Schmalzing G. A vector for the synthesis of cRNAs encoding Myc epitope-tagged proteins in Xenopus laevis oocytes. *Gene.* (1995) 160:213–7. doi: 10.1016/0378-1119(95)00226-V
- 56. Jager V, Bussow K, Wagner A, Weber S, Hust M, Frenzel A, et al. High level transient production of recombinant antibodies and antibody fusion proteins in HEK293 cells. *BMC Biotechnol.* (2013) 13:52. doi: 10.1186/1472–6750-13–52
- 57. Stahler T, Danquah W, Demeules M, Gonde H, Hardet R, Haag F, et al. Development of antibody and nanobody tools for P2X7. *Methods Mol Biol.* (2022) 2510:99–127. doi: 10.1007/978–1-0716–2384-8\_6
- 58. Dobbs LG. Isolation and culture of alveolar type II cells. Am J Physiol. (1990) 258:L134–147. doi: 10.1152/ajplung.1990.258.4.L134
- 59. Corti M, Brody AR, Harrison JH. Isolation and primary culture of murine alveolar type II cells. *Am J Respir Cell Mol Biol.* (1996) 14:309–15. doi: 10.1165/ajrcmb.14.4.8600933
- 60. Weber J, Rajan S, Schremmer C, Chao YK, Krasteva-Christ G, Kannler M, et al. TRPV4 channels are essential for alveolar epithelial barrier function as protection from lung edema. *JCI Insight*. (2020) 5:e134464. doi: 10.1172/jci.insight.134464
- 61. Schindelin J, Arganda-Carreras I, Frise E, Kaynig V, Longair M, Pietzsch T, et al. Fiji: an open-source platform for biological-image analysis. *Nat Methods.* (2012) 9:676–82. doi: 10.1038/nmeth.2019
- 62. Schmittgen TD, Livak KJ. Analyzing real-time PCR data by the comparative C (T) method. *Nat Protoc.* (2008) 3:1101–8. doi: 10.1038/nprot.2008.73
- 63. Wareham K, Vial C, Wykes RC, Bradding P, Seward EP. Functional evidence for the expression of P2X1, P2X4 and P2X7 receptors in human lung mast cells. *Br J Pharmacol.* (2009) 157:1215–24. doi: 10.1111/j.1476-5381.2009.00287.x
- 64. Wang R, Zhang P, Wang J, Ma L, Weigao E, Suo S, et al. Construction of a cross-species cell landscape at single-cell level. *Nucleic Acids Res.* (2023) 51:501–16. doi: 10.1093/nar/gkac633
- 65. Horie M, Castaldi A, Sunohara M, Wang H, Ji Y, Liu Y, et al. Integrated single-cell RNA-sequencing analysis of aquaporin 5-expressing mouse lung epithelial cells identifies GPRC5A as a novel validated type I cell surface marker. *Cells*. (2020) 9:2460. doi: 10.3390/cells9112460
- 66. Sim JA, Young MT, Sung HY, North RA, Surprenant A. Reanalysis of P2X7 receptor expression in rodent brain. *J Neurosci.* (2004) 24:6307–14. doi: 10.1523/JNEUROSCI.1469–04.2004
- 67. Anderson CM, Nedergaard M. Emerging challenges of assigning P2X7 receptor function and immunoreactivity in neurons. *Trends Neurosci.* (2006) 29:257–62. doi: 10.1016/j.tins.2006.03.003
- 68. Ramirez-Fernandez A, Urbina-Trevino L, Conte G, Alves M, Rissiek B, Durner A, et al. Deviant reporter expression and P2X4 passenger gene overexpression in the soluble EGFP BAC transgenic P2X7 reporter mouse model. *Sci Rep.* (2020) 10:19876. doi: 10.1038/s41598-020-76428-0

- 69. Jooss T, Zhang J, Zimmer B, Rezzonico-Jost T, Rissiek B, Felipe Pelczar P, et al. Macrophages and glia are the dominant P2X7-expressing cell types in the gut nervous system-No evidence for the role of neuronal P2X7 receptors in colitis. *Mucosal Immunol.* (2023) 16:180–93. doi: 10.1016/j.mucimm.2022.11.003
- 70. Chen Z, Jin N, Narasaraju T, Chen J, McFarland LR, Scott M, et al. Identification of two novel markers for alveolar epithelial type I and II cells. *Biochem Biophys Res Commun.* (2004) 319:774–80. doi: 10.1016/j.bbrc.2004.05.048
- 71. Mishra A. New insights of P2X7 receptor signaling pathway in alveolar functions. *J BioMed Sci.* (2013) 20:26. doi: 10.1186/1423-0127-20-26
- 72. Donovan KM, Leidinger MR, McQuillen LP, Goeken JA, Hogan CM, Harwani SC, et al. Allograft inflammatory factor 1 as an immunohistochemical marker for macrophages in multiple tissues and laboratory animal species. *Comp Med.* (2018) 68:341–8. doi: 10.30802/AALAS-CM-18–000017
- 73. Vargas-Martinez EM, Gomez-Coronado KS, Espinosa-Luna R, Valdez-Morales EE, Barrios-Garcia T, Barajas-Espinosa A, et al. Functional expression of P2X1, P2X4 and P2X7 purinergic receptors in human monocyte-derived macrophages. *Eur J Pharmacol.* (2020) 888:173460. doi: 10.1016/j.ejphar.2020.173460
- 74. Bobanovic LK, Royle SJ, Murrell-Lagnado RD. P2X receptor trafficking in neurons is subunit specific. J Neurosci. (2002) 22:4814–24. doi: 10.1523/JNEUROSCI.22–12-04814.2002

- 75. Toulme E, Garcia A, Samways D, Egan TM, Carson MJ, Khakh BS. P2X4 receptors in activated C8-B4 cells of cerebellar microglial origin. *J Gen Physiol.* (2010) 135:333–53. doi: 10.1085/jgp.200910336
- 76. Toyomitsu E, Tsuda M, Yamashita T, Tozaki-Saitoh H, Tanaka Y, Inoue K. CCL2 promotes P2X4 receptor trafficking to the cell surface of microglia. *Purinergic Signal.* (2012) 8:301–10. doi: 10.1007/s11302-011-9288-x
- 77. Bertin E, Deluc T, Pilch KS, Martinez A, Pougnet JT, Doudnikoff E, et al. Increased surface P2X4 receptor regulates anxiety and memory in P2X4 internalization-defective knock-in mice. *Mol Psychiatry*. (2021) 26:629–44. doi: 10.1038/s41380-019-0641-8
- 78. Sorge RE, Trang T, Dorfman R, Smith SB, Beggs S, Ritchie J, et al. Genetically determined P2X7 receptor pore formation regulates variability in chronic pain sensitivity. *Nat Med.* (2012) 18:595–9. doi: 10.1038/nm.2710
- 79. Er-Lukowiak M, Duan Y, Rassendren F, Ulmann L, Nicke A, Ufer F, et al. A P2rx7 passenger mutation affects the vitality and function of T cells in congenic mice. *iScience*. (2020) 23:101870. doi: 10.1016/j.isci.2020.101870
- 80. Nobili P, Ulmann L, Rassendren F, Hirbec H. Limited contribution of the of P2X4 receptor to LPS-induced microglial reaction in mice. *Purinergic Signal.* (2024). doi: 10.1007/s11302-023-09984-5

Table S1: Antibodies used for Western blotting and immunohistochemistry

Primary antibodies	Supplier	Cat.# / RRID	Dilution	
P2X7	Synaptic Systems	177003,	1:500	
(rb pAb)		AB_887755	WB 1:1500	
7E2-rbFc / 7E2-hFc	Nolte lab Nanobody fused rabbit or human I		0.1 μg/mL	
P2X4	Alomone	APR-002, AB 2040058	1:200 WB 1:1000	
(rb pAb)		AD_2040036	WB 1.1000	
(RG96 rt mAb)	Nolte lab		$0.2 \mu g/mL$	
GFP	Abcam	ab6556,	1:2000	
(rb pAb)		AB_305564		
GFP (chk pAb)	Thermo Fisher	CA10262, AB_2534023	1:400	
GFP (rat 3H9)	Chromotek	3h9-100, AB 10773374	WB 1:1000	
Iba1	WAKO	019–19741,	1:100	
(rb pAb)	WINO	AB_839504	1.100	
Iba1 (ch pAb)	Synaptic systems	234 009 AB 2891282	1:200	
Aquaporin-5		AQP-005		
(rb pAb)	Alomone	AB 2039736	1:200	
VE-Cadherin	Cell Signaling	2500	1:200	
(rb pAb)	Cen Signating	AB_10839118	1.200	
Podoplanin	R&D Systems	AF3244	1:200	
(gt pAb) Prosurfactant protein C		AB_2161931 AB3786		
(rb pAb)	Merk Millipore	AB 91588	1:200	
F4/80	Thermo Fisher	14-4801-82	1:200	
(rt pAb)	Thermo Tisher	AB_467558		
CD68	Biorad	MCA1957 AB 322219	1:200	
(rt pAb)		AB 322219 AB 125212	1:200	
CD68 (rb pAb)	Abcam	AB_10975465		
CD16/CD32	BD Pharmingen <sup>TM</sup>	553142	1:666	
		AB_394656 553076		
CD45	BD Pharmingen <sup>TM</sup>	AB 394606	1:666	
CD11b-Bv510	Biolegend	101245	1.100	
clone M 1/70	Biolegelia	AB_2561390	1:100	
CD45-APC-Cy7	Biolegend	103115	1:100	
clone 30-F11 Ly6G-AF700		AB_312980 127621		
clone 1A8	Biolegend	AB 10640452	1:100	
CD64-PE-Cy7	Dialogand	139313	1.100	
clone PK136	Biolegend	AB_2563903	1:100	

CD11c-PE-Dazzle clone RTK2071	Biolegend	117347 AB_2563654	1:100
P2X7-Bv421 clone 1F11	BD Bioscience	744779 AB_2742477	1:100
CD206-FITC clone RTK-2071	Biolegend	141703 AB_10900988	1:100

# Secondary antibodies

Secondary antibodies			
800CW gt anti-ms	LI-COR	925–32210, AB_2687825	WB 1:15.000
800CW gt anti-rb	LI-COR	926-32211, AB_621843	WB 1:15.000
680RD dk anti-rb	LI-COR	925–68073, AB_2716687	WB 1:15.000
680RD gt anti-rb	LI-COR	925–68071, AB_2721181	WB 1:15.000
680RD gt anti-rat	LI-COR	925-68076, AB_10956590	WB 1:15.000
A594 gt anti-rb	Thermo Fisher	A11037, AB_2534095	1:400
A594 gt anti-ms	Thermo Fisher	A11032, AB_2534091	1:400
A594 gt anti-rat	Thermo Fisher	A11007, AB_10561522	1:400
A546 gt anti-ms	Thermo Fisher	A-11003, AB_2534071	1:400
A488 gt anti-rb	Thermo Fisher	A11008, AB_143165	1:400
A488 gt anti-chk	Thermo Fisher	A11039, AB_142924	1:400
Alexa fluor 405 gt anti-rb	Thermo Fisher	A48254 AB_2890548	1:400
Alexa fluor 488 gt anti-rb F(ab')2	Jackson ImmunoResearch	109-546-088 AB_2337848	1:400
Alexa fluor 647 gt anti-ch	Thermo Fisher	A-21449 AB_2535866	1:400
Alexa fluor 647 gt anti-hs	Jackson ImmunoResearch	127-605-160 AB_2339001	1:400

**Table S2: Primers** 

Name	Sequence	Position
P2rx7 fwd-a	CTGGTTTTCGGCACTGGA	Exon 9
P2rx7 fwd-b	GAGCACGAATTATGGCACCG	Exon 1
P2rx7 rev-a	CCAAAGTAGGACAGGGTGGA	Exon 10
P2rx7 rev-b	GATGCTGTGTCCTAACTTCG	Exon 2
P2rx4 fwd	CCAACACTTCTCAGCTTGGAT	Exon 2
P2rx4 rev	TGGTCATGATGAAGAGGGAGT	Exon 3
PPIA fwd	AGGGTGGTGACTTTACACGC	
PPIA rev	CTTGCCATCCAGCCATTCAG	
RPLP0 fwd	GGACCGCCTGGTTCTCCTAT	
RPLP0 rev	ACGATGTCACTCCAACGAGG	



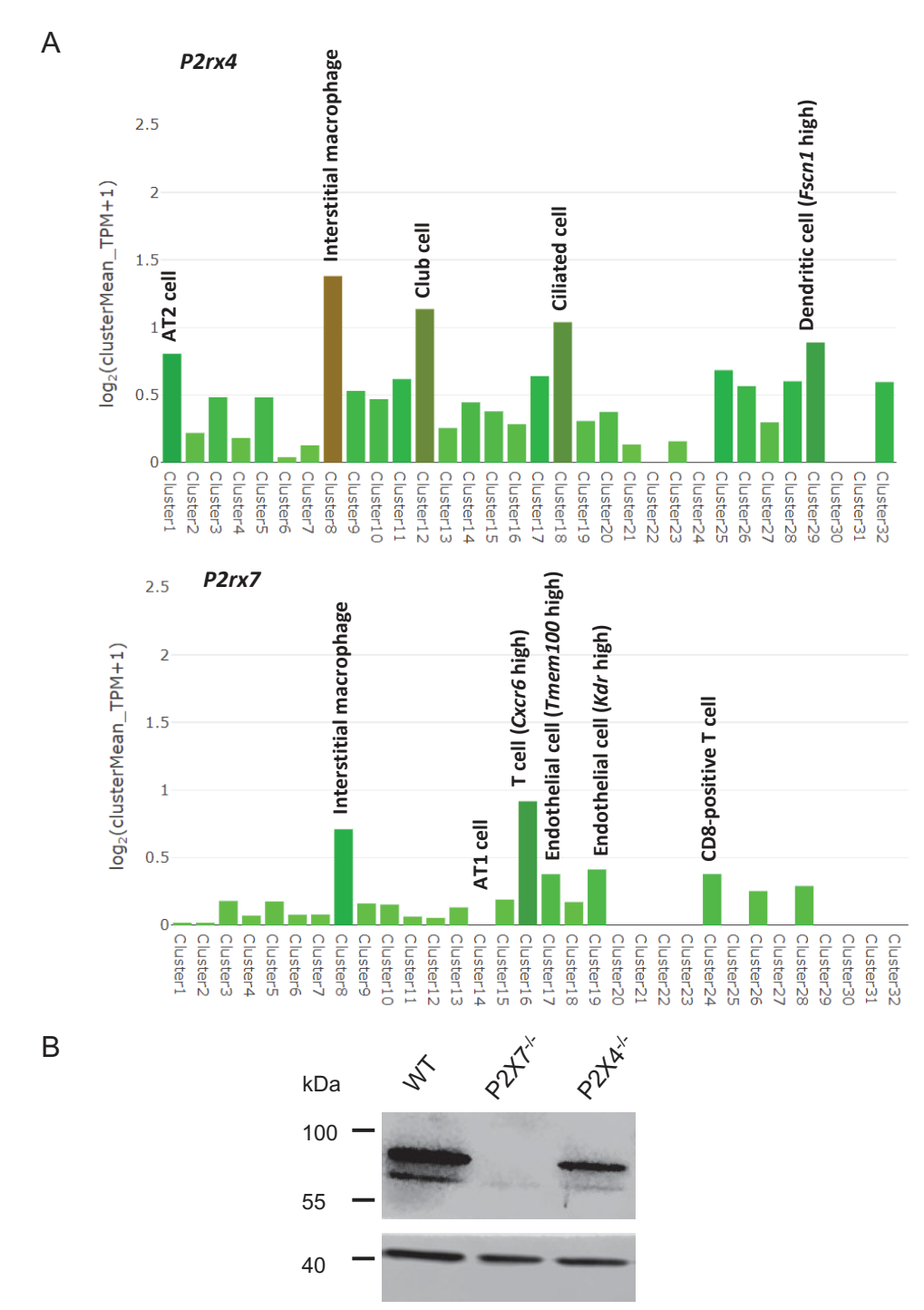
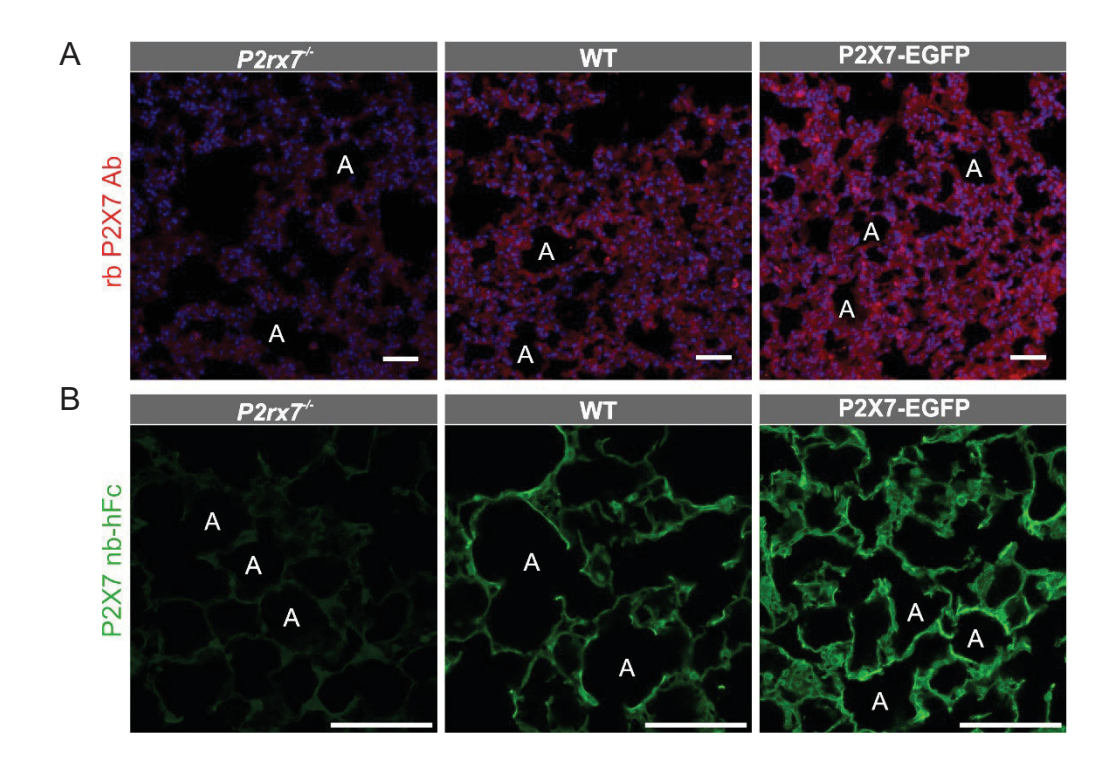


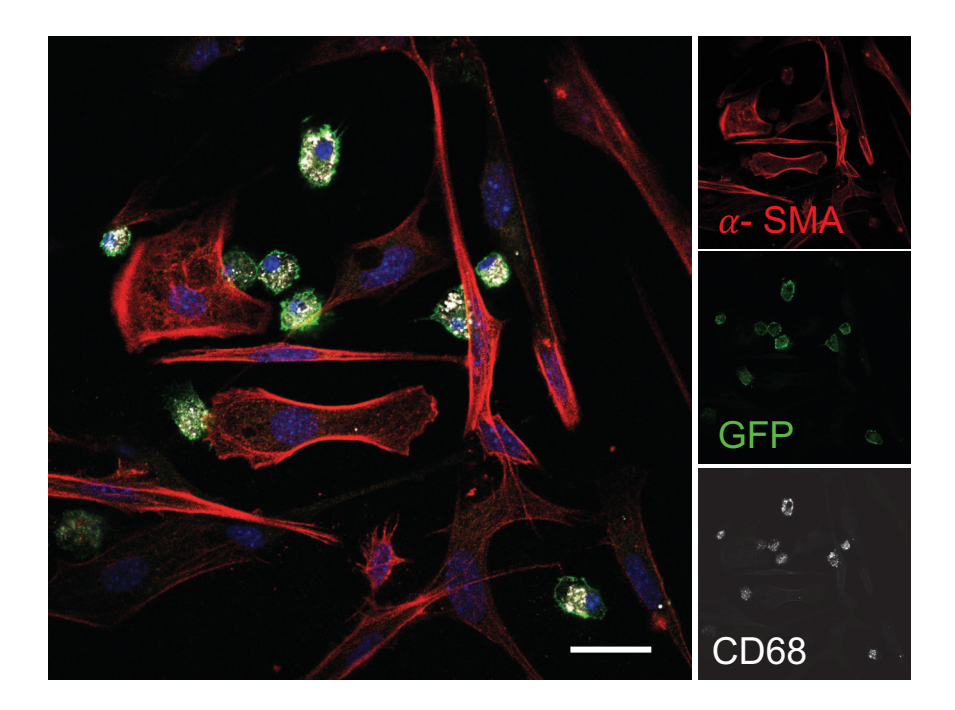
Figure S1: Expression of P2X4 and P2X7 in mouse lung.

- (A) With the exception of interstitial macrophages, publicly available scRNA-Seq data data indicate comparably little co-expression of *P2rx4* and *P2rx7* in the lung. Data is derived from the Mouse Cell Atlas 3.0 (MCA3.0, Wang R et al, Nucleic Acids Research 51(2), 2023) and was extracted by a search for the two genes within data derived from the tissue "Lung-Adult-lung". For both genes, the top 5 expressing cell types are specified. For more details, refer to the MCA3.0 webtool (<a href="https://bis.zju.edu.cn/MCA/search2.html">https://bis.zju.edu.cn/MCA/search2.html</a>).
- (B) Western blot data confirm presence P2X7 protein in primary AT2 cells despite a limited expression found at the RNA level. 1 x  $10^6$  AT2 cells from the indicated genotypes were plated on a 6-well plate and after one day, solubilized in RIPA buffer ( $100 \mu l/well$ ). 12  $\mu l$  extract were separated by SDS-Page. P2X7 and  $\beta$ -actin (loading control) were detected with an anti-P2X7 and anti- $\beta$ -actin antibody (Synaptic Systems, 1:1000, Merck #A3854, 1:10.000 dilution) and anti-rabbit peroxicase-coupled secondary antibody (Sigma A6154, 1:10.000 dilution).



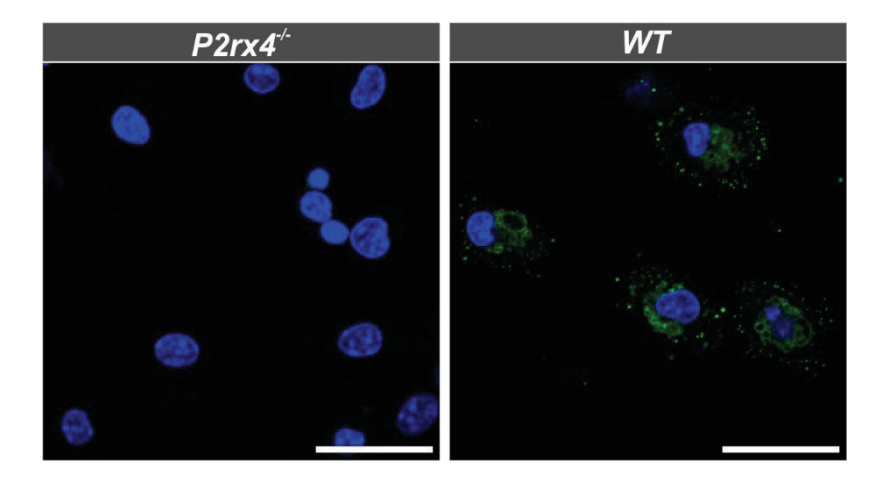
## Specificity of P2X7-EGFP expression in lung tissue.

Lung cryosections from the indicated genotypes were stained with (A) an anti-P2X7 antibody (Synaptic Systems 173 003) and (B) the 7E2 P2X7-specific nanobody fused to a human Fc domain (7E2-hFc). DAPI staining is shown in blue. Scale bar 100  $\mu$ m. A=Alveoli.



Immunostaining of primary murine lung fibroblasts (pmLF) from transgenic mice with antibodies against GFP and the fibroblast marker a-SMA.

Note that cells showing high EGFP expression were identified as contaminating macrophages by staining of the macrophage marker CD68. Nuclear DAPI staining is shown in blue. Scale bar 30  $\mu$ m. a-SMA = alpha- smooth muscle actin.



## Specificity of the rat anti-mP2X4 antibody.

Macrophages were isolated by alveolar lavage from the indicated genotypes and stained with rat anti-P2X4 (RG96 rt mAb) after 24 hours in culture (37°C, 5% CO2), supplemented with RPMI1640 media containing 10% FCS, Pen/Strep and  $\beta$ -mercaptoethanol. Nuclear DAPI staining is shown in blue. Scale bar 25  $\mu$ m.

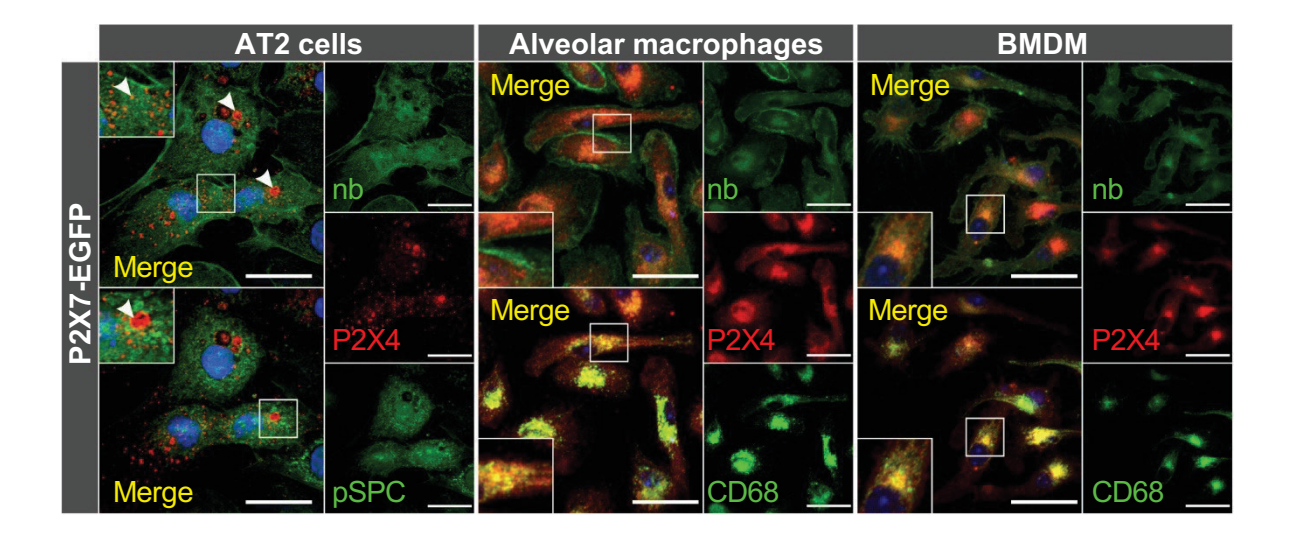
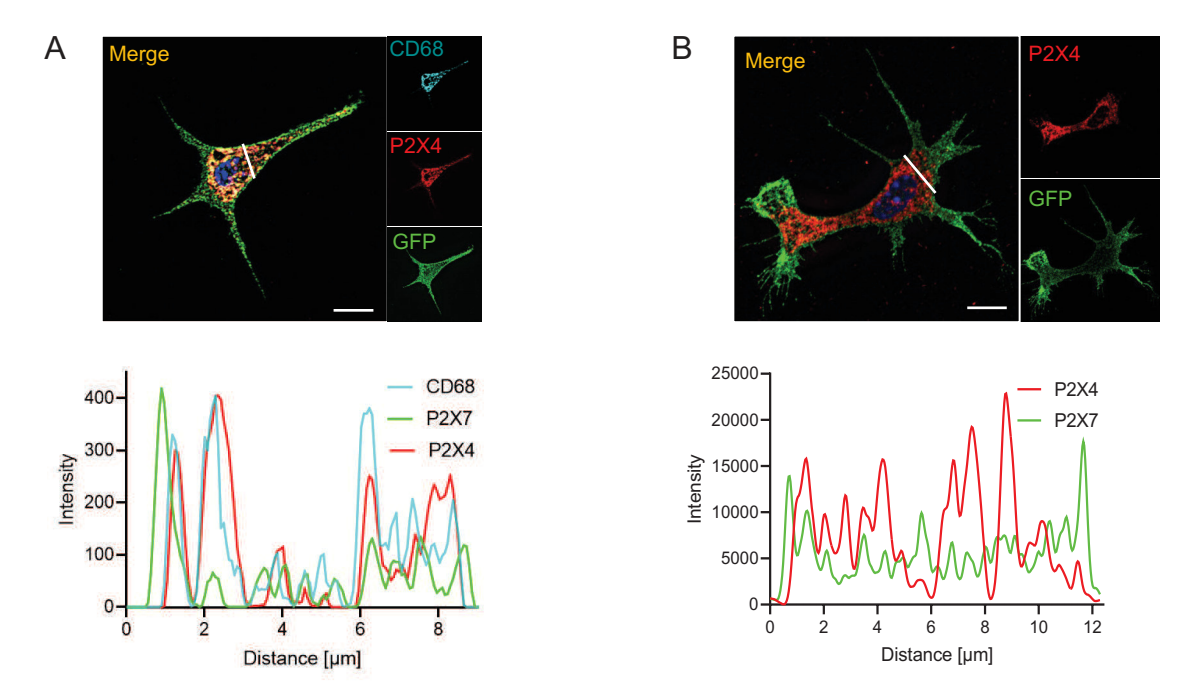
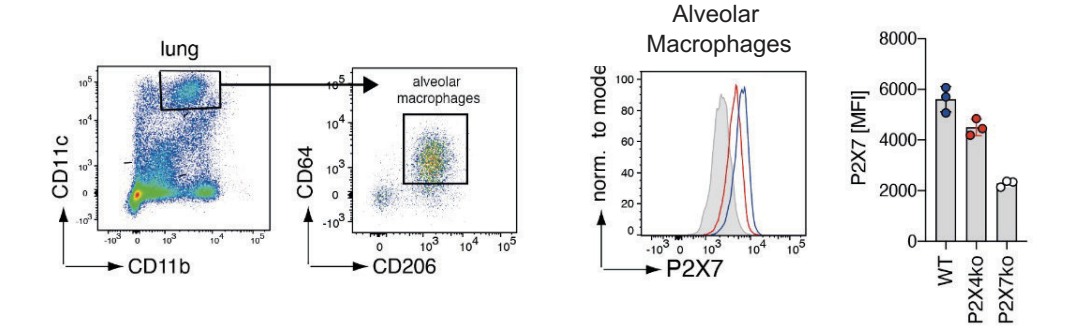


Figure S5. Comparison of the subcellular localization of P2X4 and P2X7 in isolated cells from the P2X7-EGFP mouse. Primary AT2 epithelial cells, alveolar macrophages, and bone marrow-derived macrophages (BMDM) were stained with the P2X7-specific nanobody (7E2-hFc), anti-P2X4 antibody, anti-prosurfactant protein C (SPC) for AT2 cells, and anti-CD68 for the macrophages. Arrowhead show lamellar bodies in AT2 cells, and insets display the distinct membrane pattern for P2X7, and perinuclear puncta staining for P2X4 and CD68. Nuclear staining with TO-PRO-3 is shown in blue. Scale bar 25  $\mu$ m.

Fig. S6



Different subcellular localization of P2X4 and P2X7-EGFP in peritoneal macrophage (A) and primary microglia (B). Cells were stained with antibodies against P2X4 (Alomone, APR-002) and GFP (from chicken, Thermo Fisher, CA10262) and imaged using the Airyscan on confocal laser scanning Zeiss LSM 880. Co-staining with the moncyte endosome marker CD68 was performed in the peritoneal macrophage. Intensity profiles show dominant membrane localization of P2X7 while P2X4 is absent in the membrane. Nuclear DAPI staining is shown in blue. Scale bars 10 μm.



P2X7 on alveolar macrophages (CD11b+CD11c+CD64+CD206+) as determined by by flow cytometry. Mean fluorescence intensity (MFI) of anti-P2X7-Bv421 was calculated for alveolar macrophages from wt (blue),  $P2rx4^{-1}$  (red) and  $P2rx7^{-1}$  (grey) mice (n = 3).

Mice were anesthesized and sacrificed by CO<sub>2</sub> exposure and cervical dislocation. Lungs were removed, digested for 30 min at 37°C (1 mg/ml collagenase (Roche), 0.1 mg/ml DNAse I (Roche) in DMEM (Gibco)), and passed through a 70 μm cell strainer to generate a single cell suspension. Cells were incubated with ACK erythrocyte lysis buffer on ice and washed once with FACS buffer (PBS + 1% BSA). Percoll (GE Healthcare, 33% with PBS) gradient centrifugation was performed and cells were cell surface stained for 30 min at 4°C with antibodies against CD11b-Bv510, CD45-APC-Cy7, Ly6G-AF700, CD64-PE-Cy7, CD11c-PE-Dazzle, P2X7-Bv421 and CD206-FITC at a concentration of 1:100 (see Table S1). After staining, all cells were washed and resuspended in FACS buffer. Flow cytometric analyses were performed on a BD FACS-Symphony A3 flow cytometer and analyzed by FlowJo<sup>TM</sup> version 10.8 (BD Life Sciences).

#### Suppl. Methods

*Primary lung fibroblast culture.* Mice were euthanized by isoflurane inhalation and transcardially perfused with 5 ml PBS. The lung was extracted, cut into small pieces and transferred into 5 ml DMEM/F-12 (Gibco) supplemented with 1% Pen/Strep (Gibco), 20% FCS, and 1mg/ml collagenase (Biochrom) and incubated for 2h at 37°C and 350 rpm. The obtained cell suspension was filtered through a 70 μm cell strainer and that was washed with 30 ml PBS. Cells were collected by centrifugation (400 x g for 5 min at RT), resuspended in 10 ml DMEM/F-12 with 1% Pen/Strep/20% FCS, and seeded on an uncoated 10 cm petri dish. Cells were cultured at 37°C (95% O2, 5% CO2) and split every 2 days to enrich lung fibroblasts. After 3 passages, cells were plated on coverslips and used for immunofluorescence staining.

Primary microglia culture. P4-P6 mouse pups were decapitated, brains transferred into ice cold DMEM with 1% Penicillin/Streptomycin (DMEM+P/S) and genotypes determined by EGFP fluorescence (Typhoon scanner, GE Healthcare). Five brains were combined in 5 ml of preheated trypsin EDTA solution, cut into small pieces and incubated for 15 min at 37°C in a water bath. Digestion was stopped by addition of 20 ml cell culture medium. Cells were collected by centrifugation (800 x g, 3 min), resuspended in 5 ml DMEM +P/S +10% FCS, triturated with a 1 ml pipet tip, and after addition of 15 ml DMEM +P/S +10% FCS, counted. 7 x 10<sup>6</sup> cells were plated in a T75 flasks and kept at 37°C (95% O2, 5% CO2) with medium changes every 2-3 days. After 14 days, microglia were detached from astrocytes by shaking for 3-4 hrs at 300 rpm and subsequent vigorous tapping. Detached microglia were collected (1500 rpm for 5 min), resuspended in 1 ml DMEM +P/S +10% FCS, plated on poly-L-lysin coated cover slips, and stained the following day.

Isolation of peritoneal macrophages. Mice were euthanized with isoflurane and 5 ml of ice cold HBSS were injected into the peritoneal cavity using a 27 G needle. The peritoneum was gently massaged to detach the cells and the fluid was collected in a syringe and transferred into a 50 ml reaction tube. This step was repeated and the combined cells centrifuged (800 x g for 10 min at 4°C), and resuspended in 2-5 ml DMEM +P/S +10% FCS. 10<sup>5</sup> cells were plated on poly-L-lysin-coated cover slips, cultured overnight at 37°C (95% O2, 5% CO2) and stained.

*Image analysis.* Cells were stained (see Methods) and imaged using a Zeiss LSM 880 with Airyscan. In Fig. S7, point spread functions for deconvolution of individual channels of confocal micrographs were calculated using the Diffraction PSF 3D (Bob Dougherty, Optinav Inc) plugin applying the respective numerical aperture, wavelength, image pixel spacing and size of the image. Final deconvolution was computed with the plugin Iterative Deconvolve 3D (Optinav Inc).

Flow cytometry. Mice were sacrificed and lungs removed, digested for 30 min at 37°C (1 mg/ml collagenase (Roche), 0.1 mg/ml DNAse I (Roche) in DMEM (Gibco)), and passed through a 70 μm cell strainer to generate a single cell suspension. Cells were incubated with ACK erythrocyte lysis buffer on ice and washed once with FACS buffer (PBS + 1% BSA). Percoll (GE Healthcare, 33% with PBS) gradient centrifugation was performed and cells were cell surface stained for 30 min at 4°C with antibodies against CD11b-Bv510, CD45-APC-Cy7, Ly6G-AF700, CD64-PE-Cy7, CD11c-PE-Dazzle, P2X7-Bv421 and CD206-FITC at a concentration of 1:100 (see Table S1). After staining, all cells were washed and resuspended in FACS buffer. Flow cytometric analyses were performed on a BD FACS-Symphony A3 flow cytometer and analyzed by FlowJoTM version 10.8 (BD Life Sciences).

Schindelin, J.; Arganda-Carreras, I. & Frise, E. et al. (2012), "Fiji: an open-source platform for biological-image analysis", Nature methods 9(7): 676-682, PMID 22743772, doi:10.1038/nmeth.2019.

Dougherty, R. (2005), "Extensions of DAMAS and Benefits and Limitations of Deconvolution in Beamforming", 11th AIAA/CEAS Aeroacoustics Conference (26th AIAA Aeroacoustics Conference)

# **Acknowledgements**

I am grateful to Alexander for giving me the opportunity to pursue this PhD in his lab and for trusting and fostering my initiative. His supervision and support allowed me to grow into the researcher I am today. I would also like to thank Professor Gudermann for his instrumental leadership at both the Walther Straub Institute and the GRK 2338 program. Likewise, I extend my thanks to my TAC members, Dr. Annette Nicke and Dr. Claudia Staab-Weijnitz, for their invaluable feedback.

It was a great gift to walk this road alongside the other members of the GRK 2338 program – our shared celebrations and commiserations meant the world. I would also thank my GRK predecessor, Christian, for his patience and positivity while introducing me to the methodology. I share my deep gratitude to the lovely Postdocs, Martina and Juan, for their endless support and for sharing their well-earned expertise. My thanks go to my colleagues Philipp, Isabel, Fabienne, and Randhwaj for fostering a productive and engaging research environment. The technical support of Bettina, Heinz, and Benedikt was invaluable, as were the after-work beers.

I owe so much to my friends, Ananya and Suhasini, for keeping me smiling and dancing through the stressful moments. All my love to Gonxhe, Eva, and Steffi, for reminding me to exercise, eat delicious food, and take time to reflect. Thanks to my brother, Janek, whose tireless advocacy work continues to inspire. My utmost appreciation to Marcel, Thais, Anna and Ellis, my family in this new country.

I am forever grateful to Ben, the man I love more than science, for his bravery, understanding, tolerance and trust as we navigated this chapter.

I dedicate my PhD to my dad, the man with the strongest lungs, and my mom, whose love and support shone strong across the Atlantic.